

2014

Three essays on institutional change

Kathleen M. Sheehan

Follow this and additional works at: <https://researchrepository.wvu.edu/etd>

Recommended Citation

Sheehan, Kathleen M., "Three essays on institutional change" (2014). *Graduate Theses, Dissertations, and Problem Reports*. 6624.

<https://researchrepository.wvu.edu/etd/6624>

This Dissertation is protected by copyright and/or related rights. It has been brought to you by the The Research Repository @ WVU with permission from the rights-holder(s). You are free to use this Dissertation in any way that is permitted by the copyright and related rights legislation that applies to your use. For other uses you must obtain permission from the rights-holder(s) directly, unless additional rights are indicated by a Creative Commons license in the record and/ or on the work itself. This Dissertation has been accepted for inclusion in WVU Graduate Theses, Dissertations, and Problem Reports collection by an authorized administrator of The Research Repository @ WVU. For more information, please contact researchrepository@mail.wvu.edu.

The Utility of Fine-Scale Remote Sensing Data for Modeling Habitat Characteristics and Breeding Bird Species Distributions in an Appalachian Mature Deciduous Forest.

James Sheehan

Dissertation submitted to the
Davis College of Agriculture, Natural Resources, and Design
at West Virginia University

in partial fulfillment of the requirements for the degree of

Doctor of Philosophy
in
Forest Resource Science

Petra Bohall Wood, Ph.D., Chair
James T. Anderson, Ph.D.
Amy E. Hessel, Ph.D.
Michael P. Strager, Ph.D.
Timothy A. Warner, Ph.D.

Division of Forestry and Natural Resources

Morgantown, West Virginia

2017

Keywords: Remote sensing, satellite imagery, topography, breeding forest birds, species distribution models, spatial point pattern analysis

Copyright 2013 James Sheehan

ABSTRACT

The Utility of Fine-Scale Remote Sensing Data for Modeling Habitat Characteristics and Breeding Bird Species Distributions in an Appalachian Mature Deciduous Forest.

James Sheehan

In this study, I tested the potential for remote sensing data with a high spatial resolution to model breeding forest bird species and their habitat at a fine spatial scale. The research took place on ridgetops in a large, relatively contiguous Appalachian mature deciduous forest in northwestern WV, USA. The remote sensing data sources were a leaf-on QuickBird satellite image (0.6-m panchromatic and 2.4-m multispectral) and a 3-m digital elevation model (DEM).

For the first part of the study, I extracted spectral and textural measures from the satellite image and terrain information from the DEM. I then used these data to analyze avian community survey and habitat data collected at circular plots ($n = 68$) distributed across the ridgetops. The primary results of this analysis indicated that the satellite image provided information about trends in forest composition and structure across the study site, and further that a relatively simple plot-level measure of image texture (the panchromatic pixel standard deviation calculated at plot radii of 50 and 100 m) was a useful proxy of environmental heterogeneity for predicting the distributions of certain forest canopy gap-dependent bird species.

For the second part of the study, I analyzed the habitat and remote sensing data at a finer spatial scale to develop remote sensing-based indices of forest structure and composition. These indices provided further insight into local variation in forest characteristics (e.g., in relation to topographic aspect) on the ridgetops. I also tested these indices, the DEM, and anthropogenic forest edge for modeling the breeding territory distributions of three focal species (Cerulean Warbler, *Setophaga cerulea*; Hooded Warbler, *S. citrina*; and Ovenbird, *Seiurus aurocapilla*) mapped over ~11 km of ridgetop transects. These models indicated the importance of local influences of terrain (e.g., east-facing aspects for Cerulean and Hooded Warbler, west-facing aspects for Ovenbird, and knolls for Cerulean Warbler), and forest edges (positive for Cerulean Warbler and negative for Ovenbird) on their distributions. Among the remotely-sensed indices, the index of forest structural complexity was primarily useful as a strong predictor of the distribution of the canopy gap-dependent Hooded Warbler.

For the third and final part of the study, I used the locations of singing males of the three focal species collected across a greater extent of the site (~28 km of ridgetop transects) in point pattern analyses that incorporated the remote sensing data and the potential for intraspecific interactions (attraction and repulsion) between neighboring individuals. The results of these analyses supported that intraspecific interactions in addition to environmental influences as indicated by the remote sensing data explained the species' fine-scale distribution patterns. While the individuals of all three species exhibited regular spacing over short distances that was consistent with competition for territorial space, Cerulean Warbler individuals exhibited more clustering than could be statistically accounted for by the remote sensing data, suggesting the importance of conspecific attraction in its distribution.

In summary, my findings supported the potential application of fine-scale remote sensing data for purposes such as complementing coarse-scale environmental data (e.g., land cover maps) in predicting forest breeding bird species distributions, and for comparative analyses of the local spatial distributions of these species. The capacity for remote sensing data to provide useful environmental information at a fine spatial scale is likely to improve as the technology continues to develop.

ACKNOWLEDGEMENTS

First of all, I wish to thank my advisor Dr. Petra Wood for her tremendous guidance in helping me to achieve my research goals and this dissertation, and her patience and kindness throughout this long, challenging, and ultimately rewarding process. I also thank Dr. Greg George for suggesting back in 2007 when he was a Ph.D. student of Dr. Wood that I contact her about potential graduate research in the first place. Soon after, I made my way to West Virginia and quickly realized the incredible opportunity that I had before me, both in field research on forest songbirds and at West Virginia University. Next I wish to thank Dr. Jim Anderson, Dr. Amy Hessel, Dr. Mike Strager, and Dr. Tim Warner for agreeing to be on my graduate committee, for contributing their various expertise, and for their helpful edits and comments on the various draft chapters of this dissertation. I thank Dr. Warner especially for the remote sensing classes that helped open up an exciting new world of research possibilities for me to explore.

I am grateful to the National Energy Technology Laboratory (NETL) - Department of Energy, the U.S. Fish and Wildlife Service, and the National Fish and Wildlife Foundation for funding my research. I also thank the West Virginia University Division of Forestry and Natural Resources and Dr. Joe McNeel for support. The West Virginia Department of Natural Resources and the U.S. Geological Survey West Virginia Cooperative Fish and Wildlife Research Unit provided logistical support. A special thanks to Becky Nestor in the Coop Unit for her seemingly endless administrative assistance keeping things running smoothly. Field housing at the beautiful Lantz Farm and Nature Preserve, a major perk, was provided by Wheeling Jesuit University.

My research would not have been possible without the assistance of a small army of field technicians over the years, of whom I want to particularly thank Darin Blood, Megan Napoli, and Brandon Miller for the excellent quality of their data collection even when it was most tedious. I

thank also my graduate student colleagues, especially Kyle Aldinger, Ryan Davis, Laura Farwell, Mack Frantz, and Jeremy Mizel for many interesting statistical and research-oriented discussions, or just enjoyable chats.

Finally, I cannot thank enough Laura Protzman for her love and support (and fortitude!), my best and oldest friend Joe Sargent for keeping it real and encouraging me to be my best, and my parents Alice M. and James T. Sheehan and the rest of my family for always being there even at a distance. As far as the Lewis Wetzel Wildlife Management Area, which became home to me for much too-brief a time, I hope I will forever be walking your wild ridgetops and hearing your incredible bird life in my dreams.

TABLE OF CONTENTS

TABLE OF CONTENTS.....	vi
LIST OF TABLES.....	ix
LIST OF FIGURES	xi
LIST OF APPENDICES.....	xv
CHAPTER 1: Introduction	1
Study Site	4
Remote Sensing Data.....	5
References.....	6
CHAPTER 2: Fine-scale modeling of habitat and avian biodiversity in an Appalachian deciduous forest using a QuickBird satellite image.....	9
Abstract.....	9
1. Introduction.....	11
2. Materials and methods.....	16
2.1. Study site.....	16
2.2. Field sampling.....	17
2.3. Remote sensing data.....	19
2.3.1. Satellite image variables.....	20
2.3.2. Topographic variables	23
2.4. Statistical analyses.....	24
2.4.1. Principal component analysis (PCA) of the forest data.....	24
2.4.2. Fitting of geospatial variables to the PCA.....	25
2.4.3. Avian modeling	26
3. Results.....	30
3.1. Forest variable PCA and geospatial variable fits	30
3.1.1. Selection of multiple variable linear regression models.....	32
3.1.2. Spatial trends in principal components and geospatial variables	33
3.2. Single and multiple variable 50-m scale avian species richness models	34
3.2.1. Effect of 100-m scale on species richness results.....	37
3.2.2. Effect of year on species richness results	38

3.3. Species occurrence and abundance models.....	39
4. Discussion.....	40
4.1. Avian relations to principal component 1 (PC1) and image texture.....	43
4.2. Spatial trends.....	49
4.3. Comparisons with other studies.....	50
4.4. Image texture analysis and application considerations.....	52
5. Conclusions.....	55
Acknowledgments.....	57
References.....	57
Appendix A.....	85
Appendix B.....	86
Appendix C.....	87
Appendix D.....	92

CHAPTER 3: Development of remotely-sensed indices of fine-scale forest characteristics for modeling breeding bird species distributions in an Appalachian deciduous forest..... 98

Abstract.....	98
1. Introduction.....	100
2. Methods.....	102
2.1. Study site.....	102
2.2. Field sampling.....	103
2.3. Remote sensing data.....	106
2.4. Remote sensing index development.....	108
2.5. Species distribution modeling.....	111
2.5.1. Initial model predictions.....	113
3. Results.....	115
3.1. Forest structure and composition modeling.....	115
3.2. Validation and mapping of the indices.....	118
3.3. Territory maps and SDM covariate selection.....	120
3.4. SDM single and multiple covariate effects.....	122
3.4.1. Hooded Warbler.....	123
3.4.2. Ovenbird.....	124
3.4.3. Cerulean Warbler.....	126
3.4.4. Separability of effects.....	127
4. Discussion.....	128

4.1. SDM-based habitat selection and predictions	131
4.1.1. Hooded Warbler	131
4.1.2. Ovenbird	133
4.1.3. Cerulean Warbler.....	135
5. Conclusions.....	137
Acknowledgments.....	139
References.....	139
Appendix A.....	160
Appendix B.....	161
Appendix C.....	166
Appendix D.....	167
Appendix E	168
Appendix F.....	175
 CHAPTER 4: Modeling the distributions of three Appalachian deciduous forest songbirds as point patterns using fine-scale remote sensing data.....	190
ABSTRACT.....	190
INTRODUCTION	192
METHODS	196
Study Site	196
Field Data Collection	196
Analyses	198
Point pattern analysis background.....	199
Environmental covariates	201
Modeling procedure.....	203
RESULTS.....	206
DISCUSSION	210
Conclusions	216
ACKNOWLEDGMENTS	218
LITERATURE CITED.....	218
APPENDIX.....	234

LIST OF TABLES

CHAPTER 2.

Table 1. The moving window analysis neighborhood sizes and their respective ground distances for the panchromatic (PAN; 0.6-m resolution) and normalized difference vegetation index (NDVI; 2.4-m resolution) images.66

Table 2. The four categories of geospatial variables used in this study. The variables were obtained using geoprocessing tools in ArcGIS 10.1 (described in the footnotes) applied at the two plot-level spatial scales of the sampling points (50 and 100 m radii) to the data sources: the panchromatic (PAN) and normalized difference vegetation index (NDVI) images, the moving window analysis texture images from the PAN and NDVI images, and the digital elevation model (DEM). The pixel neighborhood size (see Table 1) is appended for identifying specific first- and second-order texture variables (e.g., PAN_{AVG_SD03} indicates that the texture image from which this plot-level measure was obtained was calculated using a 3 x 3 pixel neighborhood).67

Table 3. Principal components (PC1-PC3) with eigenvalues >1.0 that were retained from the principal components analysis (% of the total variance each explained is in parentheses), and the factor loading for the 14 forest variables. The factor loadings that appeared to provide the most differentiation of the 68 sampling points for each retained component are in bold.68

Table 4. Vector and surface fits of the reduced set of geospatial variables to the PC1:PC2 (principal components 1 and 2) ordination (Figure 3a). Surface fits are not provided (--) if the R^2 fit was the same as the vector R^2 fit. Geospatial variables in bold were used as the basis for the initial avian richness, occurrence, and abundance modeling.69

Table 5. Results of the forward selection procedure (Blanchet et al. 2008) of geospatial variables for predicting principle component 1 (PC1) and the dominant PC1 forest characteristics (the six forest variables in bold for PC1 in Table 3). Model fit was evaluated using leave-one-out cross validation and the cross validated root mean square error (RMSE) is reported along with the RMSE as a percentage of the range of the response variable.70

Table 6. Single variable generalized additive model (GAM) results for the species richness measures at the two spatial scales (significant results are underlined). The principal components analysis (PCA) axes PC1 and PC2, which are 50-m scale field habitat data-derived variables (see Figure 3a), are presented for comparison with the 50-m scale geospatial (image and topographic) variables. The 100-m scale geospatial variables are presented for comparison with their respective 50-m scale results.71

Table 7. Generalized additive model (GAM) multiple variable selection results for the species richness measures at the 50-m scale.72

Table 8. Generalized additive model (GAM) multiple variable selection results for the addition of image variables to the best single image/topographic variable models for total, common, and rare species richness at the 50-m scale.73

Table 9. Best single image variable generalized additive models (GAMs) for total, common, and gap species richness in 2009-11 at the two spatial scales using the reduced dataset of 42 sampling points (significant results are underlined). No significant results were found for rare species richness (not reported).74

Table 10. Single variable generalized additive model (GAM) results for species occurrence (50-m scale) and abundance (100-m scale) for the species with at least one significant effect (underlined) found for the principal component 1 (PC1) and best image texture models. The number of absences ($N = 0$) and presences ($N = 1$) for each species over the 68 sampling points at the 50-m scale are also provided.....75

CHAPTER 3.

Table 1. Forward-backward selection of explanatory variables for the forest structure (RDAs), forest composition (CCA_C), and forest structure plus composition (RDAs_{+C}) models, and model significance tests. Percent values in parentheses are the proportions of the total model inertia (i.e., variance in the field data) explained by the models. See Appendix C for the key to the labels for the explanatory variables and their descriptions.147

Table 2. The WA-LC (i.e., ‘species-environment’) Pearson’s correlations (r) for the first and second axes of the constrained ordination models, and results of the leave-one-out cross validation (LOOCV). The internal validation was for the stability of r between the site (i.e., field subplot) WA scores (weighted averages of the field variables) and LC scores (linear combinations of the remote sensing explanatory variables), by resampling the data used to create the models. The external validation was for the r between the WA and LC scores predicted at the locations ($n = 97$) where additional habitat samples were collected (see Appendix B). The RMSE (Root Mean Squared Error) of the model is given as a percentage of the WA score range.148

CHAPTER 4.

Table 1. Parameter estimates for the environmental covariates from univariate inhomogeneous Poisson (PS), hard core (HC), and hard core-Geyer (HC-G) point process models by species across the three sampling bouts. Environmental covariate estimate 95% confidence intervals (CI) in bold do not overlap zero.226

Table 2. Final inhomogeneous Poisson (PS), hard core (HC), and hard core-Geyer (HC-G) point process models by species across the three sampling bouts obtained from the AIC step procedure. The AIC values for the final models are presented for comparison within a species within a sampling bout. The model formula begins with the intercept followed by the covariate coefficients (key: IF = impacted forest, E = eastness, N = northness, El = elevation, RDAs = forest structural complexity index, Kd = knoll distance).....228

LIST OF FIGURES

CHAPTER 1.

Figure 1. Study site at the Lewis Wetzel Wildlife Management Area in northwest WV, with the 68 ridgetop sampling point locations and the six line transects overlaid on a QuickBird satellite 0.6-m resolution panchromatic image (left) and on a 3-m resolution (± 3 m vertical accuracy) digital elevation model (DEM; right). The QuickBird satellite image was acquired August 2009 at 11:18 AM local time (solar azimuth = 127°). The 1/9 arc-second DEM was obtained as a seamless product from <http://viewer.nationalmap.gov/>.8

CHAPTER 2.

Figure 1. Study site at the Lewis Wetzel Wildlife Management Area in northwest WV, with the 68 ridgetop sampling point locations shown on the August 2009 QuickBird satellite panchromatic (0.6-m resolution) image (left). The points were located >150 m from anthropogenic forest impacts on the ridgeline (i.e., the crest) of prominent ridges (right), spaced ≥ 250 m apart for avian point count survey considerations. The 4-landform classification was obtained from a 3-m digital elevation model (used here as a shaded-relief underlay of the landform classification set at 50% transparency) using the Topographic Position Index function in Topography Tools for ArcGIS 10.1 (Dilts 2015).76

Figure 2. Diagram of the QuickBird satellite image processing and extraction of the zonal statistics (i.e., the image variables used in the analyses) for the 68 sampling point locations at the 50- and 100-m radius plot-level scales. In extraction step 1, the zonal statistics were obtained directly from the PAN and NDVI images. In extraction step 2, the zonal statistics were obtained from images of first- and second-order texture statistics processed from the PAN and NDVI images.77

Figure 3. Principal components analysis (PCA) results and geospatial variable fits. See Table 3 for the key to the forest variable labels for the PC1:PC2 (principal components 1 and 2) ordination plot, and Table 4 for the vector and surface fits (R^2) of the geospatial variables to the PC1:PC2 ordination plot.78

Figure 4. Sampling point images ranked by principal component 1 (PC1) scores. The sampling points with the minimum and 25th percentile values (negative PC1 scores; see Figure 3a) are dominated by a smooth canopy. The sampling points with the 75th percentile and maximum values (positive PC1 scores; see Figure 3a) exhibit a more heterogeneous canopy, with distinctly brighter patches of pixels that likely indicate greater reflectance by understory vegetation in canopy gaps and/or grapevines.80

Figure 5. Spatial bubble plots of principal component 1 (PC1) scores and select geospatial variables for the 68 sampling points. The x- and y-axes are in Universal Transverse Mercator Zone 17, North American Datum 1983 coordinates. The sizes of the points are in proportion to their values. The values for PAN_{SD}, elevation (ELEV), and the topographic variation index (TVI) were mean-centered to more clearly illustrate spatial patterns.81

Figure 6. Generalized additive model (GAM) response curves for the best-fitting multiple variable models for (a) total and (b) gap species richness at the 50-m scale. The curves show the functional forms of the responses (with 95% confidence bands) to the geospatial variables. The y-axes are at the scale of the linear predictor, and the labels provide the estimated degrees of freedom (e.d.f.) of the scale-invariant tensor product (te) smooths used in the GAMs to obtain the response curves. The tick marks above the x-axes indicate the geospatial variable values for the 68 sampling points. Note that for gap species richness, elevation was effectively removed as an effect (e.d.f. ≈ 0) by the GAM variable selection technique (Marra and Wood 2011).....82

Figure 7. Generalized additive model (GAM) response curves plotted at the scale of the original response data (number of species) from the overall best-fitting single variable models for (a) total and (b) gap species richness at the 50- and 100-m scales. The dots indicate the individual richness values for the sampling points ($n = 68$).83

Figure 8. Annual generalized additive model (GAM) response curves plotted at the scale of the original response data (number of species) for (a) total and (b) gap species richness at the 50- and 100-m scales using the 42 sampling points surveyed 2009-11 (solid lines = significant trends). The black dots indicate the individual richness values for the sampling points. For the 2011 graphs, the GAM response curves using the 68 total sampling points, and the individual species richness values for the 26 additional 2011 points, are shown in gray.84

CHAPTER 3.

Figure 1. QuickBird satellite 0.6-m panchromatic band image (August 2009) of the study area showing the 68 ridgetop sampling points located in mature forest >150 m from anthropogenic canopy disturbances. Also shown are the six ridgetop transects where the breeding territories of the three bird species were mapped. The OR and SR transects (shown with the boundaries used to define the point pattern analysis windows) had two years of territory mapping data (2010 and 2011) for analysis. The inset shows the 5-subplot habitat sampling arrangement per point where forest composition and structure data were collected for the remote sensing-based forest indices.149

Figure 2. Constrained ordination triplots (axes 1 and 2) showing species scores (red labels = field variables), site scores (open circles = subplots), and environmental constraints (blue arrows = remote sensing variables) from the (a) redundancy analysis of forest structure (RDAs), (b) canonical correspondence analysis of forest composition (CCA_c), and (c) redundancy analysis of forest structure plus tree species richness and chestnut oak/sugar maple composition (RDA_{s+c}). See Appendix A for field variable label key and Appendix C for remote sensing variable key.151

Figure 3. Panchromatic QuickBird satellite and RDA¹_{s+c} index images for portions of the SR and OR transects (indicated with boxes in the overview). The arrows point to deep blue patches of very smooth canopy on each transect, with predicted high basal area/chestnut oak composition. Deep red patches indicate high structural complexity/sugar maple composition.....152

Figure 4a. Mapped territory centers of the three species in 2010.....	153
Figure 4b. Mapped territory centers of the three species in 2011.....	154
Figure 5. Spatial covariates used in the species distribution models. A Gaussian (15 m s.d.) filter was applied to the forest indices RDA^1_s , CCA^1_c , and RDA^1_{s+c} (similar to RDA^1_s and not shown). Knolls (triangles) and the SR transect impact (lines) used to compute distance grids (not shown) are mapped on the elevation layer. The eastness and northness layers were arcsine square-root transformed.	155
Figure 6. Hooded Warbler 2010 and 2011 territory intensity (λ) as predicted by the fitted PPMs and as nonparametric functions of spatial covariates. The bivariate functions show λ as a function of two spatial covariates (circles indicate covariate values for the individual territories).	156
Figure 7. Ovenbird 2010 and 2011 territory intensity (λ) as predicted by the fitted PPMs and as nonparametric functions of spatial covariates. The univariate functions show λ with pointwise 95% confidence limits (gray shadings). The bivariate functions show λ as a function of two covariates (circles indicate covariate values for the individual territories).	157
Figure 8. Cerulean Warbler 2010 and 2011 territory intensity (λ) as predicted by the fitted PPMs and as nonparametric functions of spatial covariates. The univariate functions show λ with pointwise 95% confidence limits (gray shadings). The bivariate functions show λ as a function of two covariates (circles indicate covariate values for the individual territories).	158
Figure 9. Hooded Warbler and Ovenbird 2010 and 2011 territory intensity (λ) as nonparametric functions of the RDA^1_s index. The functions show λ with pointwise 95% confidence limits (gray shadings) after controlling for eastness effects on λ using a parametric point process model. For comparison, the dashed lines show λ modeled separately using only the RDA^1_s index.	159

CHAPTER 4.

Figure 1. The six ridgetop transects in the Lewis Wetzel Wildlife Management Area, WV, for mapping the locations of Cerulean Warbler, Hooded Warbler, and Ovenbird singing males. See the Appendix for additional transect details.....	229
Figure 2. Rank envelope tests of the homogeneous and final inhomogeneous hard core models for the Cerulean Warbler point patterns by survey bout using the centered L - and L_{inhom} -functions ($\hat{L}(r) - r$ and $\hat{L}_{inhom}(r) - r$; r = distance in m), which are linearized versions of the Ripley's K -function for detecting clustering or regularity in a point pattern. The thick line is the function obtained from the observed point pattern, the dashed lines are the upper and lower bounds of the 95% global envelope for the distance interval (hard core distance to 300 m) based on 2499 simulations of the fitted model, and the dotted line is the simulation mean (i.e., the estimated theoretical expectation of the null hypothesis). The p -value interval for the test is in parentheses	

(lower p -value, upper p -value) and where the function is above the envelope suggests distances up to which individuals exhibited clustering.230

Figure 3. Rank envelope tests of the final inhomogeneous hard core-Geyer interaction hybrid models for the Cerulean Warbler point patterns by survey bout (figure and test descriptions as in Figure 2). The table shows the key parameters for interpreting the Geyer saturation interaction: $r(m)$ is the interaction radius distance, σ is the number of neighboring points typically involved in the interaction, *Gamma* is the interaction parameter (>1 indicates clustering), and the estimate is the positive attraction effect estimate and its 95% confidence interval (CI).....231

Figure 4. Rank envelope tests of the homogeneous and final inhomogeneous hard core models for the Hooded Warbler point patterns by survey bout (figure and test descriptions as in Figure 2).232

Figure 5. Rank envelope tests of the homogeneous and final inhomogeneous hard core models for the Ovenbird point patterns by survey bout (figure and test descriptions as in Figure 2).233

LIST OF APPENDICES

CHAPTER 2.

Appendix A. Bird species common names, scientific names, detection type(s) used for the analysis, and relatively common/relatively rare designation.....	85
Appendix B. Spearman's correlations for the reduced set of geospatial variables. See Appendix D for the full set of correlations.....	86
Appendix C. Overview map of the 68 sampling points and the Quickbird satellite 0.6-m panchromatic band images of the points ordered by their principal component 1 (PC1) scores from the principal components analysis (PCA) of the field habitat data (collected within the inner 50-m radius circle). For the images, the value in the parentheses is the 50-m radius pixel s.d. (PAN _{SD}), with the numeric rank for the point from low to high PAN _{SD} in brackets. Image labels for the 26 points added in 2011 are in bold.	87
Appendix D. Spearman's correlations for the full set of geospatial variables.....	92

CHAPTER 3.

Appendix A. List of field variables with subplot statistics and data transformations. ...	160
Appendix B. Comparative analyses of forest habitat characteristics at Cerulean Warbler and Ovenbird territory centers, and at Cerulean Warbler territory centers and non-use locations	161
Appendix C. List of remote sensing variables with subplot statistics and data transformations.	166
Appendix D. Spearman's correlations for the set of remote sensing variables used in the constrained ordinations (top), and over the combined OR and SR transect extent for the species distribution model (SDM) spatial covariates (bottom).	167
Appendix E. SR and OR transect QuickBird satellite image and remote sensing index maps, and combined-year territory center maps by species.....	168
Appendix F. Complete annual point process model (PPM) results by species. All single spatial covariate and covariate by transect interaction model results are presented. For models including multiple spatial covariates, those presented vary by species (see section 3.4.). Modeling comments, diagnostic plots, and predicted intensity plots are also provided for select models.	175

CHAPTER 4.

Appendix. Forest impacts mapped within the areas of the transects (Figure 6), and the point patterns of the singing male Cerulean Warblers, Hooded Warblers, and Ovenbirds by survey bout (Figures 7-9).	234
--	-----

CHAPTER 1: Introduction

The research contained in this dissertation centers on testing the utility of fine-scale remote sensing data (here 0.6-m to 3-m spatial resolution) for modeling habitat characteristics and breeding bird species distributions on ridgetops in an Appalachian mature deciduous forest in WV, USA. I organized this dissertation into four chapters, with three of the chapters intended for publication and formatted as such. Chapter 1 provides a general dissertation outline, the primary motivations and some key background for my research, an introduction to the study site, and an overview of the remote sensing data used in the analyses. Chapter 2 is formatted for submission to the journal *Remote Sensing of Environment* and focuses on the use of the remote sensing data to model forest habitat characteristics and avian community point count survey data. Chapter 3 is also formatted for submission to the journal *Remote Sensing of Environment* and focuses on the development of remote sensing-based indices of forest structure and composition. These indices were then tested along with ancillary terrain data for modeling the distributions of the mapped territories of three focal forest songbird species (Cerulean Warbler, *Setophaga cerulea*; Hooded Warbler, *S. citrina*; and Ovenbird, *Seiurus aurocapilla*). Chapter 4 is formatted for submission to the journal *The Auk: Ornithological Advances*, and focuses on the singing male locations of the three focal species as point patterns. These patterns were analyzed using point process models that incorporated the remote sensing data, to assess their territorial spacing behavior in addition to the environmental factors underlying their distributions.

There were two primary motivations for my research. The first was the avian community I studied, which I broadly define here as comprised of breeding forest bird species of central Appalachian deciduous forests. This community contained several species of high conservation

attention, including the severely declining Cerulean Warbler (Sauer et al. 2014), and the region in which I studied this community has been recognized particularly for its importance to mature forest bird species (Farwell 2016). The second motivation was the recent advancement of satellite remote sensing technology capable of providing environmental information at increasingly finer spatial scales (He et al. 2015, Velázquez et al. 2016). With the acquisition of a high resolution QuickBird satellite image (see details in Remote Sensing Data, below) of a large, mostly contiguous mature deciduous forest, I saw an important opportunity to test the use of this image along with ancillary remote sensing data on terrain and anthropogenic forest impacts for fine-scale modeling of this bird community and its ridgetop forest habitat.

The modeling was a progression, both in what (and how) field data were analyzed and in the processing of the remote sensing data for these analyses. I began with the analysis of avian community point count survey data (Chapter 2) to examine broader community- and species-level trends across the site. This required much initial processing of particularly the satellite image (and many lessons learned therein), to attempt to extract meaningful information for modeling the field data. At this point, I relied on individual remotely-sensed measures (particularly of image texture) for analyzing the avian and habitat data; for example to identify specific measures that were related to environmental heterogeneity and thus could potentially predict bird species richness and occurrence. I then used a multivariate analysis technique (Torontow and King 2011) to relate the remote sensing data to the field-collected habitat data and thus allow highly-detailed continuous mapping of predicted forest structure and composition on the ridgetops (Chapter 3). This was a critical development phase for testing the use of these maps, along with ancillary terrain and forest impact remote sensing data, for modeling the intensively mapped distributions of the three focal species at a finer within-ridgetop spatial scale.

Finally, in a more application-oriented study (Chapter 4), I used the forest structure map and the ancillary remote sensing data in point pattern analyses of the singing male locations of the three focal species that also incorporated the potential for attraction or repulsion between individuals.

Because of their conspicuousness and potential value as indicator species of environmental conditions, birds have long been the focus of remote sensing-based ecological studies (Gottschalk et al. 2005). Several of these many studies were particularly important to the development of my research questions. St-Louis et al. (2006, 2009) first introduced me to the concept of using aerial and satellite image texture for predicting avian biodiversity. Although they investigated at a much coarser spatial scale (across the state of Maine) than I did, Hepinstall and Sader (1997) led me to focus on disturbance-dependent bird species as those likely to show trends in relation to remotely-sensed measures of fine-scale environmental heterogeneity. Melles et al. (2009) in their study of Hooded Warbler nesting patterns provided much of the inspiration behind my use of point pattern analysis and the remote sensing data at a finer spatial scale to better examine avian spacing behavior.

In thinking about how my findings on the utility of fine-scale remote sensing data for studying forest birds and habitat could apply to avian management or conservation, I became most interested in two potential applications with multi-scale implications. One is the use of fine-scale remote sensing data (e.g., on forest structural complexity; Chapter 2) to improve predictions of species distributions made using coarse-scale environmental data (e.g., see Camathias 2013). The other is for fine-scale remote sensing data to be used in comparative analyses of the local distribution patterns of species (Chapters 3 and 4). Such analyses may provide important information on how individuals of a species select habitat, including on the potential influences of both the environment and neighboring individuals, and thus contribute to

a better understanding of the likely multi-scale nature of avian habitat selection (Sherry and Holmes 1985). For my research, I used two remote sensing data sources among many of potential value (e.g., active remote sensing such as lidar; hyper-spectral imagery), simply because they were the ones available (albeit not without cost for the QuickBird image). While this investigation was at one site, these sources appeared to contain a variety of potentially useful fine-scale information that may be generally applicable to forest habitats elsewhere. Future such investigations will hopefully take advantage of the continual improvement (and hopefully greater availability at reduced cost) of remote sensing data for modeling avian habitat and species distributions.

Study Site

I conducted the research within the 5,500 ha (13,590 acre) Lewis Wetzel Wildlife Management Area (WMA), located in Wetzel County in northwestern West Virginia (Figure 1). The site is in the Permian Hills subdivision of the Western Allegheny Plateau Ecoregion, and well-represents the rugged topography and dense Appalachian Oak Forest and Mixed Mesophytic Forest that is characteristic of the Permian Hills (Woods et al. 1999). The WMA has also been recognized for supporting a large Cerulean Warbler breeding population (National Audubon Society 2013), a primarily ridge-associated species in this region (Weakland and Wood 2005). At the time of the field work (ca. 2009–11), the site was >92% mature second-growth deciduous forest (Farwell et al. 2016) comprised of a mix of these two forest types. The field sampling took place entirely on the convoluted networks of ridgetops covering the site (right image in Figure 3). I sampled 68 locations with avian community point count surveys and for habitat data, and on six transects (totaling 28 km in length) for collecting territory distribution

data on the three focal bird species. The existence of a largely contiguous, mature forest on the complex topography of ridgetops, along with a diverse forest bird community with large populations of the three focal species, likely provided an ideal situation for conducting my remote sensing-based research.

Remote Sensing Data

In addition to the study site characteristics, the type and quality of the remote sensing data sources that were used were likely important to the research. The 6° off-nadir, August 2009 QuickBird satellite image (left image in Figure 1) was acquired near mid-day (11:18 AM local time, solar azimuth = 127°) for good illumination of forest canopy characteristics, and the image quality appeared to be optimal, with no clouds or obvious haze visible over the study region. This image contained a 0.6-m resolution panchromatic band, and four 2.4-m resolution spectral bands (red, green, blue, and near-infrared), which allowed a relative comparison of their fine-scale information for modeling the field data. The 1/9 arc-second (3-m resolution, ± 3 m vertical accuracy) DEM (right image in Figure 1) was a seamless product downloaded for the study site from <http://viewer.nationalmap.gov/>. The DEM well-represented the complex topography, providing detailed terrain information such as knolls (local elevation high points) and the diverse aspects and slopes of the ridgetops. The DEM also produced accurate ridgetop centerlines for the transects, and helped ensure the placement of the sampling points on the absolute peak of the ridges for consistency and accuracy in the collection of the habitat and bird distribution data. Together, the two remote sensing data sources provided a large suite of potential environmental explanatory variables that were crucial to the fine-scale nature of the analyses.

References

- Camathias, L., Bergamini, A., Küchler, M., Stofer, S., Baltensweiler, A., Rocchini, D., 2013. High-resolution remote sensing data improves models of species richness. *Applied Vegetation Science* 16:539–551.
- Farwell, L.S., Wood, P.B., Sheehan, J., George, G.A., 2016. Shale gas development effects on the songbird community in a central Appalachian forest. *Biological Conservation* 201:78–91.
- Gottschalk, T.K., Huettmann, F., Ehlers, M., 2005. Thirty years of analysing and modelling avian habitat relationships using satellite imagery data: A review. *International Journal of Remote Sensing* 26: 2631–2656.
- He, K.S., Bradley, B.A., Cord, A.F., Rocchini, D., Tuanmu, M.N., Schmidtlein, S., Turner, W., Wegmann, M., Pettorelli, N., 2015. Will remote sensing shape the next generation of species distribution models? *Remote Sensing in Ecology and Conservation* 1:4–18.
- Hepinstall, J., Sader, S., 1997. Using Bayesian statistics, Thematic Mapper satellite imagery, and breeding bird survey data to model bird species probability of occurrence in Maine. *Photogrammetric Engineering and Remote Sensing* 63:1231–1237.
- Melles, S. J., Badzinski, D., Fortin, M. J., Csillag, F., Lindsay, K., 2009. Disentangling habitat and social drivers of nesting patterns in songbirds. *Landscape Ecology* 24:519–531.
- National Audubon Society, 2013. Important Bird Area Reports: Lewis Wetzel Wildlife Management Area. [Online] <http://netapp.audubon.org/IBA/Reports/3447>.
- Sauer, J.R., Hines, J.E., Fallon, J.E., Pardieck, K.L., Ziolkowski, D.J., Link, W.A., 2014. The North American Breeding Bird Survey, Results and Analysis 1966–2013 version 01.30.2015. USGS Patuxent Wildlife Research Center, Laurel, Maryland ([Online] <http://www.mbr-pwrc.usgs.gov/bbs/>. Accessed Mar.15, 2016).

- Sherry, T.W., Holmes, R.T., 1985. Dispersion patterns and habitat responses of birds in northern hardwoods forests. In *Habitat Selection in Birds*. (M. L. Cody, Editor). Academic Press, NY, USA.
- St-Louis, V., Pidgeon, A.M., Radeloff, V.C., Hawbaker, T.J., Clayton, M.K., 2006. High-resolution image texture as a predictor of bird species richness. *Remote Sensing of Environment* 105:299–312.
- St-Louis, V., Pidgeon, A.M., Clayton, M.K., Locke, B.A., Bash, D., Radeloff, V.C., 2009. Satellite image texture and a vegetation index predict avian biodiversity in the Chihuahuan Desert of New Mexico. *Ecography*, 32:468–480.
- Torontow, V., King, D., 2011. Forest complexity modelling and mapping with remote sensing and topographic data: A comparison of three methods. *Canadian Journal of Remote Sensing* 37:387–402.
- Velázquez, E., Martínez, I., Getzin, S., Moloney, K.A., Wiegand, T., 2016. An evaluation of the state of spatial point pattern analysis in ecology. *Ecography* 39:1–14.
- Weakland, C.A., Wood, P.B., 2005. Cerulean warbler (*Dendroica cerulea*) microhabitat and landscape-level habitat characteristics in southern West Virginia. *The Auk* 122:497–508.
- Woods, A.J., Omernik, J.M., Brown, D.D., 1999. Level III and IV Ecoregions of Delaware, Maryland, Pennsylvania, Virginia, and West Virginia., U.S. Retrieved November 4, 2009 from U.S. Environmental Protection Agency, National Health and Environmental Effects Research Laboratory. Corvallis, OR.
- ftp://ftp.epa.gov/wed/ecoregions/reg3/reg3_eco_desc.doc.

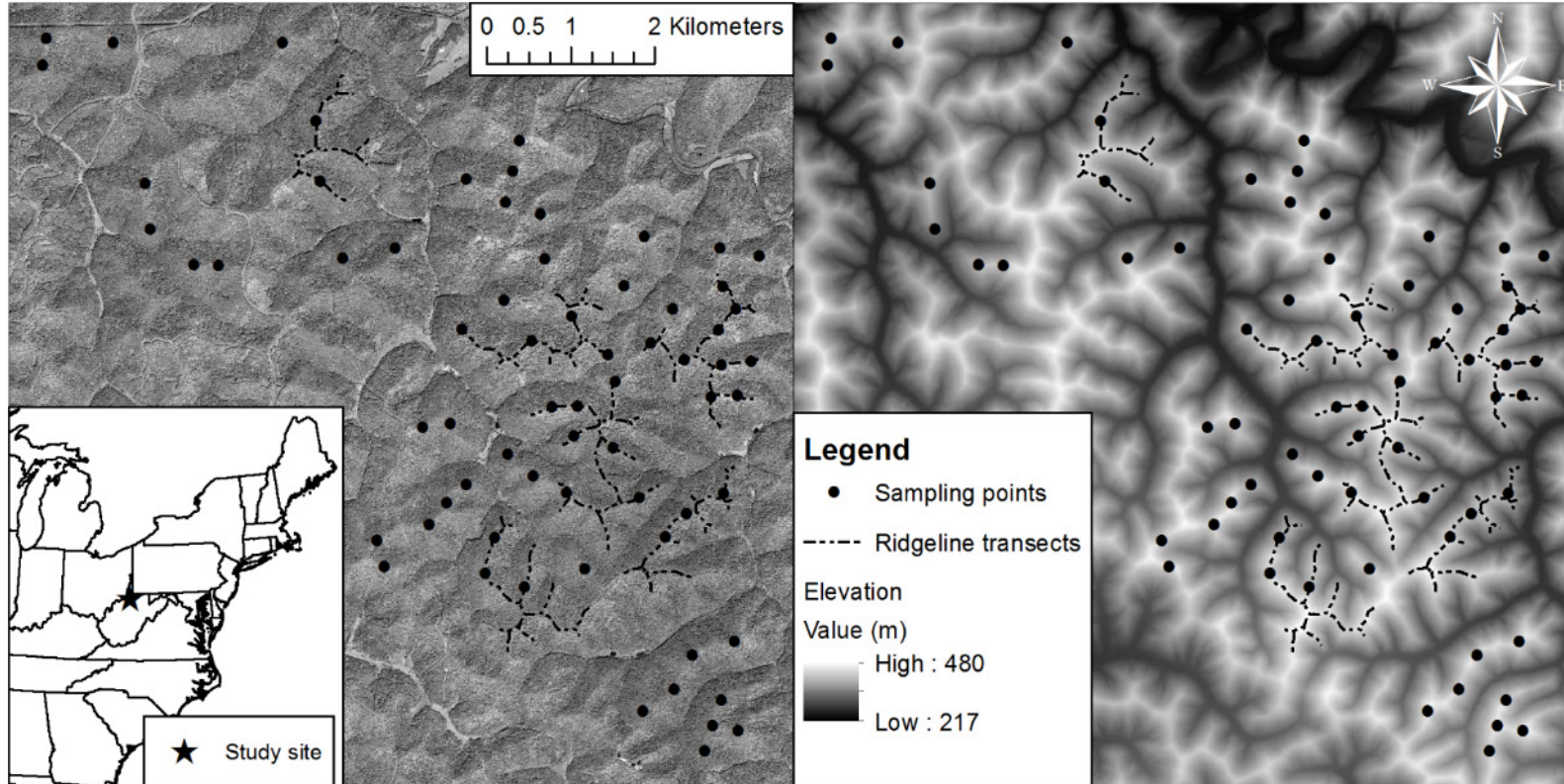


Figure 1. Study site at the Lewis Wetzel Wildlife Management Area in northwest WV, with the 68 ridgetop sampling point locations and the six line transects overlaid on a QuickBird satellite 0.6-m resolution panchromatic image (left) and on a 3-m resolution (± 3 m vertical accuracy) digital elevation model (DEM; right). The QuickBird satellite image was acquired August 2009 at 11:18 AM local time (solar azimuth = 127°). The 1/9 arc-second DEM was obtained as a seamless product from <http://viewer.nationalmap.gov/>.

CHAPTER 2: Fine-scale modeling of habitat and avian biodiversity in an Appalachian deciduous forest using a QuickBird satellite image.

Abstract. High resolution satellite imagery shows promise for assessing biodiversity at a fine spatial scale. To test this, we used the panchromatic band (PAN; 0.6-m resolution) and the normalized difference vegetation index band combination (NDVI; 2.4-m resolution) from a leaf-on QuickBird satellite image to model habitat and avian community data from circular field plots ($n = 68$) on ridgetops in a mature deciduous forest in WV, USA. We extracted the pixel value mean and standard deviation (s.d.) from the PAN and NDVI images, and from first- and second-order PAN and NDVI image textures, using (1) a plot radius of 50 m to analyze 50-m radius-scale habitat and avian species richness and occurrence; and (2) a plot radius of 100 m to analyze 100-m radius-scale avian species richness and abundance. Several image textures and the PAN mean had the strongest vector fits to a principal components analysis-derived gradient in forest structure and composition among the field plots (PC1; 39.3% variance explained), which ranged from less complex, chestnut oak (*Quercus montana*)-dominated forest to more complex, sugar maple (*Acer saccharum*)-dominated forest. We used generalized additive models (GAMs) to then test if PC1, the satellite image variables, and additional topographic variables were predictors of the avian data. We evaluated model fit using the adjusted deviance explained (D^2_a). Among the significant ($p < 0.05$) models, the PAN s.d. and NDVI s.d. usually provided the best fit. These likely proxies of environmental heterogeneity were positively related to total species richness, and the richness subset of relatively common (but not relatively rare) species, at the 50- and 100-m scales (range of $D^2_a = 0.14$ – 0.23). However, the strongest fits at both scales (range of $D^2_a = 0.45$ – 0.48) were for a positive relation between the PAN s.d. (also the best predictor of

PC1) and the richness subset of six forest canopy gap-dependent species. The occurrence and abundance GAMs for the 26 species tested also supported the PAN s.d. as the best overall predictor, likely most-indicative of habitat for the gap-dependent species. The lone species with an opposing trend in occurrence and abundance, the Eastern Wood-Pee-wee (*Contopus virens*), was positively related to the s.d. of a second-order PAN image texture likely indicative of chestnut oak composition. Our results supported the potential for remote sensing of forest habitat and avian biodiversity at a fine spatial scale, given careful consideration of the scale of field data collection and image data extraction, and the components of biodiversity being modeled.

Keywords: Remote sensing, image texture, avian biodiversity, environmental heterogeneity

1. Introduction

Concern over the continuing loss of the earth's biodiversity (e.g., Rands et al. 2010, Dirzo et al. 2014) has spurred the use of advanced technology that allows biodiversity to be assessed remotely (Turner et al. 2003, Gillespie et al. 2008). For example, imagery from airborne and spaceborne remote sensors can be used to detect biodiversity hotspots and examine biodiversity changes over space and time (Rochini et al. 2015). Advantages of a remote sensing approach to biodiversity assessment include data collection for remote or otherwise inaccessible locations (Buchanon et al. 2008), and at broad spatial scales and temporal frequencies not possible in the field (Duro et al. 2007). However, the value of remotely-sensed data for biodiversity assessment depends on its information content, and this should be judged in comparison to what can be obtained by intensive field surveys (e.g., Rhodes et al. 2015). It is important to continue to collect field data on the locations of plants and animals so that researchers can continue to test or validate remote sensing-based biodiversity models (Gillespie et al. 2008).

Remote sensing of biodiversity often relies on the link between environmental heterogeneity and species richness (the most common metric for characterizing biodiversity; von Wehrden et al. 2016). While potentially dependent on spatial scale and the taxonomic group considered, areas with higher environmental heterogeneity (e.g., habitats that are structurally more complex) often support a higher number of species (Tews et al. 2004). Remotely-sensed measures of environmental heterogeneity have been linked to species richness at multiple spatial scales. A common approach applied at coarse (i.e., landscape) scales is to model species richness using spatial heterogeneity metrics obtained from a remote sensing-based map of habitat patches (e.g., Luoto 2004, Schindler et al. 2013). Spectral heterogeneity obtained directly from remote sensing imagery is used to model species richness both within and among habitats (Rocchinni et al.

2010). Modeling species richness using increasingly fine-scaled measures of environmental heterogeneity has become possible through the use of remote sensing data of high spectral and spatial resolution (e.g., from hyperspectral sensors; Jones et al. 2013). These data may also be used along with coarse scale environmental data to improve models of species richness over large areas (Camathias 2013), and supplement or replace use of active remote sensing data such as lidar for biodiversity modeling (Wallis et al. 2016).

Birds have often been the focus of remote sensing biodiversity assessment, due in part to their conspicuousness and potential usefulness as bioindicators (Gottschalk 2005). Among the remotely-sensed proxies of environmental heterogeneity, fine-scale image texture has shown promise for modeling avian species richness and other indices of avian biodiversity. Image texture is defined as the spatial variation in the tonal values of the pixels in an image (Harralick et al. 1973), and depends in part on image spectral characteristics and grain (i.e., pixel) size. Here, we consider fine-scale image texture as that obtained from high spatial resolution imagery (commonly ≤ 4 m pixels for multispectral images and ≤ 1 m pixels for panchromatic images). Image texture from 1-m resolution panchromatic aerial imagery predicted avian species richness among semi-arid habitats in New Mexico (St-Louis et al. 2006) and among grassland, savannah, and woodland habitats in Wisconsin (Wood et al. 2013). Similarly, image texture from 2.4-m resolution multispectral QuickBird satellite imagery predicted avian (Shannon) diversity and an index of community composition in a tropical mountain ecosystem comprised of multiple forest types in southeastern Ecuador (Wallis et al. 2016).

Determination of a positive correlation between species richness and some measure of image texture (e.g., an increase in the variance of pixel values) likely requires that (1) the number of species and the amount of environmental heterogeneity are in fact positively correlated; (2) the

spectral heterogeneity of the image pixels adequately reflects this environmental heterogeneity; and (3) image texture sufficiently measures this spectral heterogeneity to model the richness data. While this predictive potential alone may be of value for biodiversity assessment, species richness provides no information about species composition. As individual species' occurrences are the fundamental units of species richness, the occurrences of species with negative trends, or without trends, may be included in an overall positive image texture - species richness correlation. To better understand how biodiversity is being modeled by image texture, analyzing trends in individual species along with species richness is desirable, as is understanding the functional types of species involved. Other than several indicator species also tested by Wood et al. (2013), however, such combined approaches appear to be lacking. St-Louis et al. (2006) suggested that because image texture was related to the spatial heterogeneity of vegetation across the habitat cover types they studied, bird species associated with heterogeneous habitats were responsible for the observed image texture-species richness relations, but they did not provide species-specific results. Wallis et al. (2016) were unable to identify any morphological or life history trait patterns among the bird species in their (multivariate analysis-derived) community composition index in relation to image texture.

To the best of our knowledge, there also have been no studies of the potential for image texture to predict trends in avian biodiversity metrics such as species richness within a single, relatively homogeneous habitat cover type. This capacity would be interesting to find, as studies such as those noted above have considerable variation in habitat cover types promoting a large range of species diversity values. Fine-scale image texture has been used to model individual bird species within a single habitat cover type. For example, in the Wood et al. (2013) study, image texture also predicted Grasshopper Sparrow (*Ammodramus savannarum*) density within

the grassland habitat, and 4-m Ikonos satellite image texture predicted Hooded Warbler (*Setophaga citrina*) nesting habitat within a forest in southern Ontario (Pasher et al. 2007). These single-species results suggest that fine-scale image texture can model within-habitat trends in species richness, assuming environmental heterogeneity in the habitat is positively correlated with enough individual species' occurrences for a trend to exist. Information on what environmental heterogeneity is actually being measured by image texture also appears to be lacking. Understanding how specific image texture measures, of which there are many, relate to habitat characteristics that are important to particular species may guide the broader application of these measures for predicting the occurrence of these species or in modeling their habitat elsewhere.

In this study, we obtained image texture measures from a QuickBird satellite image (0.6-m panchromatic and 2.4-m multispectral band resolution) of an Appalachian mature deciduous forest (~5,500 ha) and used them to model, at the level of individual field plots ($n = 68$) located on the ridgetops, forest composition and structure data along with breeding season avian survey data. We evaluated the general prediction that total avian species richness was positively correlated with image texture measures of environmental heterogeneity within this forest, and examined how trends in individual species occurrences compared to the total species richness trend. In particular, we expected that certain disturbance-dependent mature forest bird species (Hunter et al. 2001) would be modeled individually (and as a species richness subset) by image texture, if texture measures sufficiently indicated structural complexity in the form of gaps in the forest canopy with well-developed understories. In addition, because common species have often been found to largely determine total species richness patterns (e.g., Pearman and Weber 2007,

Sizling et al. 2009), we evaluated the richness of relatively common and relatively rare species (as we defined them; see section 2.4.3.) as subsets of total species richness.

We investigated two spatial scales of data collection (50 and 100 m radii) for the plots to examine issues of scalability in both the avian data and the image texture measures. Because image texture measures are seldom the only geospatial (i.e., remotely-sensed) data included when modeling avian or habitat data (e.g., see St-Louis et al. 2006; Torontow and King 2011), we incorporated topographic and image spectral brightness variables in the models. These variables served as covariates potentially resulting in better fitting models (as in St-Louis et al. 2006), and also allowed us to examine potential confounding of image texture effects with topography or image brightness effects. At the 50-m scale, at which the habitat data were collected, we examined the strength of the correlation between habitat characteristics and the geospatial data, and also compared the relative strength of the field-collected habitat data to the geospatial data for modeling the bird data. At the 100-m scale, we further examined the potential for the geospatial data to additionally model individual bird species abundances. Finally, in the discussion we add to the suggestions of others (e.g., Wood et al. 2012) on selecting among the many possible image texture measures, and choosing suitable analysis parameters for creating them. Through such efforts in multiple habitats, important contrasts or commonalities among image texture measures may become evident, and guide the selection and creation of appropriate image texture measures for future avian biodiversity assessment efforts.

2. Materials and methods

2.1. Study site

This study was conducted in mature deciduous forest on ridgetops at the Lewis Wetzel Wildlife Management Area, in northwestern WV, USA (Figure 1). The site is in the Permian Hills region of the Western Allegheny Plateau, and typifies the high topographic relief and extensive forest cover described for the Permian Hills (Woods et al. 1999). Elevation was 221–480 m (\bar{x} = 356 m) above sea level. We used the Topographic Position Index function in Topography Tools for ArcGIS 10.1 (Dilts 2015) to perform a landform classification of a 3-m resolution (± 3 m vertical accuracy) digital elevation model (DEM; source: <http://viewer.nationalmap.gov/>) of the site. We selected a circular neighborhood of 175 m and a 4-landform classification (based on Jenness 2006) for the function, to generally define the ridgetops and associated steep side-slopes that were the focus of our study (Figure 1). We found our ad-hoc classification useful for characterizing the complex terrain; for example, the ridgetops that were broader and flatter and those that were more sharply defined (i.e., in closer proximity to steep side-slopes). We note, however, that our analyses are based on data obtained within a maximum distance of 100 m from locations established on the ridgeline (i.e., the peak of the ridgetop) as obtained by hydrological modeling of the DEM. We did this for logistical reasons because of the difficult terrain and the extent of the site that we wished to cover. We thus do not make specific inferences from our results regarding the ridgetops and side-slopes as defined by the classification, as this would require much more intensive field sampling to sufficiently cover these two landforms.

Major tree species on the ridgetops included chestnut oak (*Quercus montana*), sugar maple (*Acer saccharum*), northern red oak (*Q. rubra*), red maple (*A. rubrum*), hickories (*Carya* spp.),

black oak (*Q. velutina*), white oak (*Q. alba*), and black locust (*Robinia pseudoacacia*) (Chapter 3, Appendix A). The ridgetop forest at the site has been previously described as occurring in two general types: mesic and dominated by sugar maple, and xeric and dominated by chestnut oak (Perkins and Wood 2014). Canopy gaps located on topographic aspects with high solar exposure often contained dense grapevine (*Vitis* spp.) that appeared to inhibit forest succession, and occasionally the invasive tree-of-heaven (*Ailanthus altissima*). The understory of the xeric, chestnut oak ridgetops was often dominated by shrub-like greenbrier (*Smilax* spp.).

2.2. Field sampling

We conducted breeding season fixed-radius point count surveys of the avian community at a total of 68 points (42 in 2009–11; an additional 26 in 2011) that were located within mature forest lacking recent anthropogenic disturbances (Figure 1). The 42 initial 2009–11 points were obtained from 87 points systematically placed ≥ 250 m apart along the ridgetops for surveys analyzed by Farwell et al. (2016), by retaining the points that were located > 150 m from anthropogenic canopy disturbances (e.g., forest roads, pipelines, and timber harvests) as indicated by aerial photos and site visits. The 250-m minimum distance between points was to reduce the potential that the same individual bird could be counted at more than one point. To increase the point sample size to 68 in 2011 (the primary focus of our analyses) we similarly placed an additional 26 points. Distances between the 68 points were 298–1021 m ($\bar{x} = 446$ m, SE = 17 m), and the points were located on the ridgeline using a Garmin© 60CSX Geographic Positioning System (GPS) unit (WAAS-enabled ± 5 –10 m positional accuracy).

The points were visited twice during the peak of the breeding season (~May 15–June 30) to conduct the surveys, which followed standard avian point count survey protocols (e.g., Ralph et al. 1995). To survey during peak bird activity, the surveys were completed between local sunrise

and 4-hrs after sunrise, under optimal weather conditions (calm winds, no precipitation or heavy fog). For each bird detected during the 10 minute length of a survey, the species, detection type (singing, calling, or visual), sex (if possible), and distance category (0–50 m or >50–100 m from the point) were recorded. We used the distance categories to group the detections at two spatial sampling scales for the analyses: the 0–50 m distance category (50-m radius scale) and the combined 50 m and >50–100 m distance categories (100-m radius scale). Different starting locations were used within a season to vary the time of morning that a point was sampled over the two visits within a season. Surveys were conducted by observers trained in bird identification by sight and sound, and in distance estimation. Observers ($n = 5–7$) in each season were rotated among the points over the two visits as much as was logistically possible.

We collected data on forest structure and composition at the points during July–August in 2010 and 2011, using a 5-subplot arrangement designed to encompass the topographic variability (e.g., multiple aspects) of the often sharply-defined ridgetops. The subplot arrangement and vegetation measurements were adapted from standardized methods for collecting forest habitat data for bird studies (Martin et al. 1997). A central subplot was located on the point, and four surrounding subplots were located 35 m from the point using an initial random bearing and 90° intervals. Within an 11.3-m subplot radius, the species and dbh (diameter at breast height at 1.4 m) to the nearest cm for each tree ≥ 8 cm dbh, the number of snags (≥ 8 cm dbh and ≥ 8 m in height), and the number of grapevines that ascended trees were recorded. Within a 5-m subplot radius, the number of saplings (< 8 cm dbh and ≥ 1.4 m in height) by species, and visual estimates of the percent cover (to the nearest 5%) of saplings, low woody plants (including shrubs, tree seedlings, and shrub-like greenbrier), and herbaceous plants were recorded. A spherical densiometer was used to estimate the canopy closure in the four cardinal directions at the subplot

center, and a clinometer was used to measure the height of a tree visually selected to represent the dominant canopy height of the 11.3-m subplot.

2.3. Remote sensing data

A 6° off-nadir, cloud-free QuickBird 2 (DigitalGlobe®) satellite image (Standard OrthoReady product; 0.6-m panchromatic and 2.4-m multispectral band resolution) was acquired 25 August 2009 at 16:18 GMT (solar azimuth = 127°) for the study area. The image was orthorectified in Erdas Imagine 9.3 using the 3-m DEM, the rational polynomial coefficients supplied with the image, and six ground control points obtained from 1-m resolution leaf-on orthophotos (2007 National Agriculture Imagery Program) matched to the panchromatic image. The root mean squared error of the rectified image was 3.3 m (*X* direction) and 2.6 m (*Y* direction). No major disturbances (e.g., severe windstorms) occurred between the date the image was acquired and the field sampling, and based on the 2009–11 field sampling new tree falls were infrequent, so for this study we assumed the image and the field data were a sufficient temporal match.

We selected the panchromatic (PAN) band and also the normalized difference vegetation index (NDVI) band combination of the near-infrared (NIR) and the Red bands ($NDVI = \frac{NIR - Red}{NIR + Red}$) images for this study. We selected the higher resolution PAN image as a potentially better indicator of fine textural detail (e.g., pixel variation within tree crowns) in the forest image. The NDVI is commonly used to remotely assess vegetation productivity and structural characteristics such as biomass (Pettorelli et al. 2011), and we selected it as a potentially better indicator of more coarse-scale forest structural variability via the lower resolution NDVI pixels. Because the NDVI was developed to minimize the effects of different sun illumination angles on remote sensing indices of vegetation (Rouse et al., 1973), we

suspected it could help compensate for brightness variation in the satellite image caused by the complex topography. Prior to the NDVI calculation, we used the absolute radiometric calibration factors and effective bandwidths supplied with the image to convert the Red and NIR bands to top-of-atmosphere reflectance. Although this did not correct for atmospheric effects, we had difficulty correcting haze with the method we tested (improved dark object subtraction; Chavez Jr. 1989), perhaps because of the complex topography and dense forest cover throughout the scene. While not ideal, we used the NDVI as calculated because it provided some image texture measures that were less correlated with those obtained from the panchromatic band, and thus potentially contained different information.

2.3.1. Satellite image variables

The satellite image processing and image variable extraction steps are diagrammed in Figure 2. We used the zonal statistics function in ArcGIS 10.1 to extract the image variables for each sampling point using radii of 50 and 100 m (i.e., at the plot level) to match (respectively) the sampling radii of the bird data (50 m and 100 m), and for the 50-m radius image variables to match the radius of the forest data (subsampled within ~50 m). In extraction step 1 (middle of Figure 2), we obtained the plot-level mean and standard deviation (s.d.) of the PAN and NDVI pixel values directly. To potentially capture variability in pixel values at multiple spatial scales (e.g., within and between scene objects; Pasher and King 2010), in extraction step 2 (the sides of Figure 2) we obtained these plot-level pixel summaries from images of first- and second-order statistics (the two primary classes of texture; Mihran and Jain 1998). The texture images were processed from the PAN and NDVI images using the moving window analysis procedure in GRASS GIS 6.4.3 (GRASS Development Team, 2013). In this procedure, a square, odd-numbered neighborhood of pixels (e.g., 3×3 pixels) is iteratively centered on each pixel of an

image, and a neighborhood statistic (e.g., mean value of the 3×3 pixels) is calculated for the pixel. A new image is then created that is comprised of the neighborhood statistic values. We used a range in size for the pixel neighborhoods from the smallest possible (3×3 pixels) to a neighborhood size representing $\sim 25 \times 25$ m ground distance (PAN = 41×41 pixels, NDVI = 11×11 pixels; Table 1). Preliminary tests of larger neighborhoods indicated that image statistic values leveled off or peaked within the 25×25 m range, suggesting larger neighborhoods would not provide additional textural information for this forest scene. To reduce the number of moving window analyses, we increased the neighborhoods for the PAN image in ~ 5 m ground distance increments following the initial 3×3 pixel neighborhoods.

First-order texture statistics are based on the histogram of pixel values in a pixel neighborhood, such as their mean, s.d., and range (Mihran and Jain 1998). For our study, we selected the first-order mean and s.d., following St-Louis et al. (2006) who found that these textures best predicted bird species richness out of the first-order statistics they evaluated. Because of the two spatial scales of our image data extraction and the number of pixel neighborhoods used for the moving window analysis (6 PAN and 5 NDVI), we thus obtained $n = 88$ plot-level measures of these first-order statistics per sampling point (2 plot-level pixel summaries $\times 2$ scales $\times 2$ texture statistics $\times 11$ moving window analyses). We considered the plot-level PAN and NDVI pixel s.d. measures from extraction step 1 with these moving window analysis-based measures as a general class of first-order statistics. However, while technically also first-order statistics, for the purposes of this study we considered the PAN and NDVI pixel means from extraction step 1 as spectral measures, potentially providing different forest information than textural measures based on the variance of pixel values. We discarded the $n = 22$ plot-level pixel means obtained from the first-order mean PAN and NDVI images, as these

were almost perfectly correlated ($r > 0.98$) with their respective PAN and NDVI spectral measures.

Second-order texture statistics are based on the spatial relations of pairs of pixel values in a pixel neighborhood (Mihran and Jain 1998) and are calculated using the gray-level co-occurrence matrix (GLCM; Hall-Bayer 2007). Additional parameters required by the GLCM are the offset, which is the distance between the pairs of pixels that are compared within the neighborhood, and the direction (0° , 45° , 90° , and 135°) of the offset. We selected an offset of one pixel because statistic values for larger offset distances within a particular neighborhood size became highly correlated with statistic values from other neighborhood sizes. Because image texture appeared to be isotropic (i.e., non-directional), we used an averaged statistic over the four offset directions. While the number of gray scale values (i.e., the image spectral resolution) is also an important GLCM consideration (Patel et al. 2008), we used the spectral resolution of the QuickBird imagery as acquired (8 bit = 256 gray scale values). Of the 14 second-order statistics defined by Haralick et al. (1973), we initially selected six that are commonly used in remote sensing image analysis: angular second moment, contrast, correlation, entropy, homogeneity, and variance (Kayitakire et al. 2006). Due to high plot-level correlation among these statistics, however, we retained only the contrast (CON) and correlation (COR). The COR statistic is computationally different and therefore often less correlated with other second-order statistics (Hall-Bayer 2007). As above for the first-order statistics, we obtained $n = 88$ plot-level measures of these second-order texture statistics per sampling point (of which none were discarded).

The image variables used in this study are summarized in Table 2. To consistently label them in the text, tables, and figures, the image source ('PAN' or 'NDVI') is provided, followed by a subscript identifying the variable as a plot-level pixel mean or s.d. ('AVG' or 'SD');

respectively). If the measure was extracted from a moving window analysis texture image, a subscript is added after an underscore to identify the specific neighborhood statistic (first-order mean ['AVG'] or s.d. ['SD']; second-order 'CON' or 'COR') and the pixel neighborhood size. As examples, PAN_{SD} denotes the plot-level pixel s.d. obtained from the original PAN image, and PAN_{AVG_SD09} denotes the plot-level pixel mean obtained from the PAN first-order s.d. texture image calculated with a 9x9 pixel neighborhood. The 50- or 100-m radius plot-level scale of the measure is referenced as needed.

2.3.2. Topographic variables

We obtained three topographic variables from the DEM at the two plot-level scales using ArcGIS 10.1 geoprocessing tools: mean elevation (ELEV), an index of topographic variation (TVI) calculated as the surface area divided by the planar area, and an index of direct solar radiation (DSR) at the time of image acquisition (see Table 2 for details on the tools and parameter settings used to obtain these variables). The tools were applied using the native 3-m DEM resolution, as resampling to coarser resolutions (tested up to 9 m) to minimize noise in the elevation values had little effect on the variables as summarized at the 50 and 100 m scales. We selected these topographic variables as likely to be related to the bird and the forest habitat data collected at the sampling points. For example, variation in ridgetop elevation (sampling point range: 354–456 m) could relate to local variation in exposure to wind. Ridgetops that are flatter (low TVI values) likely retain more soil moisture than those that are more sharply defined (high TVI values). DSR may relate to productivity effects on forest structure (Pasher and King 2010). Furthermore, as obtained at the time of image acquisition, DSR may reflect sun illumination angle differences among the sampling points (e.g., sampling points on predominantly east-west ridges could encompass relatively darker north-facing slopes) and be an important control

variable when included with variables such as the satellite image spectral measures in the analyses. We rejected other potential topographic variables because the sampling point scales encompassed multiple aspects and slopes (e.g., the mean aspect was not informative) or because they were correlated with the selected variables (e.g., the s.d. of elevation with TVI).

2.4. Statistical analyses

2.4.1. Principal component analysis (PCA) of the forest data

We calculated forest composition and structure variables for each sampling point as the mean of the data collected at the five subplots. We selected for analysis 11 forest structure variables and three forest composition variables (basal area of chestnut oak and sugar maple, and tree species richness). Chestnut oak and sugar maple accounted for 51.8% of the total basal area (29.5 and 22.3%; respectively), and as the primary canopy dominants we expected the structural characteristics of these species to potentially have the greatest influence on image texture. These two tree species were distributed differently within as well as among the studied ridgetops (likely due to different shade and soil moisture tolerances) and have structural differences (e.g., in leaf shape, thickness, and arrangement; and in branching pattern) that potentially influence their reflectance, and subsequently their textural pattern. We initially tested the inclusion of additional tree species in the analysis (e.g., northern red oak; 10.5% of the total basal area), and tree species diversity measures, but these inclusions had no appreciable effects on the results.

We used principal components analysis (PCA), a multivariate analysis technique that has been used previously to detect gradients in forest composition and structure (e.g., Torontow and King 2011). We conducted the PCA using the *rda* function in the *vegan* R package (Oksanen et al. 2012). Prior to the analysis, we checked the 14 variables to ensure linearity and normality (required by PCA; Franklin et al. 1995), and transformed them if necessary. Spearman's pairwise

correlations for all 14 variables were $r < 0.80$. Because the forest variables were measured in different units, we ran the PCA with the variables scaled to equalize the amount of variance they could contribute to the total variance explained by the entire set of variables (*rda* function scale parameter = TRUE). We retained the orthogonal (i.e., mutually uncorrelated) linear combinations of variables, referred to as axes or principal components, that were produced by the PCA if their eigenvalues (proportion of total variance explained) were > 1.0 (Kaiser 1960). We graphically examined the retained principal components with ordination diagrams and used the component scores as candidate field-based explanatory variables for the avian models.

2.4.2. *Fitting of geospatial variables to the PCA*

As in Torontow and King (2011), we examined if the geospatial variables were related to gradients in forest composition and structure as characterized by the retained principal components from the PCA. The geospatial variables were fit as smooth surfaces and as vectors to the ordinations using the *ordisurf* and *envfit* functions in the *vegan* R package. Subsequently, the geospatial variables that provided the strongest explanatory potential as indicated by their level of fit (evaluated using R^2) were retained as candidate explanatory variables, in addition to the retained principal components, for the avian modeling. Evaluating both the surface and the vector fits allowed us to determine when the nature of the relation of a geospatial variable to an ordination gradient was linear (surface $R^2 =$ vector R^2) or non-linear (surface $R^2 >$ vector R^2). To assess how well the remote sensing data could predict the ordination results (e.g., for use in forest complexity mapping; see Torontow and King 2011), we tested if multiple geospatial variables could more powerfully predict principle component scores, as well as dominant forest characteristics apparent from the ordinations, using multiple variable linear regression. To obtain the best fitting models, we used a forward selection procedure (Blanchet et al. 2008) that uses

two stopping rules (the significance of the added variable and the adjusted R^2 of the global model) to avoid overestimating the amount of explained variance. We used leave-one-out cross validation in the boot R package (Canty and Ripley 2015) to evaluate the predictive ability of the models.

Because the forest variables were sampled within a 50 m radius of the sampling points, we fit only the 50-m radius plot-level geospatial variables to the ordinations. To reduce the number of variables to fit, we examined Spearman's correlations to obtain a set of plot-level variables with pairwise $r < 0.80$. We selected this correlation threshold to balance variable reduction with the retention of variables that, despite being correlated, might contain different information to explain variation in the forest data. We first applied this threshold within each of the four categories of geospatial variables (Table 2). Of the two spectral variables, we selected PAN_{AVG} over $NDVI_{AVG}$ ($r = 0.90$). Within the other categories we selected 35 first-order texture, 44 second-order texture, and 3 topographic variables. We then compared across the categories to further reduce the remaining variables to below the threshold, ultimately yielding 20 variables (Appendix B). In this second variable reduction step, we selected simpler statistics over more complicated ones. Thus, we retained PAN_{SD} and $NDVI_{SD}$ over first-order texture measures obtained from the moving window analyses, and finally considered the second-order texture measures. We retained all three topographic variables, as these were relatively uncorrelated with the other geospatial variables.

2.4.3. Avian modeling

We calculated avian species richness and species-specific occurrence and abundance for each sampling point in each year based on the two visits, and at the 50-m and 100-m radius scales. We based occurrence and abundance on species-specific detection types (e.g., singing males for

small territorial songbirds; see Appendix A). We defined occurrence of a species as 1 (present) or 0 (absent) over the two annual visits, and abundance of a species as the maximum number of individuals detected over the two annual visits. We calculated a simple index of total species richness as the sum of all individual species' occurrences. We selected this richness index over other potential indices for ease of comparison between the total species richness results and the results for individual species occurrences and different subsets of total species richness. To ensure that this index was a relatively stable estimate of species richness at a point, we also assessed the use of mean species richness over the two visits, and species richness per visit, and obtained similar results.

In addition to total species richness, we calculated the richness of three subsets of species: relatively common species, relatively rare species, and the six species most closely associated with the understory of distinct canopy gaps in this forest (Appendix A). We ranked the species by their total number of occurrences using the 2011 100-m data, and selected the species above and including the midpoint of the ranking as relatively common, and below the midpoint of the ranking as relatively rare. We based canopy gap association on the literature (e.g., The Birds of North America Online: <http://bna.birds.cornell.edu/bna/>) and extensive knowledge of the species in the study area. We considered the six species to be those most often detected within canopy gaps, to differentiate them from other species that may associate with canopy gaps (e.g., Cerulean Warbler; Perkins and Wood 2014), but are also often detected away from them.

Due to sample size considerations, we relied primarily on the 2011 data ($n = 68$) for the bulk of the avian modeling. We used generalized additive models (GAMs), which are a semi-parametric alternative to generalized linear models (GLMs; McCullagh and Nelder 1989), to examine if, singly, the 50- and 100-m scale geospatial variables and 50-m scale principal

components representing forest gradients were related to the bird species richness measures as calculated at these respective scales in 2011. GAMs fit scatterplot smoother functions (e.g., regression splines) to response data and thus allow assessment of non-linear effects of model covariates (Hastie and Tibshirani 1990). We ran the GAMs with the *mgcv* R package (Wood 2011) and used thin plate regression splines with smoothness selection (i.e., degree of smoothness) via restricted maximum likelihood (REML) estimation. Because the species richness data were counts, we used the Poisson (log link) error structure. We evaluated the significance of the smoother functions using $\alpha = 0.05$. Nonlinear responses are indicated if the effective degrees of freedom (e.d.f.) of the smoother function is >1 . We graphically examined the smoother functions to assess the nature of the linear or nonlinear relations between the explanatory variables and the richness measures, and evaluated model fit using the adjusted proportion of deviance explained (D^2_a ; Guisan and Zimmermann 2000).

To determine if models could contain multiple variables as predictors of the bird species richness measures in 2011 at the 50-m scale, we used a GAM-based variable selection technique (Marra and Wood 2011). This technique uses shrinkage methods to essentially drop unimportant predictor variables from a model by shrinking their effects to zero (evaluated as e.d.f. ≈ 0 for the term), with the goal of achieving a parsimonious subset of variables that improve model interpretability and prediction accuracy. We used the double shrinkage approach (Marra and Wood 2011) option in the *mgcv* package. As with the single variable GAMs, we used thin plate regression splines and REML smoothness selection, and the Poisson (log link) error structure; however, because the variables were often in different units, we used scale-invariant tensor product smooths (Wood 2011). To reduce the potential for adverse effects of collinearity on variable selection (Mansfield and Helms 1982), we included variables in the models on the basis

of limiting their concurvity, a measure available in the *mgcv* package for GAMs that is a generalization of the collinearity measures for variables in linear models (Wood 2011). As with the single variable GAMs, we graphically examined the smoother functions and evaluated the D^2_a model fit.

To examine the effects of spatially scaling up the data for the multiple variable models, we recomputed the best-fitting 50-m scale GAMs for 2011 species richness obtained from the variable selection procedure using 100-m radius scale data. To examine the stability of richness results over the three years, we modeled species richness with single variable GAMs at both the 50-m and 100-m radius scale in each year. We used only single variable models for this analysis because multiple variable models tended to be overfit with the reduced number of sampling points ($n = 42$) available over the three years. To examine which species likely contributed most to the 50-m scale 2011 richness results, we modeled the occurrence (50-m radius scale) of species in 2011 with single variable binomial (logit link) GAMs. For this analysis, we selected 24 species with at least seven presences or absences across the 68 sampling points, because this was the minimum number for detecting significant effects without over-fitting. We did not use multiple variable binomial GAMs because these models were too often overfit. We also examined the effect of spatially scaling up the data at the species level, by analyzing these species with Poisson GAMs using their 100-m radius scale abundances. We did not attempt to model 50-m radius scale abundances because at this scale the data consisted primarily of ones and zeros

3. Results

3.1. Forest variable PCA and geospatial variable fits

The PCA of the 14 forest variables resulted in three principal components with eigenvalues greater than 1.0, which together accounted for 67.1% of the total variance. Examination of the ordination diagrams (e.g., Figure 3a) and the factor loadings for the forest variables (Table 3) indicated that the first PCA axis (PC1; 39.3% of the variance) reflected a gradient in forest composition and structure among the field plots. Compositionally, this gradient ranged from plots with higher chestnut oak basal area (negative on PC1) to plots with higher sugar maple basal area (positive on PC1). Structural variables most negative on PC1 along with chestnut oak included DBH s.d. and total basal area. Structural variables most positive on PC1 along with sugar maple included herbaceous cover and grapevine density. Other structural variables with lower factor loadings such as snag density and canopy cover were also clearly separated (positively and negatively; respectively) along PC1. Inspection of the plot images ordered by their site scores for PC1 (e.g., Figure 4; Appendix C) furthermore indicated a canopy closure gradient, with the plots most negative on PC1 appearing as a mostly closed forest canopy and the plots most positive on PC1 appearing as a more open forest canopy.

The second PCA axis (PC2; 16.3% of the variance) appeared to primarily reflect a negative relation between tree density/tree species richness and the DBH mean. Along this axis, the plots negative on PC2 had a lower density and less species of trees that were larger in diameter, and the plots positive on PC2 had a higher density and more species of trees that were smaller in diameter. The third PCA axis (PC3; 11.2% of the variance) was more difficult to interpret, and at least in part appeared to be influenced by several plots with low canopy cover yet high shrub cover. In contrast, for PC1 canopy cover and shrub cover were positively associated, likely due

to the increased cover of shrub-like greenbrier, *Vaccinium*, and tree seedlings (all classed as shrub cover) that we observed under the more closed chestnut oak-dominated forest canopy. For PC1, low canopy cover was instead associated with high herbaceous cover and grapevine density. With no clear interpretation of a habitat gradient among the plots for PC3, we did not consider this axis further, and only fit geospatial variables to the PC1:PC2 ordination.

Of the 13 image geospatial variables with significant vector fits to the ordination (Table 4), we focused on four (PAN_{AVG} , PAN_{SD} , $NDVI_{SD}$, and PAN_{SD_COR09}) because of their relative strength and differences in how they were oriented to the ordination axes (Figure 3b). The remaining significant image variables were similarly oriented (e.g., PAN_{SD_COR41} with PAN_{SD_COR09}) but with weaker fits, and so provided no additional interpretation. The fits of PAN_{AVG} , PAN_{SD} , and $NDVI_{SD}$ were all positively correlated with PC1, thus oriented toward higher complexity sugar maple plots. The strongest vector fit was obtained for PAN_{SD} ($R^2 = 0.63$). Despite PAN_{SD} and $NDVI_{SD}$ being close to the correlation threshold ($r = 0.74$), the fit of $NDVI_{SD}$ ($R^2 = 0.29$) was oriented more toward PC2, in the direction of plots with lower tree density but larger diameter trees. While PAN_{AVG} and PAN_{SD} were also relatively correlated ($r = 0.69$), the fit of PAN_{AVG} ($R^2 = 0.40$) was oriented slightly towards plots with higher grapevine density. The next strongest vector fit was obtained for PAN_{SD_COR09} ($R^2 = 0.52$), which was negatively correlated with PC1 and thus oriented toward lower complexity/chestnut oak plots.

Most of the surface fits for the image variables were equivalent or nearly so to their vector fits (Table 4; e.g., for $NDVI_{SD}$ the surface R^2 was +0.03), so we did not consider them further. While other surface fit increases were more substantial, none were particularly large. The largest increase was for PAN_{SD_SD41} (surface $R^2 = 0.25$), from a non-significant vector fit. As indicated by tighter contours (Figure 3c), this surface mostly indicated decreasing plot values for the

statistic toward the extremes of the PC1 gradient. The increase in surface fits for $\text{NDVI}_{\text{SD_SD11}}$ and $\text{NDVI}_{\text{SD_COR03}}$ ($R^2 = 0.24$ and 0.27 ; respectively) in part reflected their weaker vector fits (Figure 3d and e), but helped to identify that these vectors did not represent general gradients across the axes, and were somewhat biased as a result. For example, the surface fit for $\text{NDVI}_{\text{SD_SD11}}$ indicated that a vector fit would best apply to the plots negative on the PC2 axis, and be oriented more closely along the axis. Similarly, the surface fit for $\text{NDVI}_{\text{SD_COR03}}$ indicated that a vector fit would best apply to the plots positive on the PC1 axis, and be oriented more toward PC2.

Of the topographic variables fit to the ordination, ELEV and TVI were significant as vectors and surfaces (Table 4). While as surface fits ELEV and TVI increased, the fits remained low ($R^2 < 0.20$). As vectors, ELEV was positively related to PC2 and TVI was negatively related to PC1. The surface fits for ELEV and TVI supported these linear relations, but also indicated some inconsistency in how well these topographic variables reflected general gradients across the ordination axes (Figure 3f and g). In the case of ELEV, plots also increased in value toward the positive and negative extremes of PC1; while for TVI, plots also increased in value toward the positive and negative extremes of PC2. DSR was not significant as a vector or a surface, even though this measure of solar radiation at the time of image acquisition was correlated with PAN_{AVG} ($r = 0.62$). The PAN_{AVG} measure thus appeared to be primarily related to variation in the spectral brightness of vegetation in the image, rather than simply being a function of general solar illumination differences as calculated by DSR.

3.1.1. Selection of multiple variable linear regression models

Because PC2 explained relatively little of the field data, and was not well-modeled by the geospatial variables, we performed the forward selection using only PC1 and its associated forest

variables. Multiple geospatial variables more strongly modeled PC1 and five of the six forest variables that were most differentiated along this axis (Table 5). In all cases, PAN_{SD} was selected first and explained most of the variance as measured by cumulative R^2_a , with PAN_{SD_COR09} the next most frequently selected (for PC1 and four forest variables) to explain additional variance. The highest cumulative fits were obtained for PC1 ($R^2_a = 0.70$), followed by chestnut oak basal area ($R^2_a = 0.67$), sugar maple basal area ($R^2_a = 0.65$), herbaceous cover ($R^2_a = 0.64$), and grapevine density ($R^2_a = 0.54$). The most substantial addition to the cumulative fit was made by PAN_{SD_COR09} for chestnut oak basal area ($R^2_a + 0.13$). PAN_{AVG} and NDVI_{SD} were not included in any model. Of the topographic variables, ELEV provided a small increase in cumulative fit for sugar maple basal area and herbaceous cover ($R^2_a + 0.02$ for both), and TVI a more substantial increase for grapevine density ($R^2_a + 0.09$). The cross validation indicated that adding geospatial variables reduced prediction error, although this remained relatively high when calculated as a percentage of the range of the response variable. The best model for prediction was PAN_{SD} + PAN_{SD_COR09} for PC1, with a cross validated RMSE of 15.1% of the range of PC1 values.

3.1.2. Spatial trends in principal components and geospatial variables

A number of moderate to broad scale spatial gradients across the study area were evident for the PCA axis scores and geospatial explanatory variables. The PC1 plot scores (Fig 5a) exhibited a clear southwest to northeast increase from negative to positive, as well as some clustering of similar values. The PC2 plot scores (not shown) were spatially more mixed, but tended to be more highly negative in the north and more highly positive in the south. Not surprisingly, a pattern similar to PC1 was evident for the plot values for PAN_{SD} (Fig 5b), the geospatial variable most highly (and positively) correlated with PC1, and the other image variables (not shown) also had a general southwest to northeast directional pattern, albeit not as strong. Of the topographic

variables, ELEV (Fig 5c) generally increased from north to south, and TVI (Fig 5d) indicated that steeper plots tended to be located in the central portion of the study area. No clear spatial patterns were evident for DSR (not shown). This accounting of spatial trends, while qualitative and not exhaustive, indicated the presence of spatial structure in explanatory environmental variables, and we considered this in evaluating the results of the avian models.

3.2. Single and multiple variable 50-m scale avian species richness models

For the single variable avian models at the 50-m scale (Table 6), we focused on PC1, PC2, the image variables with the highest PC1-associated vector fits, and the topographic variables. While other image variables in the reduced set were also related to the richness measures, they produced results mostly similar to those obtained for the PC1-associated image variables. In several cases where different results were obtained, model fits for these image variables were low and difficult to interpret based on the PCA results. We considered these image variables later for inclusion in the multiple variable models. Total, gap, and common species richness were positively related to PC1 (i.e., avian richness increased with forest structural complexity/sugar maple basal area), with gap species richness providing the strongest fit ($D^2_a = 0.36$). No avian species richness measures were related to PC2. Total, gap, and common species richness were also positively related to PAN_{AVG} , PAN_{SD} , and $NDVI_{SD}$; furthermore, for total and common species richness the fits for PAN_{SD} ($D^2_a = 0.20$ and 0.23 ; respectively) and $NDVI_{SD}$ ($D^2_a = 0.21$) increased over those obtained for PC1 ($D^2_a = 0.10$ and 0.11 ; respectively). Only PAN_{SD} had a stronger fit than PC1 for gap species richness ($D^2_a = 0.45$), however. Gap species richness was also the only richness measure related (negatively) to PAN_{SD_COR09} . Rare species richness was not related to PC1 or any of the image variables. Of the three topographic variables, TVI and

DSR provided only weak fits ($D^2_a < 0.05$) to total and gap species richness (both negatively related to TVI) and to rare species richness (positively related to DSR).

We used PAN_{SD} , $NDVI_{SD}$, and PC1 as the initial basis for the GAM multiple variable selection (Table 7). We chose PAN_{SD} and $NDVI_{SD}$ because they were among the strongest of the image explanatory variables for the avian richness measures, and varied in how strongly they modeled gap species richness. We included PC1 so we could compare between models with geospatial variables added to PC1 (i.e., remote sensing data plus field data) and geospatial variable-only models for modeling the avian data. To test the inclusion of topographic effects, we added two of the three topographic variables (ELEV and TVI) to the models after preliminary testing indicated the unimportance (i.e., e.d.f. ≈ 0) of DSR as an effect for all the richness measures. Model concurvity measures remained uniformly low when ELEV and TVI were added to the models. Substantial increases in model concurvity prevented the inclusion of PAN_{AVG} and PAN_{SD_COR09} in the models, as well as all potential combinations of PC1, PAN_{SD} , and $NDVI_{SD}$ in the same model. We evaluated the addition of other, less-related image variables following the addition of the topographic variables.

The inclusion of topographic effects, even if insignificant as single explanatory variables (e.g., ELEV), often improved the fit of the models, albeit slightly over their respective single variable models (D^2_a increases < 0.10 ; Table 7 vs. Table 6). The inclusion of ELEV and TVI improved the fit of the PC1 models for all richness measures but gap species richness. The inclusion of ELEV and TVI improved the fit of the PAN_{SD} and $NDVI_{SD}$ models for total and common species richness, which remained higher than their respective PC1 model fits. The fit of the PAN_{SD} model for gap species richness remained the highest of all models, with a small increase in fit (to $D^2_a = 0.47$) because of the inclusion of TVI. The models for rare species

richness resulted in only minimal fits, although with ELEV and TVI included the NDVI_{SD} model fit increased, and NDVI_{SD} became significant.

We chose the best of the single image variable plus topographic effects models for each richness measure to test the inclusion of additional image variables (Table 8). No additional image variables were selected for the gap species richness PAN_{SD} model. For both the total and common species richness NDVI_{SD} models, a single image variable (PAN_{SD_COR03}) uncorrelated with NDVI_{SD} ($r = -0.25$) was selected and increased the fit (to $D^2_a = 0.42$ and 0.39 for total and common species richness; respectively). The other variables remained in the total and common species richness models largely unchanged, other than a small increase in evidence for an ELEV effect (see e.d.f. and P -values; Table 8 vs. Table 7). For the rare species richness NDVI_{SD} models, another image variable (NDVI_{SD_COR03}) somewhat more correlated with NDVI_{SD} ($r = 0.47$) was selected and provided an increase in fit (to $D^2_a = 0.16$). In this case, ELEV and TVI remained in the rare species richness model largely unchanged, but the evidence for the NDVI_{SD} effect was somewhat lessened.

We present the GAM curves from the best-fitting multiple variable models for total and gap species richness (Figure 6) to illustrate the various relations we found between the explanatory variables and the species richness measures. For total, common, and gap species richness, PC1 and the PAN_{SD}/NDVI_{SD} image variables tended to provide the dominant effect, as indicated by the relative steepness of the relation to species richness in comparison to the topographic effects, and any additional image variables. The ELEV effect was a slightly curved one, with higher species richness at middle elevations. The TVI effect was a slightly negative one, with species richness decreasing as the topography of the plots ranged from flatter to steeper. The increase in gap species richness showed some evidence of leveling off at high values for PC1, PAN_{SD}, and

NDVI_{SD}. In contrast, only linear relations with PC1, PAN_{SD}, and NDVI_{SD} were found with the larger counts for total and common species richness. The PAN_{SD_COR03} and NDVI_{SD_COR03} relations were more distinctly hump-shaped than ELEV.

3.2.1. Effect of 100-m scale on species richness results

We found fewer significant results for single image variable models at the 100-m scale than at the 50-m scale for both total and common species richness (Table 6). These richness measures remained positively related only to NDVI_{SD}, although the model fits were somewhat reduced from those at the 50-m scale (from $D^2_a = 0.21$ to $D^2_a = 0.14$ for both measures). The gap species richness models, however, remained significant for all four image variables at the 100-m scale and had comparable model fits. The PAN_{SD} model for gap species richness again had the highest fit at the 100-m scale, which increased slightly from that obtained at the 50-m scale (from $D^2_a = 0.45$ to $D^2_a = 0.48$). We found no significant results for single image variable models of rare species richness at the 100-m scale, and across the richness measures the few topographic models that were significant at the 50-m scale were no longer significant.

There were also some differences in how the image variables fit the 100-m richness measures that we assessed graphically. The relation of total species richness to NDVI_{SD} at 100 m (Figure 7a) showed an increase in species richness over that found at 50 m. Notably, the NDVI_{SD} values for most of the plots increased but not beyond the maximum NDVI_{SD} value at 50 m (i.e., the NDVI_{SD} gradient was shortened). While the 100-m scale total species richness relation to NDVI_{SD} was still positive, it became flatter at high NDVI_{SD}. The relation between gap species richness and PAN_{SD} at the 100-m scale (Figure 7b), as with total species richness, also showed a species richness increase (fewer points had no species and one point had the maximum six species) and a shortening of the PAN_{SD} gradient. The 100-m scale gap species richness relation

to PAN_{SD} was positive with a similar slope to that of the 50-m scale relation, but did not exhibit the slight flattening at high PAN_{SD}.

When the best multiple variable models for species richness were tested at the 100 m scale, the total species richness model retained three of the four model terms (NDVI_{SD} e.d.f. = 1.40 and $P = 0.018$; ELEV e.d.f. = 0.99 and $P = 0.077$; TVI e.d.f. = 0.70 and $P = 0.065$; PAN_{SD_COR03} e.d.f. ≈ 0) and model fit decreased somewhat from $D^2_a = 0.31$ to $D^2_a = 0.26$. Similar results were found for common species richness (PAN_{SD_COR03} e.d.f. ≈ 0), although TVI no longer had an effect. The rare species richness model remained similarly and weakly modeled ($D^2_a = 0.09$), with three of the four model terms retained (NDVI_{SD} e.d.f. = 1.45 and $P = 0.096$; ELEV e.d.f. = 0.51 and $P = 0.193$; TVI e.d.f. = 0.68 and $P = 0.075$; NDVI_{SD_COR03} e.d.f. ≈ 0). The best gap species richness model tested at the 100-m scale retained only PAN_{SD} (e.d.f. = 1.00 and $P < 0.001$) but the model fit remained similar ($D^2_a = 0.48$).

3.2.2. Effect of year on species richness results

Across the three breeding seasons with the reduced set of 42 sampling points, total and common species richness were only positively related to NDVI_{SD} in 2011 at the 50-m scale (Table 9). While the fits in 2009 (at both scales) and in 2011 at the 100 m scale were not significant, the general trends in relation to NDVI_{SD} were still positive (Figure 8a). In 2010, however, at both scales the trend for higher total and common species richness at high NDVI_{SD} was lost, with a large reduction in species richness particularly obvious for the point with the highest NDVI_{SD}. With this potential influential outlier removed and the data reanalyzed, the downward trend for species richness at high NDVI_{SD} remained. No significant results were found for rare species richness. In contrast to the variable nature of the total and common species richness results across years, gap species richness was significantly and similarly related to

PAN_{SD} in all years at both the 50- and 100-m scales (Table 9; Figure 8b). Also, within all years the gap species richness fit was highest at the 100-m scale, although marginally so in 2011. In comparison to 2009 and 2011, the 2010 gap species richness fits at both scales were somewhat lower, however. A slightly nonlinear fit for gap species richness was also only apparent in 2011 at the 50-m scale.

3.3. *Species occurrence and abundance models*

Of the 24 species analyzed for 2011 occurrence at the 50-m scale, five species (Eastern Towhee, Hooded Warbler, Kentucky Warbler, Northern Cardinal, and Ovenbird) were positively related to PC1, and one species (Eastern Wood-Pee-wee) was negatively related to PC1 (Table 10). Except for Ovenbird, the species positively related to PC1 were gap species. Occurrences of 11 species (the same PC1 species plus American Redstart, Black-and-white Warbler, Cerulean Warbler, Red-eyed Vireo, and Rose-breasted Grosbeak) were positively related to their respective best image textures (i.e., to increasing plot level pixel heterogeneity). Additionally, for the four gap species fit by PC1, their respective image texture model fits increased, and were among the highest overall for these models (D^2_a range: 0.18–0.28). While the image texture model fit for Eastern Wood-Pee-wee was also relatively high ($D^2_a = 0.19$), the PC1 model fit was higher ($D^2_a = 0.25$). The image texture models fits for Ovenbird and the five additional species were relatively low ($D^2_a < 0.10$).

At the 100-m scale, abundance was positively related to image texture for six species (Table 10). The highest abundance fits were obtained for the gap species Eastern Towhee, Hooded Warbler, and Northern Cardinal (D^2_a range: 0.20–0.25); and for Eastern Wood-Pee-wee ($D^2_a = 0.40$). Two additional species (the gap species Indigo Bunting and Kentucky Warbler) were detected only as lone individuals and thus analyzed with 100-m scale binomial models. Indigo

Bunting occurrence was positively related to image texture, and provided the highest fit of any binomial model at either scale ($D^2_a = 0.41$). Kentucky Warbler occurrence remained positively related to image texture, but model fit ($D^2_a = 0.11$) decreased from the 50-m scale model ($D^2_a = 0.28$). The modeled abundances of the remaining species provided relatively weak fits ($D^2_a < 0.10$). These included one new species, Hairy Woodpecker, negatively related to PAN_{SD} ; and two species (American Redstart and Rose-breasted Grosbeak) with similar fits to those obtained at the 50-m scale. Four species (Black-and-white Warbler, Cerulean Warbler, Ovenbird, and Red-eyed Vireo) were no longer related to image texture at the 100-m scale.

4. Discussion

We found that fine-scale satellite image texture was related to several habitat features that represented environmental heterogeneity in this forest, and that much of this heterogeneity appeared to be structural in nature. An increase in grapevine density, herbaceous cover, and snag density at the sampling locations (as calculated at the 50-m scale) was most closely tied to an increase in the s.d. of the pixel values in the panchromatic image (50-m scale PAN_{SD}). This image texture appeared to reflect a forest canopy that was structurally more heterogeneous (i.e., more open), thus allowing more light to reach through it. A more open forest canopy is also consistent with the lower basal area for these sampling locations. Because the mean of the pixel values in the panchromatic image (50-m scale PAN_{AVG}) increased along with the s.d., it seems likely that spectrally brighter vegetation, such as the grapevines and understory found in canopy gaps, contrasted with a relatively darker forest canopy to cause much of the higher variability in the image pixel values. Images for the sampling locations at the high end of the PAN_{SD} spectrum (e.g., Figure 2c and d; Appendix C) have noticeably brighter patches of pixels in support of this.

At the low end of the PAN_{SD} spectrum were the sampling locations with the highest basal area, and an additional texture measure; the s.d. of the second-order COR calculated with a 9x9 pixel neighborhood (50-m scale PAN_{SD_COR09}) was positively correlated with these locations. While the field-based canopy cover estimate did not strongly differentiate among the sampling locations in the PCA ordination, canopy cover was positively correlated with basal area. This tendency, in addition to the large patches of smooth canopy at these locations (e.g., Figure 2a and b; Appendix C), appeared to characterize a forest canopy exhibiting greater closure. Underneath this canopy, sapling cover increased and we observed that the increased woody understory cover was often dominated by greenbrier, *Vaccinium* spp., and tree seedlings. Unlike the locations with a more open forest canopy, the saplings and understory at these locations would not be directly reflected in the satellite image from within canopy gaps. Further, because the canopy had fewer gaps it would have fewer bright patches of pixels in the image, and this contributed to less variation in the pixel values for the PAN_{SD} measure.

Beyond the structural characteristics that were linked to image texture, the chestnut oak-sugar maple dichotomy in the PCA suggested a strong gradient in forest composition among the sampling locations. Forest composition and structure are often considered as separate influences in avian studies (e.g., Lee and Rottenberry 2005, Jayapal et al. 2009); however, they are also likely interdependent (Hewson et al. 2011). That the basal areas of chestnut oak and sugar maple were closely aligned with the most important structural variables in the PCA suggested that the observed structural gradient was closely intertwined with the compositional one. It is likely that the structure of this forest depends at least in part on its composition; for example, there may have been increased tree fall rates and more grapevines present to inhibit gap succession where sugar maple is dominant, leading to more and longer-term canopy gaps. While structure leading

to composition is also a likely possibility, teasing out these different influences would be difficult if not impossible. We focus here on forest composition as a likely underlying influence on structural heterogeneity, as we suspect structure is more directly linked to the strongest of the image texture measures.

The contrast between the relatively xerophytic chestnut oak and the relatively mesophytic sugar maple as canopy dominants also suggested potential productivity differences among the sampling locations. In support of this, as a productivity measure (Pettorelli et al. 2011) the NDVI pixel value mean (NDVI_{AVG}) was highly correlated ($r = 0.90$) with PAN_{AVG} at the 50 m scale and was thus also indicative of sugar maple dominance. However, this meant that NDVI_{AVG} was indicative of the associated structural characteristics as well. The NDVI has been linked to vegetation structure within and among habitats elsewhere, at least as obtained from coarser-scale (30-m resolution) Landsat satellite imagery (e.g., Wood et al. 2012), so determining what NDVI_{AVG} is actually measuring here does not seem to be possible. Still, it is important to recognize that productivity may be an underlying influence in this forest that has led to some of the observed patterns in its structure and composition, and thus correlation with information in the satellite image. The ability of fine-scale multispectral imagery, such as that used here, to detect productivity gradients within forests warrants further study.

Other than PC1 as the dominant PCA axis, other gradients within this forest as indicated by the PCA were more difficult to discern, with only relatively weak associations with the remote sensing data. One potential issue for the PCA (and subsequent fitting of geospatial variables) was the ridgetop sampling arrangement, because the field subplot data were summarized at the sampling point level for the analysis. This analysis decision prevented the ordination of potential influences such as aspect and slope on forest structure and composition within the sampled area

surrounding each point. The solution for this is to perform additional analysis at the individual field subplot level, which is the focus of Chapter 3. Still, some additional interpretation was provided by PC2 (e.g., tree density/species richness versus DBH mean), and elevation was aligned with this axis, albeit partially according to the surface fit. Also, PC2 indicated some differentiation at the extremes of PC1, and this resulted in the orientation of spectral brightness more toward grapevine density and NDVI pixel variation more toward sugar maple basal area.

While there were relatively strong vector fits aligned primarily with PC1, additional geospatial information relevant to the PCA ordination was scarce, and when found was not strongly modeled even if fit as a nonlinear surface. The surface modeling did serve an important purpose, however, in supporting stronger fits such as PAN_{SD} as being consistently linear across the PC1 gradient. It was also important to include surface modeling to fully test the potential for confounding of topography, including how this relates to sun angle-induced brightness effects in the satellite image, with the image variables seemingly providing useful information about the habitat. The solar radiation index and the other topographic variables did not appear to have much influence on this information, however. Although relatively weak, elevation and the index of topographic complexity instead provided some additional interpretation, and also were of some use for the avian modeling. Finally, the opportunity for spurious fits should also be noted. For example, the PAN_{SD_SD41} surface fit (Figure 3c) did not provide much interpretation regarding PC1, and could have been simply a consequence of fitting a large number of geospatial variables.

4.1. Avian relations to principal component 1 (PC1) and image texture

Of the richness measures, gap species richness was most strongly related to the PC1 forest structure/composition gradient. This suggested that an important component of the forest

heterogeneity indicated by this PCA axis was canopy gaps with well-developed understories. The Indigo Bunting and Blue-winged Warbler in this richness group are species that are also found in open habitats outside of forests, and unlikely to be found within mature forests without the presence of large, well-vegetated canopy gaps. Their occurrence when added to that of the other gap species is a particularly strong indication of areas with high structural heterogeneity within the largely contiguous ridgetop forest at this site. PAN_{SD}, the texture most highly correlated with PC1, modeled gap species richness even more strongly than PC1. Promisingly, Wood et al. (2013) also found that image texture was more strongly related to avian species richness, and also the densities of three species, than field-measured habitat structure. Here, perhaps PAN_{SD} reflected structural characteristics over the entire area of the sampling locations more comprehensively than the sub-sampled field data, or more accurately indicated canopy gaps and their associated vegetation, which were not directly measured in the field. If so, PAN_{SD} may be a relatively strong remote sensing proxy of this kind of structural heterogeneity, potentially useful if applied elsewhere within this forest type.

Not surprisingly given the species richness results, four of the six species with significant occurrence trends in relation to PC1 were gap species. At the 50-m scale, the PAN_{SD} binomial model produced the best fit for these gap species, and furthermore the model fit increased over that of PC1. Of the gap species that were relatively common, the Hooded Warbler (occurrence: 41/68 points) had the strongest results. That PAN_{SD} may have indicated the presence of canopy gaps with well-developed understories is consistent with other research for this species. Satellite (Ikonos and Landsat) image texture also discriminated between Hooded Warbler nest and non-nest sites in Ontario, where nesting was linked in the field to the presence of overhead canopy gaps (Pasher et al. 2007). Occurrences of Eastern Towhee, Kentucky Warbler, and Northern

Cardinal were also more strongly modeled by PAN_{SD} , and these species are also likely to be primarily dependent on canopy gaps for nesting within this forest. As noted above, canopy gaps are likely required for nesting by Indigo Bunting and Blue-winged Warbler. While Indigo Bunting occurrence was not significantly related to PAN_{SD} at the 50 m scale, it was strongly so at the 100 m scale. Blue-winged Warbler could not be modeled with only five occurrences (at both scales), but given a greater sample size would likely have been strongly related to PAN_{SD} as well, since its occurrences were all at higher PAN_{SD} values.

The lone species that was negatively related to PC1 was the Eastern Wood-Pee-wee, thus its occurrence was linked to locations with higher chestnut oak basal area and a more continuous forest canopy. This species favored nesting on drier ridgetops dominated by xeric oaks including chestnut oak in southeastern Ohio (Newell and Rodewald 2011). The PAN_{SD_COR09} binomial model was the best for Eastern Wood-Pee-wee among the image texture models, although the fit was not as strong as that obtained using PC1. It may be that both composition and a closed canopy structure contribute to the occurrence of Eastern Wood-Pee-wee on forested ridgetops at this site, since PC1 represented both potential influences. However, the species is known to tolerate a wide range in the amount of tree cover (Kendrick et al. 2013), and for Newell and Rodewald (2011) was an abundant nester in both shelterwood harvests and closed canopy mature second growth. At the 100-m scale, Eastern Wood-Pee-wee abundance was relatively strongly modeled by PAN_{SD_COR09} as the best image texture. As this texture when added to PAN_{SD} more strongly modeled chestnut oak basal area, this lends support to chestnut oak composition over canopy closure as the primary influence on its occurrence in this forest.

The positive trends in total species richness in 2011 in relation to PC1 and image texture need to be considered in light of the species with the strongest trends in occurrence. Because

there were relatively weak positive trends, or no apparent trends, for most of the species tested (17 of the 24 species), much of the total species richness trend was due to the occurrences of the gap species. As a group, the gap species occurrences would also overwhelm the competing negative occurrence trend for the Eastern Wood-Pewee. We tested the removal of the gap species and Eastern Wood-Pewee occurrences from the best total species richness single variable model (NDVI_{SD}) and still found a positive, albeit considerably weaker trend ($D^2_a = 0.12$; $P = 0.001$). This occurred despite the gap species not being as strongly modeled by NDVI_{SD}. It is likely that this “remainder” of the trend in species richness was mostly due to the occurrences of species that were positively but relatively weakly modeled with image texture (species with $D^2_a < 0.10$ in Table 10). Thus, in addition to the gap species, these species in tandem probably contributed most to the total species richness pattern observed in 2011.

With the reduced across-year dataset, the total species richness trend was not significant in 2009 and 2010, and showed evidence of diverging toward lower richness at high NDVI_{SD} in 2010. The 26 additional 2011 sampling points helped to fill in the rather sparse sample at the low end of the NDVI_{SD} spectrum, so perhaps if these points had been sampled in 2009, the slightly positive trend in this year would have been stronger. More surprising is the drop in total species richness suggested for high NDVI_{SD} in 2010. Examination of the 2010 data at the visit level supported this pattern, with weather and wind conditions, observers, time of morning, and survey date appearing to have little bearing on the lower 2010 species counts for these points. Potentially some unmeasured environmental influence had an effect in 2010 but not the other years, or total bird species richness as measured for this study has abundant annual variation causing inconsistent results. As discussed below (section 4.3), more sampling at the point level

may be needed to gain a better estimate of total species richness, particularly if sampling is done within one habitat cover type.

In terms of relatively common versus relatively rare species, the occurrences of common species were likely more responsible for the total species richness trends we observed. In all analyses, the trend for common species richness was closely similar to the trend for total species richness, whereas rare species richness had no trend, or was only weakly related to the total species richness trend. It is notable that this occurred despite the fact that the rare species group included the occurrences of three of the gap species. One potential explanation is that rare species are dispersed more randomly than common species (Ricotta et al 2008), and therefore are less likely to exhibit a group-level trend in relation to specific environmental factors. In contrast, common species are more likely to influence trends in total species richness simply due to their commonness (Lennon et al. 2004). Of the species included in common species richness, the most common (Red-eyed Vireo) showed some positive trend, along with Hooded Warbler (ranked 2nd in occurrence) with its considerably stronger positive trend, and so were influential in determining the overall positive trend. On the other hand, there were common species with no apparent trends (e.g., Scarlet Tanager; ranked 3rd in occurrence), and one with a negative trend (Eastern Wood Peewee; ranked 9th in occurrence). This suggests the importance of including analyses also at the species level, or using other functional groupings of species (e.g., as in the gap-associated species for this study), if possible.

The attempt to use multiple geospatial variables for the avian modeling was at least partly successful. While the topographic influences on species richness were relatively weak, their interpretation was rather straightforward (e.g., flatter topography and mid-elevations supporting more species), and they resulted in some model improvements. It was also important to include

them, as in the PCA, to potentially control for these effects. The same could not be said of additional image information beyond that which was most strongly linked to the PCA results. This was actually beneficial for this study because interpretation of image information content was the goal. In the few cases where an additional image variable resulted in model improvement, we could not interpret what it meant in terms of habitat information. For example, while PAN_{SD_COR03} was interesting in that it produced stronger models for total and common species richness when added to NDVI_{SD} and the topographic variables, it did not explain any PCA results. As this statistic only applied in 2011 at 50 m scale, it is perhaps safer in the absence of additional research to consider the potential, as noted above for the PCA geospatial variable fitting, for spurious effects (including nonlinear ones) to be found when considering a large number of explanatory variables.

Depending on the scale of the analysis, some of the species richness responses in relation to image texture suggested threshold effects, although none were particularly strong. For example, at the 50-m scale the increase in gap species richness in relation to PAN_{SD} began to plateau. This result would be expected if a level of environmental heterogeneity was reached prior to the maximum heterogeneity (as measured at this scale), that tended to support the maximum number of the species in this group (also as measured at this scale). Why this threshold would not also occur at the 100-m scale for this group is more difficult to explain, but could be related to the increase in heterogeneity as measured by PAN_{SD} at the low end of the gradient, which supported more gap species and increased this portion of the trend. Curiously, a threshold was also apparent for total species richness at high NDVI_{SD}, but only at the 100-m scale. In comparison to gap species richness there was considerably more scatter in the richness values, so perhaps a total species richness trend was only modeled for lower NDVI_{SD} at the 100-m scale. While both of

these thresholds are very subtle, they do emphasize the importance of carefully considering the spatial scale of the sampling. Sampling at a large enough scale within this habitat would likely cause any species richness trend to vanish, with an increasing tendency for the maximum richness to be obtained for each sample. Finally, it may be helpful to study response thresholds for individual species, including the use of abundance data as this could allow for stronger modeling of thresholds. For example, a relatively strong threshold was indicated for Eastern Wood-Pee-wee abundance at the 100-m scale, which confirmed its occurrence trend.

4.2. Spatial trends

As previously described, forest composition at the site was known to differ on the ridgetops (Perkins 2006); however, it was not known to be so spatially structured (i.e., exhibiting a southwest to northeast trend across the study area). The image textures and the forest structure and composition characteristics that were differentiated along PC1 exhibited closely related spatial trends. It seems unlikely that image texture measures such as PAN_{SD} were idiosyncratic in their spatial distribution at this study area, and merely correlated with the observed forest composition and structure differences rather than indicate them. It is also unlikely that the occurrences of the gap species were the result of other influences on their distribution, rather than the presence of increased structural heterogeneity that was captured with image texture. These multiple lines of evidence strengthen support for image texture as truly representing environmental heterogeneity in this forest that is important to some species. It is also interesting that this heterogeneity was so spatially structured, as this may indicate a larger (i.e., macroecological) environmental pattern such as a broad-scale trend in forest composition across the region. While this study was likely too small and opportunistic, future studies in the region could perhaps detect pure spatial versus pure environmental control of avian diversity patterns

(*sensu* Gianuca et al. 2013) with a larger number of sampling locations distributed more regularly over a larger spatial scale.

4.3. Comparisons with other studies

Comparing our results with those from other studies that use image texture to model avian species richness is complicated by a number of factors, including differences in study design, habitats studied, and remote sensing data sources. Probably the most important study design-related difference was that we modeled species richness using image texture obtained for a single habitat cover type (mature forest), whereas the other studies modeled species richness using image texture obtained for multiple habitat cover types. For instance, the habitats studied by St-Louis et al. (2006) ranged from finer-textured grasslands to coarser-textured shrublands and a woodland, and avian species richness was previously known to increase as the structural complexity of these habitats increased from the grasslands to the shrublands to the woodland (Pidgeon et al. 2001). Image texture appeared to strongly reflect this gradient in structural complexity, and thus strongly modeled avian species richness (St-Louis et al. 2006). Although we cannot exactly quantify the differences between our studies, ours probably lacked the amount of contrast in both species richness and image texture values that is to be expected from multiple habitat cover types. It is perhaps not surprising, therefore, that we did not find particularly strong (or consistent) results for total species richness in relation to image texture. Comparison with Wallis et al.'s (2016) forested sites is somewhat complicated by our use of different biodiversity measures. Assuming richness is well correlated with Shannon diversity, their sampling of three forest types over a 700 m elevation gradient (including valleys, midslopes, and ridges) likely provided much more contrast in forest composition and structure than the ridgetop forest we studied, for modeling species richness.

Another study design-related factor pertains to the avian richness data itself. Both St-Louis et al. (2006) and Wood et al. (2013) conducted avian point counts over more within-breeding season visits (4–5 and 3–4; respectively) to their sampling points. Furthermore, St-Louis et al. (2006) combined three breeding seasons of data to obtain species richness for their sampling points and then calculated average species richness for their plot-level analyses using 12 sampling points in each plot. Wood et al. (2013) also combined three breeding seasons of data to obtain species richness for their point-level analyses. Through greater sampling effort, both of these studies likely had a more stable and perhaps more accurate estimate of species richness than our study, for which we analyzed species richness computed for each sampling point based on two visits. We chose not to combine the three breeding seasons of data that we had based on sample size considerations for the multiple variable models (i.e., because of problems with over-fitting). Future studies should consider increased sampling effort, within and perhaps across multiple breeding seasons, and use of species accumulation curves to assess the stability of the species richness estimate (see Wood et al. 2013) if analysis at the point-level is the goal and sample sizes are expected to be minimal.

For Wood et al. (2013), the best image texture for predicting Grasshopper Sparrow density within grassland habitat was the plot-level pixel s.d. from second-order contrast derived from a 1-m resolution infrared air photo, and the best predictor for Ovenbird density within forest habitat was the plot-level pixel mean from a 30-m resolution Landsat NDVI image. Despite the difference in habitats and remote sensing data, the measures appeared to capture similar types of habitat information (low contrast representing unbroken grasslands important for the sparrow, and high NDVI values representing dense forest for the Ovenbird) and model the species relatively strongly (Wood et al. 2013). Other than the Eastern Wood-Pee-wee, the best modeled

species in our study were gap species, and a plot-level image statistic (PAN_{SD}) likely representing habitat structural variability was the strongest. Comparing among our studies is difficult due to the myriad of differences. However, based on this limited comparison we suggest future studies include focus at the species level, with attention to how image texture and other remote sensing data characterize the habitat(s) in question, and features important to particular species within the habitat(s). With greater understanding at the species level, how remote sensing information relates to broader community-level trends (e.g., in species richness) may be better understood.

4.4. Image texture analysis and application considerations

We found that the best image texture measure for modeling the forest characteristics indicating high structural heterogeneity, as well as the avian species associated with this heterogeneity, was PAN_{SD} . This first-order statistic was also easy to obtain, being the s.d. of the pixel values extracted at the plot level from the original panchromatic image. The pixel value s.d. from the coarser grained NDVI image was not as effective, which suggests that the panchromatic image provided a spatial resolution that was a better match to the forest structural variability important to some of the bird species we evaluated. Pasher and King (2010) degraded 0.2-m resolution aerial photos of a northern hardwood forest to 0.6-m and 1-m resolutions, and found a loss of canopy spatial information and a decrease in the visibility of canopy gaps, so a finer grain than the 0.6 m panchromatic image we used could perhaps have provided a more powerful measure than PAN_{SD} . On the other hand, during the reduction of highly correlated image texture variables to a more manageable set, we found that the second-order $NDVI_{AVG_CON}$ measure increased to the $r = 0.80$ correlation threshold with PAN_{SD} as the NDVI neighborhood size increased to 11x11 pixels (Appendix D). Processing of the coarser 2.4 m resolution NDVI image

thus provided information that was similar to PAN_{SD}, so it could have been a potentially useful alternative if the finer-grained panchromatic image had not been available.

Processing of the panchromatic image provided plot-level measures of first- and second-order statistics that were nearly to completely redundant with PAN_{SD} (Appendix D).

Interestingly, there were competing trends in the moving window pixel neighborhood sizes for particular measures to achieve redundancy. For example, both the PAN_{SD_AVG} and the PAN_{SD_SD} measures became most redundant ($r = 1.00$ and 0.95 ; respectively) with PAN_{SD} at the smallest neighborhood size (3x3 pixels) whereas for the PAN_{AVG_SD} measure the most redundancy ($r = 0.98$) was achieved at the largest neighborhood size (41x41 pixels). Thus, at the 50-m scale at which the correlations were computed, the mean of the pixel s.d. obtained with the largest (24.6 m x 24.6 m) neighborhood was most redundant with the s.d. of the pixel mean and s.d. obtained with the smallest (1.8 x 1.8 m) neighborhood. This suggests that the scale at which a statistic is summarized at the plot level is important to consider, for example, when attempting to interpret the meaning of the scale of a moving window statistic (e.g., is fine- or course-scale variability being characterized?). The differences we found when scaling up the statistics to 100 m (e.g., increasing the values, but shortening the range of pixel heterogeneity) also suggests caution in choosing a spatial scale for summarizing texture values. If the remote sensing data are available prior to collecting the field data, to help select the most appropriate spatial scale(s) for the field data collection, calculating area summaries of pixel values from raw and processed images at multiple spatial scales and evaluating their correlation may be useful.

We addressed in two ways the potential confounding influence of topography and acquisition-induced (e.g., sun angle) image brightness variations on the image spectral and texture information. First, we used the NDVI image in part to potentially correct for these

brightness variations (Rouse et al. 1973). However, NDVI_{AVG} was only slightly less correlated with DSR ($r = 0.55$) than PAN_{AVG} was with DSR ($r = 0.62$). For the image textures, there was a reduction in NDVI correlation with DSR for a given statistic (e.g., $r = -0.06$ and 0.25 for NDVI_{SD} and PAN_{SD} ; respectively), but all pairwise correlations with DSR were $r < 0.50$ (Appendix D). Second, we assessed the inclusion of DSR as a variable throughout the modeling. Despite the moderate correlation with PAN_{AVG} , the fit of DSR to the PC1:PC2 ordination was small and not significant while the fit of PAN_{AVG} was relatively strong and significant. DSR also was unimportant as a single variable and in combination with other image variables in the avian models. The summer date and the near-solar noon acquisition time for the QuickBird image were probably close to optimal for texture calculation in rough terrain such as this. Imagery collected under less than optimal acquisition conditions may require removal of brightness variation prior to image texture calculation. Pasher and King (2010) review brightness correction techniques and apply one of these techniques to airborne imagery exhibiting much brightness variation to good effect. At a minimum, estimating a measure of solar illumination at the time of image acquisition should be done to examine if it relates more strongly to image brightness variation (i.e., noise) than to field data.

Wood et al. (2012) recommend using a subset of first- and second-order texture measures to characterize vegetation heterogeneity due to the often high correlation between texture measures. The results from this study support this. While we found that a first-order statistic was most strongly related to forest composition and structure, one of the less correlated second-order COR statistics ($\text{PAN}_{\text{SD_COR09}}$) appeared to provide unique information related to a more closed canopy dominated by chestnut oak. For their texture measures, Wood et al. (2012) found that while the pixel mean summaries were usually highly correlated, the correlations among the pixel s.d.

summaries were more variable. We calculated a number of the latter (e.g., PAN_{SD_SD41}) that were relatively uncorrelated with other image texture statistics (Appendix D). While these additional s.d. summaries did not seem to be important in this study, such statistics may reflect important habitat variability at different spatial scales (St-Louis et al. 2006), and should be considered for inclusion. Finally, a spectral measure appeared to provide some unique vegetation information in this study and was useful when considered along with image texture for its likely contribution to the sampling point pixel s.d. To be comprehensive, studies using image texture should include spectral measures. In some cases (e.g., as in Wood et al. 2012), spectral measures may even provide more forest structural information than image texture.

5. Conclusions

The results of this study illustrate both the opportunities and the challenges for the use of high spatial resolution imagery to model forest habitat and avian biodiversity. Textural information contained in the satellite image was relatively strongly related to some of the forest characteristics measured in the field. The image information modeled the main structural complexity/chestnut oak-sugar maple composition gradient rather well, with potentially enough predictive accuracy to be ecologically informative if applied throughout the contiguous mature ridgetop forest at the site. As the model was assessed only within one site, it is important to attempt to validate these results elsewhere. These results also need to be validated with other imagery of a similarly fine resolution. Both the availability and quality of remote sensing data, including high resolution imagery, continues to increase (Li et al. 2014), so there is much future potential for studies such as this one. Although other kinds of remote sensing data should better provide certain information (e.g., vertical forest structure via active sensors such as Lidar),

standard optical imagery with a high spatial resolution should retain some advantages, such as the ease of producing relatively simple yet effective image statistics and for a larger area at a comparatively reduced cost (Wallis et al. 2016). This imagery also may add local, fine-scale information to other coarser-scale remote sensing data on forests (e.g., from the National Land Cover Database 2011; Homer et al. 2015).

We found that the total avian species richness trend in relation to image texture was relatively weak, and results were inconsistent across the spatial scales of the analysis and when tested across years. This was a potentially interesting result in that it may call into question the general applicability of environmental heterogeneity as a driver of total species richness, at least when considered within a single, relatively homogeneous habitat cover type. Of likely greater interest was the relative strength and consistency of the gap species richness trends. This finding was encouraging, as it suggested that these bird species as a group may be a dependable signal of forest heterogeneity that can also be detected with high resolution imagery. The results at the species level, including both occurrence and abundance, also supported this finding. More intensive investigation at the habitat and species level may provide more certainty as to what is actually being measured by remote sensing data. The results of our study suggest that better estimation of point-based total species richness may be needed if the analysis is performed at the level of individual sampling points, with careful attention given to the spatial scale at which species are counted and remote sensing data are quantified.

Acknowledgments

We thank D. Blood, B. Miller, M. Napoli, and numerous other field technicians for their assistance with data collection and Wheeling Jesuit University for providing field housing. This research was funded by NETL Department of Energy, U.S. Fish and Wildlife Service, National Fish and Wildlife Foundation, and West Virginia University Division of Forestry and Natural Resources. West Virginia Department of Natural Resources and U.S. Geological Survey West Virginia Cooperative Fish and Wildlife Research Unit provided logistical support.

References

- Bellis, L.M., Pidgeon, A.M., Radeloff, V.C., St-Louis, V., Navarro, J.L., Martella, M.B., 2008. Modeling habitat suitability for Greater Rheas based on satellite image texture. *Ecological applications* 18(8): 1956-1966.
- Blanchet, F.G., Legendre, P., Borcard, D., 2008. Forward selection of explanatory variables. *Ecology* 89: 2623-2632.
- Camathias, L., Bergamini, A., Küchler, M., Stofer, S., Baltensweiler, A., Rocchini, D., 2013. High-resolution remote sensing data improves models of species richness. *Applied Vegetation Science* 16(4): 539-551.
- Canty, A., Ripley, B., 2015. boot: Bootstrap R (S-Plus) Functions. R package version 1.3-17.
- Chavez Jr., P.S., 1989. Radiometric calibration of Landsat Thematic Mapper multispectral images, *Photogrammetric Engineering and Remote Sensing* 55(9): 1285-1294.
- Culbert, P.D., Radeloff, V.C., St-Louis, V., Flather, C.H., Rittenhouse, C.D., Albright, T.P. and Pidgeon, A.M., 2012. Modeling broad-scale patterns of avian species richness across the

- Midwestern United States with measures of satellite image texture. *Remote Sensing of Environment* (118): 140-150.
- Dilts, T.E., 2015. Topography Tools for ArcGIS 10.1. University of Nevada Reno. Available at: <http://www.arcgis.com/home/item.html?id=b13b3b40fa3c43d4a23a1a09c5fe96b9>
- Dirzo, R., Young, H.S., Galetti, M., Ceballos, G., Isaac, N.J., Collen, B., 2014. Defaunation in the Anthropocene. *Science* 345(6195): 401-406.
- Duro, D.C., Coops, N.C., Wulder, M.A. and Han, T., 2007. Development of a large area biodiversity monitoring system driven by remote sensing. *Progress in Physical Geography*, 31(3): 235-260.
- Franklin, S.B., Gibson, D.J., Robertson, P.A., Pohlmann, J.T., Fralish, J.S., 1995. Parallel Analysis: a method for determining significant principal components. *Journal of Vegetation Science* 6: 99-106.
- Gianuca, A.T., Bastazini, V.A.G., Dias, R.A., Hernández, M.I.M., 2013. Independent and shared effects of environmental features and space driving avian community beta diversity across a coastal gradient in southern Brazil. *Austral Ecology* 38(8): 864-873.
- Gillespie, T.W., Foody, G.M., Rocchini, D., Giorgi, A.P., Saatchi S., 2008. Measuring and modelling biodiversity from space. *Progress in Physical Geography* 32(2): 203-221.
- Gottschalk, T.K., Huettmann, F., Ehlers, M., 2005. Thirty years of analysing and modelling avian habitat relationships using satellite imagery data: A review. *International Journal of Remote Sensing* 26(12): 2631-2656.
- GRASS Development Team, 2013. Geographic Resources Analysis Support System (GRASS) Software, Version 6.4.3. Open Source Geospatial Foundation. <http://grass.osgeo.org>.

- Guisan, A., Zimmermann, N.E., 2000. Predictive habitat distribution models in ecology. *Ecological Modelling* 135(2): 147-186.
- Hall-Beyer, M. 2007. The GLCM texture tutorial, current version: 2.10 February 2007. <http://www.fp.ucalgary.ca/mhallbey/tutorial.htm>. (Accessed: February 15, 2014).
- Harralick, R.M., Shanmugam, K., Dinstein, I., 1973. Textural features for image classification. *IEEE Transactions on Systems, Man, and Cybernetics*, SMC-3, 610-621.
- Hastie, T., Tibshirani, R., 1990. *Generalized Additive Models*. Chapman and Hall, New York, NY, USA.
- Hewson, C.M., Austin, G.E., Gough, S.J., Fuller, R.J., 2011. Species-specific responses of woodland birds to stand-level habitat characteristics: the dual importance of forest structure and floristics. *Forest Ecology and Management* 261: 1224-1240.
- Homer, C.G., Dewitz, J.A., Yang, L., Jin, S., Danielson, P., Xian, G., Coulston, J., Herold, N.D., Wickham, J.D., Megown, K., 2015. Completion of the 2011 National Land Cover Database for the conterminous United States-Representing a decade of land cover change information. *Photogrammetric Engineering and Remote Sensing* 81(5): 345-354
- Hunter, W.C., Buehler, D.A., Canterbury, R.A., Confer, J.L., Hamel, P.B., 2001. Conservation of Disturbance-Dependent Birds in Eastern North America. *Wildlife Society Bulletin* 29(2): 440-455.
- Jayapal, R., Qureshi, Q., Chellam, R., 2009. Importance of forest structure versus floristics to composition of avian assemblages in tropical deciduous forests of Central Highlands, India. *Forest Ecology and Management* 257: 2287-2295.
- Jenness, J., 2006. Topographic Position Index extension (tpi_jen.avx) for ArcView 3.x, v. 1.3a. Jenness Enterprises. Available at: <http://www.jennessent.com/arcview/tpi.htm>.

- Jones, T., Arcese, P., Sharma, T., Coops, N., 2013. Describing avifaunal richness with functional and structural bioindicators derived from advanced airborne remotely sensed data. *International Journal of Remote Sensing* 34(8): 2689-2713.
- Kaiser, H.F., 1960. The application of electronic computers to factor analysis. *Educational and Psychological Measurement* 20: 141-151.
- Kayitakire, F., Hamel, C., Defourny, P., 2006. Retrieving forest structure variables based on image texture analysis and IKONOS-2 imagery. *Remote Sensing of Environment* 102(3-4): 390-401.
- Kendrick, S.W., Thompson III, F.R., Reidy, J.L., 2013. Eastern Wood-Pewee (*Contopus virens*) breeding demography across a gradient of savanna, woodland, and forest in the Missouri Ozarks. *Auk* 130: 355-363.
- Lee, P.-Y., Rotenberry, J.T., 2005. Relationships between bird species and tree species assemblages in forested habitats of eastern North America. *Journal of Biogeography*. 32: 1139-1150.
- Lennon, J.J., Koleff, P., Greenwood, J.J.D., Gaston, K.J., 2004. Contribution of rarity and commonness to patterns of species richness. *Ecology Letters* 7: 81-87.
- Li, Z., Xu, D., Guo, X., 2014. Remote Sensing of Ecosystem Health: Opportunities, Challenges, and Future Perspectives. *Sensors* 14(11): 21117-21139.
- Luoto, M., Virkkala, R., Heikkinen, R.K., Rainio, K., 2004. Predicting Bird Species Richness Using Remote Sensing in Boreal Agricultural-Forest Mosaics. *Ecological Applications* 14(6): 1946-1962.
- Mansfield, E.R., Helms, B.P., 1982. Detecting Multicollinearity. *The American Statistician* 36(3): 158-160.

- Marra, G., Wood, S.N., 2011. Practical variable selection for generalized additive models. *Computational Statistics and Data Analysis* 55(7): 2372-2387.
- McCullagh, P., Nelder, J.A., 1989. *Generalized Linear Models*. 2nd ed. Chapman and Hall/CRC, Boca Raton, FL.
- Mihran, T., Jain, A.K., 1998. Texture analysis. pp. 207-248 in Chen, C.H., Pau, L.F., Wang, P.S.P. (Eds.), *The handbook of pattern recognition and computer vision*. Word Scientific Publishing Co.
- Newell, F.L., Rodewald, A.D., 2011. Role of topography, canopy structure, and floristics in nest-site selection and nesting success of canopy songbirds. *Forest Ecology and Management* 262: 739-749.
- Oksanen, J., Guillaume Blanchet, F., Kindt, R., Legendre, P., Minchin, P.R., O'Hara, R.B., Simpson, G.L., Solymos, P., Henry, M., Stevens, H., Wagner, H., 2012. *vegan: Community Ecology Package*. R package version 2.0-5. <http://CRAN.R-project.org/package=vegan>
- Pasher, J., King, D., Lindsay, K., 2007. Modelling and mapping potential hooded warbler (*Wilsonia citrina*) habitat using remotely sensed imagery. *Remote Sensing of Environment* 107(3): 471-483.
- Pasher, J., King, D.J. 2010. Multivariate forest structure modelling and mapping using high resolution airborne imagery and topographic information. *Remote Sensing of Environment* 114(8): 1718-1732.
- Patel, M.B., Rodriguez, J.J., Gmitro, A.F., 2008. Effect of gray-level re-quantization on co-occurrence based texture analysis. 15th IEEE International Conference on Image Processing (pp. 585-588). IEEE.

- Pearman, P.B., Weber, D., 2007. Common species determine richness patterns in biodiversity indicator taxa. *Biological Conservation* 138(1): 109-119.
- Perkins, K.A. 2006. Cerulean warbler selection of forest canopy gaps. Morgantown, WV: West Virginia University. 89 p. M.S. thesis.
- Perkins, K.A., Wood, P.B., 2014. Selection of forest canopy gaps by male cerulean warblers in West Virginia. *Wilson Journal of Ornithology* 126: 288-297.
- Pettorelli, N., Ryan, S., Mueller, T., Bunnefeld, N., Jędrzejewska, B., Lima, M., Kausrud, K., 2011. The normalized difference vegetation index (NDVI): unforeseen successes in animal ecology. *Climate Research* 46: 15-27.
- Pidgeon, A.M., Mathews, N.E., Benoit, R., Nordheim, E.V., 2001. Response of avian communities to historic habitat change in the Northern Chihuahuan Desert. *Conservation Biology* 15: 1772-1788.
- Ralph, C.J., Droege, S., Sauer, J.R., 1995. Managing and monitoring birds using point counts: standards and applications. In: Ralph, C.J., Sauer, J.R., Droege, S. (Eds.), *Monitoring Bird Populations by Point Counts*. Gen.Tech.Rep.PSW-GTR-149. U.S. Department of Agriculture, Forest Service, Pacific Southwest Research Station, Albany, California, pp. 161-168.
- Rands, M.R.W., Scharlemann, J.P.W., Sutherland, W.J., Vira, B., Adams, W.M., Bennun, L., Butchart, S.H.M., Clements, A., Coomes, D., Entwistle, A., Hodge, I., Kapos, V., 2010. Biodiversity conservation: challenges beyond 2010. *Science* 329(5997): 1298-1303.
- Rhodes, C.J., Henrys, P., Siriwardena, G.M., Whittingham, M.J., Norton, L.R., 2015. The relative value of field survey and remote sensing for biodiversity assessment. *Methods in Ecology and Evolution* 6(7): 772-781.

- Ricotta, C., Godefroid, S., Celesti-Grapow, L., 2008. Common species have lower taxonomic diversity evidence from the urban floras of Brussels and Rome. *Diversity and Distributions*, 14(3): 530-537.
- Rocchini, D., Luoto, M., Nagendra, H., Oldeland, J., Ricotta, C., Southworth, J., Neteler, M., Balkenhol, N., Carter, G.A., Foody, G.M., Gillespie, T.W., He, K.S., Kark, S., Levin, N., Lucas, K., 2010. Remotely sensed spectral heterogeneity as a proxy of species diversity: Recent advances and open challenges. *Ecological Informatics* 5(5): 318-329.
- Rocchini, D., Hernández-Stefanoni, J.L., He, K.S., 2015. Advancing species diversity estimate by remotely sensed proxies: A conceptual review. *Ecological Informatics* 25: 22-28.
- Rouse, J.W., Haas, R.H., Schell, J.A., Deering, D.W., 1973. Monitoring vegetation systems in the Great Plains with ERTS. pp. 309-317 in 3rd ERTS Symposium, NASA SP-351 I.
- Schindler, S., von Wehrden, H., Poirazidis, K., Wrbka, T., Kati, V., 2013. Multiscale performance of landscape metrics as indicators of species richness of plants, insects and vertebrates. *Ecological Indicators* 31: 41-48.
- Šizling, A.L., Šizlingová, E., Storch, D., Reif, J.í., Gaston, K.J., 2009. Rarity, Commonness, and the Contribution of Individual Species to Species Richness Patterns. *The American Naturalist* 174(1): 82-93.
- St-Louis, V., Pidgeon, A.M., Radeloff, V.C., Hawbaker, T.J., Clayton, M.K., 2006. High-resolution image texture as a predictor of bird species richness. *Remote Sensing of Environment* 105(4): 299-312.
- St-Louis, V., Pidgeon, A.M., Kuemmerle, T., Sonnenschein, R., Radeloff, V.C., Clayton, M.K., Locke, B.A., Bash, D., Hostert, P., 2014. Modelling avian biodiversity using raw,

- unclassified satellite imagery. Philosophical Transactions of the Royal Society of London B: Biological Sciences 369(1643): 20130197.
- Tews, J., Brose, U., Grimm, V., Tielbörger, K., Wichmann, M.C., Schwager, M., Jeltsch, F., 2004. Animal species diversity driven by habitat heterogeneity/diversity: the importance of keystone structures. Journal of Biogeography 31(1): 79-92.
- Torontow, V., King, D., 2011. Forest complexity modelling and mapping with remote sensing and topographic data: A comparison of three methods. Canadian Journal of Remote Sensing 37(4): 387-402.
- Turner, W., Spector, S., Gardiner, N., Fladeland, M., Sterling, E., Steininger, M., 2003. Remote sensing for biodiversity science and conservation. Trends in Ecology and Evolution 18(6): 306-314.
- Tuttle, E., Jensen, R., Formica, V., Gonser, R., 2006. Using remote sensing image texture to study habitat use patterns: a case study using the polymorphic white-throated sparrow (*Zonotrichia albicollis*). Global Ecology and Biogeography 15(4): 349-357.
- von Wehrden, H., von Oheimb, G., Abson, D. J., Härdtle, W., 2016. Sustainability and Ecosystems. pp. 61-70 in Sustainability Science. Springer Netherlands.
- Wallis, C.I., Paulsch, D., Zeilinger, J., Silva, B., Fernández, G.F.C., Brandl, R., Farwig, N., Bendix, J., 2016. Contrasting performance of Lidar and optical texture models in predicting avian diversity in a tropical mountain forest. Remote Sensing of Environment 174: 223-232.
- Wood E.M., Pidgeon A.M., Radeloff, V.C., Keuler N.S., 2012. Image texture as a remotely sensed measure of vegetation structure. Remote Sensing of Environment 121: 516-526.
- Wood, E.M., Pidgeon, A.M., Radeloff, V.C., Keuler, N.S., 2013. Image texture predicts avian density and species richness. PloS one 8(5): e63211.

Wood, S.N., 2011. Fast stable restricted maximum likelihood and marginal likelihood estimation of semiparametric generalized linear models. *Journal of the Royal Statistical Society: Series B (Statistical Methodology)* 73: 3-36.

Woods, A.J., Omernik, J.M., Brown, D.D., 1999. Level III and IV Ecoregions of Delaware, Maryland, Pennsylvania, Virginia, and West Virginia., U.S. Retrieved November 4, 2009 from U.S. Environmental Protection Agency, National Health and Environmental Effects Research Laboratory. Corvallis, OR.
ftp://ftp.epa.gov/wed/ecoregions/reg3/reg3_eco_desc.doc.

Table 1. The moving window analysis neighborhood sizes and their respective ground distances for the panchromatic (PAN; 0.6-m resolution) and normalized difference vegetation index (NDVI; 2.4-m resolution) images.

PAN image neighborhoods		NDVI image neighborhoods	
<u>pixels</u>	<u>meters</u>	<u>pixels</u>	<u>meters</u>
3 x 3	1.8 x 1.8	3 x 3	7.2 x 7.2
9 x 9	5.4 x 5.4	5 x 5	12.0 x 12.0
17 x 17	10.2 x 10.2	7 x 7	16.8 x 16.8
25 x 25	15.0 x 15.0	9 x 9	21.6 x 21.6
33 x 33	19.8 x 19.8	11 x 11	26.4 x 26.4
41 x 41	24.6 x 24.6		

Table 2. The four categories of geospatial variables used in this study. The variables were obtained using geoprocessing tools in ArcGIS 10.1 (described in the footnotes) applied at the two plot-level spatial scales of the sampling points (50 and 100 m radii) to the data sources: the panchromatic (PAN) and normalized difference vegetation index (NDVI) images, the moving window analysis texture images from the PAN and NDVI images, and the digital elevation model (DEM). The pixel neighborhood size (see Table 1) is appended for identifying specific first- and second-order texture variables (e.g., PAN_{AVG_SD03} indicates that the texture image from which this plot-level measure was obtained was calculated using a 3 x 3 pixel neighborhood).

Geospatial variable	Plot-level measure ^a	Source
<u><i>Spectral</i></u>		
PAN _{AVG}	mean	PAN image
NDVI _{AVG}	mean	NDVI image
<u><i>First-order texture</i></u>		
PAN _{SD}	s.d.	PAN image
NDVI _{SD}	s.d.	NDVI image
PAN _{AVG_SD03-41}	mean	6 PAN moving window s.d. images
NDVI _{AVG_SD03-11}	mean	5 NDVI moving window s.d. images
PAN _{SD_AVG03-41}	s.d.	6 PAN moving window mean images
NDVI _{SD_AVG03-11}	s.d.	5 NDVI moving window mean images
PAN _{SD_SD03-41}	s.d.	6 PAN moving window s.d. images
NDVI _{SD_SD03-11}	s.d.	5 NDVI moving window s.d. images
<u><i>Second-order texture</i></u>		
PAN _{AVG_CON03-41}	mean	6 PAN moving window CON images
NDVI _{AVG_CON03-11}	mean	5 NDVI moving window CON images
PAN _{SD_CON03-41}	s.d.	6 PAN moving window CON images
NDVI _{SD_CON03-11}	s.d.	5 NDVI moving window CON images
PAN _{AVG_COR03-41}	mean	6 PAN moving window COR images
NDVI _{AVG_COR03-11}	mean	5 NDVI moving window COR images
PAN _{SD_COR03-11}	s.d.	6 PAN moving window COR images
NDVI _{SD_COR03-11}	s.d.	5 NDVI moving window COR images
<u><i>Topographic</i></u>		
ELEV	mean	Elevation from DEM
TVI	area ratio	Topographic variation index: 3D DEM area/2D area ^b
DSR	mean	Direct solar radiation at time of image acquisition from DEM ^c

a. The plot-level pixel summary statistic: mean or standard deviation (s.d.) as obtained using the Zonal Statistics tool, or the area ratio (for TVI), at radii of 50 and 100 m for the sampling points ($n = 68$).

b. For TVI, the 3-dimensional (3D) area was calculated from the DEM using the Surface Volume tool, which also provided the 2-dimensional (2D) area.

c. The DSR image was calculated using the Area Solar Radiation tool. The parameters for the tool were: Latitude = 40°; Sky size = 200; Julian date = 237 (August 25); Start/End (local) time = 11:18; Azimuth directions = 32; Zenith divisions = 8; Azimuth divisions = 8; Diffuse radiation model = Uniform sky; Diffuse proportion = 0.3; Transmittivity = 0.5.

Table 3. Principal components (PC1-PC3) with eigenvalues >1.0 that were retained from the principal components analysis (% of the total variance each explained is in parentheses), and the factor loading for the 14 forest variables. The factor loadings that appeared to provide the most differentiation of the 68 sampling points for each retained component are in bold.

Forest variable	Label for Fig. 1a	PC1 (39.3%)	PC2 (16.3%)	PC3 (11.5%)
Chestnut oak basal area	CHOA	-0.38	-0.04	-0.08
Sugar maple basal area	SUMA	0.30	0.23	0.33
Total basal area	BA	-0.33	0.04	0.34
Tree density	Tr_N	-0.03	-0.51	0.36
Tree height	Hgt	-0.21	0.25	0.05
Tree species richness	Tr_R	-0.13	-0.51	0.14
DBH mean	xDBH	-0.26	0.45	0.09
DBH standard deviation	sdDBH	-0.33	0.17	0.17
Snag density	Snag_N	0.22	0.03	0.05
Grapevine density	Gv_N	0.33	-0.21	0.07
Herbaceous % cover	Hb	0.36	0.14	0.20
Shrub % cover	Sb	-0.22	-0.15	-0.51
Sapling % cover	Sp	-0.26	-0.21	0.20
Canopy % cover	Can	-0.14	0.06	0.48

Table 4. Vector and surface fits of the reduced set of geospatial variables to the PC1:PC2 (principal components 1 and 2) ordination (Figure 3a). Surface fits are not provided (--) if the R^2 fit was the same as the vector R^2 fit. Geospatial variables in bold were used as the basis for the initial avian richness, occurrence, and abundance modeling.

Geospatial variable	Vector fit				Surface fit	
	axis correlation		R^2	P	R^2	P
	PC1	PC2				
<i>Image</i>						
PAN_{AVG}	0.99	0.11	0.40	0.001	--	
PAN_{SD}	0.99	-0.15	0.63	0.001	--	
PAN _{SD_AVG41}	0.98	-0.22	0.26	0.001	0.33	<0.001
PAN _{SD_SD41}	0.93	-0.37	0.03	0.414	0.25	0.007
PAN _{AVG_CON03}	0.99	-0.11	0.43	0.001	0.44	<0.001
PAN _{SD_CON03}	0.93	-0.38	0.26	0.001	--	
PAN _{SD_COR03}	-0.96	-0.26	0.05	0.165	--	
PAN_{SD_COR09}	-0.99	-0.17	0.52	0.001	--	
PAN _{SD_COR41}	-1.00	-0.05	0.35	0.001	0.38	<0.001
NDVI_{SD}	0.83	-0.55	0.29	0.001	0.32	<0.001
NDVI _{SD_SD11}	0.44	-0.90	0.11	0.025	0.24	0.005
NDVI _{AVG_CON03}	0.94	-0.35	0.39	0.001	--	
NDVI _{SD_CON03}	0.90	-0.44	0.20	0.002	--	
NDVI _{AVG_COR03}	0.98	-0.22	0.38	0.001	0.42	<0.001
NDVI _{SD_COR03}	1.00	-0.02	0.14	0.010	0.27	0.002
NDVI _{SD_COR05}	-0.74	-0.68	0.01	0.791	--	
NDVI _{SD_COR11}	-1.00	0.10	0.00	0.874	--	
<i>Topographic</i>						
ELEV	-0.16	0.99	0.11	0.026	0.19	0.008
TVI	-0.98	-0.19	0.10	0.040	0.18	0.014
DSR	0.77	0.64	0.07	0.084	--	

Table 5. Results of the forward selection procedure (Blanchet et al. 2008) of geospatial variables for predicting principle component 1 (PC1) and the dominant PC1 forest characteristics (the six forest variables in bold for PC1 in Table 3). Model fit was evaluated using leave-one-out cross validation and the cross validated root mean square error (RMSE) is reported along with the RMSE as a percentage of the range of the response variable.

Response variable	Variable selection			Model fit		
	Geospatial variables	<i>F</i>	<i>P</i>	Cumulative R^2_a	RMSE	% RMSE
PC1	PAN _{SD}	103.0	0.001	0.61	0.431	17.3
	+ PAN _{SD_COR09}	21.8	0.001	0.70	0.377	15.1
Chestnut oak basal area	PAN _{SD}	78.0	0.001	0.54	0.208	19.9
	+ PAN _{SD_COR09}	27.5	0.001	0.67	0.178	17.0
Sugar maple basal area	PAN _{SD}	114.4	0.001	0.63	0.145	16.5
	+ ELEV	4.4	0.044	0.65	0.144	16.4
Total basal area	PAN _{SD}	27.5	0.001	0.29	4.76	16.8
DBH standard deviation	PAN _{SD}	18.8	0.001	0.21	1.80	21.0
	+ PAN _{SD_COR09}	5.0	0.028	0.26	1.76	20.5
Grapevine density	PAN _{SD}	46.7	0.001	0.41	0.594	19.8
	+ TVI	12.1	0.002	0.50	0.554	18.5
	+ PAN _{SD_COR09}	7.2	0.015	0.54	0.534	17.8
Herbaceous % cover	PAN _{SD}	78.4	0.001	0.54	0.182	18.5
	+ PAN _{SD_COR09}	13.9	0.001	0.62	0.167	17.0
	+ ELEV	5.8	0.017	0.64	0.163	16.5

Table 6. Single variable generalized additive model (GAM) results for the species richness measures at the two spatial scales (significant results are underlined). The principal components analysis (PCA) axes PC1 and PC2, which are 50-m scale field habitat data-derived variables (see Figure 3a), are presented for comparison with the 50-m scale geospatial (image and topographic) variables. The 100-m scale geospatial variables are presented for comparison with their respective 50-m scale results.

Category (and scale)	Variable	T ^a	Richness											
			Total			Common			Rare			Gap		
			edf	Wald P	D ² _a	edf	Wald P	D ² _a	edf	Wald P	D ² _a	edf	Wald P	D ² _a
PCA axis (50-m)	PC1	(+)	1.00	<u>0.001</u>	0.10	1.00	<u>0.003</u>	0.11	1.00	0.236	0.00	1.63	<u><0.001</u>	0.36
	PC2		1.00	0.202	0.00	1.00	0.147	0.01	2.01	0.645	0.00	1.00	0.434	0.00
Image (50-m)	PAN _{AVG}	(+)	1.00	<u>0.012</u>	0.05	1.00	<u>0.016</u>	0.06	1.00	0.370	0.00	1.00	<u><0.001</u>	0.25
	PAN _{SD}	(+)	1.00	<u><0.001</u>	0.20	1.00	<u><0.001</u>	0.23	1.00	0.133	0.01	2.04	<u><0.001</u>	0.45
	NDVI _{SD}	(+)	1.00	<u><0.001</u>	0.21	1.00	<u><0.001</u>	0.21	1.87	0.170	0.05	2.66	<u><0.001</u>	0.23
	PAN _{SD_COR09}	(-)	1.00	0.171	0.01	1.00	0.127	0.02	1.00	0.904	0.00	1.00	<u><0.001</u>	0.19
Image (100-m)	PAN _{AVG}	(+)	1.00	0.703	-0.01	1.00	0.719	-0.01	1.60	0.572	0.00	1.00	<u><0.001</u>	0.30
	PAN _{SD}	(+)	1.00	0.057	0.06	1.28	0.123	0.10	1.00	0.426	-0.01	1.00	<u><0.001</u>	0.48
	NDVI _{SD}	(+)	1.60	<u>0.034</u>	0.14	1.00	<u>0.028</u>	0.14	2.01	0.235	0.05	1.36	<u>0.001</u>	0.24
	PAN _{SD_COR09}	(-)	1.00	0.809	-0.01	1.00	0.616	-0.01	1.47	0.692	0.00	1.00	<u><0.001</u>	0.23
Topographic (50-m)	ELEV		2.58	0.072	0.07	2.52	0.116	0.08	1.11	0.228	0.01	2.14	0.568	0.01
	TVI	(-)	1.00	<u>0.043</u>	0.03	1.00	0.148	0.01	1.00	0.107	0.02	1.00	<u>0.024</u>	0.04
	DSR	(+)	1.64	0.430	0.00	1.45	0.731	0.00	1.00	<u>0.048</u>	0.04	3.19	0.091	0.06
Topographic (100-m)	ELEV		2.41	0.148	0.12	2.12	0.336	0.10	1.59	0.478	0.01	1.29	0.533	0.00
	TVI		1.73	0.305	0.05	1.27	0.777	0.00	1.25	0.237	0.02	1.00	0.799	-0.01
	DSR		1.00	0.764	-0.01	1.00	0.336	0.01	1.68	0.485	0.01	1.00	0.567	-0.01

a. For significant results, species richness trend is in relation to increasing forest structural heterogeneity/sugar maple composition (PC1 models), to increasing pixel heterogeneity (image models), and to increasing TVI and DSR (topographic models).

Table 7. Generalized additive model (GAM) multiple variable selection results for the species richness measures at the 50-m scale.

Richness	PC1 models				PAN _{SD} models				NDVI _{SD} models			
	Term	edf ^a	Wald <i>P</i>	<i>D</i> ² _a	Term	edf ^a	Wald <i>P</i>	<i>D</i> ² _a	Term	edf ^a	Wald <i>P</i>	<i>D</i> ² _a
Total	PC1	0.85	0.009	0.17	PAN _{SD}	0.94	<0.001	0.27	NDVI _{SD}	0.95	<0.001	0.31
	ELEV	1.35	0.011		ELEV	1.20	0.025		ELEV	0.97	0.088	
	TVI	0.62	0.100		TVI	0.72	0.060		TVI	0.88	0.004	
Common	PC1	0.87	0.005	0.16	PAN _{SD}	0.94	<0.001	0.27	NDVI _{SD}	0.94	<0.001	0.29
	ELEV	1.16	0.047		ELEV	0.96	0.083		ELEV	0.84	0.154	
	TVI	0			TVI	0.36	0.210		TVI	0.80	0.027	
Rare	PC1	0		0.05	PAN _{SD}	0.41	0.190	0.05	NDVI _{SD}	1.11	0.040	0.08
	ELEV	0.83	0.112		ELEV	0.76	0.140		ELEV	0.32	0.255	
	TVI	0.67	0.082		TVI	0.63	0.100		TVI	0.72	0.059	
Gap	PC1	1.55	<0.001	0.36	PAN _{SD}	1.96	<0.001	0.47	NDVI _{SD}	2.24	<0.001	0.30
	ELEV	0			ELEV	0			ELEV	0.12	0.298	
	TVI	0			TVI	0.59	0.120		TVI	0.87	0.005	

a. Double penalized estimated degrees of freedom (Marra and Wood 2011). If edf = 0 then the term was completely penalized out of the model.

Table 8. Generalized additive model (GAM) multiple variable selection results for the addition of image variables to the best single image/topographic variable models for total, common, and rare species richness at the 50-m scale.

Total species richness				Common species richness				Rare species richness			
Term	edf ^a	Wald <i>P</i>	<i>D</i> ² _a	Term	edf ^a	Wald <i>P</i>	<i>D</i> ² _a	Term	edf ^a	Wald <i>P</i>	<i>D</i> ² _a
NDVI _{SD}	0.96	<0.001	0.42	NDVI _{SD}	0.94	<0.001	0.39	NDVI _{SD}	0.61	0.102	0.16
ELEV	1.25	0.062		ELEV	1.29	0.096		ELEV	0.21	0.251	
TVI	0.87	0.006		TVI	0.79	0.029		TVI	0.68	0.075	
PAN _{SD_COR03}	1.59	0.003		PAN _{SD_COR03}	1.38	0.017		NDVI _{SD_COR03}	1.60	0.011	

a. Double penalized estimated degrees of freedom (Marra and Wood 2011).

Table 9. Best single image variable generalized additive models (GAMs) for total, common, and gap species richness in 2009-11 at the two spatial scales using the reduced dataset of 42 sampling points (significant results are underlined). No significant results were found for rare species richness (not reported).

		Year (n = 42 sampling points each year)								
Richness	Model	2009			2010			2011		
		edf	Wald <i>P</i>	<i>D</i> ² _{<i>a</i>}	edf	Wald <i>P</i>	<i>D</i> ² _{<i>a</i>}	edf	Wald <i>P</i>	<i>D</i> ² _{<i>a</i>}
<i>Total</i>										
50 m	NDVI _{SD}	1.00	0.203	0.02	3.06	0.064	0.20	1.00	<u><0.001</u>	0.16
100 m	NDVI _{SD}	1.00	0.266	0.03	2.02	0.294	0.12	1.69	0.097	0.17
<i>Common</i>										
50 m	NDVI _{SD}	1.00	0.186	0.05	2.86	0.196	0.22	1.00	<u>0.002</u>	0.19
100 m	NDVI _{SD}	1.00	0.417	0.02	1.86	0.475	0.11	1.00	0.088	0.11
<i>Gap</i>										
50 m	PAN _{SD}	1.00	<u><0.001</u>	0.28	1.06	<u>0.012</u>	0.18	2.12	<u><0.001</u>	0.44
100 m	PAN _{SD}	1.00	<u><0.001</u>	0.45	1.00	<u>0.003</u>	0.28	1.00	<u><0.001</u>	0.47

Table 10. Single variable generalized additive model (GAM) results for species occurrence (50-m scale) and abundance (100-m scale) for the species with at least one significant effect (underlined) found for the principal component 1 (PC1) and best image texture models. The number of absences (N = 0) and presences (N = 1) for each species over the 68 sampling points at the 50-m scale are also provided.

Species	PC1 models						Best image textures models								
	N (50 m)		50 m occurrence				Model	T ^a	50 m occurrence				100 m abundance		
	0	1	T ^a	edf	Wald <i>P</i>	<i>D</i> ² _{<i>a</i>}			edf	Wald <i>P</i>	<i>D</i> ² _{<i>a</i>}	edf	Wald <i>P</i>	<i>D</i> ² _{<i>a</i>}	
American Redstart	36	32		2.06	0.428	0.02	NDVI _{SD}	(+)	1.00	<u>0.043</u>	0.03	1.00	<u>0.023</u>	0.05	
Black-and-white Warbler	32	36		1.00	0.691	0.00	NDVI _{SD}	(+)	1.00	<u>0.007</u>	0.08	1.00	0.744	0.00	
Cerulean Warbler	45	23		1.00	0.151	0.01	PAN _{SD}	(+)	1.00	<u>0.029</u>	0.04	1.76	0.268	0.04	
Eastern Towhee ^b	39	29	(+)	1.00	<u>0.002</u>	0.11	PAN _{SD}	(+)	1.44	<u><0.001</u>	0.23	1.00	<u><0.001</u>	0.25	
Eastern Wood-Pewee	40	28	(-)	1.73	<u>0.002</u>	0.25	PAN _{SD_COR09}	(+)	1.00	<u><0.001</u>	0.19	2.50	<u>0.003</u>	0.40	
Hairy Woodpecker	53	15		1.00	0.108	0.03	PAN _{SD}	(-)	2.09	0.157	0.08	1.00	<u>0.048</u>	0.06	
Hooded Warbler ^b	27	41	(+)	1.00	<u><0.001</u>	0.22	PAN _{SD}	(+)	1.22	<u><0.001</u>	0.28	1.00	<u>0.004</u>	0.20	
Indigo Bunting ^{b, c}	61	7		1.82	0.092	0.26	PAN _{SD}	(+)	2.25	0.135	0.27	1.00	<u>0.001</u>	0.41	
Kentucky Warbler ^{b, c}	61	7	(+)	1.00	<u>0.009</u>	0.21	PAN _{SD}	(+)	1.00	<u>0.008</u>	0.28	1.00	<u>0.006</u>	0.11	
Northern Cardinal ^b	49	19	(+)	1.97	<u>0.013</u>	0.15	PAN _{SD}	(+)	2.56	<u>0.041</u>	0.18	2.20	<u>0.012</u>	0.25	
Ovenbird	34	34	(+)	1.00	<u>0.008</u>	0.07	PAN _{SD}	(+)	1.00	<u>0.022</u>	0.05	1.00	0.090	0.04	
Red-eyed Vireo	16	52		1.00	0.052	0.04	PAN _{SD}	(+)	1.00	<u>0.042</u>	0.05	1.00	0.121	0.07	
Rose-breasted Grosbeak	57	11		2.01	0.283	0.04	PAN _{SD}	(+)	1.00	<u>0.045</u>	0.06	1.00	<u>0.026</u>	0.07	

a. Trend (+ = positive, - = negative) is in relation to increasing forest structural heterogeneity/sugar maple composition (significant PC1 models) and to increasing pixel heterogeneity (significant best image texture models).

b. Included in canopy gap-associated species richness.

c. Binomial 100 m occurrence model applied because relative abundance per sampling point was not higher than 1

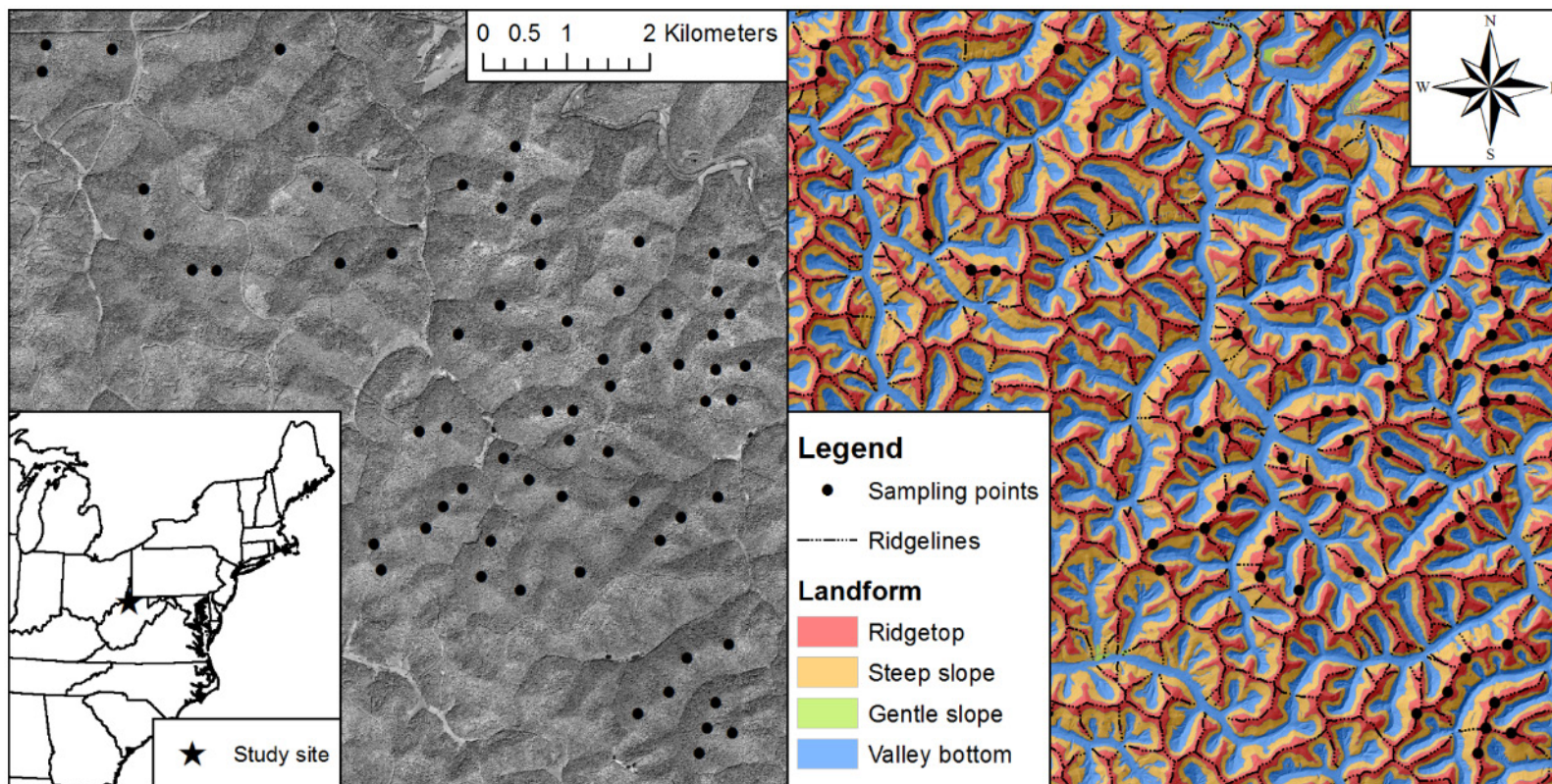


Figure 1. Study site at the Lewis Wetzel Wildlife Management Area in northwest WV, with the 68 ridgetop sampling point locations shown on the August 2009 QuickBird satellite panchromatic (0.6-m resolution) image (left). The points were located >150 m from anthropogenic forest impacts on the ridgeline (i.e., the crest) of prominent ridges (right), spaced ≥ 250 m apart for avian point count survey considerations. The 4-landform classification was obtained from a 3-m digital elevation model (used here as a shaded-relief underlay of the landform classification set at 50% transparency) using the Topographic Position Index function in Topography Tools for ArcGIS 10.1 (Dilts 2015).

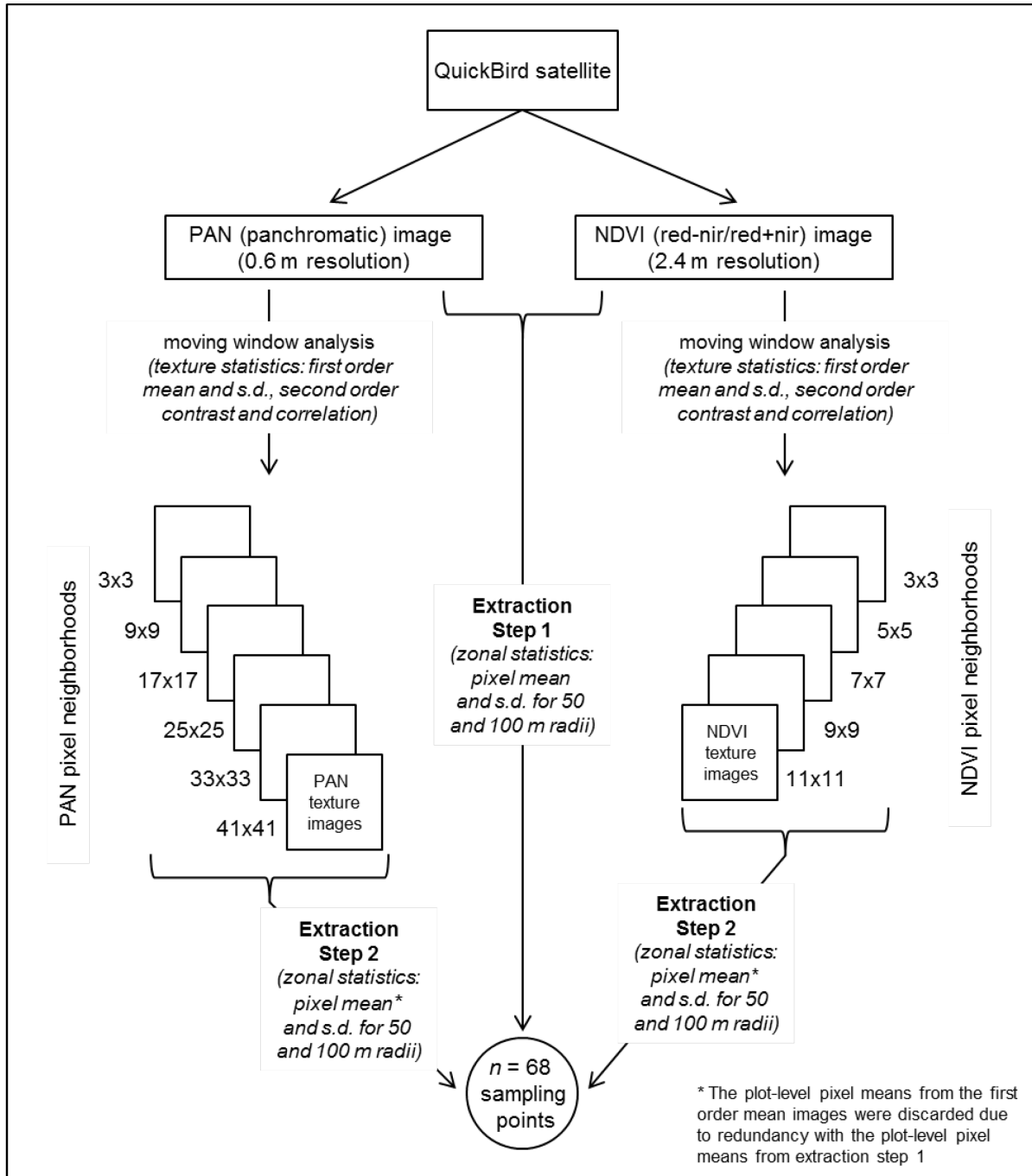
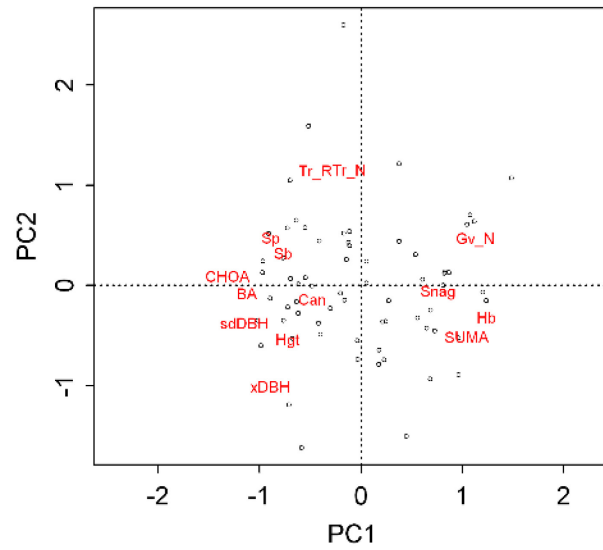
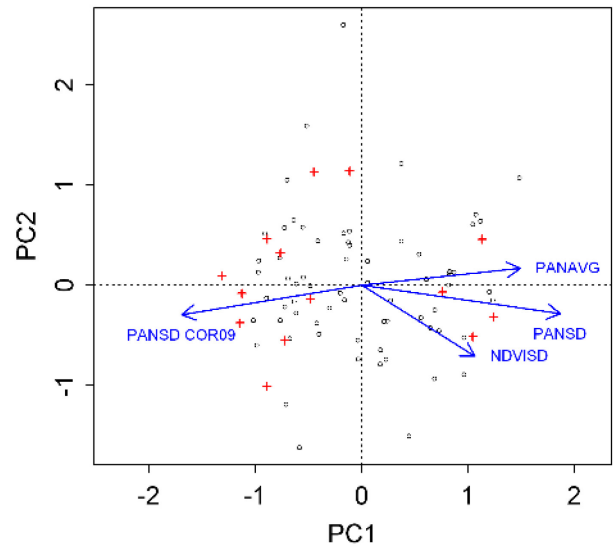


Figure 2. Diagram of the QuickBird satellite image processing and extraction of the zonal statistics (i.e., the image variables used in the analyses) for the 68 sampling point locations at the 50- and 100-m radius plot-level scales. In extraction step 1, the zonal statistics were obtained directly from the PAN and NDVI images. In extraction step 2, the zonal statistics were obtained from images of first- and second-order texture statistics processed from the PAN and NDVI images.

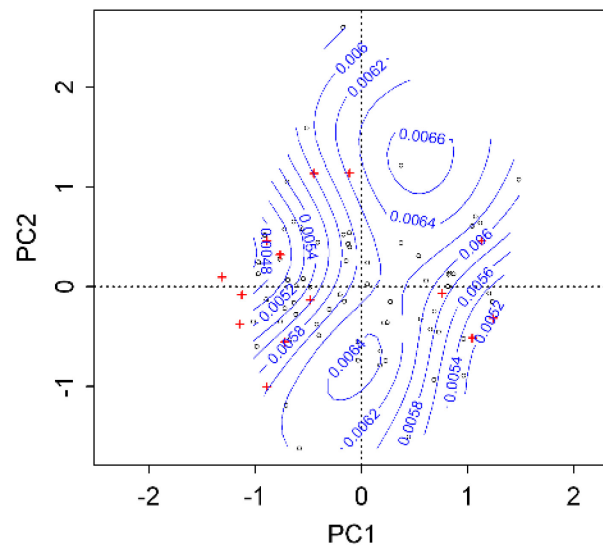
(a) PC1:PC2 ordination plot



(b) Image variable vector fits



(c) PAN_{SD}_SD41 surface fit



(d) NDVI_{SD}_SD11 surface and vector fits

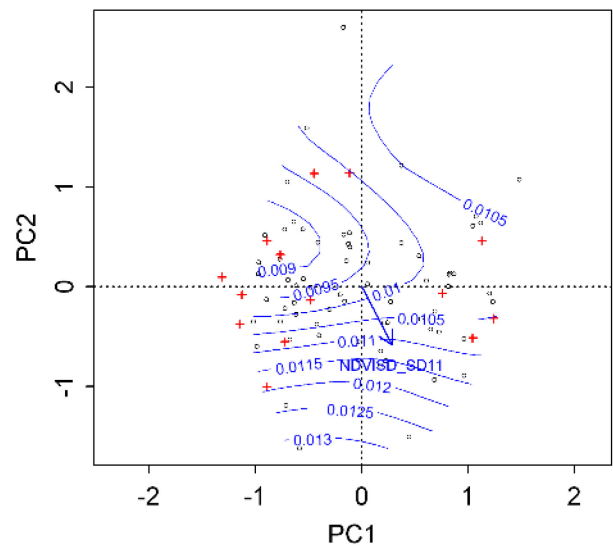
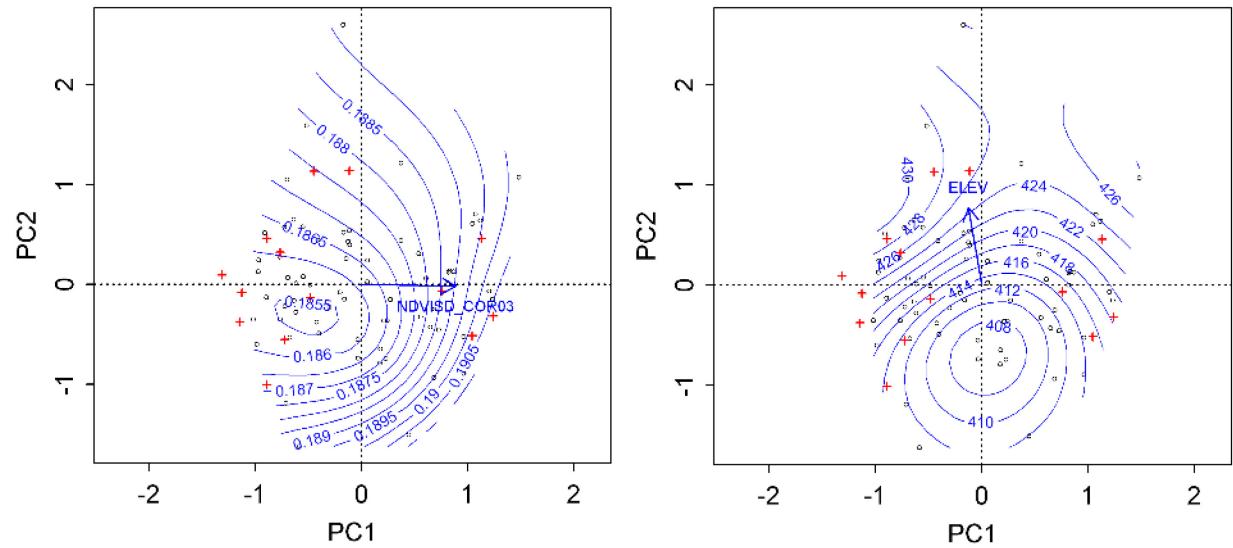


Figure 3. Principal components analysis (PCA) results and geospatial variable fits. See Table 3 for the key to the forest variable labels for the PC1:PC2 (principal components 1 and 2) ordination plot, and Table 4 for the vector and surface fits (R^2) of the geospatial variables to the PC1:PC2 ordination plot.

(f) ELEV surface and vector fits



(g) TVI surface and vector fits

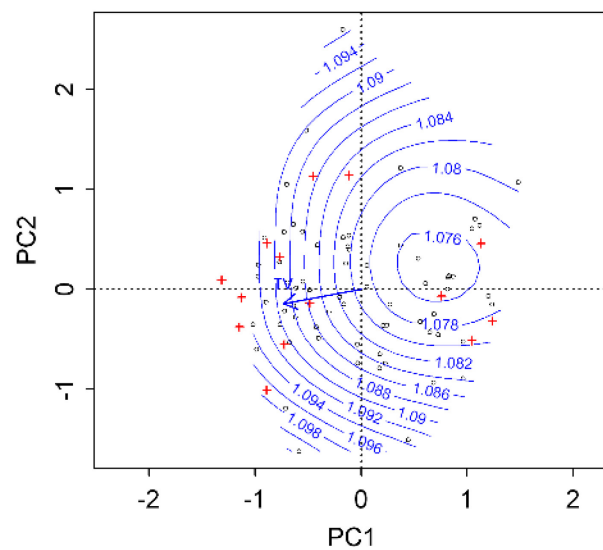


Figure 3. cont. Principal components analysis (PCA) results and geospatial variable fits. See Table 3 for the key to the forest variable labels for the PC1:PC2 (principal components 1 and 2) ordination plot, and Table 4 for the vector and surface fits (R^2) of the geospatial variables to the PC1:PC2 ordination plot.

Panchromatic image (0.6 m resolution) 50 m radius plot PC1 scores

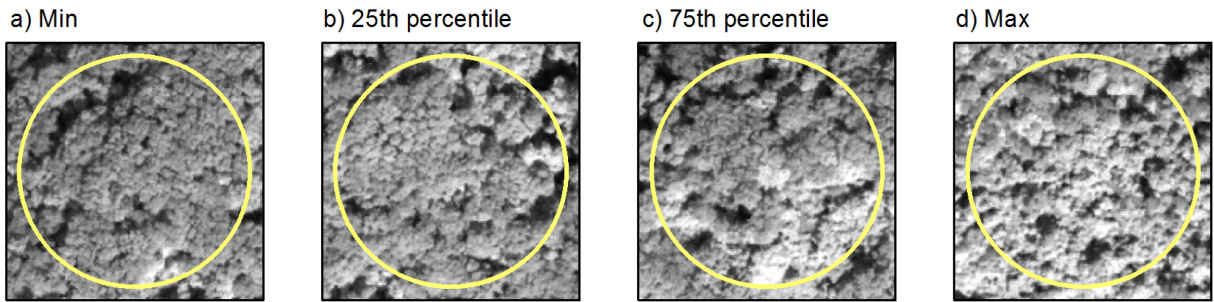
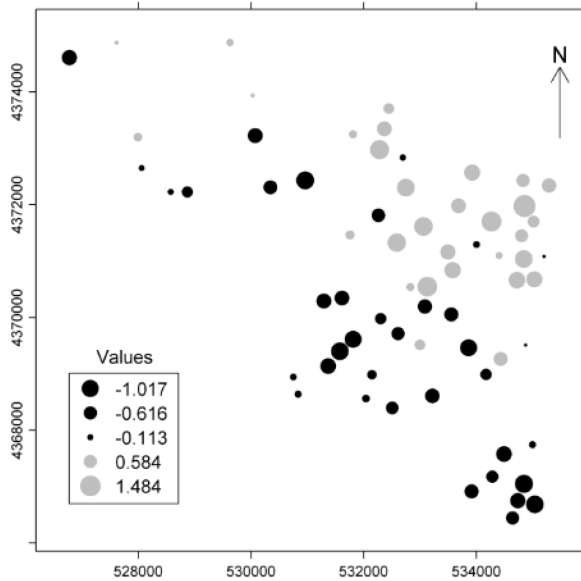
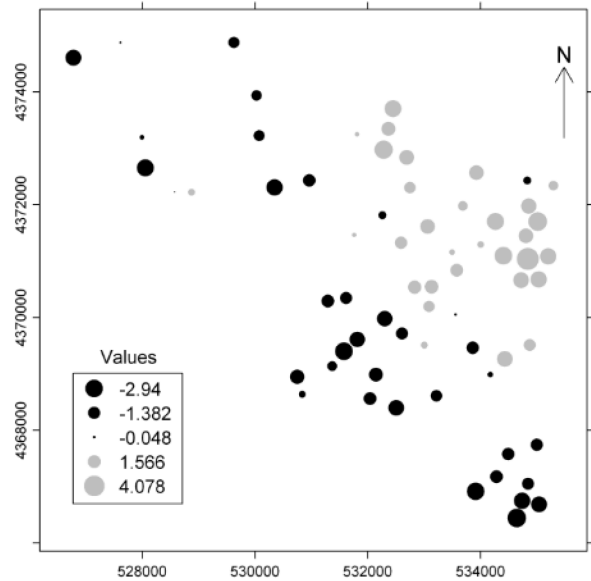
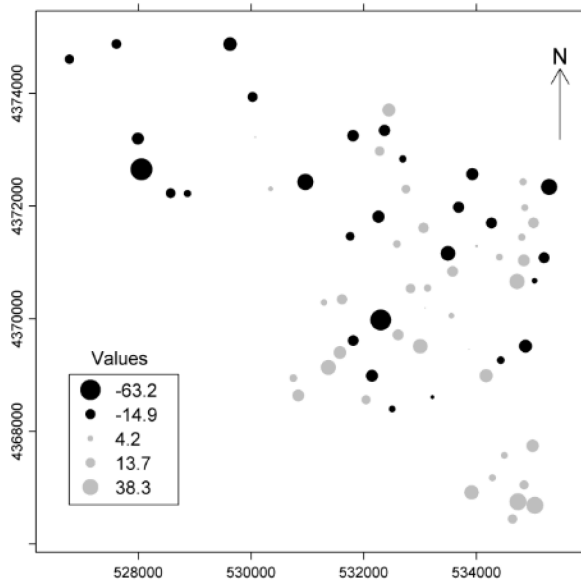


Figure 4. Sampling point images ranked by principal component 1 (PC1) scores. The sampling points with the minimum and 25th percentile values (negative PC1 scores; see Figure 3a) are dominated by a smooth canopy. The sampling points with the 75th percentile and maximum values (positive PC1 scores; see Figure 3a) exhibit a more heterogeneous canopy, with distinctly brighter patches of pixels that likely indicate greater reflectance by understory vegetation in canopy gaps and/or grapevines.

(a) PC1

(b) PAN_{SD}

(c) ELEV



(d) TVI

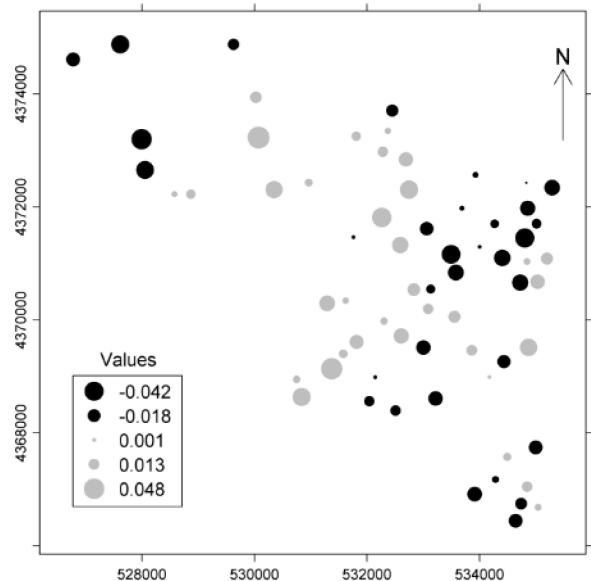


Figure 5. Spatial bubble plots of principal component 1 (PC1) scores and select geospatial variables for the 68 sampling points. The x- and y-axes are in Universal Transverse Mercator Zone 17, North American Datum 1983 coordinates. The sizes of the points are in proportion to their values. The values for PAN_{SD}, elevation (ELEV), and the topographic variation index (TVI) were mean-centered to more clearly illustrate spatial patterns.

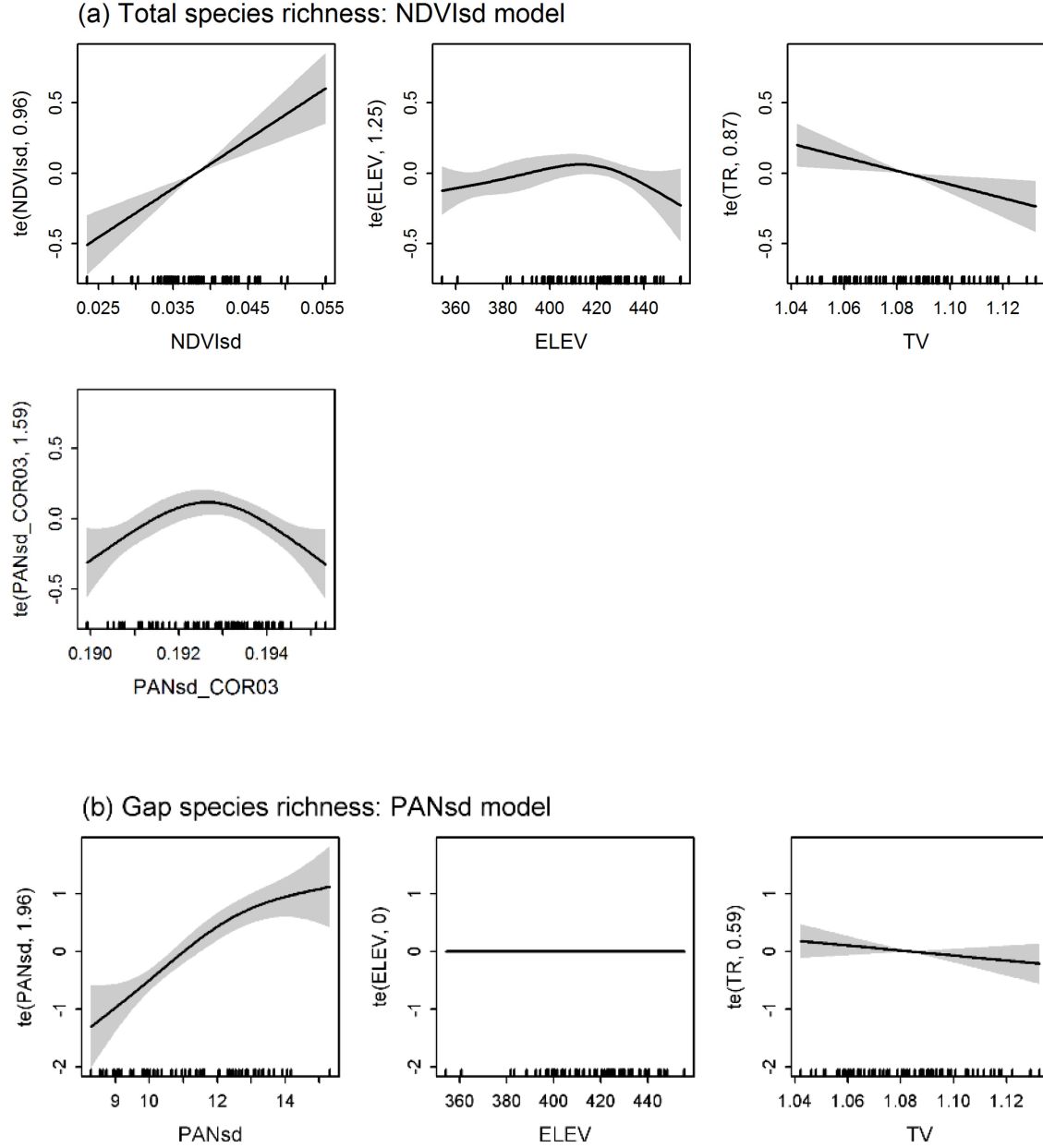
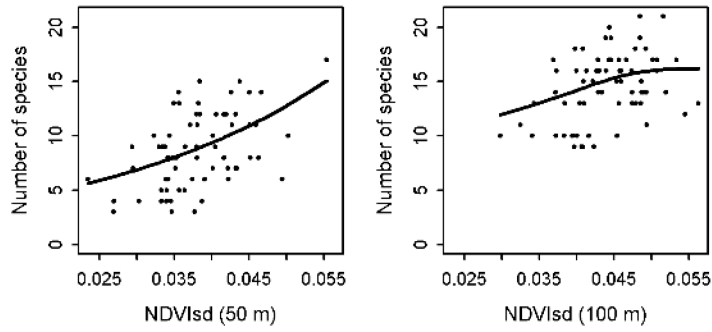


Figure 6. Generalized additive model (GAM) response curves for the best-fitting multiple variable models for (a) total and (b) gap species richness at the 50-m scale. The curves show the functional forms of the responses (with 95% confidence bands) to the geospatial variables. The y-axes are at the scale of the linear predictor, and the labels provide the estimated degrees of freedom (e.d.f.) of the scale-invariant tensor product (te) smooths used in the GAMs to obtain the response curves. The tick marks above the x-axes indicate the geospatial variable values for the 68 sampling points. Note that for gap species richness, elevation was effectively removed as an effect (e.d.f. ≈ 0) by the GAM variable selection technique (Marra and Wood 2011).

(a) Total species richness: NDVI_{sd} 50 and 100 m models



(b) Gap species richness: PAN_{sd} 50 and 100 m models

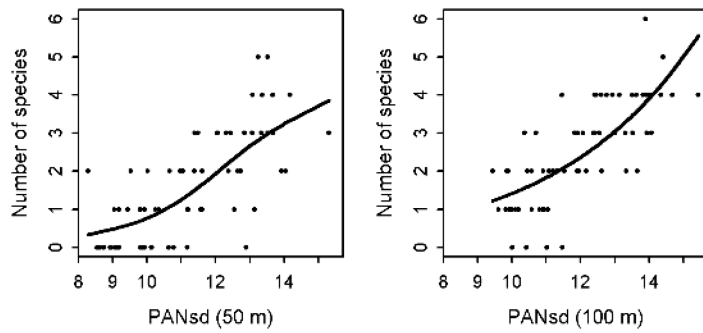
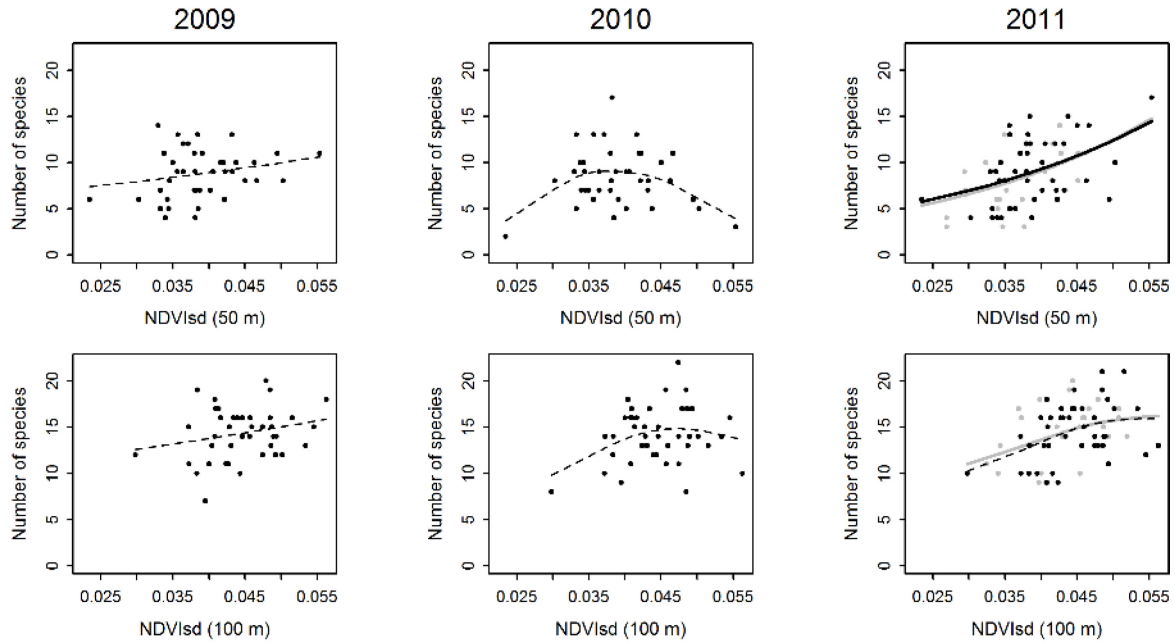


Figure 7. Generalized additive model (GAM) response curves plotted at the scale of the original response data (number of species) from the overall best-fitting single variable models for (a) total and (b) gap species richness at the 50- and 100-m scales. The dots indicate the individual richness values for the sampling points ($n = 68$).

(a) Total species richness: NDVI_{SD} models



(b) Gap species richness: PAN_{SD} models

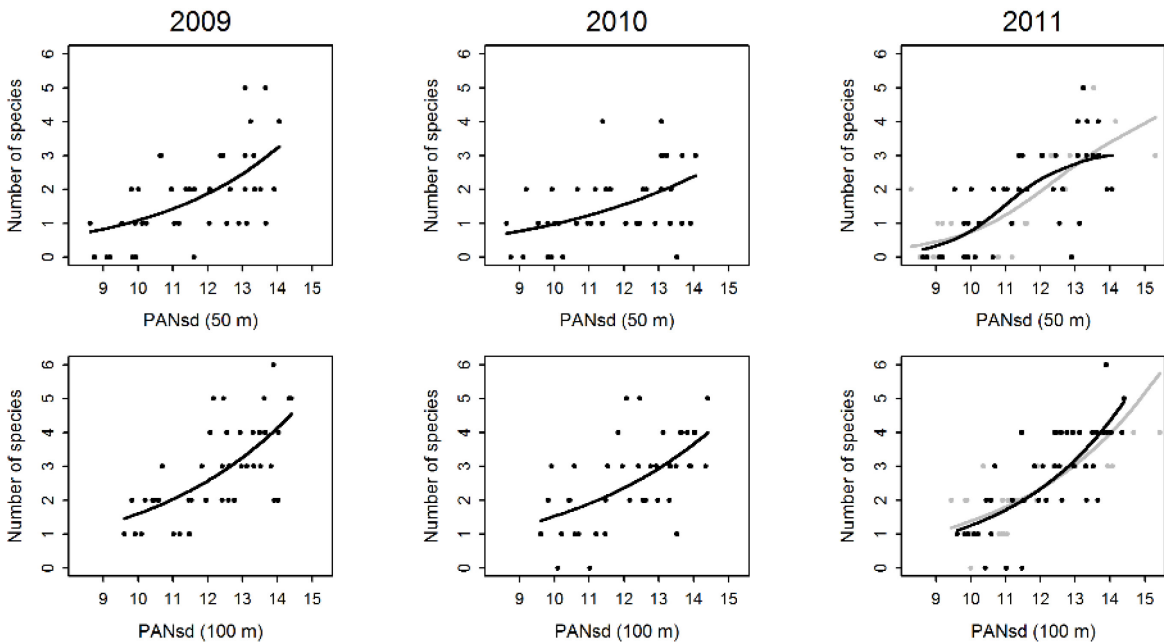


Figure 8. Annual generalized additive model (GAM) response curves plotted at the scale of the original response data (number of species) for (a) total and (b) gap species richness at the 50- and 100-m scales using the 42 sampling points surveyed 2009-11 (solid lines = significant trends). The black dots indicate the individual richness values for the sampling points. For the 2011 graphs, the GAM response curves using the 68 total sampling points, and the individual species richness values for the 26 additional 2011 points, are shown in gray.

Appendix A. Bird species common names, scientific names, detection type(s) used for the analysis, and relatively common/relatively rare designation.

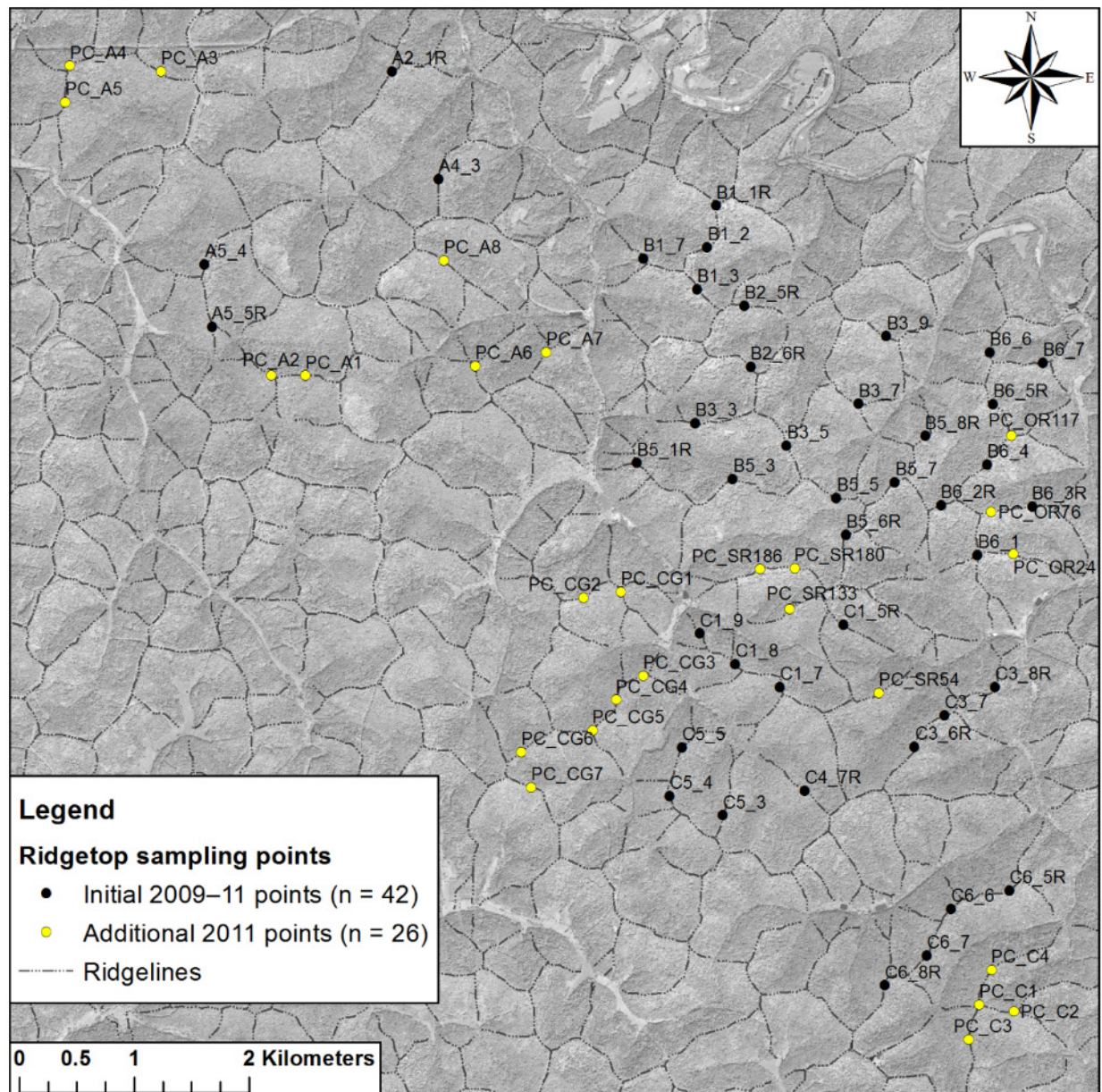
Common name ^a	Scientific name	Detection type(s)	(C)ommon or (R)are
Acadian Flycatcher	<i>Empidonax vireescens</i>	song	R
<u>American Redstart</u>	<i>Setophaga ruticilla</i>	song	C
<u>American Robin</u>	<i>Turdus migratorius</i>	song + call	C
Baltimore Oriole	<i>Icterus galbula</i>	song	R
<u>Black-and-white Warbler</u>	<i>Mniotilta varia</i>	song	C
Black-throated Green Warbler	<i>Setophaga virens</i>	song	R
<u>Blue-gray Gnatcatcher</u>	<i>Poliophtila caerulea</i>	song + call	R
Blue-headed Vireo	<i>Vireo solitarius</i>	song	R
<u>Blue Jay</u>	<i>Cyanocitta cristata</i>	call + visual	C
Blue-winged Warbler	<i>Vermivora cyanoptera</i>	song	R
<u>Carolina Chickadee</u>	<i>Poecile carolinensis</i>	song + call	R
Carolina Wren	<i>Thryothorus ludovicianus</i>	song	R
<u>Cerulean Warbler</u>	<i>Setophaga cerulea</i>	song	C
<u>Downy Woodpecker</u>	<i>Picoides pubescens</i>	call + visual	R
<u>Eastern Towhee</u>	<i>Pipilo erythrophthalmus</i>	song + call	C
<u>Eastern Wood-Pewee</u>	<i>Contopus virens</i>	song	C
Great-crested Flycatcher	<i>Picoides villosus</i>	call	R
<u>Hairy Woodpecker</u>	<i>Picoides villosus</i>	call + visual	R
<u>Hooded Warbler</u>	<i>Setophaga citrina</i>	song	C
<u>Indigo Bunting</u>	<i>Passerina cyanea</i>	song	R
<u>Kentucky Warbler</u>	<i>Geothlypis formosus</i>	song	R
Mourning Dove	<i>Zenaida macroura</i>	song	R
<u>Northern Cardinal</u>	<i>Cardinalis cardinalis</i>	song	C
Northern Flicker	<i>Colaptes auratus</i>	call + visual	R
Northern Parula Warbler	<i>Seiurus aurocapilla</i>	song	R
<u>Ovenbird</u>	<i>Seiurus aurocapilla</i>	song	C
Pileated Woodpecker	<i>Dryocopus pileatus</i>	call + visual	R
Red-bellied Woodpecker	<i>Melanerpes carolinus</i>	call + visual	R
<u>Red-eyed Vireo</u>	<i>Vireo olivaceus</i>	song	C
<u>Rose-breasted Grosbeak</u>	<i>Pheucticus ludovicianus</i>	song	C
Ruby-throated Hummingbird	<i>Archilochus colubris</i>	call + visual	R
<u>Scarlet Tanager</u>	<i>Piranga olivacea</i>	song	C
<u>Tufted Titmouse</u>	<i>Baeolophus bicolor</i>	song + call	C
<u>White-breasted Nuthatch</u>	<i>Sitta carolinensis</i>	call	C
<u>Wood Thrush</u>	<i>Hylocichla mustelina</i>	song	C
Worm-eating Warbler	<i>Helmitheros vermivorum</i>	song	R
<u>Yellow-billed Cuckoo</u>	<i>Coccyzus americanus</i>	call	R
<u>Yellow-throated Vireo</u>	<i>Vireo flavifrons</i>	song	R

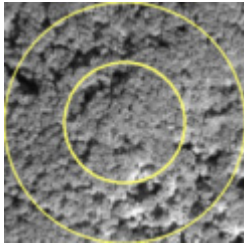
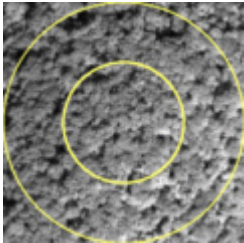
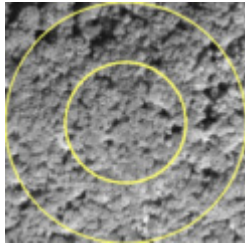
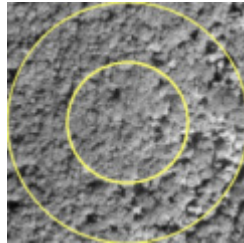
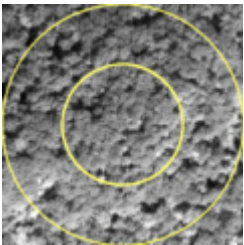
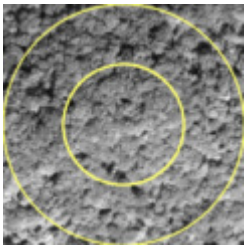
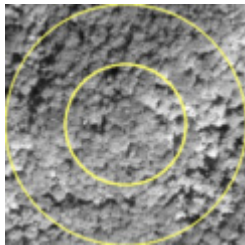
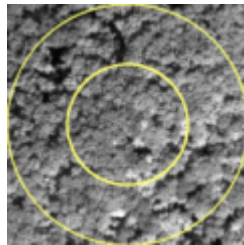
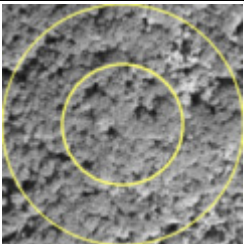
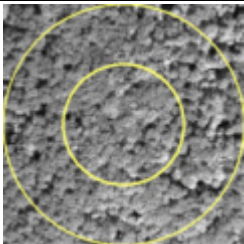
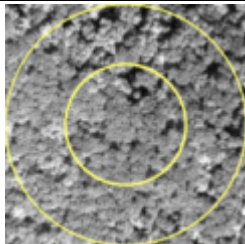
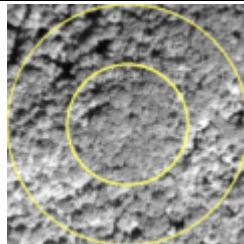
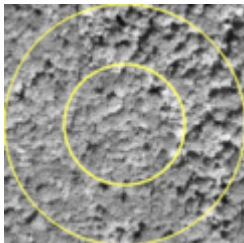
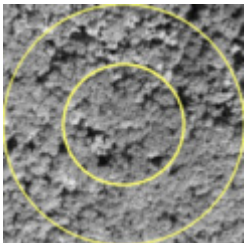
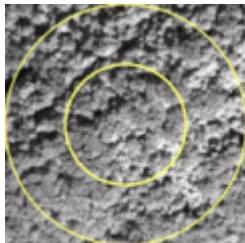
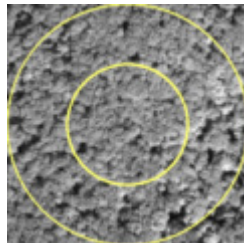
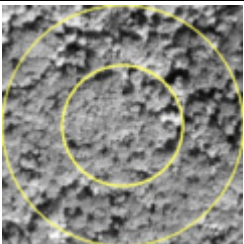
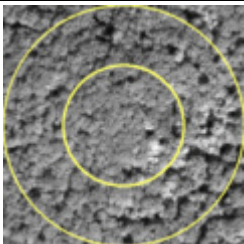
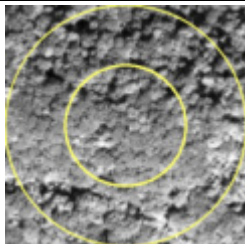
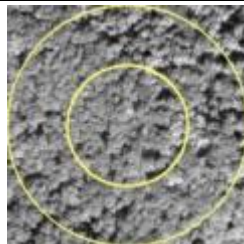
^a Species in bold (n=6) are those whose occurrences appeared to be most closely tied to distinct canopy gaps in this forest and those underlined (n=24) were analyzed with binomial (occurrence) models.

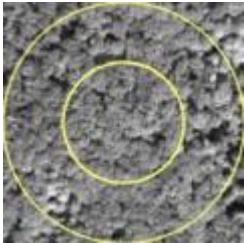
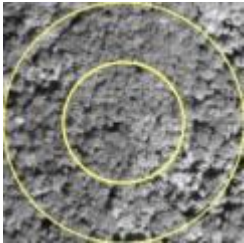
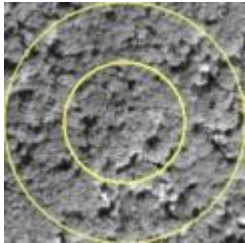
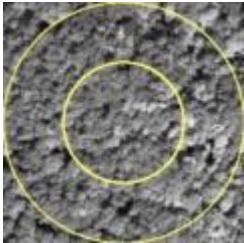
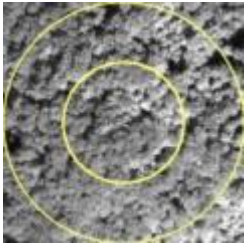
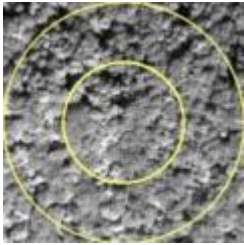
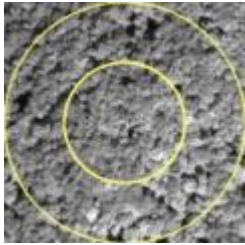
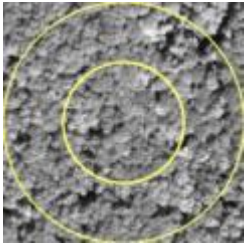
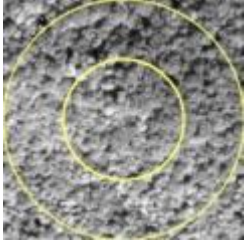
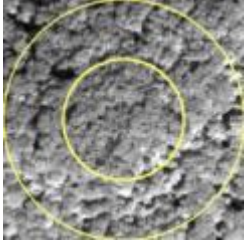
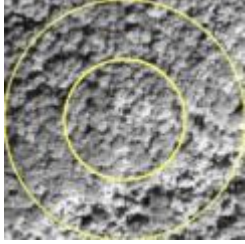
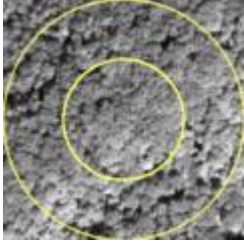
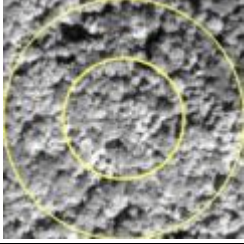
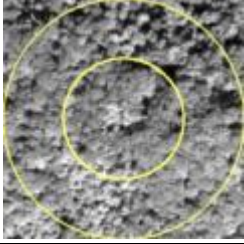
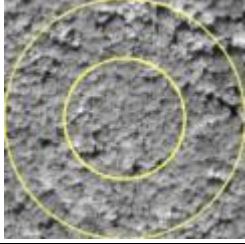
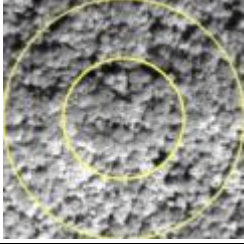
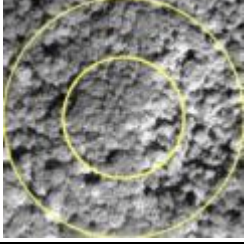
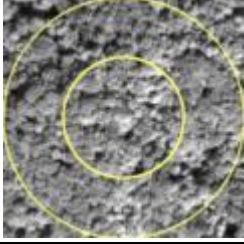
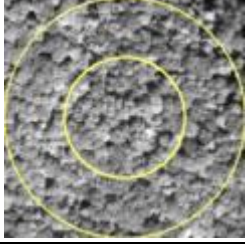
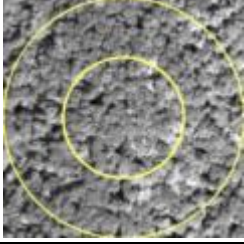
Appendix B. Spearman's correlations for the reduced set of geospatial variables. See Appendix D for the full set of correlations.

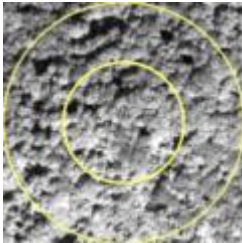
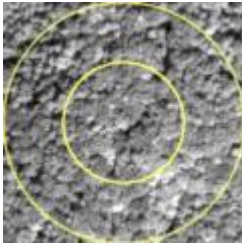
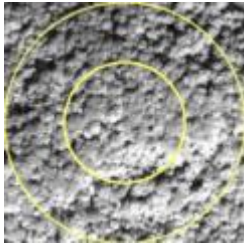
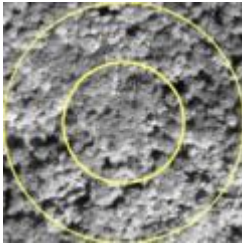
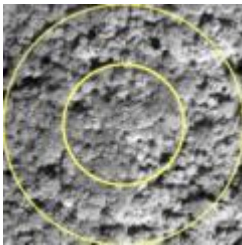
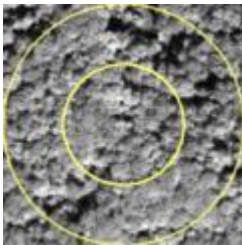
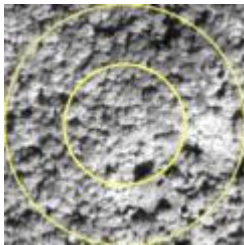
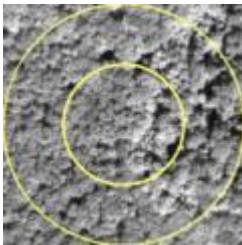
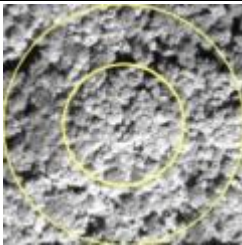
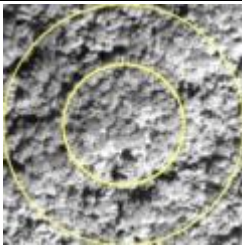
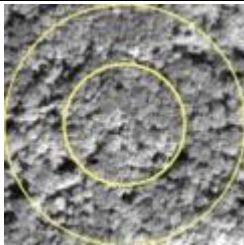
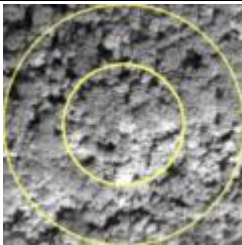
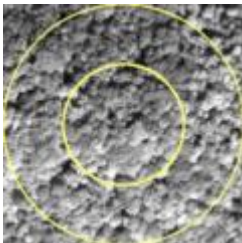
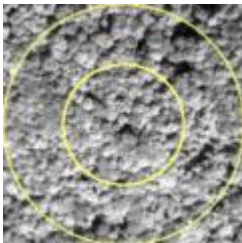
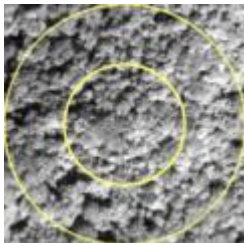
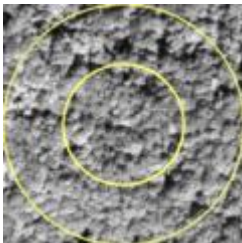
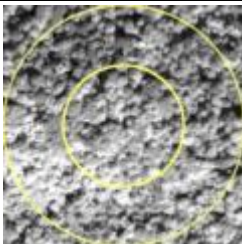
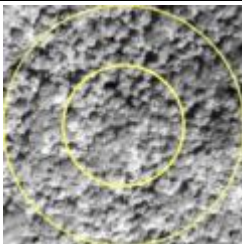
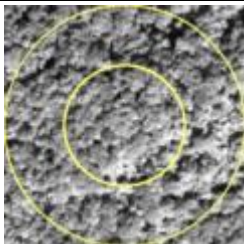
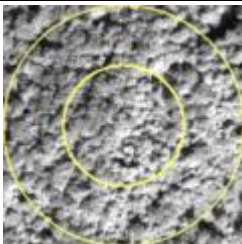
	PAN _{AVG}	PAN _{SD}	PAN _{SD_AVG41}	PAN _{SD_SD41}	PAN _{AVG_CON03}	PAN _{SD_CON03}	PAN _{SD_COR03}	PAN _{SD_COR09}	PAN _{SD_COR41}	NDVI _{SD}	NDVI _{SD_SD11}	NDVI _{AVG_CON03}	NDVI _{SD_CON03}	NDVI _{AVG_COR03}	NDVI _{SD_COR03}	NDVI _{SD_COR05}	NDVI _{SD_COR11}	ELEV	TVI	DSR
PAN _{AVG}		0.69	0.51	0.16	0.78	0.49	-0.26	-0.55	-0.54	0.17	0.04	0.14	0.23	0.32	0.18	-0.19	-0.08	0.18	-0.16	0.62
PAN _{SD}	0.69		0.76	0.33	0.74	0.64	-0.32	-0.60	-0.60	0.74	0.45	0.62	0.56	0.76	0.43	0.04	0.05	0.00	-0.07	0.25
PAN _{SD_AVG41}	0.51	0.76		0.16	0.52	0.30	-0.32	-0.40	-0.46	0.65	0.37	0.41	0.37	0.56	0.21	0.02	0.10	-0.05	0.11	0.07
PAN _{SD_SD41}	0.16	0.33	0.16		0.10	0.21	0.08	0.07	0.30	0.36	0.60	0.04	0.33	0.32	0.04	0.17	0.23	0.07	0.11	-0.10
PAN _{AVG_CON03}	0.78	0.74	0.52	0.10		0.71	-0.03	-0.51	-0.60	0.27	0.11	0.36	0.36	0.33	0.21	-0.26	-0.10	0.04	-0.11	0.36
PAN _{SD_CON03}	0.49	0.64	0.30	0.21	0.71		0.13	-0.24	-0.29	0.45	0.35	0.36	0.38	0.33	0.37	0.05	-0.03	0.09	0.05	0.14
PAN _{SD_COR03}	-0.26	-0.32	-0.32	0.08	-0.03	0.13		0.49	0.34	-0.25	0.07	-0.40	-0.19	-0.42	-0.13	-0.07	-0.01	0.09	0.15	-0.21
PAN _{SD_COR09}	-0.55	-0.60	-0.40	0.07	-0.51	-0.24	0.49		0.76	-0.27	0.08	-0.55	-0.23	-0.48	-0.23	0.19	0.06	-0.06	0.28	-0.34
PAN _{SD_COR41}	-0.54	-0.60	-0.46	0.30	-0.60	-0.29	0.34	0.76		-0.21	0.24	-0.55	-0.25	-0.43	-0.13	0.34	0.32	0.02	0.33	-0.40
NDVI _{SD}	0.17	0.74	0.65	0.36	0.27	0.45	-0.25	-0.27	-0.21		0.72	0.65	0.52	0.72	0.47	0.36	0.25	-0.13	0.10	-0.06
NDVI _{SD_SD11}	0.04	0.45	0.37	0.60	0.11	0.35	0.07	0.08	0.24	0.72		0.23	0.35	0.38	0.30	0.35	0.44	-0.03	0.32	-0.24
NDVI _{AVG_CON03}	0.14	0.62	0.41	0.04	0.36	0.36	-0.40	-0.55	-0.55	0.65	0.23		0.56	0.57	0.37	0.07	-0.01	-0.18	-0.13	0.01
NDVI _{SD_CON03}	0.23	0.56	0.37	0.33	0.36	0.38	-0.19	-0.23	-0.25	0.52	0.35	0.56		0.39	0.29	0.20	-0.05	-0.07	0.02	0.01
NDVI _{AVG_COR03}	0.32	0.76	0.56	0.32	0.33	0.33	-0.42	-0.48	-0.43	0.72	0.38	0.57	0.39		0.33	0.05	0.13	-0.09	-0.15	0.02
NDVI _{SD_COR03}	0.18	0.43	0.21	0.04	0.21	0.37	-0.13	-0.23	-0.13	0.47	0.30	0.37	0.29	0.33		0.39	0.11	-0.01	0.12	0.03
NDVI _{SD_COR05}	-0.19	0.04	0.02	0.17	-0.26	0.05	-0.07	0.19	0.34	0.36	0.35	0.07	0.20	0.05	0.39		0.44	-0.02	0.12	-0.16
NDVI _{SD_COR11}	-0.08	0.05	0.10	0.23	-0.10	-0.03	-0.01	0.06	0.32	0.25	0.44	-0.01	-0.05	0.13	0.11	0.44		0.09	0.09	-0.06
ELEV	0.18	0.00	-0.05	0.07	0.04	0.09	0.09	-0.06	0.02	-0.13	-0.03	-0.18	-0.07	-0.09	-0.01	-0.02	0.09		0.00	0.15
TVI	-0.16	-0.07	0.11	0.11	-0.11	0.05	0.15	0.28	0.33	0.10	0.32	-0.13	0.02	-0.15	0.12	0.12	0.09	0.00		-0.43
DSR	0.62	0.25	0.07	-0.10	0.36	0.14	-0.21	-0.34	-0.40	-0.06	-0.24	0.01	0.01	0.02	0.03	-0.16	-0.06	0.15	-0.43	

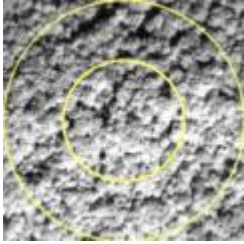
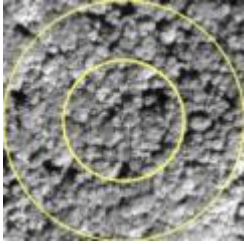
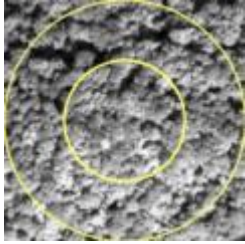
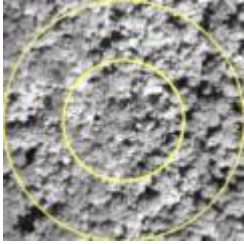
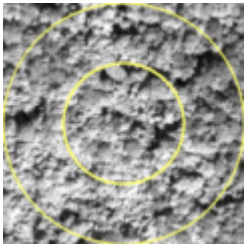
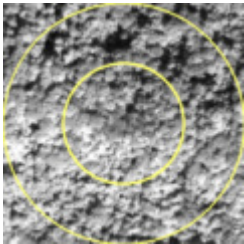
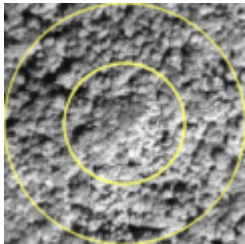
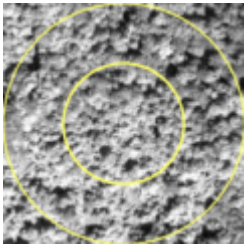
Appendix C. Overview map of the 68 sampling points and the Quickbird satellite 0.6-m panchromatic band images of the points ordered by their principal component 1 (PC1) scores from the principal components analysis (PCA) of the field habitat data (collected within the inner 50-m radius circle). For the images, the value in the parentheses is the 50-m radius pixel s.d. (PAN_{SD}), with the numeric rank for the point from low to high PAN_{SD} in brackets. Image labels for the 26 points added in 2011 are in bold.



			
-1.017 PC_C4 (9.938 [22])	-0.987 PC_A7 (9.842 [17])	-0.970 PC_C2 (9.056 [7])	-0.969 PC_CG4 (8.547 [2])
			
-0.909 PC_SR54 (9.845 [18])	-0.894 PC_CG3 (9.191 [11])	-0.768 PC_CG5 (10.357 [28])	-0.764 C6_6 (9.849 [19])
			
-0.724 PC_C1 (8.959 [6])	-0.720 PC_A5 (9.082 [8])	-0.711 PC_A8 (10.145 [26])	-0.700 PC_CG2 (9.797 [14])
			
-0.694 PC_CG1 (9.939 [23])	-0.674 C4_7R (10.020 [24])	-0.637 PC_SR133 (12.311 [46])	-0.635 C6_8R (8.631 [3])
			
-0.617 C1_5R (11.178 [34])	-0.614 PC_A6 (8.934 [5])	-0.583 B3_3 (10.643 [29])	-0.552 C1_8 (9.932 [21])

			
-0.548 PC_C3 (8.286 [1])	-0.516 C5_3 (9.103 [9])	-0.484 C6_7 (9.811 [15])	-0.420 C1_9 (9.190 [10])
			
-0.412 C3_6R (10.968 [32])	-0.399 PC_A1 (11.606 [42])	-0.302 C5_5 (9.541 [13])	-0.203 C5_4 (9.814 [16])
			
-0.172 PC_CG7 (10.790 [31])	-0.168 C6_5R (9.922 [20])	-0.163 B5_7 (11.604 [41])	-0.142 PC_CG6 (9.442 [12])
			
-0.125 B2_5R (13.131 [57])	-0.113 PC_A2 (11.214 [36])	-0.111 A5_5R (8.748 [4])	-0.036 B6_3R (13.525 [61])
			
-0.032 C3_8R (12.447 [48])	0.000 PC_A4 (11.575 [40])	0.055 PC_A3 (11.184 [35])	0.056 A4_3 (10.246 [27])

			
0.175 B6_2R (13.918 [65])	0.180 A2_1R (10.130 [25])	0.213 PC_SR186 (12.737 [51])	0.227 B1_7 (11.385 [37])
			
0.244 A5_4 (11.050 [33])	0.272 B5_1R (11.391 [38])	0.374 B1_1R (13.670 [63])	0.375 C1_7 (11.617 [43])
			
0.447 PC_OR117 (14.169 [67])	0.541 B6_4 (13.077 [56])	0.559 B6_6 (10.663 [30])	0.609 C3_7 (13.331 [59])
			
0.647 B6_7 (12.059 [45])	0.684 B3_7 (12.048 [44])	0.687 B1_2 (12.900 [53])	0.726 B5_5 (11.493 [39])
			
0.813 PC_OR24 (13.528 [62])	0.822 B3_9 (13.077 [55])	0.828 B5_6R (12.651 [50])	0.868 B6_1 (13.359 [60])

			
0.962 PC_OR76 (15.305 [68])	0.963 B2_6R (12.375 [47])	1.046 B5_3 (12.548 [49])	1.074 B3_5 (13.076 [54])
			
1.117 B1_3 (14.059 [66])	1.201 PC_SR180 (12.847 [52])	1.235 B5_8R (13.679 [64])	1.484 B6_5R (13.240 [58])

Appendix D. Spearman's correlations for the full set of geospatial variables.

Name	PAN AVG	PAN SD	PAN AVG SD03	PAN AVG SD09	PAN AVG SD17	PAN AVG SD25	PAN AVG SD33	PAN AVG SD41	PAN SD SD03	PAN SD SD09	PAN SD SD17	PAN SD SD25	PAN SD SD33	PAN SD SD41
PAN AVG	1.00													
PAN SD	0.70	1.00												
PAN AVG SD03	0.78	0.91	1.00											
PAN AVG SD09	0.74	0.95	0.98	1.00										
PAN AVG SD17	0.72	0.96	0.97	0.99	1.00									
PAN AVG SD25	0.72	0.97	0.96	0.99	1.00	1.00								
PAN AVG SD33	0.70	0.97	0.95	0.99	0.99	1.00	1.00							
PAN AVG SD41	0.70	0.98	0.95	0.98	0.99	1.00	1.00	1.00						
PAN SD SD03	0.76	0.95	0.96	0.98	0.98	0.98	0.98	0.97	1.00					
PAN SD SD09	0.67	0.91	0.86	0.91	0.92	0.93	0.93	0.93	0.95	1.00				
PAN SD SD17	0.46	0.71	0.62	0.66	0.68	0.69	0.70	0.71	0.73	0.87	1.00			
PAN SD SD25	0.31	0.52	0.42	0.45	0.47	0.49	0.51	0.51	0.53	0.71	0.94	1.00		
PAN SD SD33	0.21	0.40	0.30	0.33	0.35	0.37	0.38	0.39	0.41	0.59	0.86	0.97	1.00	
PAN SD SD41	0.16	0.33	0.24	0.26	0.28	0.29	0.31	0.32	0.34	0.51	0.80	0.93	0.99	1.00
PAN SD AVG03	0.68	1.00	0.89	0.94	0.95	0.96	0.97	0.97	0.94	0.91	0.70	0.52	0.40	0.33
PAN SD AVG09	0.62	0.98	0.83	0.88	0.90	0.91	0.92	0.92	0.89	0.87	0.70	0.54	0.43	0.35
PAN SD AVG17	0.57	0.93	0.74	0.79	0.81	0.82	0.84	0.84	0.80	0.80	0.64	0.50	0.41	0.34
PAN SD AVG25	0.55	0.86	0.67	0.71	0.72	0.74	0.75	0.75	0.72	0.71	0.54	0.42	0.34	0.28
PAN SD AVG33	0.52	0.79	0.60	0.63	0.64	0.65	0.66	0.67	0.64	0.63	0.46	0.34	0.26	0.20
PAN SD AVG41	0.51	0.76	0.56	0.60	0.60	0.61	0.62	0.63	0.61	0.60	0.42	0.31	0.23	0.17
PAN AVG CON03	0.78	0.74	0.90	0.82	0.79	0.78	0.77	0.77	0.79	0.66	0.41	0.23	0.13	0.09
PAN AVG CON09	0.78	0.89	0.99	0.96	0.94	0.93	0.92	0.92	0.94	0.83	0.60	0.40	0.29	0.23
PAN AVG CON17	0.78	0.92	1.00	0.98	0.97	0.96	0.95	0.95	0.97	0.88	0.64	0.44	0.33	0.26
PAN AVG CON25	0.78	0.92	1.00	0.98	0.97	0.96	0.96	0.96	0.97	0.88	0.65	0.45	0.34	0.27
PAN AVG CON33	0.78	0.92	1.00	0.98	0.97	0.96	0.96	0.96	0.97	0.88	0.65	0.46	0.34	0.27
PAN AVG CON41	0.78	0.93	1.00	0.98	0.97	0.96	0.95	0.96	0.97	0.88	0.65	0.45	0.34	0.27
PAN SD CON03	0.48	0.63	0.70	0.65	0.65	0.65	0.64	0.65	0.65	0.59	0.46	0.33	0.27	0.22
PAN SD CON09	0.75	0.92	0.94	0.94	0.94	0.94	0.93	0.93	0.96	0.91	0.70	0.52	0.40	0.33
PAN SD CON17	0.70	0.88	0.87	0.88	0.88	0.88	0.88	0.88	0.92	0.91	0.78	0.62	0.51	0.43
PAN SD CON25	0.66	0.81	0.82	0.81	0.81	0.81	0.81	0.82	0.86	0.86	0.77	0.64	0.53	0.46
PAN SD CON33	0.60	0.75	0.76	0.75	0.74	0.75	0.75	0.75	0.80	0.80	0.75	0.64	0.54	0.47
PAN SD CON41	0.56	0.70	0.72	0.70	0.69	0.69	0.70	0.70	0.75	0.75	0.72	0.63	0.54	0.47
PAN AVG COR03	0.56	0.88	0.83	0.90	0.91	0.91	0.91	0.91	0.87	0.83	0.57	0.38	0.27	0.20
PAN AVG COR09	0.56	0.89	0.83	0.91	0.92	0.92	0.92	0.91	0.88	0.83	0.56	0.36	0.25	0.18
PAN AVG COR17	0.54	0.91	0.82	0.90	0.92	0.92	0.93	0.92	0.87	0.85	0.61	0.42	0.32	0.24
PAN AVG COR25	0.52	0.90	0.80	0.88	0.91	0.91	0.92	0.92	0.86	0.85	0.63	0.44	0.33	0.25
PAN AVG COR33	0.50	0.90	0.78	0.87	0.89	0.90	0.91	0.91	0.85	0.86	0.65	0.47	0.36	0.28
PAN AVG COR41	0.49	0.90	0.77	0.85	0.88	0.89	0.91	0.90	0.84	0.86	0.67	0.50	0.38	0.29
PAN SD COR03	-0.26	-0.33	-0.26	-0.33	-0.33	-0.33	-0.34	-0.33	-0.33	-0.30	-0.12	-0.02	0.06	0.09
PAN SD COR09	-0.55	-0.61	-0.67	-0.68	-0.66	-0.65	-0.64	-0.63	-0.65	-0.52	-0.21	-0.06	0.03	0.08
PAN SD COR17	-0.59	-0.66	-0.71	-0.73	-0.71	-0.70	-0.69	-0.68	-0.70	-0.56	-0.21	-0.05	0.02	0.06
PAN SD COR25	-0.57	-0.66	-0.73	-0.75	-0.73	-0.71	-0.70	-0.69	-0.70	-0.56	-0.17	0.03	0.12	0.17
PAN SD COR33	-0.55	-0.62	-0.70	-0.72	-0.70	-0.68	-0.67	-0.66	-0.66	-0.53	-0.13	0.10	0.21	0.26
PAN SD COR41	-0.53	-0.59	-0.67	-0.68	-0.66	-0.65	-0.64	-0.63	-0.63	-0.49	-0.10	0.13	0.25	0.31
NDVI AVG	0.90	0.70	0.80	0.76	0.74	0.74	0.72	0.72	0.79	0.72	0.52	0.38	0.28	0.23
NDVI SD	0.17	0.72	0.48	0.56	0.60	0.62	0.64	0.65	0.58	0.63	0.61	0.52	0.45	0.37
NDVI AVG SD03	0.21	0.76	0.62	0.70	0.73	0.74	0.75	0.76	0.69	0.71	0.61	0.47	0.39	0.31
NDVI AVG SD05	0.20	0.76	0.60	0.69	0.72	0.73	0.75	0.76	0.69	0.72	0.63	0.50	0.41	0.33
NDVI AVG SD07	0.18	0.75	0.57	0.66	0.70	0.71	0.73	0.74	0.66	0.70	0.64	0.51	0.43	0.34
NDVI AVG SD09	0.17	0.74	0.56	0.65	0.68	0.69	0.72	0.72	0.65	0.68	0.63	0.52	0.44	0.36
NDVI AVG SD11	0.16	0.72	0.54	0.62	0.65	0.67	0.69	0.70	0.62	0.66	0.62	0.52	0.45	0.37
NDVI SD SD03	0.06	0.54	0.33	0.40	0.45	0.47	0.49	0.51	0.45	0.57	0.67	0.63	0.59	0.52
NDVI SD SD05	0.01	0.45	0.24	0.30	0.35	0.37	0.39	0.41	0.35	0.48	0.62	0.63	0.60	0.55
NDVI SD SD07	-0.01	0.41	0.20	0.26	0.30	0.32	0.35	0.36	0.30	0.43	0.60	0.63	0.62	0.58
NDVI SD SD09	0.00	0.41	0.21	0.26	0.30	0.32	0.34	0.36	0.30	0.43	0.60	0.64	0.63	0.60
NDVI SD SD11	0.04	0.43	0.23	0.28	0.32	0.33	0.36	0.37	0.32	0.44	0.60	0.63	0.63	0.60
NDVI SD AVG03	0.14	0.67	0.40	0.47	0.51	0.53	0.56	0.57	0.50	0.55	0.54	0.48	0.43	0.35
NDVI SD AVG05	0.11	0.60	0.31	0.38	0.41	0.43	0.45	0.47	0.40	0.46	0.44	0.40	0.35	0.28
NDVI SD AVG07	0.15	0.56	0.29	0.34	0.37	0.39	0.41	0.42	0.37	0.41	0.37	0.33	0.27	0.21
NDVI SD AVG09	0.16	0.54	0.28	0.32	0.34	0.36	0.38	0.39	0.35	0.38	0.34	0.29	0.24	0.18
NDVI SD AVG11	0.19	0.51	0.26	0.30	0.31	0.33	0.34	0.35	0.33	0.36	0.32	0.28	0.23	0.17
NDVI AVG CON03	0.14	0.62	0.57	0.63	0.64	0.64	0.65	0.65	0.58	0.51	0.30	0.15	0.09	0.04
NDVI AVG CON05	0.22	0.70	0.63	0.71	0.71	0.71	0.72	0.72	0.66	0.60	0.40	0.25	0.17	0.11
NDVI AVG CON07	0.28	0.77	0.68	0.75	0.77	0.77	0.78	0.78	0.72	0.69	0.53	0.37	0.29	0.22
NDVI AVG CON09	0.28	0.79	0.68	0.76	0.77	0.78	0.79	0.79	0.74	0.72	0.56	0.41	0.32	0.25
NDVI AVG CON11	0.29	0.80	0.68	0.76	0.78	0.79	0.80	0.80	0.75	0.74	0.59	0.43	0.35	0.27
NDVI SD CON03	0.23	0.57	0.54	0.57	0.57	0.58	0.59	0.59	0.56	0.60	0.55	0.41	0.35	0.33
NDVI SD CON05	0.31	0.71	0.56	0.63	0.65	0.66	0.67	0.68	0.66	0.71	0.67	0.58	0.52	0.46
NDVI SD CON07	0.31	0.71	0.54	0.61	0.63	0.64	0.65	0.66	0.65	0.71	0.70	0.63	0.57	0.51
NDVI SD CON09	0.29	0.69	0.52	0.58	0.61	0.62	0.63	0.64	0.63	0.68	0.68	0.61	0.55	0.50
NDVI SD CON11	0.26	0.67	0.49	0.55	0.58	0.59	0.61	0.62	0.61	0.67	0.69	0.62	0.57	0.53
NDVI AVG COR03	0.32	0.75	0.59	0.67	0.70	0.72	0.73	0.73	0.65	0.69	0.58	0.47	0.39	0.31
NDVI AVG COR05	0.29	0.71	0.54	0.62	0.65	0.67	0.69	0.69	0.61	0.66	0.59	0.48	0.39	0.31
NDVI AVG COR07	0.23	0.66	0.45	0.54	0.58	0.60	0.62	0.63	0.53	0.60	0.57	0.49	0.39	0.31
NDVI AVG COR09	0.20	0.63	0.41	0.49	0.53	0.55	0.58	0.58	0.49	0.56	0.56	0.49	0.40	0.32
NDVI AVG COR11	0.18	0.61	0.37	0.44	0.48	0.51	0.53	0.54	0.45	0.53	0.55	0.50	0.42	0.34
NDVI SD COR03	0.18	0.43	0.37	0.41	0.44	0.44	0.43	0.43	0.43	0.36	0.24	0.13	0.06	0.03
NDVI SD COR05	-0.18	0.04	-0.13	-0.10	-0.05	-0.04	-0.02	-0.02	-0.04	0.02	0.13	0.16	0.16	0.16
NDVI SD COR07	-0.18	0.03	-0.17	-0.13	-0.09	-0.07	-0.05	-0.04	-0.08	-0.01	0.12	0.19	0.20	0.21
NDVI SD COR09	-0.12	0.05	-0.13	-0.09	-0.06	-0.04	-0.02	-0.01	-0.04	0.04	0.14	0.22	0.23	0.23
NDVI SD COR11	-0.07	0.06	-0.09	-0.07	-0.04	-0.03	-0.01	0.00	-0.03	0.05	0.15	0.22	0.22	0.23
ELEV	0.18	0.00	0.03	0.01	0.02	0.02	0.02	0.02	0.06	0.07	0.05	0.06	0.08	0.07
TVI	-0.16	-0.08	-0.16	-0.16	-0.14	-0.14	-0.14	-0.13	-0.12	-0.07	0.03	0.08	0.11	0.12
DSR	0.62	0.25	0.35	0.33	0.32	0.31	0.30	0.29	0.37	0.31	0.09	0.00	-0.05	-0.09

Name	PAN SD AVG03	PAN SD AVG09	PAN SD AVG17	PAN SD AVG25	PAN SD AVG33	PAN SD AVG41	PAN AVG CON03	PAN AVG CON09	PAN AVG CON17	PAN AVG CON25	PAN AVG CON33	PAN AVG CON41	PAN SD CON03	PAN SD CON09
PAN AVG														
PAN SD														
PAN AVG SD03														
PAN AVG SD09														
PAN AVG SD17														
PAN AVG SD25														
PAN AVG SD33														
PAN AVG SD41														
PAN SD SD03														
PAN SD SD09														
PAN SD SD17														
PAN SD SD25														
PAN SD SD33														
PAN SD SD41														
PAN SD AVG03	1.00													
PAN SD AVG09	0.99	1.00												
PAN SD AVG17	0.94	0.97	1.00											
PAN SD AVG25	0.87	0.92	0.97	1.00										
PAN SD AVG33	0.80	0.86	0.93	0.98	1.00									
PAN SD AVG41	0.77	0.83	0.91	0.97	1.00	1.00								
PAN AVG CON03	0.72	0.65	0.60	0.56	0.53	0.51	1.00							
PAN AVG CON09	0.86	0.80	0.72	0.65	0.58	0.55	0.92	1.00						
PAN AVG CON17	0.90	0.84	0.76	0.68	0.61	0.57	0.89	0.99	1.00					
PAN AVG CON25	0.90	0.84	0.76	0.69	0.61	0.58	0.89	0.99	1.00	1.00				
PAN AVG CON33	0.91	0.85	0.76	0.69	0.61	0.58	0.89	0.99	1.00	1.00	1.00			
PAN AVG CON41	0.91	0.85	0.77	0.69	0.62	0.58	0.89	0.99	1.00	1.00	1.00	1.00		
PAN SD CON03	0.60	0.56	0.49	0.40	0.34	0.31	0.70	0.73	0.70	0.71	0.71	0.71	1.00	
PAN SD CON09	0.91	0.86	0.80	0.73	0.66	0.63	0.79	0.92	0.95	0.95	0.95	0.95	0.67	1.00
PAN SD CON17	0.87	0.84	0.78	0.72	0.65	0.62	0.70	0.85	0.89	0.89	0.89	0.89	0.55	0.95
PAN SD CON25	0.80	0.78	0.73	0.68	0.61	0.58	0.66	0.80	0.83	0.83	0.83	0.83	0.51	0.91
PAN SD CON33	0.74	0.72	0.68	0.62	0.56	0.52	0.61	0.75	0.78	0.78	0.78	0.78	0.45	0.86
PAN SD CON41	0.68	0.68	0.63	0.58	0.51	0.48	0.57	0.71	0.73	0.73	0.73	0.74	0.44	0.81
PAN AVG COR03	0.88	0.85	0.77	0.69	0.60	0.56	0.57	0.78	0.83	0.83	0.82	0.82	0.43	0.84
PAN AVG COR09	0.89	0.85	0.77	0.69	0.61	0.57	0.58	0.78	0.83	0.83	0.83	0.83	0.44	0.83
PAN AVG COR17	0.91	0.89	0.81	0.72	0.63	0.59	0.56	0.77	0.82	0.82	0.82	0.81	0.48	0.83
PAN AVG COR25	0.91	0.89	0.82	0.72	0.63	0.60	0.54	0.75	0.80	0.80	0.80	0.80	0.49	0.82
PAN AVG COR33	0.91	0.90	0.83	0.73	0.64	0.60	0.52	0.73	0.79	0.79	0.79	0.79	0.47	0.81
PAN AVG COR41	0.91	0.90	0.83	0.74	0.65	0.62	0.50	0.71	0.77	0.77	0.77	0.77	0.46	0.80
PAN SD COR03	-0.34	-0.34	-0.30	-0.30	-0.31	-0.30	-0.05	-0.20	-0.25	-0.24	-0.24	-0.24	0.14	-0.29
PAN SD COR09	-0.60	-0.55	-0.50	-0.46	-0.41	-0.39	-0.52	-0.64	-0.66	-0.66	-0.66	-0.66	-0.23	-0.67
PAN SD COR17	-0.65	-0.61	-0.56	-0.52	-0.47	-0.45	-0.60	-0.69	-0.71	-0.70	-0.70	-0.70	-0.29	-0.70
PAN SD COR25	-0.65	-0.60	-0.55	-0.52	-0.48	-0.47	-0.64	-0.70	-0.72	-0.72	-0.72	-0.72	-0.32	-0.70
PAN SD COR33	-0.61	-0.55	-0.50	-0.48	-0.46	-0.45	-0.63	-0.67	-0.70	-0.69	-0.69	-0.68	-0.29	-0.65
PAN SD COR41	-0.58	-0.52	-0.47	-0.45	-0.43	-0.42	-0.60	-0.64	-0.66	-0.65	-0.65	-0.65	-0.26	-0.61
NDVI AVG	0.67	0.61	0.55	0.50	0.47	0.45	0.79	0.81	0.81	0.81	0.81	0.81	0.57	0.80
NDVI SD	0.74	0.79	0.80	0.75	0.69	0.66	0.26	0.45	0.49	0.50	0.51	0.51	0.45	0.57
NDVI AVG SD03	0.77	0.77	0.72	0.64	0.56	0.53	0.36	0.58	0.62	0.62	0.63	0.63	0.48	0.65
NDVI AVG SD05	0.77	0.78	0.72	0.63	0.55	0.51	0.34	0.56	0.61	0.61	0.62	0.62	0.48	0.66
NDVI AVG SD07	0.76	0.77	0.73	0.63	0.55	0.51	0.31	0.54	0.58	0.59	0.59	0.59	0.47	0.64
NDVI AVG SD09	0.75	0.77	0.72	0.63	0.55	0.51	0.30	0.52	0.57	0.57	0.58	0.58	0.46	0.62
NDVI AVG SD11	0.74	0.76	0.72	0.63	0.54	0.51	0.28	0.50	0.55	0.55	0.56	0.56	0.45	0.60
NDVI SD SD03	0.55	0.58	0.57	0.49	0.42	0.40	0.12	0.31	0.35	0.36	0.36	0.36	0.43	0.42
NDVI SD SD05	0.46	0.49	0.50	0.43	0.36	0.34	0.06	0.23	0.26	0.27	0.27	0.27	0.40	0.33
NDVI SD SD07	0.42	0.46	0.48	0.42	0.35	0.33	0.04	0.19	0.22	0.23	0.23	0.23	0.37	0.30
NDVI SD SD09	0.43	0.47	0.49	0.44	0.38	0.36	0.06	0.20	0.22	0.23	0.24	0.24	0.36	0.31
NDVI SD SD11	0.44	0.48	0.51	0.47	0.40	0.39	0.09	0.22	0.25	0.26	0.26	0.26	0.36	0.34
NDVI SD AVG03	0.69	0.76	0.81	0.78	0.73	0.71	0.21	0.37	0.41	0.42	0.43	0.43	0.37	0.50
NDVI SD AVG05	0.62	0.70	0.78	0.80	0.78	0.77	0.17	0.28	0.33	0.33	0.34	0.34	0.28	0.42
NDVI SD AVG07	0.58	0.67	0.77	0.82	0.84	0.84	0.21	0.28	0.31	0.32	0.32	0.32	0.27	0.40
NDVI SD AVG09	0.56	0.65	0.76	0.82	0.85	0.85	0.22	0.27	0.29	0.30	0.31	0.31	0.24	0.39
NDVI SD AVG11	0.53	0.62	0.73	0.80	0.85	0.86	0.22	0.25	0.28	0.28	0.29	0.29	0.22	0.37
NDVI AVG CON03	0.63	0.61	0.55	0.49	0.44	0.41	0.37	0.54	0.56	0.56	0.56	0.56	0.35	0.55
NDVI AVG CON05	0.71	0.69	0.63	0.57	0.50	0.47	0.41	0.60	0.63	0.63	0.63	0.62	0.37	0.63
NDVI AVG CON07	0.78	0.76	0.71	0.65	0.56	0.53	0.42	0.64	0.68	0.68	0.68	0.68	0.41	0.70
NDVI AVG CON09	0.80	0.78	0.74	0.67	0.59	0.55	0.43	0.65	0.68	0.68	0.69	0.68	0.43	0.72
NDVI AVG CON11	0.81	0.80	0.75	0.68	0.60	0.56	0.43	0.65	0.69	0.69	0.69	0.69	0.45	0.73
NDVI SD CON03	0.57	0.55	0.51	0.44	0.39	0.37	0.36	0.51	0.53	0.53	0.53	0.53	0.38	0.52
NDVI SD CON05	0.73	0.75	0.73	0.67	0.61	0.59	0.36	0.53	0.58	0.58	0.58	0.58	0.40	0.62
NDVI SD CON07	0.73	0.75	0.76	0.71	0.65	0.63	0.34	0.52	0.56	0.56	0.56	0.56	0.41	0.62
NDVI SD CON09	0.71	0.73	0.74	0.70	0.64	0.62	0.33	0.50	0.54	0.54	0.54	0.54	0.42	0.61
NDVI SD CON11	0.68	0.71	0.73	0.68	0.63	0.61	0.31	0.47	0.51	0.51	0.52	0.52	0.42	0.59
NDVI AVG COR03	0.77	0.79	0.74	0.66	0.58	0.54	0.33	0.54	0.59	0.60	0.60	0.60	0.31	0.61
NDVI AVG COR05	0.72	0.75	0.70	0.61	0.53	0.49	0.26	0.48	0.54	0.55	0.55	0.55	0.28	0.58
NDVI AVG COR07	0.68	0.72	0.69	0.60	0.53	0.49	0.17	0.39	0.46	0.47	0.47	0.47	0.24	0.51
NDVI AVG COR09	0.65	0.70	0.68	0.60	0.53	0.49	0.14	0.36	0.42	0.42	0.43	0.43	0.23	0.48
NDVI AVG COR11	0.63	0.69	0.68	0.61	0.54	0.51	0.11	0.32	0.38	0.39	0.39	0.39	0.22	0.45
NDVI SD COR03	0.44	0.42	0.37	0.28	0.21	0.18	0.22	0.38	0.38	0.39	0.39	0.39	0.35	0.42
NDVI SD COR05	0.05	0.08	0.09	0.02	0.00	-0.01	-0.25	-0.14	-0.13	-0.12	-0.12	-0.11	0.03	-0.01
NDVI SD COR07	0.05	0.09	0.11	0.07	0.05	0.05	-0.22	-0.17	-0.17	-0.16	-0.15	-0.15	0.00	-0.03
NDVI SD COR09	0.08	0.11	0.13	0.10	0.08	0.07	-0.16	-0.13	-0.13	-0.12	-0.11	-0.11	-0.01	0.00
NDVI SD COR11	0.08	0.11	0.14	0.12	0.10	0.09	-0.09	-0.09	-0.09	-0.08	-0.07	-0.07	-0.03	0.00
ELEV	-0.02	-0.04	-0.03	-0.01	-0.03	-0.04	0.04	0.05	0.04	0.05	0.05	0.05	0.09	0.07
TVI	-0.07	-0.03	0.03	0.08	0.11	0.13	-0.12	-0.15	-0.16	-0.15	-0.15	-0.15	0.07	-0.11
DSR	0.24	0.19	0.13	0.10	0.08	0.07	0.36	0.33	0.35	0.35	0.34	0.34	0.14	0.32

Name	PAN SD CON17	PAN SD CON25	PAN SD CON33	PAN SD CON41	PAN AVG COR03	PANAV G COR09	PAN AVG COR17	PAN AVG COR25	PAN AVG COR33	PAN AVG COR41	PAN SD COR03	PAN SD COR09	PAN SD COR17	PAN SD COR25
PAN AVG														
PAN SD														
PAN AVG SD03														
PAN AVG SD09														
PAN AVG SD17														
PAN AVG SD25														
PAN AVG SD33														
PAN AVG SD41														
PAN SD SD03														
PAN SD SD09														
PAN SD SD17														
PAN SD SD25														
PAN SD SD33														
PAN SD SD41														
PAN SD AVG03														
PAN SD AVG09														
PAN SD AVG17														
PAN SD AVG25														
PAN SD AVG33														
PAN SD AVG41														
PAN AVG CON03														
PAN AVG CON09														
PAN AVG CON17														
PAN AVG CON25														
PAN AVG CON33														
PAN AVG CON41														
PAN SD CON03														
PAN SD CON09														
PAN SD CON17	1.00													
PAN SD CON25	0.98	1.00												
PAN SD CON33	0.95	0.98	1.00											
PAN SD CON41	0.91	0.96	0.99	1.00										
PAN AVG COR03	0.79	0.72	0.67	0.61	1.00									
PAN AVG COR09	0.77	0.70	0.64	0.58	0.98	1.00								
PAN AVG COR17	0.77	0.69	0.63	0.57	0.96	0.98	1.00							
PAN AVG COR25	0.77	0.70	0.63	0.58	0.95	0.96	0.99	1.00						
PAN AVG COR33	0.77	0.70	0.64	0.58	0.94	0.95	0.99	1.00	1.00					
PAN AVG COR41	0.77	0.71	0.64	0.59	0.93	0.94	0.98	0.99	1.00	1.00				
PAN SD COR03	-0.28	-0.26	-0.24	-0.21	-0.55	-0.54	-0.47	-0.47	-0.46	-0.45	1.00			
PAN SD COR09	-0.62	-0.58	-0.55	-0.50	-0.76	-0.77	-0.68	-0.64	-0.62	-0.59	0.50	1.00		
PAN SD COR17	-0.64	-0.58	-0.54	-0.49	-0.76	-0.79	-0.73	-0.70	-0.67	-0.63	0.42	0.93	1.00	
PAN SD COR25	-0.61	-0.55	-0.49	-0.44	-0.76	-0.79	-0.74	-0.71	-0.68	-0.65	0.42	0.86	0.96	1.00
PAN SD COR33	-0.56	-0.49	-0.43	-0.38	-0.71	-0.74	-0.69	-0.67	-0.64	-0.61	0.38	0.79	0.89	0.97
PAN SD COR41	-0.53	-0.47	-0.41	-0.36	-0.67	-0.70	-0.65	-0.63	-0.61	-0.59	0.35	0.76	0.84	0.93
NDVI AVG	0.73	0.68	0.63	0.58	0.58	0.59	0.56	0.54	0.52	0.51	-0.20	-0.54	-0.55	-0.54
NDVI SD	0.57	0.53	0.50	0.46	0.61	0.60	0.67	0.69	0.71	0.72	-0.24	-0.25	-0.27	-0.24
NDVI AVG SD03	0.65	0.60	0.57	0.54	0.76	0.75	0.79	0.80	0.81	0.81	-0.30	-0.41	-0.45	-0.45
NDVI AVG SD05	0.65	0.61	0.58	0.55	0.76	0.75	0.79	0.81	0.82	0.83	-0.30	-0.40	-0.42	-0.41
NDVI AVG SD07	0.64	0.60	0.57	0.54	0.73	0.72	0.77	0.79	0.81	0.82	-0.28	-0.37	-0.38	-0.38
NDVI AVG SD09	0.63	0.59	0.56	0.53	0.72	0.70	0.76	0.78	0.80	0.81	-0.28	-0.36	-0.38	-0.36
NDVI AVG SD11	0.60	0.57	0.54	0.51	0.70	0.68	0.74	0.76	0.78	0.80	-0.26	-0.34	-0.36	-0.34
NDVI SD SD03	0.42	0.39	0.36	0.34	0.41	0.39	0.47	0.51	0.53	0.55	0.01	0.02	0.01	0.05
NDVI SD SD05	0.34	0.31	0.29	0.27	0.28	0.27	0.36	0.39	0.42	0.44	0.10	0.13	0.13	0.18
NDVI SD SD07	0.32	0.29	0.27	0.25	0.24	0.22	0.32	0.35	0.38	0.40	0.12	0.15	0.15	0.21
NDVI SD SD09	0.32	0.31	0.28	0.27	0.23	0.22	0.31	0.34	0.37	0.39	0.10	0.14	0.14	0.21
NDVI SD SD11	0.35	0.33	0.31	0.30	0.24	0.24	0.32	0.34	0.37	0.39	0.08	0.10	0.10	0.17
NDVI SD AVG03	0.50	0.48	0.45	0.42	0.54	0.53	0.60	0.62	0.64	0.66	-0.25	-0.22	-0.23	-0.20
NDVI SD AVG05	0.42	0.40	0.38	0.35	0.44	0.44	0.51	0.53	0.55	0.57	-0.25	-0.17	-0.19	-0.18
NDVI SD AVG07	0.40	0.39	0.36	0.33	0.37	0.38	0.43	0.45	0.47	0.49	-0.23	-0.15	-0.19	-0.19
NDVI SD AVG09	0.39	0.37	0.35	0.32	0.34	0.34	0.39	0.41	0.43	0.45	-0.21	-0.14	-0.19	-0.19
NDVI SD AVG11	0.37	0.36	0.34	0.31	0.30	0.30	0.35	0.37	0.39	0.41	-0.20	-0.11	-0.16	-0.17
NDVI AVG CON03	0.50	0.46	0.43	0.40	0.73	0.72	0.72	0.70	0.69	0.68	-0.41	-0.55	-0.61	-0.63
NDVI AVG CON05	0.61	0.57	0.54	0.50	0.81	0.79	0.78	0.77	0.76	0.76	-0.46	-0.58	-0.63	-0.63
NDVI AVG CON07	0.69	0.65	0.62	0.58	0.85	0.83	0.83	0.83	0.83	0.82	-0.44	-0.57	-0.61	-0.61
NDVI AVG CON09	0.71	0.66	0.63	0.59	0.84	0.83	0.84	0.83	0.84	0.83	-0.41	-0.55	-0.58	-0.58
NDVI AVG CON11	0.71	0.67	0.63	0.59	0.83	0.82	0.84	0.84	0.84	0.84	-0.39	-0.53	-0.56	-0.56
NDVI SD CON03	0.54	0.51	0.47	0.44	0.51	0.51	0.53	0.53	0.53	0.52	-0.19	-0.23	-0.32	-0.33
NDVI SD CON05	0.62	0.58	0.56	0.53	0.61	0.61	0.66	0.67	0.67	0.67	-0.28	-0.24	-0.30	-0.28
NDVI SD CON07	0.62	0.59	0.56	0.53	0.58	0.58	0.62	0.63	0.64	0.65	-0.22	-0.20	-0.25	-0.22
NDVI SD CON09	0.60	0.57	0.54	0.51	0.55	0.55	0.60	0.61	0.62	0.63	-0.18	-0.17	-0.22	-0.20
NDVI SD CON11	0.58	0.55	0.52	0.49	0.52	0.52	0.58	0.59	0.61	0.62	-0.16	-0.14	-0.19	-0.17
NDVI AVG COR03	0.62	0.57	0.53	0.50	0.79	0.80	0.84	0.85	0.87	0.88	-0.42	-0.49	-0.51	-0.50
NDVI AVG COR05	0.60	0.56	0.53	0.50	0.75	0.75	0.80	0.83	0.85	0.86	-0.41	-0.42	-0.42	-0.42
NDVI AVG COR07	0.55	0.53	0.50	0.47	0.68	0.67	0.73	0.77	0.80	0.82	-0.42	-0.34	-0.32	-0.32
NDVI AVG COR09	0.52	0.51	0.49	0.46	0.62	0.61	0.67	0.71	0.75	0.77	-0.40	-0.29	-0.26	-0.26
NDVI AVG COR11	0.50	0.49	0.47	0.45	0.58	0.57	0.63	0.67	0.71	0.74	-0.38	-0.27	-0.24	-0.22
NDVI SD COR03	0.33	0.29	0.25	0.24	0.41	0.41	0.43	0.42	0.41	0.41	-0.14	-0.24	-0.20	-0.20
NDVI SD COR05	0.02	0.03	0.05	0.07	-0.01	-0.05	0.01	0.05	0.07	0.08	-0.08	0.17	0.21	0.26
NDVI SD COR07	0.00	0.01	0.04	0.04	-0.01	-0.05	0.01	0.04	0.06	0.08	-0.10	0.13	0.19	0.28
NDVI SD COR09	0.04	0.05	0.07	0.07	0.02	0.00	0.05	0.06	0.09	0.11	-0.09	0.07	0.14	0.23
NDVI SD COR11	0.05	0.06	0.08	0.07	0.00	-0.01	0.02	0.03	0.05	0.07	-0.01	0.05	0.12	0.22
ELEV	0.11	0.10	0.09	0.09	-0.04	-0.07	-0.08	-0.08	-0.08	-0.08	0.09	-0.05	-0.01	0.02
TVI	-0.14	-0.16	-0.17	-0.19	-0.21	-0.16	-0.12	-0.12	-0.12	-0.13	0.16	0.30	0.28	0.28
DSR	0.29	0.25	0.23	0.20	0.26	0.26	0.22	0.20	0.18	0.17	-0.21	-0.34	-0.36	-0.33

Name	PAN SD COR33	PAN SD COR41	NDVI AVG	NDVI SD	NDVI AVG SD03	NDVI AVG SD05	NDVI AVG SD07	NDVI AVG SD09	NDVI AVG SD11	NDVI SD SD03	NDVI SD SD05	NDVI SD SD07	NDVI SD SD09	NDVI SD SD11
PAN AVG														
PAN SD														
PAN AVG SD03														
PAN AVG SD09														
PAN AVG SD17														
PAN AVG SD25														
PAN AVG SD33														
PAN AVG SD41														
PAN SD SD03														
PAN SD SD09														
PAN SD SD17														
PAN SD SD25														
PAN SD SD33														
PAN SD SD41														
PAN SD AVG03														
PAN SD AVG09														
PAN SD AVG17														
PAN SD AVG25														
PAN SD AVG33														
PAN SD AVG41														
PAN AVG CON03														
PAN AVG CON09														
PAN AVG CON17														
PAN AVG CON25														
PAN AVG CON33														
PAN AVG CON41														
PAN SD CON03														
PAN SD CON09														
PAN SD CON17														
PAN SD CON25														
PAN SD CON33														
PAN SD CON41														
PAN AVG COR03														
PAN AVG COR09														
PAN AVG COR17														
PAN AVG COR25														
PAN AVG COR33														
PAN AVG COR41														
PAN SD COR03														
PAN SD COR09														
PAN SD COR17														
PAN SD COR25														
PAN SD COR33	1.00													
PAN SD COR41	0.98	1.00												
NDVI AVG	-0.52	-0.49	1.00											
NDVI SD	-0.19	-0.18	0.16	1.00										
NDVI AVG SD03	-0.40	-0.38	0.21	0.88	1.00									
NDVI AVG SD05	-0.37	-0.35	0.21	0.90	0.99	1.00								
NDVI AVG SD07	-0.33	-0.32	0.19	0.91	0.98	0.99	1.00							
NDVI AVG SD09	-0.31	-0.30	0.17	0.91	0.97	0.98	1.00	1.00						
NDVI AVG SD11	-0.28	-0.27	0.15	0.91	0.95	0.97	0.99	1.00	1.00					
NDVI SD SD03	0.08	0.10	0.06	0.85	0.74	0.77	0.79	0.79	0.79	1.00				
NDVI SD SD05	0.23	0.24	0.02	0.79	0.63	0.67	0.69	0.70	0.71	0.97	1.00			
NDVI SD SD07	0.27	0.29	0.00	0.76	0.57	0.61	0.64	0.65	0.66	0.92	0.98	1.00		
NDVI SD SD09	0.27	0.29	0.02	0.74	0.54	0.58	0.61	0.63	0.63	0.89	0.96	0.99	1.00	
NDVI SD SD11	0.24	0.27	0.06	0.73	0.52	0.56	0.59	0.60	0.62	0.85	0.93	0.97	0.99	1.00
NDVI SD AVG03	-0.15	-0.13	0.12	0.97	0.78	0.81	0.83	0.84	0.84	0.78	0.74	0.73	0.74	0.73
NDVI SD AVG05	-0.13	-0.11	0.08	0.90	0.67	0.69	0.71	0.72	0.73	0.67	0.65	0.66	0.67	0.67
NDVI SD AVG07	-0.16	-0.14	0.11	0.82	0.57	0.58	0.59	0.60	0.61	0.58	0.56	0.57	0.60	0.61
NDVI SD AVG09	-0.17	-0.15	0.12	0.77	0.52	0.52	0.54	0.54	0.55	0.53	0.51	0.52	0.55	0.57
NDVI SD AVG11	-0.14	-0.13	0.13	0.72	0.46	0.46	0.48	0.48	0.49	0.50	0.48	0.50	0.53	0.55
NDVI AVG CON03	-0.58	-0.55	0.12	0.63	0.84	0.80	0.78	0.78	0.77	0.38	0.27	0.23	0.22	0.22
NDVI AVG CON05	-0.58	-0.56	0.20	0.69	0.90	0.87	0.84	0.83	0.81	0.45	0.33	0.28	0.27	0.26
NDVI AVG CON07	-0.55	-0.53	0.27	0.77	0.94	0.92	0.90	0.89	0.87	0.54	0.42	0.38	0.37	0.36
NDVI AVG CON09	-0.53	-0.50	0.28	0.81	0.96	0.95	0.93	0.91	0.90	0.60	0.48	0.43	0.42	0.42
NDVI AVG CON11	-0.51	-0.49	0.29	0.83	0.97	0.96	0.94	0.93	0.91	0.63	0.52	0.47	0.46	0.46
NDVI SD CON03	-0.30	-0.25	0.24	0.51	0.60	0.59	0.58	0.57	0.55	0.48	0.42	0.37	0.36	0.34
NDVI SD CON05	-0.24	-0.21	0.32	0.80	0.76	0.76	0.75	0.74	0.72	0.71	0.65	0.62	0.62	0.63
NDVI SD CON07	-0.18	-0.15	0.32	0.83	0.75	0.75	0.75	0.74	0.72	0.76	0.72	0.70	0.72	0.72
NDVI SD CON09	-0.15	-0.12	0.30	0.83	0.74	0.74	0.74	0.73	0.71	0.78	0.74	0.73	0.75	0.75
NDVI SD CON11	-0.12	-0.09	0.29	0.82	0.72	0.72	0.72	0.71	0.70	0.80	0.77	0.77	0.78	0.79
NDVI AVG COR03	-0.46	-0.43	0.34	0.69	0.73	0.75	0.76	0.75	0.75	0.49	0.40	0.36	0.36	0.35
NDVI AVG COR05	-0.38	-0.37	0.29	0.69	0.71	0.75	0.76	0.76	0.76	0.51	0.43	0.40	0.40	0.38
NDVI AVG COR07	-0.29	-0.29	0.22	0.73	0.69	0.74	0.76	0.77	0.78	0.54	0.48	0.45	0.44	0.42
NDVI AVG COR09	-0.22	-0.22	0.18	0.74	0.67	0.72	0.75	0.77	0.78	0.55	0.50	0.48	0.47	0.45
NDVI AVG COR11	-0.18	-0.18	0.15	0.75	0.65	0.70	0.74	0.76	0.78	0.55	0.52	0.50	0.49	0.48
NDVI SD COR03	-0.15	-0.15	0.23	0.44	0.40	0.42	0.42	0.41	0.42	0.31	0.31	0.28	0.26	0.25
NDVI SD COR05	0.30	0.29	-0.13	0.32	0.17	0.22	0.25	0.26	0.28	0.30	0.34	0.34	0.32	0.30
NDVI SD COR07	0.35	0.37	-0.16	0.34	0.17	0.21	0.25	0.28	0.31	0.32	0.39	0.42	0.41	0.40
NDVI SD COR09	0.31	0.33	-0.12	0.31	0.17	0.21	0.24	0.27	0.30	0.29	0.37	0.41	0.41	0.42
NDVI SD COR11	0.28	0.30	-0.08	0.24	0.11	0.14	0.17	0.19	0.23	0.26	0.35	0.40	0.41	0.43
ELEV	0.02	0.03	0.12	-0.12	-0.13	-0.11	-0.11	-0.11	-0.12	-0.06	-0.01	-0.01	-0.01	-0.02
TVI	0.32	0.35	-0.14	0.12	-0.08	-0.08	-0.06	-0.07	-0.07	0.18	0.26	0.29	0.32	0.34
DSR	-0.37	-0.39	0.55	-0.06	0.02	0.01	-0.02	-0.02	-0.04	-0.10	-0.17	-0.21	-0.23	-0.24

Name	NDVI SD AVG03	NDVI SD AVG05	NDVI SD AVG07	NDVI SD AVG09	NDVI SD AVG11	NDVI AVG CON03	NDVI AVG CON05	NDVI AVG CON07	NDVI AVG CON09	NDVI AVG CON11	NDVI SD CON03	NDVI SD CON05	NDVI SD CON07	NDVI SD CON09
PAN AVG														
PAN SD														
PAN AVG SD03														
PAN AVG SD09														
PAN AVG SD17														
PAN AVG SD25														
PAN AVG SD33														
PAN AVG SD41														
PAN SD SD03														
PAN SD SD09														
PAN SD SD17														
PAN SD SD25														
PAN SD SD33														
PAN SD SD41														
PAN SD AVG03														
PAN SD AVG09														
PAN SD AVG17														
PAN SD AVG25														
PAN SD AVG33														
PAN SD AVG41														
PAN AVG CON03														
PAN AVG CON09														
PAN AVG CON17														
PAN AVG CON25														
PAN AVG CON33														
PAN AVG CON41														
PAN SD CON03														
PAN SD CON09														
PAN SD CON17														
PAN SD CON25														
PAN SD CON33														
PAN SD CON41														
PAN AVG COR03														
PAN AVG COR09														
PAN AVG COR17														
PAN AVG COR25														
PAN AVG COR33														
PAN AVG COR41														
PAN SD COR03														
PAN SD COR09														
PAN SD COR17														
PAN SD COR25														
PAN SD COR33														
PAN SD COR41														
NDVI AVG														
NDVI SD														
NDVI AVG SD03														
NDVI AVG SD05														
NDVI AVG SD07														
NDVI AVG SD09														
NDVI AVG SD11														
NDVI SD SD03														
NDVI SD SD05														
NDVI SD SD07														
NDVI SD SD09														
NDVI SD SD11														
NDVI SD AVG03	1.00													
NDVI SD AVG05	0.97	1.00												
NDVI SD AVG07	0.90	0.97	1.00											
NDVI SD AVG09	0.85	0.93	0.99	1.00										
NDVI SD AVG11	0.81	0.90	0.97	0.99	1.00									
NDVI AVG CON03	0.55	0.47	0.40	0.36	0.30	1.00								
NDVI AVG CON05	0.60	0.51	0.44	0.40	0.34	0.97	1.00							
NDVI AVG CON07	0.68	0.58	0.50	0.46	0.40	0.92	0.98	1.00						
NDVI AVG CON09	0.72	0.62	0.54	0.49	0.44	0.89	0.96	0.99	1.00					
NDVI AVG CON11	0.74	0.64	0.56	0.51	0.46	0.88	0.94	0.98	1.00	1.00				
NDVI SD CON03	0.44	0.38	0.32	0.28	0.26	0.56	0.59	0.62	0.64	0.64	1.00			
NDVI SD CON05	0.75	0.69	0.65	0.64	0.61	0.56	0.66	0.73	0.76	0.77	0.64	1.00		
NDVI SD CON07	0.79	0.74	0.71	0.69	0.67	0.51	0.60	0.70	0.74	0.76	0.58	0.96	1.00	
NDVI SD CON09	0.79	0.73	0.71	0.70	0.69	0.50	0.58	0.68	0.72	0.74	0.56	0.92	0.98	1.00
NDVI SD CON11	0.78	0.74	0.72	0.70	0.69	0.46	0.54	0.64	0.69	0.72	0.56	0.89	0.96	0.99
NDVI AVG COR03	0.66	0.58	0.48	0.43	0.39	0.57	0.66	0.73	0.73	0.73	0.39	0.61	0.57	0.52
NDVI AVG COR05	0.68	0.59	0.48	0.42	0.38	0.54	0.62	0.70	0.71	0.71	0.37	0.60	0.56	0.52
NDVI AVG COR07	0.72	0.66	0.53	0.47	0.43	0.52	0.59	0.67	0.68	0.69	0.36	0.58	0.56	0.51
NDVI AVG COR09	0.75	0.69	0.56	0.50	0.46	0.50	0.56	0.63	0.65	0.66	0.36	0.56	0.55	0.51
NDVI AVG COR11	0.78	0.73	0.61	0.54	0.50	0.48	0.54	0.62	0.63	0.64	0.34	0.54	0.54	0.51
NDVI SD COR03	0.37	0.28	0.22	0.19	0.17	0.37	0.37	0.40	0.41	0.42	0.29	0.35	0.36	0.36
NDVI SD COR05	0.34	0.32	0.23	0.19	0.18	0.08	0.06	0.08	0.11	0.13	0.19	0.14	0.15	0.17
NDVI SD COR07	0.38	0.36	0.28	0.25	0.24	0.06	0.05	0.07	0.10	0.13	0.08	0.12	0.14	0.17
NDVI SD COR09	0.35	0.32	0.25	0.22	0.21	0.06	0.06	0.08	0.10	0.12	0.02	0.08	0.11	0.15
NDVI SD COR11	0.29	0.27	0.21	0.18	0.17	-0.01	-0.01	0.01	0.04	0.05	-0.05	0.03	0.07	0.10
ELEV	-0.11	-0.15	-0.16	-0.15	-0.16	-0.18	-0.14	-0.12	-0.12	-0.12	-0.07	-0.12	-0.10	-0.11
TVI	0.17	0.23	0.31	0.34	0.37	-0.13	-0.15	-0.14	-0.12	-0.10	0.02	0.14	0.19	0.22
DSR	-0.10	-0.15	-0.16	-0.15	-0.15	0.01	0.05	0.06	0.05	0.06	0.01	0.09	0.04	0.01

Name	NDVI SD CON11	NDVI AVG COR03	NDVI AVG COR05	NDVI AVG COR07	NDVI AVG COR09	NDVI AVG COR11	NDVI SD COR03	NDVI SD COR05	NDVI SD COR07	NDVI SD COR09	NDVI SD COR11	ELEV	TVI	DSR
PAN AVG														
PAN SD														
PAN AVG SD03														
PAN AVG SD09														
PAN AVG SD17														
PAN AVG SD25														
PAN AVG SD33														
PAN AVG SD41														
PAN SD SD03														
PAN SD SD09														
PAN SD SD17														
PAN SD SD25														
PAN SD SD33														
PAN SD SD41														
PAN SD AVG03														
PAN SD AVG09														
PAN SD AVG17														
PAN SD AVG25														
PAN SD AVG33														
PAN SD AVG41														
PAN AVG CON03														
PAN AVG CON09														
PAN AVG CON17														
PAN AVG CON25														
PAN AVG CON33														
PAN AVG CON41														
PAN SD CON03														
PAN SD CON09														
PAN SD CON17														
PAN SD CON25														
PAN SD CON33														
PAN SD CON41														
PAN AVG COR03														
PAN AVG COR09														
PAN AVG COR17														
PAN AVG COR25														
PAN AVG COR33														
PAN AVG COR41														
PAN SD COR03														
PAN SD COR09														
PAN SD COR17														
PAN SD COR25														
PAN SD COR33														
PAN SD COR41														
NDVI AVG														
NDVI SD														
NDVI AVG SD03														
NDVI AVG SD05														
NDVI AVG SD07														
NDVI AVG SD09														
NDVI AVG SD11														
NDVI SD SD03														
NDVI SD SD05														
NDVI SD SD07														
NDVI SD SD09														
NDVI SD SD11														
NDVI SD AVG03														
NDVI SD AVG05														
NDVI SD AVG07														
NDVI SD AVG09														
NDVI SD AVG11														
NDVI AVG CON03														
NDVI AVG CON05														
NDVI AVG CON07														
NDVI AVG CON09														
NDVI AVG CON11														
NDVI SD CON03														
NDVI SD CON05														
NDVI SD CON07														
NDVI SD CON09														
NDVI SD CON11	1.00													
NDVI AVG COR03	0.51	1.00												
NDVI AVG COR05	0.50	0.96	1.00											
NDVI AVG COR07	0.50	0.90	0.97	1.00										
NDVI AVG COR09	0.50	0.85	0.93	0.99	1.00									
NDVI AVG COR11	0.50	0.82	0.89	0.96	0.99	1.00								
NDVI SD COR03	0.35	0.34	0.38	0.39	0.40	0.38	1.00							
NDVI SD COR05	0.20	0.06	0.14	0.27	0.36	0.39	0.41	1.00						
NDVI SD COR07	0.21	0.08	0.13	0.24	0.33	0.38	0.27	0.82	1.00					
NDVI SD COR09	0.19	0.14	0.15	0.22	0.30	0.36	0.19	0.63	0.92	1.00				
NDVI SD COR11	0.14	0.14	0.12	0.17	0.24	0.29	0.12	0.44	0.76	0.93	1.00			
ELEV	-0.14	-0.10	-0.08	-0.11	-0.11	-0.11	-0.02	-0.03	-0.05	0.00	0.09	1.00		
TVI	0.24	-0.17	-0.17	-0.16	-0.13	-0.10	0.09	0.10	0.10	0.09	0.09	0.02	1.00	
DSR	-0.02	0.02	0.04	0.01	-0.01	-0.02	0.03	-0.17	-0.12	-0.07	-0.06	0.15	-0.43	1.00

CHAPTER 3: Development of remotely-sensed indices of fine-scale forest characteristics for modeling breeding bird species distributions in an Appalachian deciduous forest.

Abstract. Recent developments in remote sensing technology allow forest characteristics to be assessed at increasingly finer spatial scales. For example, high resolution optical imagery and ancillary data can be used to create continuous, predictive maps of detailed forest characteristics, by relating the remote sensing data to data collected in the field. Such maps may also be useful for studying patterns in avian biodiversity within forests. To test this, we used a QuickBird satellite 0.6-m panchromatic image and a 3-m digital elevation model of a ridgetop Appalachian deciduous forest to develop and map indices of forest structure and composition based on field data. We then tested these indices along with topographic variables and anthropogenic forest edge for modeling the spatial distributions of three sympatric forest songbirds over two breeding seasons. The indices characterized a forest structural complexity gradient across the study site that was closely related to a chestnut oak (*Quercus montana*)-sugar maple (*Acer saccharum*) dominated forest composition gradient. Applied to the bird distributions, the indices suggested the importance of high structural complexity within this forest for the Hooded Warbler (*Setophaga citrina*), the species most dependent on the understory of forest canopy gaps, in addition to higher elevations and certain east-facing aspects. West-facing aspects were most important for the Ovenbird (*Seiurus aurocapilla*), but selection for moderate structural complexity (potentially also related to higher forest productivity) was also indicated, as well as some forest edge-avoidance. East-facing aspects on knolls, as well as forest edge-attraction, were most important for the Cerulean Warbler (*Setophaga cerulea*), suggesting that other remote sensing data (e.g., three-dimensional lidar) may provide better information on its forest habitat

characteristics. Overall, the indices suggested habitat-based explanations for many of the observed differences among the three species' distributions, as well as new predictions to test regarding their spatial segregation on the ridgetops in this forest.

Keywords: Forest complexity mapping, remote sensing, redundancy analysis, canonical correspondence analysis, avian habitat selection

1. Introduction

Remote sensing of forest characteristics has a long history, and has become increasingly sophisticated. Aerial photography was used for rudimentary forest surveys as early as 1927 (Standish 1945). By the 1940s, however, the availability of high quality aerial photos and advances in photogrammetric equipment and photo-mensuration techniques provided a powerful inventory and mapping tool for foresters (Spurr 1948). Currently, there are numerous aerial and satellite remote sensors capable of forest assessment from very coarse (global; e.g., Hansen et al. 2013) to very fine (individual tree; e.g., Wulder et al. 2004, Ferraz et al. 2016) spatial scales. New active (i.e., radar-based) sensors such as synthetic aperture radar (SAR) and light detection and ranging (lidar) can provide detailed, three-dimensional forest structure information (Schmitt et al. 2013, White et al. 2016). Passive (i.e., reflection-based) sensors have also been developed that can provide detailed, albeit two-dimensional, forest structure information (Beguet et al. 2012). While classifying forest composition at the species level may be best achieved using hyperspectral imagery (Martin et al. 1998, Ferreira et al. 2016) or active sensors (Korpela et al. 2010), standard optical imagery can be used to map broad forest cover types (Homer et al. 2012), and high spatial resolution aerial and satellite imagery has been used to identify the species of individual tree crowns in a forest canopy (Erikson 2004, Waser et al. 2014).

There have also been advances in the geostatistical techniques used to analyze remote sensing data. One development applicable to high resolution forest imagery is the use of constrained ordination to relate the image data (and potentially other geospatial data) to data collected in the field. For example, Pasher and King (2010) and Torontow and King (2011) obtained explanatory variables from aerial and QuickBird satellite imagery (respectively), and a digital elevation model (DEM), for use in a redundancy analysis (RDA) of forest data at the field

plot level. The RDA further provided, via statistical model coefficients applied back to the remote sensing data, highly detailed maps of forest complexity throughout their study sites (for a related use, see Gomez et al. 2011). In addition to the value of such maps for forestry purposes, they may also have value for the remote assessment of biodiversity within these forests (Torontow and King 2011), based on the established link between forest complexity and forest biodiversity (Beckschäfer et al. 2013).

Eventually, active rather than passive remote sensing will likely be of greater value for collecting forest structure information at a fine spatial scale. Presently however, high spatial resolution imagery retains a number of advantages for this purpose. For aerial imagery, one is that its interpretation is more straightforward based on a long history of photographic image analysis (Pasher and King 2010). Some of the satellite imagery (e.g., Ikonos and QuickBird) with a spatial resolution comparable to that of aerial imagery appears to provide a comparably fine level of detail on forest structure (Beguet et al. 2012). Further, this satellite imagery has the advantage of greater spatial coverage with the narrow view angle per acquired image that is needed to detect fine-scale forest structure (Pasher and King 2010), and it lacks the uneven brightness and parallax distortion that is inherent in aerial imagery (Heumann 2011). Other advantages include cost and availability compared to actively-sensed data (Li et al. 2014). Research on the use of high resolution imagery for operational forestry is increasing (White et al. 2016), which may further clarify and promote its use in studying forest biodiversity.

For this study, we used a QuickBird satellite 0.6-m panchromatic image and a 3-m DEM to develop remotely-sensed indices of forest structure and composition on ridgetops in an Appalachian mature deciduous forest. We build on Chapter 2, where these remote sensing sources were used to separately model field-collected forest and avian point count survey data.

Here, we refined the analysis to better incorporate the ridgetop's complex topography, and used constrained ordinations to (1) characterize gradients in forest structure and composition as indicated by the field and remote sensing data; and (2) map these gradients as continuous indices throughout the site. In addition to obtaining information about the forest itself, we wished to discover if the mapped indices could model the spatial distributions of Cerulean Warbler (*Setophaga cerulea*), Hooded Warbler (*Setophaga citrina*), and Ovenbird (*Seiurus aurocapilla*) breeding territories. We expected the territory locations of these abundant species to differ based on known differences in their breeding habitat selection. In turn, we predicted that indices that quantified forest characteristics important to their habitat selection would help to explain their spatial distributions, in addition to the likely effects of topography and anthropogenic forest impacts. We tested these predictions using species distribution models (SDMs) of their territories mapped over two breeding seasons on two ridgetop transects.

2. Methods

2.1. Study site

This study was conducted primarily in mature deciduous forest on ridgetops at the Lewis Wetzel Wildlife Management Area, in northwestern West Virginia, USA. The site is in the topographically rugged Permian Hills region of the Western Allegheny Plateau (Woods et al. 1999), and during our study (ca. 2010–11) was >92% mature forest (Farwell et al. 2016). Elevation was 221–480 m (mean 356 m) above sea level. Major tree species included chestnut oak (*Quercus montana*), sugar maple (*Acer saccharum*), northern red oak (*Q. rubra*), red maple (*A. rubrum*), hickories (*Carya* spp.), black oak (*Q. velutina*), white oak (*Q. alba*), and black locust (*Robinia pseudoacacia*) (Appendix A). The ridgetop forest at the site has been previously

described as occurring in two general types: mesic and dominated by sugar maple, and xeric and dominated by chestnut oak (Perkins and Wood 2014). Canopy gaps located on topographic aspects with high solar exposure often contained dense grapevine (*Vitis* spp.) that appeared to inhibit forest succession, and occasionally the invasive tree-of-heaven (*Ailanthus altissima*). The understory of the xeric, chestnut oak ridgetops was often dominated by shrub-like greenbrier (*Smilax* spp.).

2.2. Field sampling

Data on forest structure and composition were collected during July–August in 2010 and 2011 at 68 ridgetop sampling points located within mature forest >150 m from anthropogenic canopy disturbances (Figure 1; see Chapter 2 for additional details), using a 5-subplot arrangement designed to encompass the topographic variability of the often sharply-defined ridgetops (Figure 1 inset). The subplot arrangement and vegetation measurements were adapted from standardized methods for collecting forest habitat data for bird studies (Martin et al. 1997). A central subplot was located on the point, and four surrounding subplots were located 35 m from the point using an initial random bearing and 90° intervals. Within an 11.3-m subplot radius, the species and dbh (diameter at breast height at 1.4 m) to the nearest cm for each tree ≥ 8 cm dbh, the number of snags (≥ 8 cm dbh and ≥ 8 m in height), and the number of grapevines that ascended trees were recorded. Within a 5-m subplot radius, the number of saplings (<8 cm dbh and ≥ 1.4 m in height) by species, and visual estimates of the percent cover (to the nearest 5%) of saplings, low woody plants (including shrubs, tree seedlings, and shrub-like greenbrier), and herbaceous plants were recorded. A spherical densiometer was used to estimate the canopy closure in the four cardinal directions at the subplot center, and a clinometer was used to measure

the height of a tree visually selected to represent the dominant canopy height of the 11.3-m subplot.

Additionally, we established six ridgetop transects (Figure 1) for territory mapping (Bibby et al. 2000) of the three bird species. Each transect was a network of primary and secondary ridge centerlines that were obtained by hydrological modeling of the 3-m DEM. We selected transects based on logistical constraints (ease of access and efficient travel routes) to cover much of the forested ridgetop conditions. For analyses in the present study, we focused on the two transects with two breeding seasons (2010 and 2011) of territory mapping data. The OR transect was 4.9 km in length and located completely within mature forest, with no obvious signs of human disturbance. The SR transect was 6.2 km in length and also within mature forest, but was impacted over a portion of this length (2.4 km) by a narrow forest road and pipeline (10–15 m wide) with four small (<0.4 ha) canopy openings for conventional natural gas and oil wells, and a 20-ha single tree selection harvest. This harvest removed about 25% of the canopy trees and was applied during the 2006–07 winter. These transects represented the topographic diversity of the site, with each containing locally high and low elevations (knolls and saddles) and a variety of ridge orientations. The SR transect further provided the opportunity to incorporate the anthropogenic impacts in the SDMs.

The territory mapping was conducted by J.S. over four sampling bouts per transect spread across each breeding season. Most of the sampling occurred between May 1 and June 30, the period of high breeding activity for the three species based on other avian breeding season research conducted at the site (Sheehan et al. 2014, Farwell et al. 2016), with some sampling in early July as long as breeding activity remained comparably high. Each bout was completed over 1–2 days, depending on the transect length that could be covered during the peak daily period of

singing by the territorial males of these species (0 to 4 hrs after local sunrise). The sampling occurred under optimal weather conditions (calm winds, no precipitation or heavy fog) for recording bird activity. During a visit, the transect was walked at a slow, regular pace (~1–2 kph), with short (<5 minute) pauses used as necessary to confirm locations of the species and record them on detailed field maps (1:5,000 scale). The maps included the transect ridgelines with points placed at 50 m intervals. A Garmin© 60CSX Geographic Positioning System (GPS) unit (WAAS-enabled ± 5 –10 m positional accuracy) containing these points was used to ensure accurate positioning for estimating the singing locations.

Because of transect side branches and 2-day bouts, logical junctures (e.g., ridgeline intersections and prominent knolls) were used to perform the surveys in segments to which even survey effort was applied. When coming back to a juncture and beginning a new map, it was compared with the previous map to help ensure that the same individual was not double-recorded. We considered 100 m to either side of the transect to be the maximum distance at which locations could be estimated with sufficient accuracy for their use in delineating territories. However, in practice the majority of individuals (>95%) were placed within 75 m of the transect. Over this distance we assumed there was little decline in detectability, although this could not be assessed because it was too difficult to also record the distance to each detected individual, especially when they were abundant. By conducting multiple surveys at the very top of the often sharply-peaked ridgetops (optimal for detecting the singing males in all directions), we also assumed that detection probabilities were sufficient for obtaining the locations of the majority of actively territorial individuals. A singing male was recorded as soon as possible after it was first heard and its location could be estimated, with adjustments for better accuracy when possible for individuals that continued to vocalize and did not appear to move. Lines were drawn

to connect simultaneous locations of individuals (conspecific males of all three species frequently countersinging) and denote individual movements on the maps.

Over the course of each season, the completed maps were scanned and then georeferenced (UTM NAD 83, Zone 17 N) and manually digitized in a geographic information system (GIS; ArcGIS 10.1, Environmental Systems Research Institute, Redlands, CA, USA) to obtain the individual locations as well as countersinging and movement events. At the end of the season, the bouts were overlaid in the GIS and ovals were drawn around clusters of locations to define individual territories. We used a minimum of two locations from >1 bout to define a territory (following Bibby et al. 2000 for when there are ≤ 8 visits), and often relied on counter-singing to separate territories. We did not consider the drawn ovals to represent physical territory boundaries because this would require more intensive techniques (e.g., burst sampling; Barg et al. 2005); instead, we determined the center coordinates of each oval in the GIS and used these points to represent the general locations of breeding territories (territory centers; hereafter). We collected habitat data as described above for a subplot for a preliminary analysis of forest characteristics at selected Cerulean Warbler and Ovenbird territory centers in 2010, and at Cerulean Warbler non-use points in 2011 (Appendix B). As collected over the extent of the SR and OR transects, this sampling also provided $n = 97$ habitat samples which we used as external data for validation of the remotely-sensed forest indices (section 2.4).

2.3. Remote sensing data

We obtained a cloud-free QuickBird 2 (DigitalGlobe®) satellite 0.6-m panchromatic image (acquired 25 August 2009 at 16:18 GMT, 6° off-nadir, solar azimuth = 127°) and a 1/9 arc-second DEM (3-m spatial resolution and ± 3 m vertical accuracy; source: <http://viewer.nationalmap.gov/>). The satellite image was orthorectified in Erdas Imagine 9.3

using the DEM, the rational polynomial coefficients supplied with the image, and six ground control points obtained from 1-m resolution leaf-on orthophotos (2007 National Agriculture Imagery Program). The root mean squared error of the rectified image was 3.3 m (X direction) and 2.6 m (Y direction). Because there were no major disturbances (e.g., severe windstorms) between the image date and the field sampling, and new tree falls were infrequent based on the 2010–11 field sampling, we assumed the image and the field data were a temporal match.

We used the zonal statistics function in ArcGIS 10.1 to obtain a set of variables from the satellite image and DEM to use in the constrained ordinations. We selected a 15-m radius from the subplot centers to extract the zonal statistics (i.e., pixel summaries; including the mean and s.d.) from the various layers (Appendix C). This was the maximum radius possible without overlapping adjacent subplots, and overall it produced remote sensing variables that were comparatively more strongly correlated with the field data variables than smaller radii (5 and 10 m), based on preliminary testing.

We first chose the three satellite image statistic measures that we previously found most useful for analyzing the forest data at a larger local scale (50-m radius plots; Chapter 2) for inclusion in the set of variables. These were the panchromatic image mean (PAN_{AVG}) and s.d. (PAN_{SD}), and the s.d. from a second-order correlation texture image computed from the panchromatic image using a 9x9 pixel moving window (PAN_{SD_COR09}). For topography, we included mean elevation, topographic slope, and the sine and cosine derivations of topographic aspect. These derivations transformed the circular aspect directions (0–360°) into linear values for eastness (-1.0–1.0; due west to due east) and northness (-1.0–1.0; due south to due north); respectively. We did not include a solar insolation index because it was highly correlated with northness (Spearman's rank-order correlation $r_s = -0.87$) and moderately correlated with eastness

($r_s = 0.53$). Use of northness and eastness allowed us to more flexibly model the complex ridge topography, and still infer the likely influence of solar insolation (e.g., on forest composition of north- versus south-facing aspects). Finally, to potentially represent different spatial scales of satellite image information, we included eight additional image texture statistic measures (Appendix C) from among a large number available (see Chapter 2 for full listing and computational details), ensuring a pairwise $r_s < 0.80$ among all variables (Appendix D) and also a variance inflation factor of < 5 (for stability of the variable selection procedure; section 2.5.).

For use only in the SDMs, we determined the coordinates of the tops of prominent knolls on the two transects based on 3-dimensional modeling of the DEM and field verification, and created a continuous distance grid from these locally high elevation points. We also digitized the anthropogenic impact to the SR transect, and created a continuous distance grid from the impact edges. This impact grid was also manipulated for inclusion as a local effect (likely more realistic for models applied at larger spatial scales) by truncating the continuous distance at various maximum distances, and also by transforming it to a categorical impact grid (i.e., “impacted” and “not impacted”) at a specified distance. We applied Gaussian filtering to the mapped forest structure and composition indices using a s.d. of 5 m at intervals up to 25 m, to examine the influence of different spatial scales for locally averaging the indices to reduce noise (and thus potentially maximize their information content). To speed processing time, all of the spatial data layers used in the SDMs (see section 3.3.) were resampled to a 5-m resolution.

2.4. Remote sensing index development

We evaluated the use of RDA and canonical correspondence analysis (CCA) for developing the indices of forest structure and composition. These constrained ordination techniques allow two matrices of data collected at the same locations to be analyzed simultaneously (Legendre and

Legendre 2012). For our study, the matrices (with one row per subplot; $n = 340$) were the field data as response variables and the remote sensing data as explanatory variables. RDA and CCA produce successive, orthogonal ordination axes that are linear combinations of explanatory variables, and these axes best explain (in decreasing amounts) the variation present in the matrix of response variables (Borcard et al. 2011). While closely related, RDA and CCA differ in application, with RDA more appropriate for linear trends in response variables over relatively short environmental gradients and CCA more appropriate for unimodal trends in response variables over longer environmental gradients (ter Braak and Prentice 1988). A common method to choose between them is to first use detrended correspondence analysis (DCA) on the paired data matrices to examine the gradient length of the first ordination axis. A gradient length of >4 s.d. units of species turnover (e.g., for community composition data) indicates that at least some species exhibit unimodal responses and the use of CCA is advised (Borcard et al. 2011).

We used DCA, RDA and CCA as implemented in the vegan R package (Oksanen et al. 2016) to analyze three sets of field variables (list and summary statistics in Appendix A), using the set of remotely-sensed explanatory variables for each of the analyses. Based on DCA as an initial step to check the gradient lengths, in the first analysis (RDA_S) we used RDA to model 11 forest structure variables; in the second analysis (CCA_C) we used CCA to model tree species composition (percent of total basal area); and in the third analysis (RDA_{S+C}) we used RDA to model the forest structure variables plus tree species richness and chestnut oak and sugar maple composition (29.5% and 22.3% of total basal area; respectively). We used percent of total basal area (i.e., a measure of relative importance) instead of actual basal area for species composition because doing so resulted in stronger CCA_C and RDA_{S+C} models. Prior to the analyses, to achieve normality and reduce the influence of outliers (Legendre and Legendre 2012), we

graphically examined the explanatory and forest structure variables and applied data transformations if necessary (noted in Appendix A and C). We applied the arcsine square root-transformation to the tree species composition data.

We used the *ordistep* function in the vegan R package to determine if there was a parsimonious set of explanatory variables for each of the analyses from among the full set. This function performs variable selection for constrained ordinations through the use of permutation tests (Oksanen et al. 2016). We used the default forward-backward variable selection, $P \leq 0.05$ to add a term to the model and $P > 0.1$ to drop a term from the model, and 999 permutations. Based on the results of the selection procedure, we re-ran the analyses to produce a final RDAs, CCA_C and RDA_{S+C} model using the reduced set of explanatory variables that were selected for each model.

For each final model, we made plots of the dominant ordination axes as judged by the proportion of the total variance they explained. These ordination plots displayed arrows originating from the plot center to represent the explanatory variables, which by their orientations and lengths (as determined by adjusted R^2 vector fits) indicated how they were associated with the field variables, as well as their correlation with the ordination axes. We examined these plots to determine gradients in forest structure and composition as indicated by the ordination axes for potential mapping. To make the maps, we used the ArcGIS 10.1 raster calculator to multiply each pixel of the spatial data layers by their respective axis model coefficients (obtained with the vegan *coef* function), then summed these new layers. Prior to this calculation, we transformed the spatial data layers as needed for the applied model coefficients, and processed them using a 15-m radius circular moving window (focal mean or s.d., depending on the layer) to match the scale used for the ordinations.

We used leave-one-out cross validation (LOOCV) to evaluate the stability of the final models using the original data (i.e., internal validation), and also how well these models predicted the externally collected data (i.e., external validation). Both evaluations used the Pearson's correlation (r) between the site (i.e., field plot) WA scores and the LC scores for the dominant ordination axes. Originally defined for CCA applied to community data (e.g., see Graffelman and Tuft 2004), WA scores are weighted averages of species scores and LC scores are linear combinations of environmental variables. The correlation between these scores is thus often called the 'species-environment relationship' (e.g., Legendre and Legendre 2012). Following McCune (1997), we refer to the species-environment relationship for our data simply as the WA-LC correlation hereafter. To evaluate model stability, we used the *vegan* R package *predict* function to iteratively predict the scores for each row of held out data from a model using the rest of the data ($n = 339$), and obtained the WA-LC correlation between the set of predicted scores to compare with the WA-LC correlation obtained for the final models. To evaluate the predictive potential of the indices (which are the LC scores mapped as a continuous surface) for modeling the bird species territory habitat, we used the function to predict the WA and LC scores for the external data, and then applied LOOCV to linear regression models relating these scores. For both evaluations, we calculated the RMSE (root mean square error) as a percentage of the range of the WA scores.

2.5. Species distribution modeling

We used point pattern analysis (PPA) in the *spatstat* R package (Baddeley et al. 2015) to perform the distribution modeling. The point patterns were the territory centers of each species on the ridgetop transects in each year, and we used a buffer of 75 m to either side of the ridge centerlines to define the sampling window for each transect (Figure 1). In this paper, we follow

PPA terminology and use ‘intensity’ to refer to the average density of points per unit area. We tested if intensity varied in relation to spatial covariates (e.g., the mapped indices) covering the sampling windows. We assumed that using points (the territory centers) to represent selection by the species of territory areas was appropriate for the relatively large spatial scale of this investigation, and we also did not consider processes of attraction and repulsion between the points in the models. We chose this application of PPA because it can closely approximate other commonly used SDM techniques such as spatial logistic regression and Maxent (Baddeley 2010, Fithian and Hastie 2013). The chief advantages of PPA (and spatstat) for our study were the variety of techniques available for statistical modeling (both parametric and nonparametric) and visualization, model diagnostics, and data handling flexibility.

The relation between intensity and a spatial covariate is tested in a spatstat point process model (PPM) through the use of quadrature points. These points provide background values for the covariate over the sampling window to compare with the covariate values obtained for the observed point pattern. To accurately estimate the background, it is important that the number of quadrature points be sufficiently large (Renner et al. 2015), and it is also important that the spatial resolution of the covariate be sufficiently fine so that individual points of the observed pattern do not share the same pixel (Aarts et al. 2012). For the point patterns of each species, inter-point distances were easily sufficient so that pixel values for the 5-m resolution covariates were unique to each point. We selected an appropriate number of quadrature points by successively increasing their number on a regular grid until the maximum likelihood estimates for the PPMs converged (Renner et al. 2015).

Our primary goal was to seek SDMs that could apply across the combined OR-SR transect extent. We focused both on finding covariates that were consistently related to intensity over the

combined transect extent, and finding covariates that differed in how they were related to intensity between the two transects (e.g., those positively related to intensity at one transect but not the other). To help indicate these two general types of covariate effects, we attached categorical transect “marks” to the points and tested the significance of transect by covariate interaction PPMs using likelihood ratio tests. To infer the presence of single covariate effects on intensity, we examined the model parameter 95% confidence intervals (CI). We also sought to combine multiple covariates to explain intensity. To evaluate PPMs, we used the Akaike Information Criterion (AIC) provided by spatstat as a measure of relative fit, examined model diagnostic plots, and mapped the predicted intensity trends for the species across the transects.

We used nonparametric techniques implemented in spatstat (the univariate *rho.hat* and bivariate *rho2.hat* functions) to visualize the relation between intensity and the spatial covariates. These functions allow covariate effects on intensity of no pre-specified form to be fit graphically, and further can provide this fit relative to a previously-fitted PPM (Baddeley et al. 2012). This second capability was valuable because it allowed us to visualize how additional covariates affected intensity, conditional to how intensity was already explained by a PPM. These additional effects could, for example, be indicated as separable from other effects (see examples in Baddeley et al. 2012). Along with the spatstat *parres* function, these nonparametric functions also helped to indicate if polynomial terms should be considered for covariates in the PPMs.

2.5.1. Initial model predictions

We tested a number of species-specific predictions for covariate effects on intensity. The first predictions were based on likely differences among the species according to habitat structure. While both the canopy-nesting Cerulean Warbler and the shrub-nesting Hooded Warbler have been associated with forest canopy gaps (e.g., Perkins and Wood 2014, Pasher et al. 2007;

respectively), during territory mapping Hooded Warblers were most often recorded within the understory of canopy gaps, whereas Cerulean Warblers were recorded on the edges of canopy gaps but also nearby in areas with a more continuous canopy. The Ovenbird has typically been associated with closed forest canopies with relatively open understories for nesting (Porneluzi et al. 2011), and during territory mapping it was primarily recorded in such areas. We thus predicted that Hooded Warbler intensity would be positively related to mapped indices that characterized forest structural complexity in the form of canopy gaps. We predicted that Cerulean Warbler intensity would also be positively related to these indices, but less strongly, and that Ovenbird intensity would be unrelated, or potentially negatively related, to these indices. Analysis of point count survey data at the site (Chapter 2) supported these predictions in part, as Hooded Warbler occurrence and abundance were positively and relatively strongly related to PAN_{SD} (calculated at a 50 and 100 m radius; respectively). For the other two species, however, only occurrence was positively (and relatively weakly) related to this image texture measure.

We made two predictions related to likely topographic influences. Several studies have found that Cerulean Warblers select particular aspects for breeding activities (e.g., Hartman et al. 2009: east-facing aspects; Weakland and Wood 2005, Barnes et al. 2016: northeast-facing aspects). In contrast, we were able to find no published information on Hooded Warbler or Ovenbird breeding habitat selection in relation to aspect. However, we suspected that aspect strongly influenced all three species, as Ovenbirds were frequently detected on opposite-facing aspects from where the other two species were detected. Because of the highly convoluted ridge orientations at the site, we tested the general prediction that differences would be found among the species' intensities in relation to eastness, northness, or both in combination. The second prediction was for a positive Cerulean Warbler distance to knoll association, as Cerulean Warblers were more often observed

near the tops of knolls, even minor ones, than the other species. We found no published information to support a potential knoll association, although prior research at the site conducted in 2008 and 2009 (included in Sheehan et al. 2014) was supportive, as particularly high Cerulean Warbler numbers were known to occur on two prominent knolls located on the SR transect, and elsewhere.

The final predictions were for potential effects on intensity from anthropogenic impacts on the SR transect. The Cerulean Warbler in particular was likely to be attracted to the internal forest edges created by the narrow SR transect impact (Rodewald 2004, Weakland and Wood 2005), and during territory mapping it was commonly recorded directly on the impact edges. Potentially the Hooded Warbler could be attracted to the impact as well (e.g., to shrubby edges for nesting), although no clear pattern in relation to the impact was observed for it during the mapping. In contrast, the Ovenbird could potentially exhibit repulsion from the impact, as found by Ortega and Capen (1999) also in a heavily forested landscape. In support of this, there appeared to be relatively few Ovenbirds in the impacted sections of the SR transect compared to unimpacted sections.

3. Results

3.1. Forest structure and composition modeling

The forward-backward selection procedure resulted in a forest structure model (RDA_S) with seven variables, and forest composition (CCA_C) and forest structure plus composition (RDA_{S+C}) models with eight variables each (Table 1). As indicated by the relatively low proportion of variance explained across the models (13.5–22.3%), there was considerable noise in the field data as fit by the remote sensing data. However, each model contained a number of significant

axes (four for RDA_S and five for CCA_C and RDA_{S+C}), suggesting there were also some potentially informative signals in the field data (e.g., general multivariate gradients; Pasher and King 2011). The PAN_{SD} measure was also consistently the first variable selected for each model (indicative of its relative strength, see also Chapter 2). All models retained a mixture of image texture and topographic variables, and included spectral brightness (PAN_{AVG}) as well as a coarser-scale version of the second-order correlation texture s.d. (PAN_{SD_COR17}). Within each model, the majority of variance was explained by the first ordination axis ($RDA_S = 12.9\%$, $CCA_C = 8.6\%$, and $RDA_{S+C} = 17.0\%$; Table 1). We made ordination plots for each model (Figure 2) using the first ordination axis and the second ordination axis, which explained an additional 2.7%, 2.1%, and 2.8% of the variance for RDA_S , CCA_C , and RDA_{S+C} ; respectively.

Basal area, herbaceous cover, and grapevine density had the most spread along the first ordination axis of RDA_S (Figure 2a). This supported the existence of a forest structure gradient among the field plots, ranging from those with higher basal area (plots to the left in Figure 2a) to plots with higher herbaceous cover and grapevine density (plots to the right in Figure 2a). As in Chapter 2, inspection of the satellite image at the plots suggested that this gradient was related to the range of canopy closure present in mature, non-anthropogenically disturbed forest at the site. We characterized this gradient overall as one of forest structural complexity, with a less complex, closed canopy (associated with higher basal area), grading into a more complex, open canopy (associated with higher herbaceous cover and grapevine density). For CCA_C , a gradient in tree species composition along the first ordination axis was indicated by the canopy dominants (Appendix A) chestnut oak (plots to the left in Figure 2b) and sugar maple (plots to the right in Figure 2b), and by additional species. For example, the other oak species were separated out with chestnut oak from tree-of-heaven and slippery elm, which were at the opposite end of the

gradient with sugar maple. While the RDA_{S+C} ordination (Figure 2c) was otherwise similar to the structure variable-only RDA_S ordination, the addition of chestnut oak and sugar maple composition resulted in these species being aligned with the first ordination axis, but having the greatest spread along it.

The difference in the relative positions of sugar maple and chestnut oak for characterizing the first ordination axis of RDA_{S+C} (located at the extremes) versus CCA_C (differentiated, but other species located at the extremes) was a likely a function of the technique's modeling of linear versus unimodal responses; respectively, and because common species have less of an influence on CCA than rare species (Legendre and Legendre 2012). Both techniques appeared to provide useful information. CCA helped to highlight less dominant tree species that were nonetheless important for characterizing the primary composition gradient. Adding chestnut oak and sugar maple composition to the structure variables in RDA_{S+C} helped to highlight the association between these canopy dominants and the primary structure gradient. The association between the primary structure and composition gradients (as modeled by the remote sensing data) was further indicated by the relatively high correlation between the first ordination axes of RDA_S and CCA_C ($r_s = 0.71$). Not surprisingly, the first ordination axes were highly correlated between RDA_S and RDA_{S+C} ($r_s = 0.93$), and between CCA_C and RDA_{S+C} ($r_s = 0.86$).

The PAN_{SD} and PAN_{SD_COR17} textures were most strongly correlated with the first ordination axis across the models (Figure 2), and were similarly orientated for each model, with PAN_{SD} positively correlated and PAN_{SD_COR17} negatively correlated with the axes. Additional variables were closely aligned with PAN_{SD} (PAN_{SD_CON09} for RDA_S and RDA_{S+C} , eastness for RDA_{S+C} , and PAN_{SD_AVG25} for CCA_C), but had shorter arrow lengths (i.e., lower R^2 fit; particularly eastness). The PAN_{AVG} measure was diagonal to the first and second ordination axis (lower right

quadrant) across the models. Compared to RDAs, the addition of forest composition to the structural variables for RDA_{S+C} increased the PAN_{AVG} association with grapevine density and herbaceous cover. Thus, while PAN_{AVG} increased in the direction of these structure variables for both models, for RDA_{S+C} this brightness measure also helped to separate these variables from sugar maple, likely indicative of larger canopy gaps. For CCA_C, PAN_{AVG} was oriented toward a number of pioneer tree species that favor disturbance (e.g., tree-of-heaven, slippery elm, and black locust), and was also closely aligned with the weaker fit provided by eastness.

The second ordination axis across the models appeared to primarily represent topographic influences on forest structure and composition (Figure 2). For RDAs and RDA_{S+C}, elevation was negatively correlated with the axes in the direction of plots with higher tree density and shrub cover (and tree species richness for RDA_{S+C}), while topographic slope and northness were both positively correlated with the axes in the direction of plots with greater tree height and the mean and s.d. of tree dbh. Although topographic slope and northness were also positively correlated with the CCA_C second axis, the slope correlation was relatively stronger. Species such as white oak and black oak became more dominant in plots with flatter slopes (i.e., plots opposite the slope arrow), and there were also species favoring steeper slopes (e.g., American beech and tulip poplar). American beech and black oak in particular were related to north- and south-facing aspects; respectively. As noted above, eastness was diagonal to the first and second axes with PAN_{AVG} for CCA_C, indicating some association between east-facing aspects and the higher spectral brightness that was related to the above-noted tree species. The image texture PAN_{SD_CON03} was also diagonal to the CCA_C axes (but in the upper right quadrant), and characterized plots with more American basswood, shagbark hickory, and sugar maple.

3.2. Validation and mapping of the indices

The WA-LC correlations (Table 2) were moderately strong for the first ordination axis across the models. Constrained ordination techniques seek to maximize this correlation, however, so it is important to note that the correlations pertain only to the relatively low amount of variance explained by the models. The correlations were higher for CCA_C ($r = 0.81$) and RDA_{S+C} ($r = 0.79$) than for RDA_S ($r = 0.72$), but again this must be interpreted with caution because of the different sets of response variables analyzed. More importantly for prediction purposes, the internal LOOCV indicated stability for the correlations across the models, with only relatively small reductions in fit. For RDA_S and RDA_{S+C} , the external LOOCV produced correlations approximately equivalent to those of the original models, with a relatively small percent RMSE increase (<5%) over the internal validation. This suggested that these models, built using data from the full study area extent, predicted within the smaller extent of the two transects similar to how they predicted more broadly. For CCA_C , the external LOOCV resulted in a larger correlation reduction (r from 0.81 to 0.66), and a larger percent RMSE increase (8%), so conversely this model predicted relatively less well when applied only within the smaller extent of the two transects.

The lower WA-LC correlations for the second ordination axis were also relatively stable across the models according to the internal LOOCV, albeit with somewhat larger RMSE. However, predictive ability was poor to nonexistent according to the external LOOCV (e.g., r became near 0 for CCA_C). For this reason, we opted to map only the first ordination axis for each model. As described above (section 2.4.), we produced continuous predictive maps (referred to hereafter as RDA^1_S , CCA^1_C , and RDA^1_{S+C}) across the area of the two ridge transects (Appendix E). Visually, the RDA^1_S and the RDA^1_{S+C} maps were nearly identical due to their high first ordination axis correlation. Portions of the RDA^1_{S+C} map (and associated panchromatic images)

are shown in Figure 3 to illustrate several key patterns. Locally within the transects, areas of predicted high structure/sugar maple composition often dominated south- and east-facing aspects. In the panchromatic image, these areas have a characteristically rough forest canopy which contains spectrally brighter gaps. Important for the generality of the index across aspects, the map also indicated a complex forest canopy on more north-facing aspects that were more shaded due to the sun angle at the time of image acquisition.

The RDA^1_S and RDA^1_{S+C} maps also indicated areas of smooth canopy in the imagery, with predicted high basal area/chestnut oak composition (e.g., see arrows in Figure 3). Across the extent of the two transects, there was a general southwest to northeast trend from where such smoother canopies were more dominant, to areas where rougher canopies were more dominant (i.e., with predicted high structure/sugar maple composition). This pattern was similar to the broader pattern (across the full study area extent) observed for several image measures such as PAN_{SD} and PAN_{AVG} at the coarser resolution that was the focus of the Chapter 2 analyses. The RDA^1_S and RDA^1_{S+C} maps, however, more clearly showed the pattern according to the multiple aspects across the two transects, which is a consequence of modeling the field and remote sensing data at the finer subplot scale. For the CCA^1_C map, while the coarser-scale pattern was still evident, much of the differentiation in the index values according to aspect appeared to be lacking.

3.3. Territory maps and SDM covariate selection

A similar number of Ovenbird territories were mapped in 2010 and 2011 ($n = 69$ and $n = 68$; respectively), but from 2010 to 2011 the number of Cerulean Warbler mapped territories substantially increased (from $n = 71$ to $n = 96$) and the number of Hooded Warbler mapped territories nearly doubled (from $n = 55$ to $n = 97$). Inspection of the point patterns as represented

by the species' territory centers revealed several patterns of interest. As a combined species pattern in each year (Figure 4), there was relatively little unoccupied area across the transects. At the local (i.e., within ridge) scale, while the three species often occurred in relatively close proximity to each other, there also were areas in which they occurred more separately. The Cerulean Warbler exhibited greater clustering than both the Hooded Warbler and Ovenbird. For these species too, however, there were areas where they occurred more densely. In 2011, territories of each species were often located in the same areas as in 2010 (combined-year maps by species are in Appendix E). This was most obvious for the Ovenbird, but was also apparent for the other two species despite their 2011 increases.

Based on preliminary modeling, we selected a 15 m s.d. for the Gaussian filtering of the mapped indices (done with the spatstat *blur* function). This amount of smoothing (shown for RDA^1_S and CCA^1_C in Figure 5a, b) provided a balance between preserving the indices' spatial patterns and maximizing how strongly they could model the species. This filter also effectively smoothed over the narrow SR transect impact (represented on the elevation layer; Figure 5c, and in Appendix E). Because of this, we did not mask out the impact from the indices, and relied on the impact covariate to account for forest edge attraction or repulsion, and the indices to account for effects of the surrounding mature forest habitat, in models combining these covariates. In support of this decision, we detected no consistent spatial pattern in the values of the smoothed or original indices over the extent of the impact. We also let the indices alone represent the selection harvest at the SR transect (Appendix E), as we could not detect any obvious signs of a harvest (e.g., a boundary) in the satellite image from this low amount of canopy tree removal.

We used the same topographic layers that were used for the constrained ordinations in the SDMs (Figure 5c-f). Of these, topographic slope (Figure 5d) remained relatively noisy despite

the 15-m radius focal mean and the 5-m resolution resampling. Further smoothing of the slope layer did not improve its ability to model the species however, and in its original form it depicted potentially interesting characteristics (e.g., flatter areas on knolls and particularly “spiny” ridges on the SR transect). Over the combined transect extent, the topographic layers were relatively uncorrelated with each other and with the indices (Appendix D), which facilitated the modeling. However, because elevation and slope were often locally correlated in modeling intensity (e.g., locally higher elevations often had flatter slopes), we selected only one of these for the multiple covariate SDMs, based on their individual AIC fit and consideration of model diagnostics.

3.4. SDM single and multiple covariate effects

We found a variety of single covariate effects on intensity among the species, and also models of combined covariate effects for each species (full results in Appendix F). We did not attempt to evaluate all possible covariate combinations, but focused on combining covariates to create plausible models of their habitat use, based on knowledge of a species and the annual consistency of effects. In summary regarding the initial predictions prior to the more detailed results presented below, the forest structure-based indices were most strongly related to Hooded Warbler intensity as predicted. Considered singly, however, the indices were mostly unrelated to Ovenbird and Cerulean Warbler intensity. Instead, topography and anthropogenic edge best differentiated them. Notably, eastness of aspect had opposite effects on their intensities (west-facing for Ovenbird and east-facing for Cerulean Warbler, consistently across the transects), as did the SR transect impact (repulsion for Ovenbird and attraction for Cerulean Warbler, as predicted). Interestingly, while the eastness effects were strong (including for Hooded Warbler in certain areas), we found little to no effects of northness. Finally, the predicted Cerulean Warbler attraction to knolls was well supported across the transects.

3.4.1. Hooded Warbler

Spatially, the Hooded Warbler intensity trend was largely consistent with the broad-scale patterns of the indices (e.g., as indicated in Figure 5a, b). Based on the predicted intensity from a PPM containing only the RDA¹s index (Figure 6), the strongest of the indices for modeling Hooded Warbler, this occurred in both years as higher intensity in the northern region of the SR transect, and at the OR transect overall. In 2010, the effect was somewhat stronger, with the relative scarcity of Hooded Warbler territories more pronounced in the central to southern region of the SR transect. Despite the territory number increase in 2011, however, this regional disparity remained. There was also no evidence in either year to support that the SR transect impact influenced this pattern.

Eastness and elevation were also relatively strong predictors of Hooded Warbler intensity, with largely consistent between-year effects. Further, an improved model AIC fit occurred when the RDA¹s index was combined with eastness (AIC Δ = 1.48 and 4.31 in 2010 and 2011; respectively) and with elevation (AIC Δ = 4.08 and 6.18 in 2010 and 2011; respectively). The bivariate RDA¹s index by eastness plots (Figure 6) indicated that high Hooded Warbler intensity coincided with higher index and eastness values (the upper right plot quadrant) in both years (also see section 3.4.1.). This trend occurred as higher predicted intensity primarily on east-facing aspects at the OR transect, however. A positively-sloped pattern in the territory covariate values (particularly discernible in 2011) was also evident for the RDA¹s index by eastness plots. This was largely an artifact of the SR transect, due to the large number of Hooded Warbler territories in low RDA¹s index areas and also ranging across west- to east-facing aspects there.

The bivariate RDA¹s index by elevation plots (Figure 6) indicated that high Hooded Warbler intensity also coincided with higher index and elevation values in both years. Outside of this

dominant pattern, the vertical spread in the territory covariate values (again more discernible in 2011) was also largely an artifact of the SR transect, because of the number of Hooded Warbler territories in low RDA^1_s index areas at higher elevations. Spatially, these two predictors of Hooded Warbler intensity were also partly in opposition to each other, as there were higher elevations at the SR transect relative to the OR transect, and mostly the opposite pattern for the RDA^1_s index (Figure 5). Combining all three covariates in one model, or just elevation with eastness, caused a number of fit issues (PPM diagnostic plots are in Appendix F), a not surprising finding given the different spatial patterns for these predictors.

3.4.2. *Ovenbird*

The dominant trend for the Ovenbird was higher intensity on west-facing aspects in both years. This trend can be seen in the predicted intensity from a PPM containing only eastness (Figure 7), and the spatial consistency of this trend was supported by the lack of significance for the eastness by transect interaction in each year ($P = 0.976$ and 0.761 for 2010 and 2011; respectively). Of the indices, a peak in intensity occurred for intermediate values of the RDA^1_s index, but only in 2010. This index was more informative in both years when considered in combination with the apparent selection by Ovenbird for west-facing aspects, however (also see section 3.4.1.). This was evident in the bivariate RDA^1_s index by eastness plots (Figure 7) as higher Ovenbird intensity coinciding with moderate values for the index and west-facing aspects. A quadratic polynomial for the RDA^1_s index added to the eastness model caused a small fit improvement in 2010 ($AIC \Delta = 0.79$) and a larger one in 2011 ($AIC \Delta = 2.77$), and improved models based on residual diagnostics in each year. Much of the selected moderate RDA^1_s index area occurred in the north of the SR transect, and at the OR transect overall.

Some repulsion from the SR transect impact was indicated for the Ovenbird in each year, with a slightly stronger effect apparent in 2011 (Figure 7). We truncated the impact edge distance at 75 m to attempt to incorporate this repulsion as a local effect along with eastness and the RDA¹_s index. This combined model resulted in better AIC fit in both years (AIC Δ = 1.21 and 7.48 in 2010 and 2011; respectively) and improvements based on residual diagnostics. Adding this modified impact covariate caused little change to the broader-scale eastness and RDA¹_s index effects in 2010, but in 2011 the RDA¹_s index effect decreased somewhat (model parameter estimate changes are noted in Appendix F), which meant that the impact and the index coincided in part in explaining Ovenbird intensity. While excluding the RDA¹_s index produced competitive eastness+impact PPMs in terms of AIC fit (AIC Δ = 0.06 and 0.29 in 2010 and 2011; respectively), these models were less valid based on residual diagnostics.

Selection for flatter to moderate slopes was also indicated for Ovenbird intensity in both years (Figure 7). Adding topographic slope to eastness, the RDA¹_s index, and the truncated impact improved model fit in both years (AIC Δ = 2.80 and 4.42 in 2010 and 2011; respectively), with residuals diagnostics unaffected. For 2011, however, this combination caused a further decrease in the RDA¹_s index effect, apparently related to the slope by transect interaction effect for 2011 (P = 0.048; with selection for flatter slopes at the OR transect), versus 2010 (P = 0.675). We considered this 5-term model to be rather complex, also considering the relatively noisy nature of the slope covariate. One interesting spatial tendency related to slope, however, was that flatter slopes often occurred in proximity to the ridgelines (Figure 5d), and a number of Ovenbird territories in each year centered near the ridgelines were thus partly responsible for this effect.

3.4.3. *Cerulean Warbler*

Eastness combined with knolls more strongly modeled Cerulean Warbler intensity in both years than eastness alone based on fit (AIC $\Delta = 14.08$ and 13.24 in 2010 and 2011; respectively). This combined trend can be seen in the predicted intensity from an eastness+knolls PPM as higher intensity for east-facing aspects in proximity to the tops of knolls (Figure 8). Covariate by transect interaction models supported the spatial consistency of the eastness trend ($P = 0.907$ and 0.169 for 2010 and 2011; respectively) and the knolls trend ($P = 0.403$ and 0.295 for 2010 and 2011; respectively) across the transects. The bivariate knolls by eastness plots indicated that highest intensities occurred approximately <100 m from the tops of knolls and for eastness values >0.5 in both years (Figure 8). Notably, while some dense clusters of territories in proximity to knolls were evident at both transects (e.g., in their southern regions), this knoll proximity was also evident for smaller clusters and even lone territories. Despite the relative strength of the combined eastness-knolls model, however, the residual diagnostic plots in particular pointed to a lack of fit where the densest clusters occurred.

Although Cerulean Warbler intensity was not related to any of the forest indices, it strongly increased near the SR transect impact in both years (Figure 8). We included this local effect with other covariates using a 10 m edge distance categorical covariate (i.e., ≤ 10 m from edge equals “impacted”), which produced a strong effect due to the number of territories centered on or close to the impact edges (including in the dense clusters). The addition of this impact covariate largely overwhelmed other covariate effects in terms of predicted intensity across the transects, however (e.g., see eastness+knolls+impact PPM in Appendix F). This also reduced the knoll effect somewhat, a consequence of the impact running through a number of the prominent SR transect knolls with abundant territories. Elevation was also a relatively strong predictor of

Cerulean Warbler intensity in both years (Figure 8), but as with Hooded Warbler, predicted intensity appeared to be positively biased toward the higher elevations of the SR transect. In combined models, the elevation effect reduced the knoll effect somewhat (i.e., intensity was modeled in part by higher elevations on knolls). The elevation and impact effects also competed, a consequence of the impact being located on the higher elevation SR transect. Despite increases in AIC fit when elevation and the impact were combined (singly or together) with eastness and knolls, residual diagnostics still indicated the fit issues apparently caused by the dense clusters.

3.4.4. Separability of effects

Along with those mentioned above, other covariates when combined sometimes competed with each other in modeling intensity. This occurred because the covariates, while relatively uncorrelated across the combined transect extent, could exhibit local correlation (e.g., as in elevation and topographic slope; described in section 3.3). Other effects were largely separable, indicated by the relative lack of parameter estimate changes when combined (e.g., eastness+knolls for the Cerulean Warbler), which could also be seen as little change in nonparametric *rho*_{hat} functions after controlling for covariate effects on intensity. We were most interested in examining how the RDA¹s index and eastness together partly explained Hooded Warbler and Ovenbird intensity (Figure 9). For the Hooded Warbler, while the intensity trend in relation to the RDA¹s index remained in both years after controlling for eastness, it was weakened at higher index values relative to the univariate trends. In other words, some of the most east-facing aspects already partly explained Hooded Warbler intensity (conversely, this could also be seen for eastness after controlling for the RDA¹s index). For the Ovenbird, not controlling for eastness prior to modeling the RDA¹s index resulted in a rather weak unimodal peak in intensity at intermediate index values. Controlling for eastness, however, helped to

clarify that within west-facing aspects there was a positive intensity trend in relation to the RDA¹_S index, and that this trend was more pronounced in 2011.

4. Discussion

As noted by Torontow and King (2011) for RDA similarly applied to a mixed hardwood forest in Quebec, Canada, we also found that the use of constrained ordination provided an information-rich display of the structure and composition of this ridgetop forest, and helped to define environmental gradients that were also characterized by the satellite image and DEM. This occurred despite the relatively low amount of variation in the field data that was explained by the remote sensing data, a result of the inclusion of a number of response variables in each analyzed set that did not contribute to the observed gradients. To manually pre-select the field variables that appeared to contribute most (e.g., through preliminary modeling) would simply have produced a deceptively high amount of explained variance. The multivariate gradients that were indicated however, notably by grapevine density, herbaceous cover, basal area, and chestnut oak and sugar maple composition, were strong enough to be related to the linear combinations of remote sensing variables. Importantly for modeling the bird species, the relative predictability of the primary forest structure and composition gradients found across the models received cross validation support.

The satellite image measures that we previously found to be most useful for modeling forest characteristics at the plot level (Chapter 2) were also the ones most useful at the smaller subplot scale. The value of the selection procedure for a more parsimonious model of each set of response variables was in selecting a version of the second order Correlation texture (PAN_{SD_COR17}) that was a better predictor at the subplot scale, and further for indicating based on

selection order that the satellite image variables tended to be stronger predictors than the DEM-derived topographic variables. While useful for explaining some forest gradients (e.g., a positive shrub cover-elevation correlation), the topographic variables mostly explained variation for the second ordination axes, and the stronger satellite image variables (PAN_{SD} , PAN_{AVG} , and PAN_{SD_COR17}), which indicated the primary structure and composition gradients, mostly explained variation for the first ordination axes. Effectively, this meant that the mapped indices were mostly independent of topography, which allowed, for example, structural complexity to be indicated for multiple topographic aspects (e.g., see Figure 3). This independence facilitated the modeling, as the indices could be included with relatively uncorrelated topographic variables. For Ovenbird for example, eastness appeared to serve as a controlling variable that helped to clarify how its intensity was related to the structural RDA^1_s index.

Of the indices, the one based only on tree species composition (CCA^1_c) was a somewhat less reliable (albeit still significant) predictor when tested on the external data from the two transects. One likely reason was the relatively long gradient length for composition as collected across the full study area extent (hence the use of CCA over RDA). When analyzing a large number of tree species, including those that are relatively rare (Appendix A), composition will often vary more over a longer environmental gradient than over a shorter one. The CCA^1_c index, more sensitive to rarer tree species, could therefore be expected to not predict as well when applied only to the extent of the two transects. In contrast, the primary structure gradient, even with the addition of composition variables, was relatively short (which makes sense as the models were built from data collected only within mature forest). The range of structural complexity (via RDA^1_s), as well as with chestnut oak and sugar maple composition added (via RDA^1_{s+C}), was predicted for

the two transects similarly to how it was predicted across the full study area extent, suggesting greater reliability for prediction (and SDMs) using these indices throughout the site.

While the pure composition index may be a less reliable predictor when applied to smaller areas within the study area, the CCA_C model itself was still informative. One important observation was that the sites (the field subplots) were mostly separated into two groups of points in the CCA_C ordination plot (Figure 2b) along the first ordination axis, suggesting that the field data were collected in two relatively distinct forest types at the site. That two dominant forest types exist here is not new information (see Perkins and Wood 2014), but it was of value to examine this spatially across the full study area extent. For example, the two transects covered some of the transition from chestnut oak to sugar maple dominance (Figure 5b), and presumably an associated xeric to mesic moisture gradient. Topographic slope also helped to indicate this, as many of the narrower, more “spiny” ridges on the SR transect (Figure 5d) were dry, rocky and dominated by chestnut oak with an often dense greenbrier ground cover. Potentially, elevation was involved in the composition gradient as well, since the SR transect was generally higher in elevation than the OR transect (Figure 5c).

Based on the satellite image variable contribution alone, the CCA_C model was likely weaker than the RDA_S and RDA_{S+C} models because the PAN_{AVG} measure explained less of the variation in composition than it did for structure (indicated by the relatively low order in which it was selected for CCA_C; Table 1). Its subsequent contribution to the dominant first ordination axis of CCA_C was also less, and it was oriented more toward the second ordination axis. This in turn was reflected in the CCA¹_C index map as a relative lack of differentiation according to topographic aspect. However, in the CCA_C model PAN_{AVG} was still of interest in helping to explain an association between topographic aspect (both northness and eastness) and several of

the tree species. For example, the invasive tree-of-heaven is indicative of disturbed sites (Call and Nilsen 2003), so higher spectral brightness where it is found may indicate the presence of long term canopy gaps (potentially due to arrested succession) on south- and east-facing aspects. Oriented away from PAN_{AVG} , the shade-tolerant American beech (Poulson and Platt 1989) occurred most on cooler, spectrally darker north-facing aspects.

4.1. SDM-based habitat selection and predictions

While we did not statistically test among the three bird species, based on the SDMs there were some important differences in their breeding territory placement in this forest. The degree to which individuals of a species placed territories in 2011 near where the prior year's territories were located helped lead to consistent between-year results, further reinforcing the differences that we found. This stability also suggested potential site fidelity by returning males, perhaps related to reproductive success in the previous year (e.g., as found for Ovenbird by Thériault et al. 2012). Whether by site fidelity or some other cue used by individuals of these taxonomically-related species, the models suggested that much of their favored breeding habitat was spatially segregated on the ridgetops. To make predictions for subsequent investigation (e.g., Chapter 4), here we summarize the study findings that appeared to best support their individual habitat selection, for which we also relied on pertinent literature on these well-studied species. We also include consideration of the species themselves as potential indicators of information (or lack thereof) contained in the remote sensing data.

4.1.1. Hooded Warbler

The occurrences of Hooded Warbler and several other forest canopy gap dependent songbirds were positively correlated with the measure of spectral heterogeneity (PAN_{SD}) that was the best indicator of structural complexity across this forest at a broad spatial scale (Chapter

2). At the finer spatial scale examined in this chapter, the PAN_{SD} measure again was clearly the single strongest variable in the development of the mapped indices. The results for Hooded Warbler intensity in relation to the RDA¹_s index helped to reinforce the specific type of structural complexity that was indicated, namely the presence of a more open canopy. In a deciduous forest in southern Ontario, Canada, Pasher et al. (2007) found that Hooded Warbler nest sites had less canopy cover (as measured using skyward hemispherical photographs) than non-use areas. It is likely that the same habitat preference applied here, and was responsible for more territories placed in or near areas mapped by the RDA¹_s index as having high (presumably horizontal) structural complexity. Importantly, this tendency held despite the species' territory increase in 2011.

The results suggest the utility of the RDA¹_s index alone to predict Hooded Warbler intensity throughout the site. However, higher structural complexity on east-facing aspects appeared to be particularly favored. While east-facing aspects were well represented across the transects (Figure 5e), those with higher structural complexity were mostly on the OR transect. The reason for this is unknown, but may involve forest composition differences as well as past land use in the study area (Perkins and Wood 2014). Regardless, it was in these areas that the potential arrested succession for canopy gaps noted above (section 2.1.) was most obvious. Hooded Warblers were often detected in these areas, and open-habitat species not often detected in mature forest (e.g., Blue-winged Warbler; *Vermivora cyanoptera*) were also found there. Although the RDA¹_s index and eastness were uncorrelated overall, in these areas their effects on Hooded Warbler intensity were not completely separable, which suggests topography is partly responsible for some of the structural complexity in this forest important to this species.

Elevation also coincided with the RDA¹_s index in part to model Hooded Warbler intensity. However, higher elevations at the SR transect that were not structurally complex according to the index also appeared to be selected. Although not a site-wide trend based on the cross validation, the positive correlation between elevation and shrub cover for the second ordination axis of RDA_s (Figure 2a) suggests elevation alone as a potential habitat indicator, and in support of this the higher elevations of the SR transect had dense greenbrier-dominated areas under a chestnut oak-dominated canopy in which the species was frequently detected, and likely nesting. The factors behind this understory characteristic are unknown, as the forest here is older with little evidence remaining of past land use, but may involve tolerance by greenbrier species (both *S. rotundifolia* and *S. glauca* occur here) for drier conditions. Regardless of the reason, elevation appeared to provide an alternative explanation for Hooded Warbler intensity other than structural complexity as mapped by the RDA¹_s index. While the satellite image is obviously limited for detecting shrub cover under a forest canopy, elevation may be a suitable surrogate indicator where ridgetops are dominated by chestnut oak according to the satellite-derived indices.

4.1.2. Ovenbird

West-facing aspects alone mostly explained Ovenbird intensity, albeit not on east-west oriented ridges where Ovenbirds also occurred but north- and south-facing aspects dominate. Partly, this apparently strong selection may be explained by avoidance of east-facing aspects where the forest canopy was too open, and instead Hooded Warblers were more prevalent (e.g., the northern portion of the OR transect; Appendix E). This habitat selection dichotomy is interesting, and makes for a testable prediction that these species are similarly segregated elsewhere at the site. In support of this, the highest territory densities of these species occurred at opposite ends of a wide timber harvest residual basal area gradient (Ovenbird: high, Hooded

Warbler: low) for prior research here and at six other sites in the Appalachians (Sheehan et al. 2014). In a natural disturbance context, albeit without the Hooded Warbler present, Ovenbird abundance declined in sites with forest canopy loss relative to undisturbed control sites following a severe ice storm in a northern hardwood forest in Vermont, USA (Faccio 2003).

Ovenbird selection for greater canopy closure conflicts with the lower intensity indicated for a less open forest canopy dominated by chestnut oak, however. Modeling its intensity with eastness and the RDA¹_s index helped to clarify that west-facing aspects with greater structural complexity, which in turn occurred more in sugar maple dominated forest, were likely selected. An alternative to a strictly habitat structure-based explanation for this result comes from studies of Ovenbirds in relation to habitat quality. Its reproductive success was positively related to forest productivity and invertebrate biomass in a Maryland, USA forest similar to this one (Seagle and Sturtevant 2005). Ovenbirds also had larger territory sizes and lower densities in selection harvest plots with decreased litter invertebrate abundance in a New Brunswick, Canada managed forest (Haché et al. 2013). It seems likely that the drier, chestnut oak dominated ridgetops were poorer quality Ovenbird habitat. This relative quality could be based on lower site productivity and thus prey biomass, and also on fewer open, deep leaf litter areas which Ovenbird may prefer to nest in (Mattsson and Niemi 2006, Leblanc et al. 2011). The mesic sugar maple dominated ridgetops had more of these areas, including on west-facing aspects. As with shrub cover, the satellite image could not detect leaf litter under the forest canopy, but perhaps did so indirectly via the closely related forest structure and composition gradients.

The level of Ovenbird edge avoidance we found is consistent with other research in predominantly forested regions on this species. In an extensive northern hardwood forest in Vermont, USA, Ortega and Capen (1999) found lower Ovenbird territory density up to 150 m

from the edges of narrow (7–10 m wide) forest roads. Pertinent because of the energy industry activity in our study area, Lankau et al. (2013) found lower Ovenbird territory density near narrow (5–12 m wide) linear seismic lines used for oil and gas exploration in a boreal forest in western Canada. Other than at the few small clearings, the access road and pipeline on SR transect was similarly narrow (10–15 m wide), and within a large, relatively contiguous forest. The relatively weak avoidance of this edge facilitated its inclusion with other covariate effects for a more generally applicable model. Potential avoidance by Ovenbirds of edges from higher-intensity timber harvests, wider roads, and larger clearings at the site requires additional testing, however, prior to including these edges in models with other covariates.

4.1.3. Cerulean Warbler

It was somewhat surprising that the forest structure index did not explain Cerulean Warbler intensity, because of its known association with forest canopy gaps (including at this site; Perkins and Wood 2014). Potentially, as indicated by its attraction to the anthropogenic edge, other forest edges not detected by the satellite image or our image processing techniques were responsible for much of its distribution. Such edges do not necessarily occur at distinct canopy gaps, and their selection could have diluted any association with the structure index. Using lidar to study Cerulean Warbler habitat use in a central hardwood forest in Indiana, Barnes et al. (2016) found no evidence to support selection for canopy gaps, but suggested that ridgetops and steep slopes created canopy edges that the species may favor (e.g., for song projection). The knoll attraction found here is potentially an indication of such topographically-induced edge, with the refinement that favored edges are mostly on the east-facing aspects of knolls.

The strong local attraction to the SR transect impact needs to be considered in light of prior research on the species here (Sheehan et al. 2014). Large clusters of Cerulean Warbler territories

were mapped during the 2006–10 breeding seasons near the two prominent knolls where the species was most densely clustered for this 2010–11 study. The portion of the impact occurring over the winter of 2008–09 was through these two knolls, so comparatively high numbers existed here both pre-impact (2006–08 breeding seasons) and post-impact (2009–11 breeding seasons). The impact likely caused a shift in the locations of a number of individuals to incorporate this new edge, while overall densities remained similar. Comparatively dense clusters were also found elsewhere in the study area in non-impacted forest, including on the OR transect for this study. Complicating the situation, the light selection harvest occurred here over the 2006–07 winter, a likely cause of a moderate territory density increase observed for 2008 (the season prior to the impact). Because of the number of potentially coincident factors (e.g., impact edges, knolls, east-facing aspects, and timber harvests), teasing out which are responsible for Cerulean Warbler territory selection is obviously complicated. Also, due to the potential strength of local edge attraction, models that also include covariates representing broader environmental gradients may under predict intensity away from the impact.

A final consideration is the degree of clustering exhibited by the Cerulean Warbler. Such strong clustering implies strong second-order effects (e.g., conspecific attraction; Ward and Schlossberg 2004) on the observed distribution pattern in addition to the environmental effects. Conspecific attraction as a cause of clustering has also been implicated elsewhere for this species (Roth and Islam 2007). This is a potential modeling issue unless controlled for in some way, because clustering causes the variance of an estimator (e.g., the CIs for the intensity functions in Figure 8) to be underestimated (Baddeley et al. 2012), thus potentially biasing inference. In contrast, estimator variance is likely to be overestimated (thus statistical tests are conservative) when a point pattern exhibits regularity (Baddeley et al. 2012), and regularity may better

characterize the Hooded Warbler and Ovenbird distributions than clustering, especially if this is evaluated within their apparently preferred habitats. Despite this potential issue, the environmental effects on the Cerulean Warbler distribution appear to be rather strong in this forest, so it is unlikely that sociality would completely negate the observed effects. Still, for potentially more robust modeling of the Cerulean Warbler, or even the other species, the inclusion of second-order interaction terms (of which there are a variety available in spatstat) along with spatial covariates in PPMs may be useful.

5. Conclusions

For this study, the forest structure-based index most capably modeled the distribution patterns of two of the three bird species, probably because the satellite image relatively strongly, and predictably, indicated forest structural characteristics. These characteristics in turn appeared to be relevant to their habitat selection, albeit in different ways. However, it is unlikely that only this form of environmental heterogeneity is important to these (and other) bird species in this forest. While the tree species composition index was less useful for the bird SDMs, it provided a potentially valuable broad-scale perspective on forest composition patterns across the study area. This perspective warrants consideration going forward, since the additional transects more fully cover a forest composition gradient previously found useful for considering trends in the bird community here (Chapter 2). In any case, as the index that included chestnut oak and sugar maple composition with the structure variables suggested, it is important to continue to try to understand the close relation between structure and composition in this forest. It may also be interesting to separately model within these two dominant forest types.

Overall, topographic effects appeared to dominate in terms of contrasting the bird distribution patterns, perhaps because of limited information on the part of the satellite image. That topography would be important for these bird species in helping to define their breeding habitat is perhaps characteristic of a ridgetop forest of such high topographic complexity. Certainly, there may be alternative explanations (e.g., based on microclimate and solar exposure) for the distribution patterns. However, topography as a major underlying factor leading to differences in forest composition (e.g., chestnut oak dominance on drier, more sharply-defined ridgetops) and forest structure (e.g., arrested succession in canopy gaps on certain east-facing aspects) provides a likely powerful explanation for much of the observed distribution patterns. Although the satellite image was a weaker predictor overall for the bird species, it helped to elucidate the dominant patterns in forest structure and composition over this complex topography. The results for the Cerulean Warbler also helped to rule out the use of optical imagery, at least as processed and analyzed here, for predicting its distribution.

We view this study as an important first step for incorporating novel remote sensing data in “next-generation SDMs” (He et al. 2015). One exciting possibility is that better accounting of potentially fine-scale environmental effects on a species’ point pattern may allow detection of second-order point interactions (attraction or repulsion). Our results show initial promise in this regard, as remote sensing technology for forest inventory purposes should continue to advance (White et al. 2016) and the remote sensing data thus obtained will hopefully also be available for such spatially-explicit avian studies. This applies not only for the high spatial resolution (now relatively standard) optical imagery such as used here, but also for hyperspectral and three-dimensional active remote sensing data, and these technologies may further be merged to better predict forest characteristics. Our study was geared toward using remote sensing to explain forest

gradients and subsequently the bird species distributions, but the ability of the birds themselves to explain what the remote sensing data do, and do not, indicate should also be considered. This was most clearly seen for the Hooded Warbler and the likelihood that it indicated the presence of a more open forest canopy, but also by the Ovenbird and Cerulean Warbler for suggesting other heterogeneity that was not indicated by the satellite image, at least not directly. Finally, this study provided a basis for generating new spatially-explicit predictions regarding the breeding distributions of these species that we further tested in Chapter 4. Ultimately, we wish to stimulate more study of the potential for remote sensing data to determine fine scale patterns in forest-associated biodiversity over considerably broad spatial extents.

Acknowledgments

We thank D. Blood, B. Miller, M. Napoli, and numerous other field technicians for their assistance with data collection and Wheeling Jesuit University for providing field housing. This research was funded by NETL Department of Energy, U.S. Fish and Wildlife Service, National Fish and Wildlife Foundation, and West Virginia University Division of Forestry and Natural Resources. West Virginia Department of Natural Resources and U.S. Geological Survey West Virginia Cooperative Fish and Wildlife Research Unit provided logistical support.

References

Aarts, G., Fieberg, J., Matthiopoulos, J., 2012. Comparative interpretation of count, presence-absence and point methods for species distribution models. *Methods in Ecology and Evolution* 3(1): 177–187.

- Baddeley, A., Berman, M., Fisher, N.I., Hardegen, A., Milne, R.K., Schuhmacher, D., Shah, R., Turner, R., 2010. Spatial logistic regression and change-of-support in Poisson point processes. *Electronic Journal of Statistics* 4: 1151–1201.
- Baddeley, A., Chang, Y., Song, Y., Turner, R., 2012. Nonparametric estimation of the dependence of a spatial point process on spatial covariates. *Statistics and Its Interface* 5: 221–236.
- Baddeley, A., Rubak, E., Turner, F., 2015. *Spatial Point Patterns: Methodology and Applications* with R. London: Chapman and Hall/CRC Press.
- Barg, J.J., Jones, J., Robertson, R.J., 2005. Describing breeding territories of migratory passerines: suggestions for sampling, choice of estimator, and delineation of core areas. *Journal of Animal Ecology* 74(1): 139–149.
- Barnes, K.W., Islam, K., Auer, S.A., 2016. Integrating LIDAR-derived canopy structure into cerulean warbler habitat models. *The Journal of Wildlife Management* 80(1): 101–116.
- Beguet, B., Chehata, N., Boukir, S., Guyon, D., 2012. Retrieving forest structure variables from very high resolution satellite images using an automatic method. *ISPRS Annals of the Photogrammetry, Remote Sensing and Spatial Information Sciences*, Volume I-7, 2012 XXII ISPRS Congress, Melbourne, Australia.
- Beckschäfer, P., Mundhenk, P., Kleinn, C., Ji, Y., Douglas, W.Y., Harrison, R.D., 2013. Enhanced structural complexity index: An improved index for describing forest structural complexity. *Open Journal of Forestry*, 3(1): 23–29.
- Bibby, C.J., Burgess, N.D., Hill, D.A., 2000. *Bird Census Techniques*. Academic Press, London, UK.

- Borcard D., Gillet F., Legendre P., 2011. Numerical Ecology with R. New York, NY: Springer, 306 pp.
- Call, L.J., Nilsen, E.T., 2003. Analysis of spatial patterns and spatial association between the invasive tree-of-heaven (*Ailanthus altissima*) and the native black locust (*Robinia pseudoacacia*). The American Midland Naturalist 150(1): 1–14.
- Erikson, M., 2004. Species classification of individually segmented tree crowns in high-resolution aerial images using radiometric and morphologic image measures. Remote Sensing of Environment 91(3): 469–477.
- Faccio, S.D., 2003. Effects of ice storm-created gaps on forest breeding bird communities in central Vermont. Forest Ecology and Management 186(1): 133–145.
- Farwell, L.S., Wood, P.B., Sheehan, J., George, G.A., 2016. Shale gas development effects on the songbird community in a central Appalachian forest. Biological Conservation 201:78–91.
- Ferraz, A., Saatchi, S., Mallet, C., Meyer, V., 2016. Lidar detection of individual tree size in tropical forests. Remote Sensing of Environment 183: 318–333.
- Ferreira, M.P., Zortea, M., Zanotta, D.C., Shimabukuro, Y.E., de Souza Filho, C.R., 2016. Mapping tree species in tropical seasonal semi-deciduous forests with hyperspectral and multispectral data. Remote Sensing of Environment 179: 66–78.
- Fithian, W., Hastie, T., 2013. Finite-sample equivalence in statistical models for presence-only data. The annals of applied statistics 7(4): 1917–1939.
- Gómez, C., Wulder, M.A., Montes, F., Delgado, J.A., 2012. Forest structural diversity characterization in Mediterranean pines of central Spain with QuickBird-2 imagery and canonical correlation analysis. Canadian Journal of Remote Sensing 37(6): 628–642.

- Graffelman, J., Tuft, R., 2004. Site scores and conditional biplots in canonical correspondence analysis. *Environmetrics* 15(1): 67–80.
- Haché, S., Villard, M.A., Bayne, E.M., 2013. Experimental evidence for an ideal free distribution in a breeding population of a territorial songbird. *Ecology* 94(4): 861–869.
- Hansen, M.C., Potapov, P.V., Moore, R., Hancher, M., Turubanova, S.A., Tyukavina, A., Thau, D., Stehman, S.V., Goetz, S.J., Loveland, T.R., Kommareddy, A., 2013. High-resolution global maps of 21st-century forest cover change. *Science* 342(6160): 850–853.
- Hartman, P.J., Maehr, D.S., Larkin, J.L., 2009. Habitat selection by Cerulean Warblers in eastern Kentucky. *The Wilson Journal of Ornithology* 121(3): 469–475.
- He, K.S., Bradley, B.A., Cord, A.F., Rocchini, D., Tuanmu, M.N., Schmidtlein, S., Turner, W., Wegmann, M., Pettorelli, N., 2015. Will remote sensing shape the next generation of species distribution models? *Remote Sensing in Ecology and Conservation*, 1(1): 4–18.
- Heumann, B.W., 2011. Satellite remote sensing of mangrove forests: Recent advances and future opportunities. *Progress in Physical Geography* 35(1): 87–108.
- Homer, C.H., Fry, J.A., Barnes, C.A., 2012. The national land cover database. *US Geological Survey Fact Sheet* 3020(4): 1–4.
- Korpela, I., Ørka, H.O., Maltamo, M., Tokola, T., Hyypä, J., 2010. Tree species classification using airborne LiDAR-effects of stand and tree parameters, downsizing of training set, intensity normalization, and sensor type. *Silva Fennica* 44(2): 319–339.
- Lankau, H.E., Bayne, E.M., Machtans, C.S., 2013. Ovenbird (*Seiurus aurocapilla*) territory placement near seismic lines is influenced by forest regeneration and conspecific density. *Avian Conservation and Ecology* 8(1): 5.

- Leblanc, J.P., Burke, D.M., Nol, E., 2011. Ovenbird (*Seiurus aurocapilla*) demography and nest-site selection in response to single-tree selection silviculture in a northern hardwood managed forest landscape. *Ecoscience* 18(1): 26–36.
- Legendre, P., Legendre, L., 2012. Numerical Ecology. Third English edition. Elsevier Science BV, Amsterdam.
- Li, Z., Xu, D., Guo, X., 2014. Remote Sensing of Ecosystem Health: Opportunities, Challenges, and Future Perspectives. *Sensors* 14(11): 21117–21139.
- Mattsson, B.J., Niemi, G.J., 2006. Factors influencing predation on Ovenbird (*Seiurus aurocapilla*) nests in northern hardwoods: Interactions across spatial scales. *The Auk* 123(1): 82–96.
- Martin, M.E., Newman, S.D., Aber, J.D., Congalton, R.G., 1998. Determining forest species composition using high spectral resolution remote sensing data. *Remote Sensing of Environment* 65(3): 249–254.
- Martin, T.E., C.R. Paine, C.J. Conway, W.M. Hochachka, P. Allen, and W. Jenkins. 1997. BBIRD Field Protocol. Montana Cooperative Wildlife Research Unit, University of Montana, Missoula, Montana, USA.
- McCune, B., 1997. Influence of noisy environmental data on canonical correspondence analysis. *Ecology*, 78(8): 2617–2623.
- Oksanen, J., Blanchet, F.G., Kindt, R., Legendre, P., Minchin, P.R., O'Hara, R.B., Simpson, G.L., Solymos, P., Stevens, M.H.H., Wagner, H., 2016. *vegan: Community Ecology Package*. R package version 2.3-3. <https://CRAN.R-project.org/package=vegan>
- Ortega, Y.K., Capen, D.E., 1999. Effects of forest roads on habitat quality for ovenbirds in a forested landscape. *The Auk*: 937–946.

- Pasher, J., King, D., Lindsay, K., 2007. Modelling and mapping potential hooded warbler (*Wilsonia citrina*) habitat using remotely sensed imagery. *Remote Sensing of Environment* 107(3): 471–483.
- Pasher, J., King, D.J., 2010. Multivariate forest structure modelling and mapping using high resolution airborne imagery and topographic information. *Remote Sensing of Environment* 114(8): 1718–1732.
- Pasher, J., King, D.J., 2011. Development of a forest structural complexity index based on multispectral airborne remote sensing and topographic data. *Canadian Journal of Forest Research*, 41(1): 44–58.
- Perkins, K.A., Wood, P.B., 2014. Selection of forest canopy gaps by male cerulean warblers in West Virginia. *Wilson Journal of Ornithology* 126: 288–297.
- Pérot, A., Villard, M.A., 2009. Putting density back into the habitat-quality equation: Case study of an open-nesting forest bird. *Conservation Biology* 23(6): 1550–1557.
- Porneluzi, P.A., Van Horn, M.A., Donovan, T.M. 2011. Ovenbird (*Seiurus aurocapilla*). In: Poole, A., editor. *The birds of North America online*. Ithaca (NY); Cornell Lab of Ornithology. accessed 2016 April from: <http://bna.birds.cornell.edu.bnaproxy.birds.cornell.edu/bna/species/088>.
- Poulson, T.L., Platt, W.J., 1989. Gap light regimes influence canopy tree diversity. *Ecology* 70(3): 553–555.
- Renner, I.W., Elith, J., Baddeley, A., Fithian, W., Hastie, T., Phillips, S.J., Popovic, G., Warton, D.I., 2015. Point process models for presence-only analysis. *Methods in Ecology and Evolution* 6(4): 366–379.

- Rodewald, A.D., 2004. Landscape and local influences of forest management on cerulean warblers in Pennsylvania. pp. 472–477 in: Proceedings of the 14th Central Hardwood Forest Conference. United States Department of Agriculture Forest Service General Technical Report NE-316, Newtown Square, Pennsylvania, USA.
- Roth, K. L., K. Islam. 2007. Do cerulean warblers (*Dendroica cerulea*) exhibit clustered territoriality? American Midland Naturalist 157: 345–355.
- Schmitt, M., Brück, A., Schönberger, J., Stilla, U., 2013. Potential of airborne single-pass millimeterwave InSAR data for individual tree recognition. pp. 427–436 in: Proceedings of 33. Wissenschaftlich-Technische Jahrestagung der DGPF. Freiburg, Germany.
- Seagle, S.W., Sturtevant, B.R., 2005. Forest productivity predicts invertebrate biomass and ovenbird (*Seiurus aurocapillus*) reproduction in Appalachian landscapes. Ecology 86(6): 1531–1539.
- Sheehan, J., Wood, P.B., Buehler, D.A., Keyser, P.D., Larkin, J.L., Rodewald, A.D., Wigley, T.B., Boves, T.J., George, G.A., Bakermans, M.H., Beachy, T.A., Evans, A., McDermott, M.E., Newell, F.L., Perkins, K.A., White, M., 2014. Avian response to timber harvesting applied experimentally to manage Cerulean Warbler breeding populations. Forest Ecology and Management 321: 5–18.
- Standish, M. 1945. The use of aerial photographs in forestry. Journal of Forestry 43: 252–257.
- Spurr, S. H. 1948. Aerial photography. Unasylva 2: 183–194. accessed 2016 April from: [http://www.fao.org/docrep/x5345e/x5345e04.htm#aerial photography](http://www.fao.org/docrep/x5345e/x5345e04.htm#aerial%20photography).
- ter Braak, C.J.F., Prentice, I.C., 1988. A theory of gradient analysis. Advances in Ecological Research 18: 271–317.

- Thériault, S., Villard, M.A., Haché, S., 2012. Habitat selection in site-faithful ovenbirds and recruits in the absence of experimental attraction. *Behavioral Ecology* 23(6): 1289–1295.
- Torontow, V., King, D., 2011. Forest complexity modelling and mapping with remote sensing and topographic data: A comparison of three methods. *Canadian Journal of Remote Sensing* 37(4): 387–402.
- Ward, M.P., Schlossberg, S., 2004. Conspecific attraction and the conservation of territorial songbirds. *Conservation Biology* 18(2): 519–525.
- Waser, L.T., Küchler, M., Jütte, K., Stampfer, T., 2014. Evaluating the potential of WorldView-2 data to classify tree species and different levels of ash mortality. *Remote sensing* 6(5): 4515–4545.
- Weakland, C.A., Wood, P.B., 2005. Cerulean Warbler (*Dendroica cerulea*) microhabitat and landscape-level habitat characteristics in southern West Virginia. *Auk* 122: 497–508.
- White, J.C., Coops, N.C., Wulder, M.A., Vastaranta, M., Hilker, T., Tompalski, P., 2016. Remote sensing technologies for enhancing forest inventories: A review. *Canadian Journal of Remote Sensing* 42(5): 619–641.
- Woods, A.J., Omernik, J.M., Brown, D.D., 1999. Level III and IV Ecoregions of Delaware, Maryland, Pennsylvania, Virginia, and West Virginia. U.S. Environmental Protection Agency, National Health and Environmental Effects Research Laboratory. Corvallis, OR. accessed 2016 April from: ftp://ftp.epa.gov/wed/ecoregions/reg3/reg3_eco_desc.doc.
- Wulder, M.A., Hall, R.J., Coops, N.C., Franklin, S.E., 2004. High spatial resolution remotely sensed data for ecosystem characterization. *BioScience* 54(6): 511–521.

Table 1. Forward-backward selection of explanatory variables for the forest structure (RDAs), forest composition (CCA_C), and forest structure plus composition (RDA_{S+C}) models, and model significance tests. Percent values in parentheses are the proportions of the total model inertia (i.e., variance in the field data) explained by the models. See Appendix C for the key to the labels for the explanatory variables and their descriptions.

Structure RDA					Composition CCA					Structure plus composition RDA				
Variable	Df	AIC	F	P	Variable	Df	AIC	F	P	Variable	Df	AIC	F	P
PAN _{SD}	1	771.87	36.04	0.005	PAN _{SD}	1	686.10	25.60	0.005	PAN _{SD}	1	836.58	54.18	0.005
PAN _{AVG}	1	762.94	11.01	0.005	SLOPE	1	682.48	5.61	0.005	PAN _{AVG}	1	828.93	9.71	0.005
ELEV	1	759.43	5.48	0.005	PAN _{SD_COR17}	1	680.26	4.20	0.005	ELEV	1	825.37	5.54	0.005
SLOPE	1	756.99	4.40	0.005	SIN	1	678.22	4.00	0.005	COS	1	822.24	5.09	0.005
PAN _{SD_COR17}	1	754.59	4.36	0.005	PAN _{AVG}	1	677.14	3.04	0.005	SLOPE	1	819.04	5.14	0.005
COS	1	752.41	4.12	0.005	COS	1	676.04	3.05	0.005	PAN _{SD_COR17}	1	816.01	4.96	0.005
PAN _{SD_CON09}	1	750.78	3.56	0.010	PAN _{SD_CON03}	1	676.03	1.97	0.015	PAN _{SD_CON09}	1	814.26	3.68	0.005
					PAN _{SD_AVG25}	1	676.20	1.79	0.035	SIN	1	814.05	2.17	0.025
ANOVA RDA _S model (18.3% of inertia explained)					ANOVA CCA _C model (13.5% of inertia explained)					ANOVA RDA _{S+C} model (22.3% of inertia explained)				
	Df	Var.	F	Pr(>F)		Df	ChiSq	F	Pr(>F)		Df	Var.	F	Pr(>F)
Model	7	2.01	10.43	0.001	Model	8	0.54	6.38	0.001	Model	8	3.20	12.09	0.001
Residuals	327	8.99			Residuals	326	3.42			Residuals	326	10.80		
ANOVA RDA _S model by axis					ANOVA CCA _C model by axis					ANOVA RDA _{S+C} model by axis				
Axis ^a	Df	Var.	F	Pr(>F)	Axis ^a	Df	ChiSq	F	Pr(>F)	Axis ^a	Df	Var.	F	Pr(>F)
RDA1 (12.9%)	1	1.42	51.53	0.001	CCA1 (8.6%)	1	0.34	32.49	0.001	RDA1 (17.0%)	1	2.38	71.87	0.001
RDA2 (2.7%)	1	0.29	10.63	0.001	CCA2 (2.1%)	1	0.08	7.85	0.001	RDA2 (2.8%)	1	0.38	11.47	0.001
RDA3 (1.9%)	1	0.21	7.46	0.001	CCA3 (1.0%)	1	0.04	3.80	0.001	RDA3 (1.6%)	1	0.22	6.75	0.001
RDA4 (0.5%)	1	0.05	1.96	0.044	CCA4 (0.7%)	1	0.03	2.58	0.001	RDA4 (0.6%)	1	0.08	2.50	0.005
RDA5	1	0.03	0.93	0.495	CCA5 (0.6%)	1	0.03	2.45	0.002	RDA5 (0.5%)	1	0.06	1.90	0.046
RDA6	1	0.01	0.37	0.949	CCA6	1	0.01	0.92	0.549	RDA6	1	0.04	1.30	0.25
RDA7	1	0.00	0.14	0.998	CCA7	1	0.01	0.63	0.903	RDA7	1	0.02	0.68	0.743
Residuals	327	8.99			CCA8	1	0.00	0.31	1	RDA8	1	0.01	0.26	0.989
					Residuals	326	3.42			Residuals	326	10.80		

a. Percent of constrained inertia explained provided for each significant ordination axis.

Table 2. The WA-LC (i.e., ‘species-environment’) Pearson’s correlations (r) for the first and second axes of the constrained ordination models, and results of the leave-one-out cross validation (LOOCV). The internal validation was for the stability of r between the site (i.e., field subplot) WA scores (weighted averages of the field variables) and LC scores (linear combinations of the remote sensing explanatory variables), by resampling the data used to create the models. The external validation was for the r between the WA and LC scores predicted at the locations ($n = 97$) where additional habitat samples were collected (see Appendix B). The RMSE (Root Mean Squared Error) of the model is given as a percentage of the WA score range.

Axis	Model ^a	LOOCV					
		Model output		Internal		External	
		r	RMSE	r	RMSE	r	RMSE
First	RDA _S	0.72	11.1%	0.69	10.7%	0.74	15.6%
	CCA _C	0.81	11.7%	0.79	12.2%	0.66	20.2%
	RDA _{S+C}	0.79	12.4%	0.77	12.3%	0.78	15.9%
Second	RDA _S	0.47	13.3%	0.41	13.7%	14.4	18.6%
	CCA _C	0.58	13.3%	0.50	16.0%	0.05	23.2%
	RDA _{S+C}	0.48	13.2%	0.41	13.2%	0.26	23.3%

a. forest structure (RDA_S), forest composition (CCA_C), and forest structure plus composition (RDA_{S+C}) models.

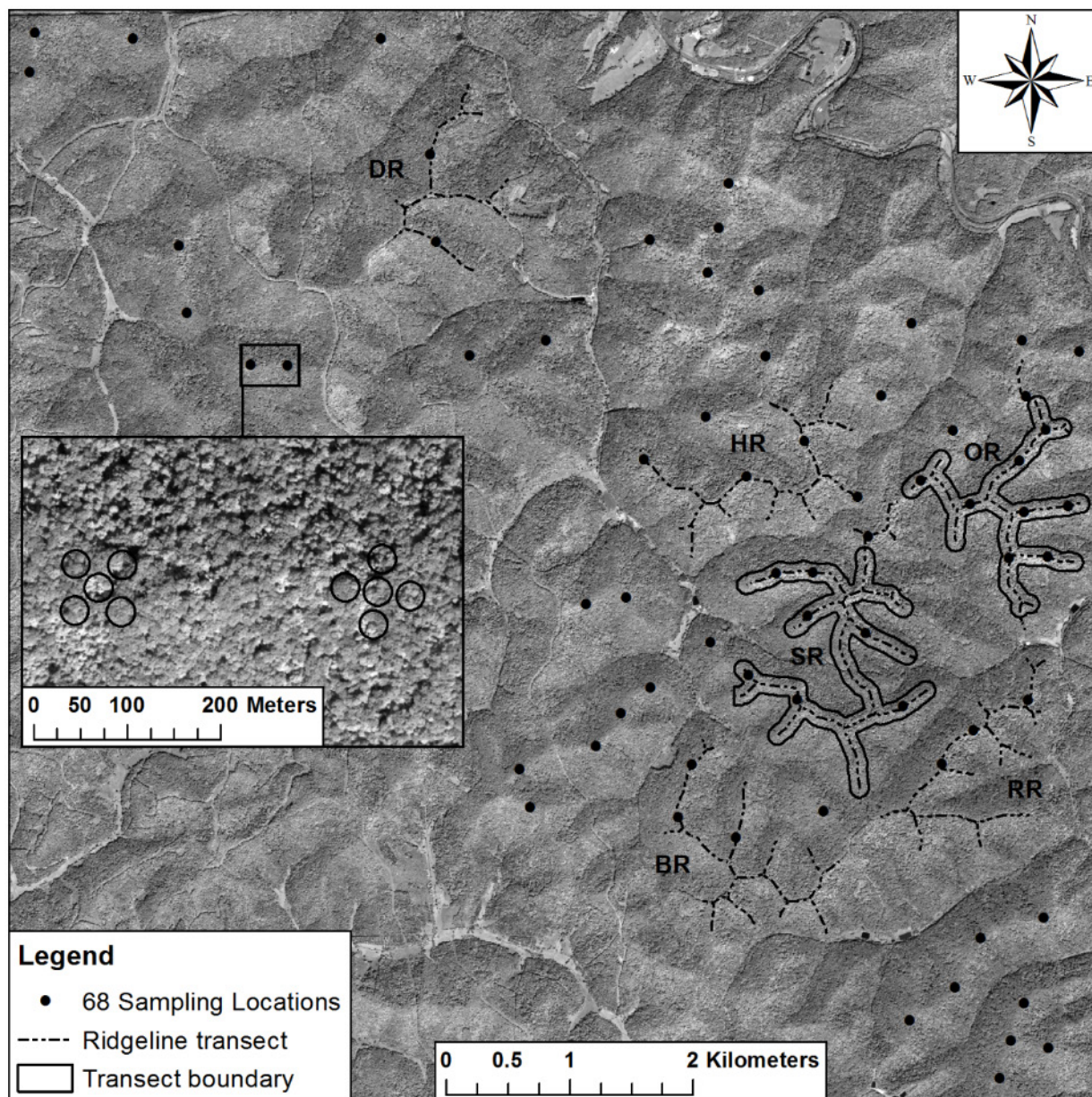
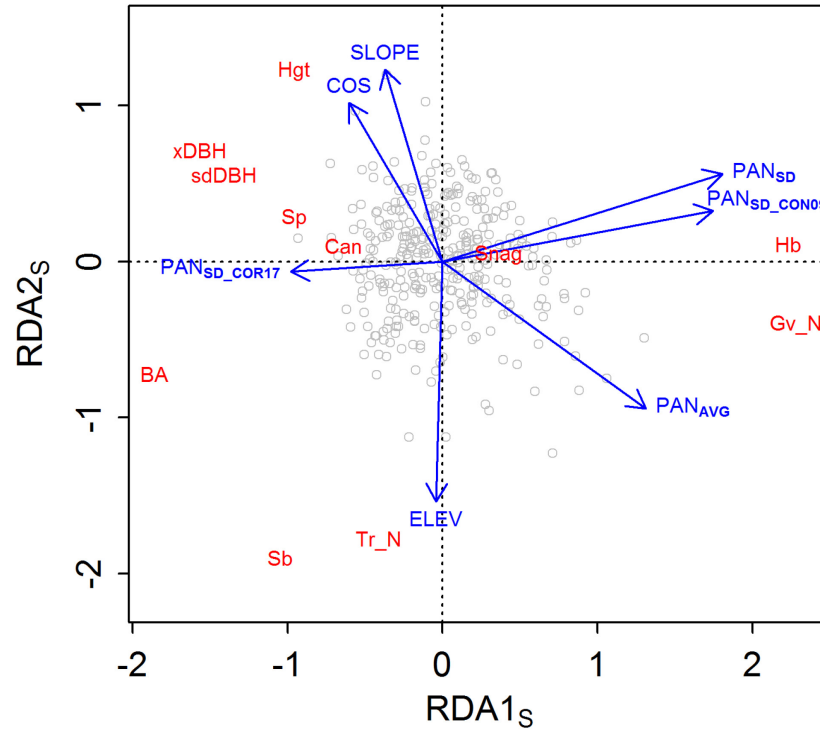
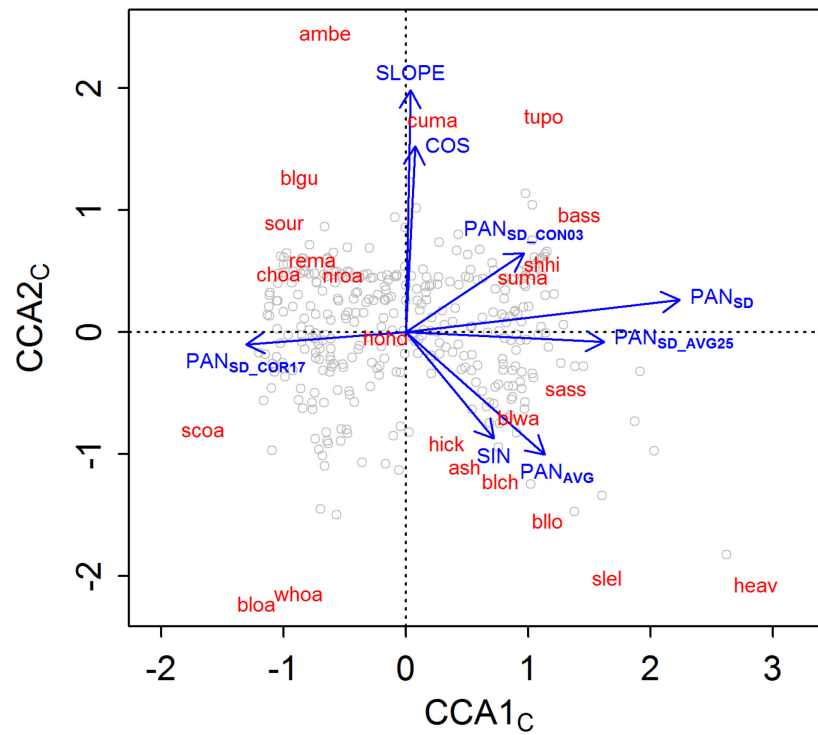


Figure 1. QuickBird satellite 0.6-m panchromatic band image (August 2009) of the study area showing the 68 ridgetop sampling points located in mature forest >150 m from anthropogenic canopy disturbances. Also shown are the six ridgetop transects where the breeding territories of the three bird species were mapped. The OR and SR transects (shown with the boundaries used to define the point pattern analysis windows) had two years of territory mapping data (2010 and 2011) for analysis. The inset shows the 5-subplot habitat sampling arrangement per point where forest composition and structure data were collected for the remote sensing-based forest indices.

a. RDA_S



b. CCA_C



c. RDA_{S+C}

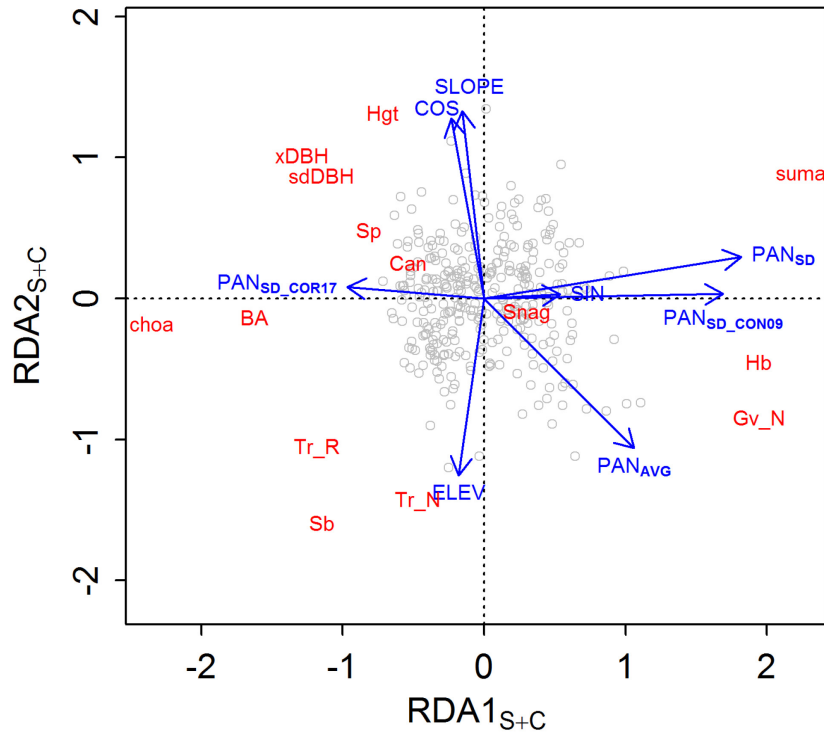
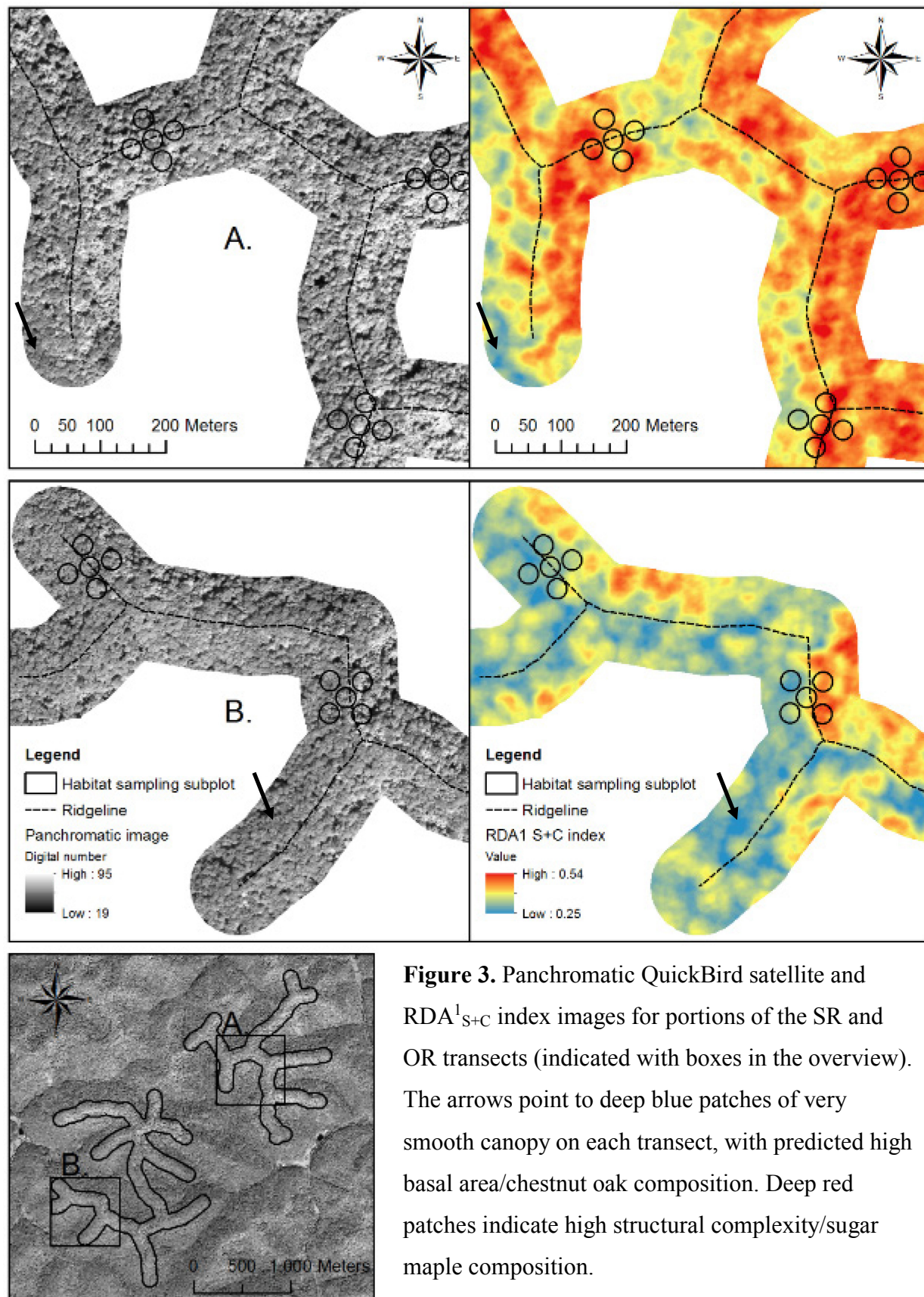


Figure 2. Constrained ordination triplots (axes 1 and 2) showing species scores (red labels = field variables), site scores (open circles = subplots), and environmental constraints (blue arrows = remote sensing variables) from the (a) redundancy analysis of forest structure (RDAs), (b) canonical correspondence analysis of forest composition (CCA_C), and (c) redundancy analysis of forest structure plus tree species richness and chestnut oak/sugar maple composition (RDA_{S+C}). See Appendix A for field variable label key and Appendix C for remote sensing variable key.



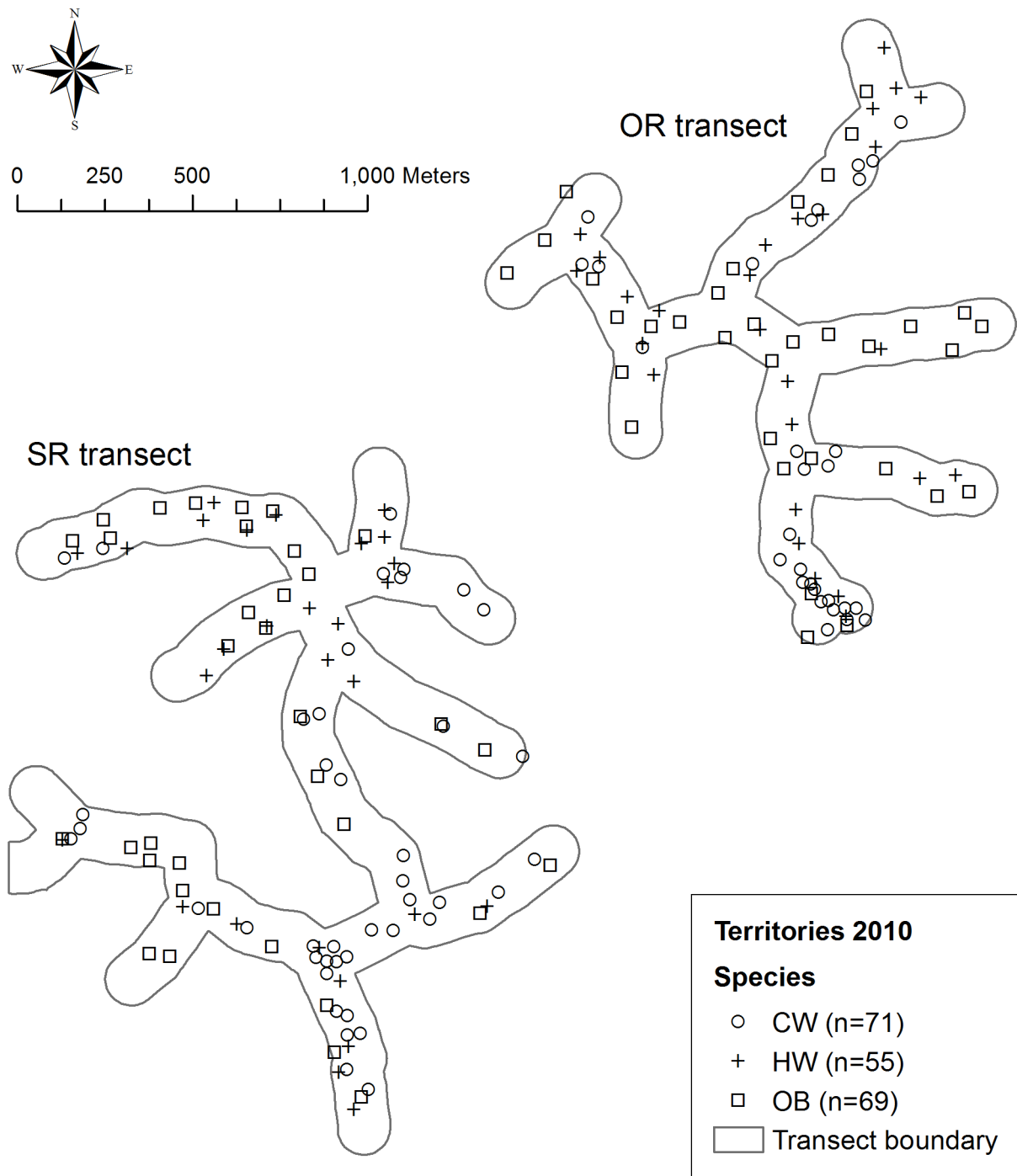


Figure 4a. Mapped territory centers of the three species in 2010.

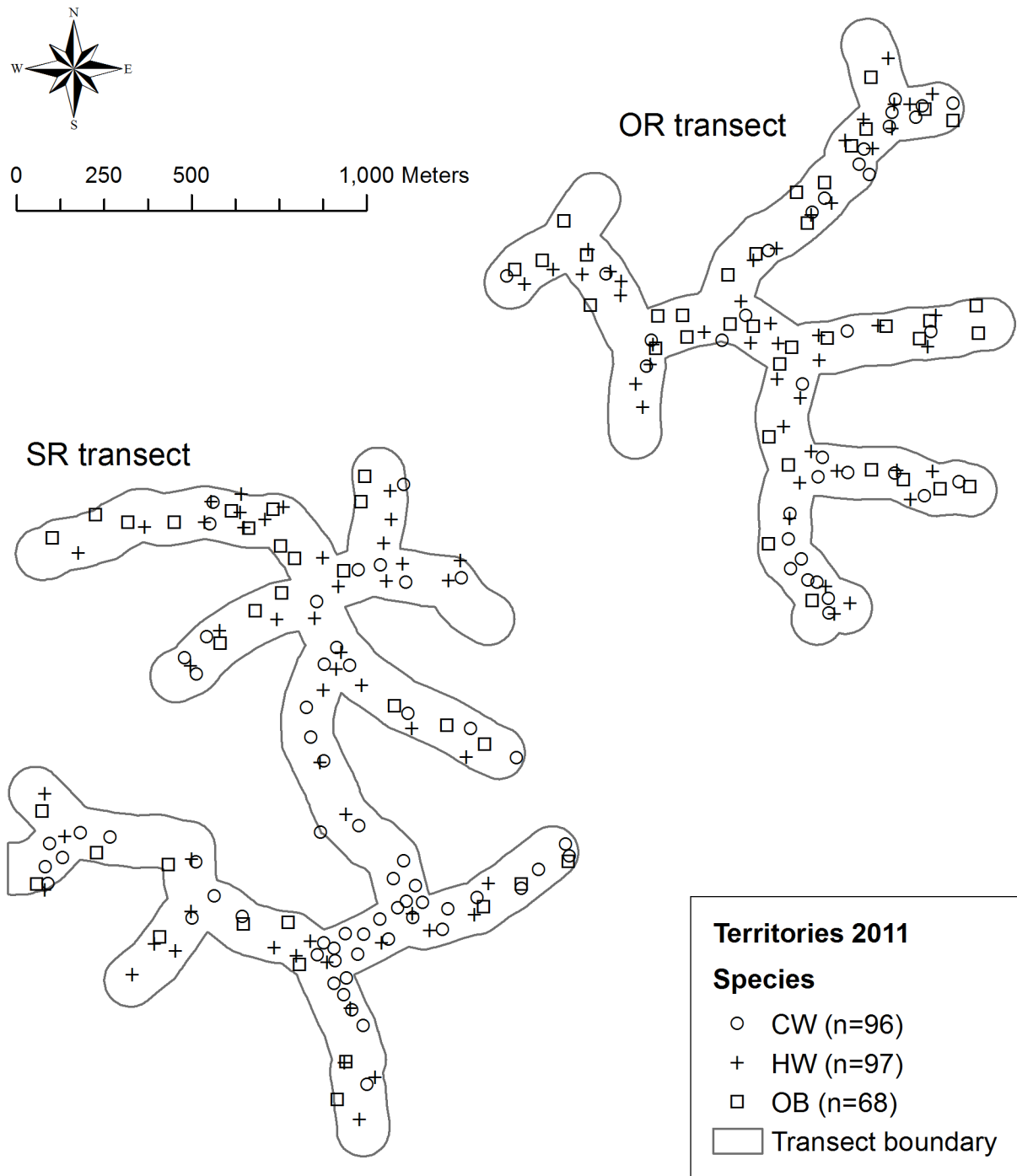


Figure 4b. Mapped territory centers of the three species in 2011.

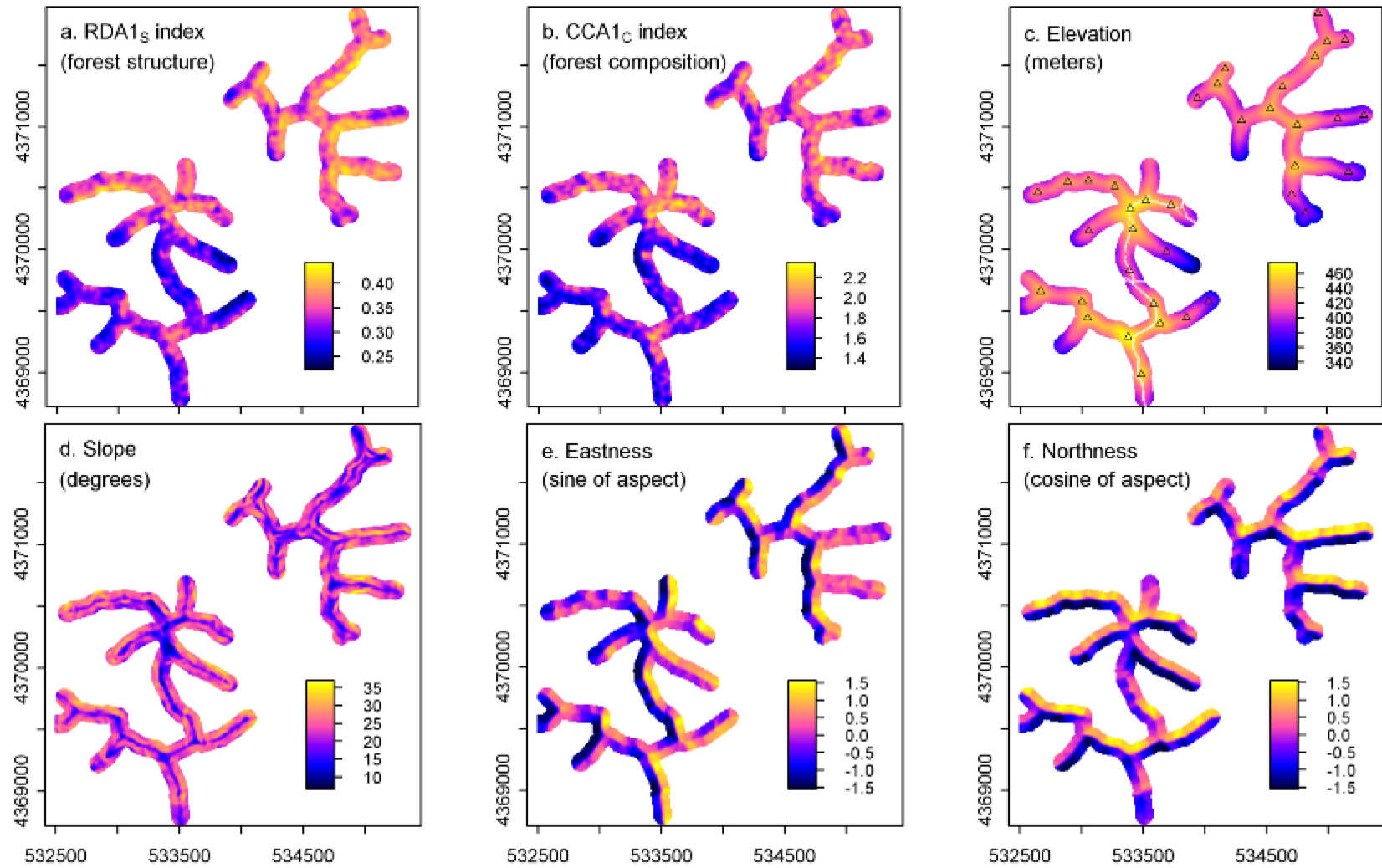
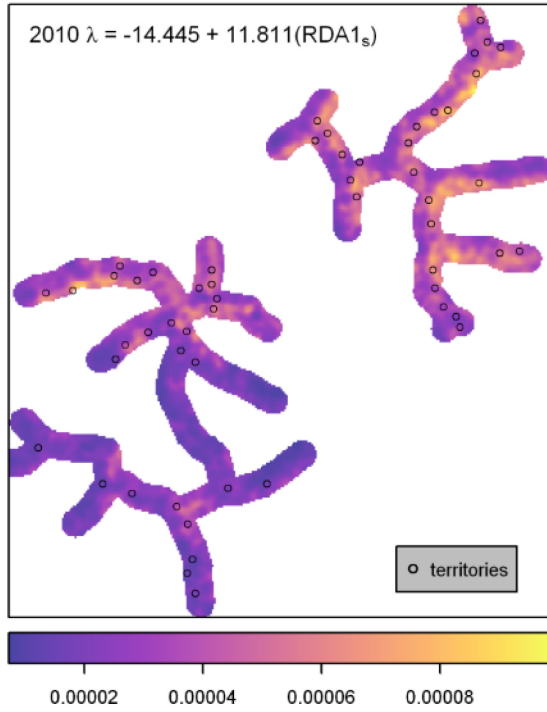
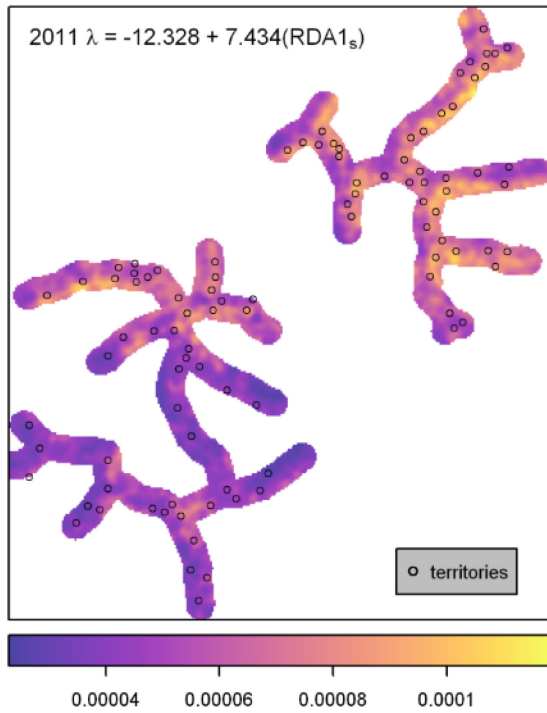
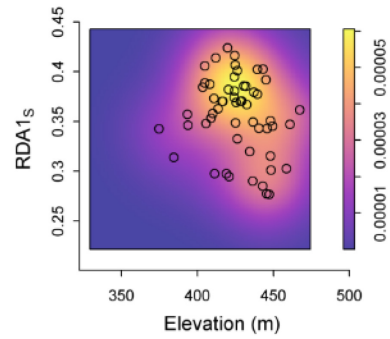
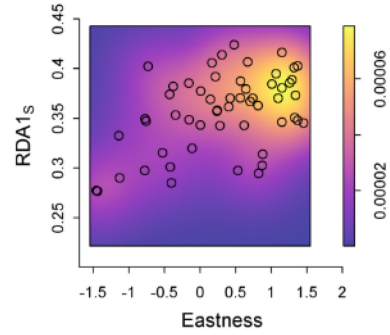


Figure 5. Spatial covariates used in the species distribution models. A Gaussian (15 m s.d.) filter was applied to the forest indices RDA^1_S , CCA^1_C , and RDA^1_{S+C} (similar to RDA^1_S and not shown). Knolls (triangles) and the SR transect impact (lines) used to compute distance grids (not shown) are mapped on the elevation layer. The eastness and northness layers were arcsine square-root transformed.



2010 nonparametric intensity functions:



2011 nonparametric intensity functions:

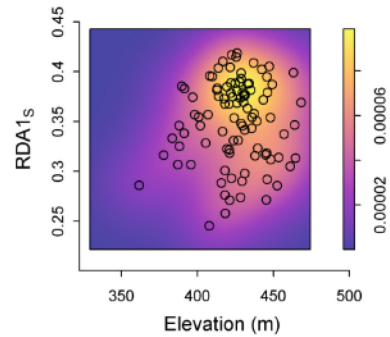
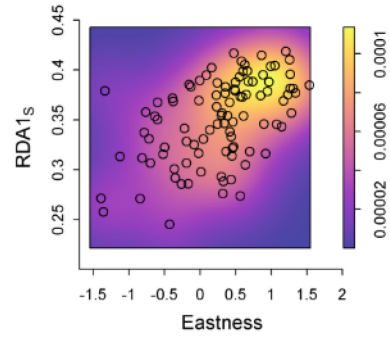
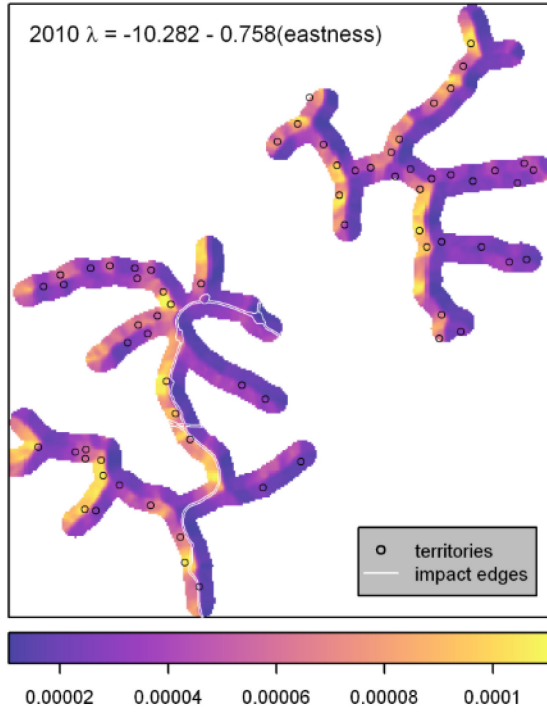
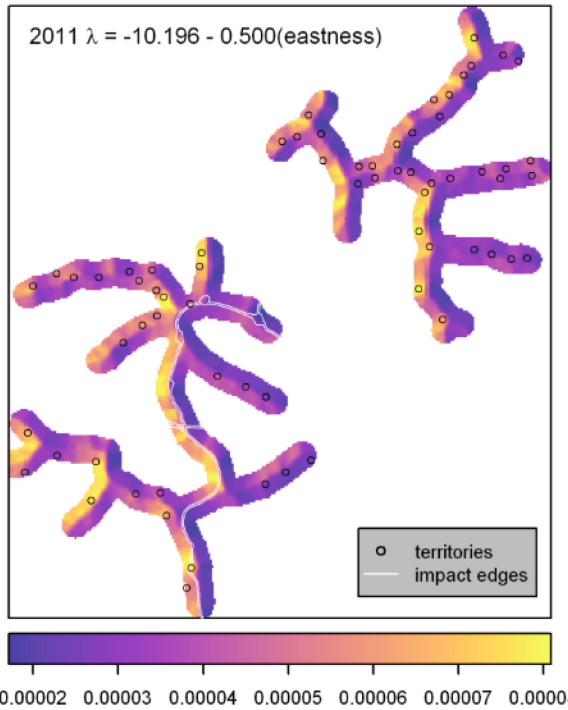
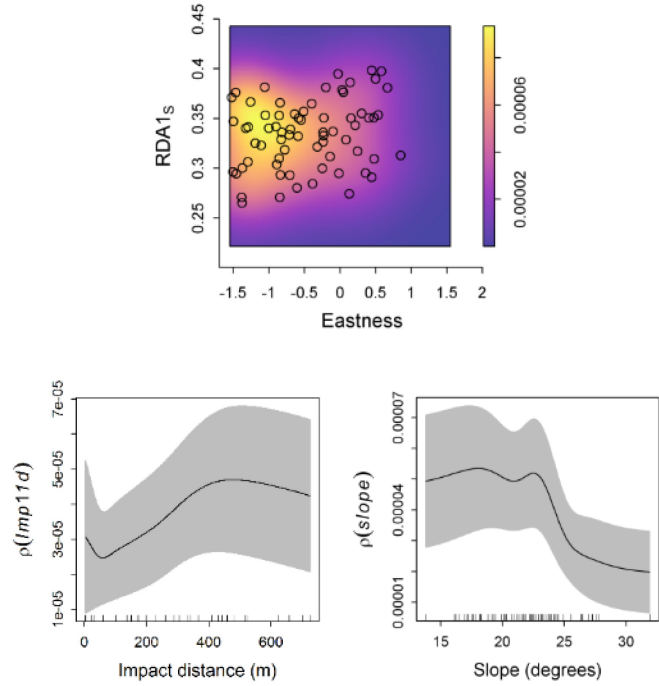


Figure 6. Hooded Warbler 2010 and 2011 territory intensity (λ) as predicted by the fitted PPMs and as nonparametric functions of spatial covariates. The bivariate functions show λ as a function of two spatial covariates (circles indicate covariate values for the individual territories).



2010 nonparametric intensity functions:



2011 nonparametric intensity functions:

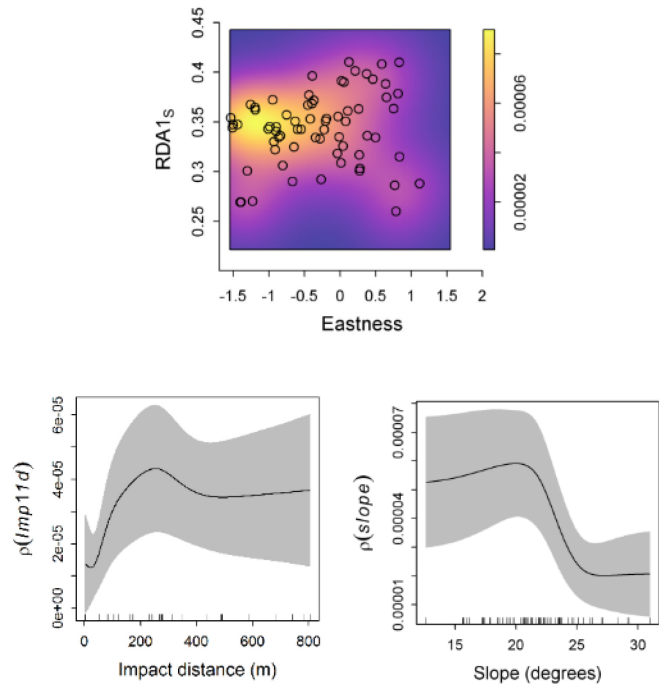
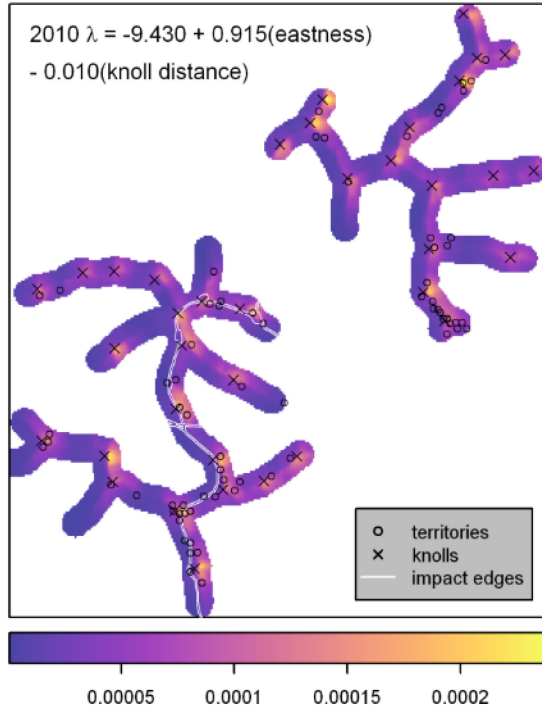
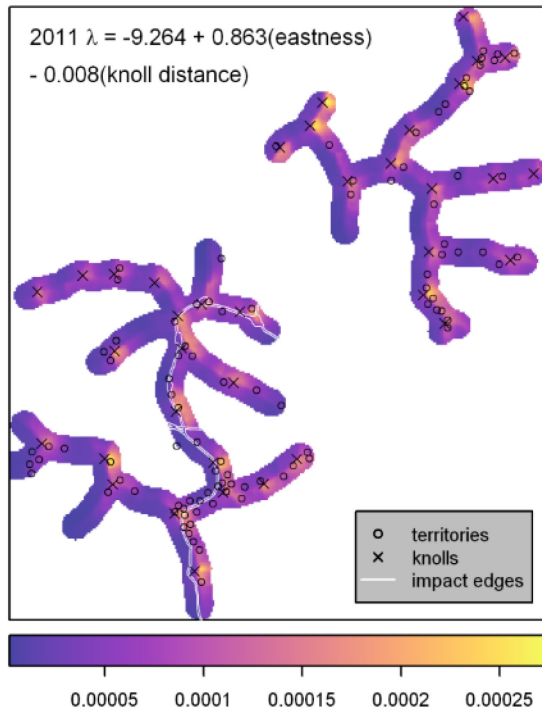
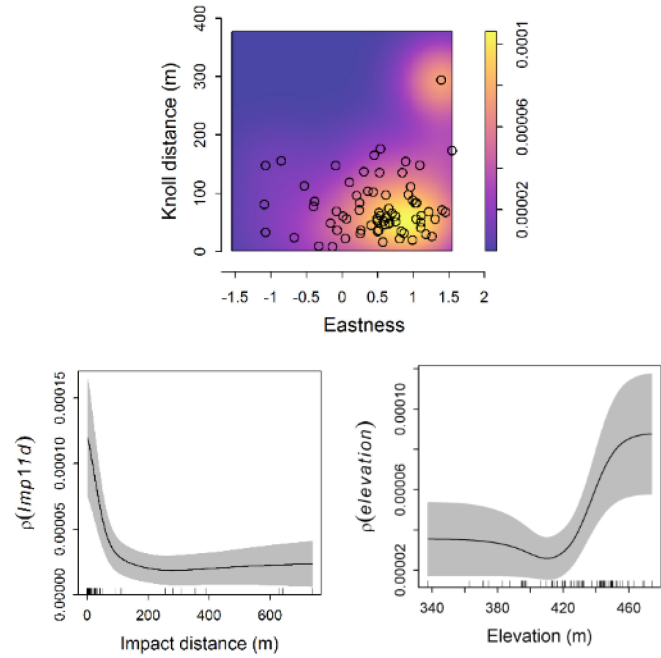


Figure 7. Ovenbird 2010 and 2011 territory intensity (λ) as predicted by the fitted PPMs and as nonparametric functions of spatial covariates. The univariate functions show λ with pointwise 95% confidence limits (gray shadings). The bivariate functions show λ as a function of two covariates (circles indicate covariate values for the individual territories).



2010 nonparametric intensity functions:



2011 nonparametric intensity functions:

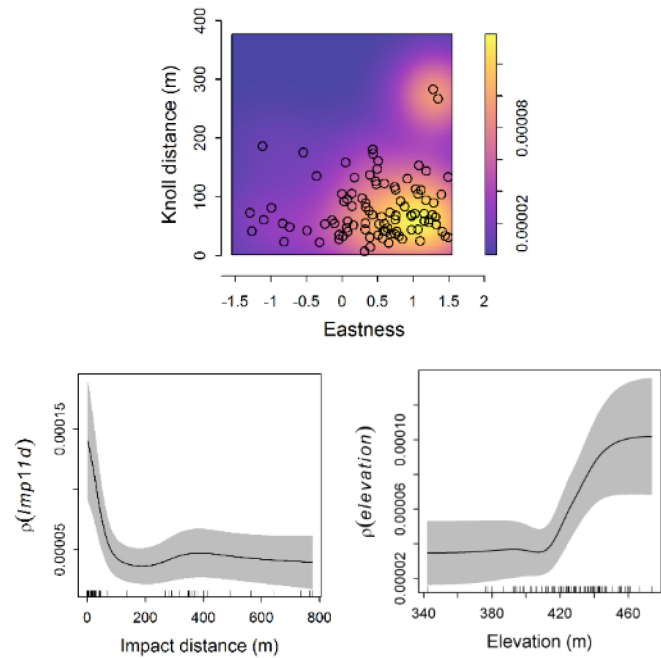
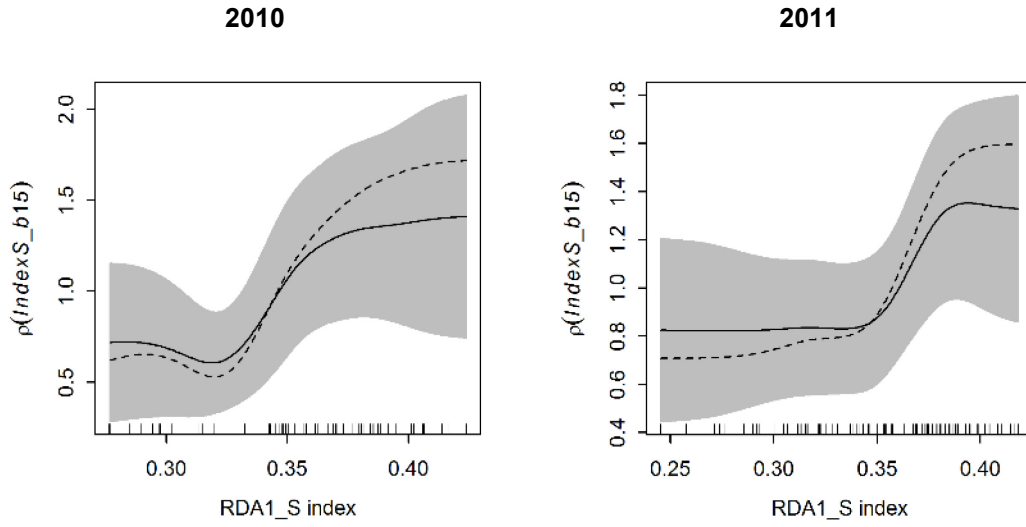


Figure 8. Cerulean Warbler 2010 and 2011 territory intensity (λ) as predicted by the fitted PPMs and as nonparametric functions of spatial covariates. The univariate functions show λ with pointwise 95% confidence limits (gray shadings). The bivariate functions show λ as a function of two covariates (circles indicate covariate values for the individual territories).

a. Hooded Warbler



b. Ovenbird

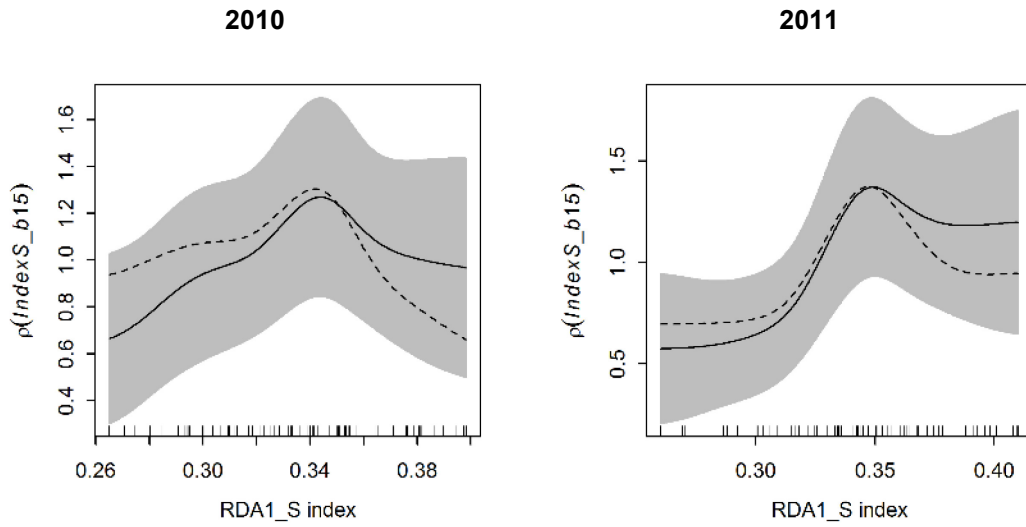


Figure 9. Hooded Warbler and Ovenbird 2010 and 2011 territory intensity (λ) as nonparametric functions of the RDA^1_s index. The functions show λ with pointwise 95% confidence limits (gray shadings) after controlling for eastness effects on λ using a parametric point process model. For comparison, the dashed lines show λ modeled separately using only the RDA^1_s index.

Appendix A. List of field variables with subplot statistics and data transformations.

Field variable ^a	Label	Mean	s.d.	min, max	Units	Subplot ^b	Transformation
Basal area (1, 3)	BA	30.25	10.57	1.95, 68.18	m ² /ha	11.3 m	none
Tree density (1, 3)	Tr_N	17.72	4.89	5, 33	#	11.3 m	none
Tree height ^c (1, 3)	Hgt	23.71	4.91	4.00, 42.00	m	11.3 m	none
DBH mean (1, 3)	xDBH	25.49	4.62	11.36, 40.17	cm	11.3 m	none
DBH s.d. (1, 3)	sdDBH	15.15	3.86	2.83, 30.18	cm	11.3 m	none
Snag density (1, 3)	Snag	0.63	0.84	0, 5	#	11.3 m	log(x+1)
Grapevine density (1, 3)	Gv_N	3.68	6.79	0, 48	#	11.3 m	log(x+1)
Herbaceous cover (1, 3)	Hb	20.78	25.43	0.00, 95.00	%	5 m	arcsine square-root(x)
Shrub cover (1, 3)	Sb	21.27	23.08	0.00, 100.00	%	5 m	arcsine square-root(x)
Sapling cover (1, 3)	Sp	19.43	17.62	0.00, 80.00	%	5 m	arcsine square-root(x)
Canopy cover (1, 3)	Can	95.65	7.59	16.67, 100.00	%	center	log(x+1)
Tree species richness (3)	Tr_R	5.17	1.99	1, 12	#	11.3 m	square-root(x)

Tree species composition data:

Common name ^a	Scientific name	Label	% of total BA ^d	% of subplot BA ^d		
				Mean	s.d.	min, max
Chestnut oak (2, 3)	<i>Quercus montana</i>	choa	29.54	26.07	28.12	0.00, 100.00
Sugar maple (2, 3)	<i>Acer saccharum</i>	suma	22.31	25.89	26.96	0.00, 100.00
Northern red oak (2)	<i>Q. rubra</i>	nroa	10.54	8.97	13.98	0.00, 59.84
Red maple (2)	<i>A. rubrum</i>	rema	5.68	5.74	10.19	0.00, 85.66
Black oak (2)	<i>Q. velutina</i>	bloa	4.93	4.54	11.67	0.00, 76.46
Hickory spp. (2)	<i>Carya spp.</i>	hick	4.46	4.76	10.17	0.00, 68.91
White oak (2)	<i>Q. alba</i>	whoa	3.21	3.08	9.33	0.00, 76.44
Black locust (2)	<i>Robinia pseudoacacia</i>	bllo	3.09	3.24	8.71	0.00, 70.08
Ash spp. (2)	<i>Fraxinus spp.</i>	ash	2.52	2.66	8.65	0.00, 76.62
American basswood (2)	<i>Tilia americana</i>	bass	2.51	2.67	7.64	0.00, 46.12
Scarlet oak (2)	<i>Quercus coccinea</i>	scoa	2.09	1.83	6.81	0.00, 65.56
Tulip poplar (2)	<i>Liriodendron tulipifera</i>	tupo	1.94	2.25	8.71	0.00, 77.39
Sassafras (2)	<i>Sassafras albidum</i>	sass	1.39	1.70	6.42	0.00, 51.98
Black cherry (2)	<i>Prunus serotina</i>	blch	1.06	1.06	4.14	0.00, 30.55
Shagbark hickory (2)	<i>Carya ovata</i>	shhi	1.03	1.05	5.32	0.00, 57.30
Black gum (2)	<i>Nyssa sylvatica</i>	blgu	0.73	0.73	2.90	0.00, 24.20
Black walnut (2)	<i>Juglans nigra</i>	blwa	0.57	0.59	3.51	0.00, 45.36
Tree-of-heaven (2)	<i>Ailanthus altissima</i>	heav	0.49	1.16	8.16	0.00, 94.25
Cucumber magnolia (2)	<i>Magnolia acuminata</i>	cuma	0.48	0.41	2.24	0.00, 17.98
Sourwood (2)	<i>Oxydendrum arboreum</i>	sour	0.36	0.33	1.36	0.00, 12.95
American beech (2)	<i>Fagus grandifolia</i>	ambe	0.33	0.32	2.04	0.00, 27.61
Slippery elm (2)	<i>Ulmus rubra</i>	slel	0.29	0.44	2.76	0.00, 40.57
Eastern hophornbeam (2)	<i>Ostrya virginiana</i>	hoho	0.28	0.30	0.99	0.00, 9.70

a. Inclusion in constrained ordination model noted in parentheses: 1 = RDA_S; 2 = CCA_C; 3 = RDA_{S+C}

b. Data collected within a radius of 5 m or 11.3 m of the subplot center (canopy cover estimated overhead at the center)

c. For tree selected to represent the dominant canopy height

d. Percent of total BA based on the sum of the 340 field subplots; subplot data arcsine square-root transformed prior to analysis

Appendix B. Comparative analyses of forest habitat characteristics at Cerulean Warbler and Ovenbird territory centers, and at Cerulean Warbler territory centers and non-use locations.

Purpose

We performed an exploratory analysis to test if field-collected forest habitat data differed between Cerulean Warbler and Ovenbird territory centers across the extent of the six ridgetop transects at our study site (blue and yellow points in Figure B1). The Hooded Warbler was excluded from this analysis because many of its territory centers were inaccessible due to dense vegetation. We also performed a separate analysis to test if the forest habitat data differed between the Cerulean Warbler territory centers and non-use locations (red points in Figure B1) randomly placed in apparently unoccupied forested areas based on the territory mapping and other field activities (e.g., regularly traversing the ridges in between the transects). As collected over the extent of the SR and OR transects, the habitat samples ($n = 97$) were further used as external data for validation of the mapped remotely-sensed indices of forest structure and composition on these transects (section 3.2).

Methods

We selected Cerulean Warbler and Ovenbird territory centers in 2010 for the habitat data collection by choosing an initial territory center as mapped on a transect for each species (e.g., the first territory center encountered from an access point), then by selecting additional territory centers that were >50 m apart (within a species) as we moved along the transect. Thus we did not obtain a completely random sample of territory centers but sampled as many over the extent of each transect as we could, given the distance requirement and time constraints of other

concurrent field work (e.g., habitat data collection at the 68 sampling points used for point count surveys). For the Cerulean Warbler non-use points, we used the ArcGIS 10.1 random point tool to generate points over the extent of each transect that were a minimum of 50 m apart and within areas of the transect buffered at >50 m from the species' 2010 and 2011 territory centers (for the SR and OR transect only), from its 2011 territory centers for the remaining transects (which were only sampled in 2011), and also in several areas near the transects that we often frequented but seldom observed them. We then randomly selected 9–10 of these points per transect. We excluded any territory centers or non-use points that would have encompassed anthropogenic impacts (e.g., forest roads, pipelines, and timber harvests) from the sampling. The data collection at the territory centers and non-use points was done in the same manner as for an individual sampling point subplot (i.e., within a 15-m radius with the same data collected; see section 2.2).

We used binomial logistic regression models to analyze single forest variables for comparing Cerulean Warbler and Ovenbird territory centers, and in a separate analysis also for comparing Cerulean Warbler territory centers and non-use points. We combined the data across the transects for both analyses due to sample size considerations (e.g., the DR transect had few Ovenbirds territory centers to sample) We evaluated model significance ($\alpha = 0.05$) using likelihood ratio tests. The forest variables were transformed as necessary (see Appendix A) prior to analysis, but we report here untransformed data means and standard errors (SE). We analyzed the same 12 forest structural variables that were used for the remote sensing index development, and for tree species composition the percent of total basal area accounted for by the canopy dominants chestnut oak and sugar maple.

Results and Discussion

We found relatively few significant differences for the forest variables with either analysis (Table B1), although several of the differences that we found potentially indicated selection of habitat for breeding territories by the species at our study site. Grapevine density was higher at the Cerulean Warbler territory centers than at the Ovenbird territory centers, and grapevines have been noted as important to nesting Cerulean Warblers (Bakermans and Rodewald 2009, Buehler et al. 2013). Herbaceous cover was lower at Ovenbird territory centers than at Cerulean Warbler territory centers, which may be a consequence of Ovenbirds favoring more open, deep leaf litter areas for nesting (Mattsson and Niemi 2006, Leblanc et al. 2011; see also section 4.1.2.). The greater sugar maple percent composition at Ovenbird territory centers than at Cerulean Warbler territory centers could indicate selection by the Ovenbird for more mesic habitat with greater food resources because of higher forest productivity (Seagle and Sturtevant 2005; see also section 4.1.2.). Tree heights were higher at the Cerulean Warbler territory centers than at the non-use locations, which is consistent with research suggesting Cerulean Warbler favor areas with taller trees (e.g., perhaps for maximizing the height of song perches; Barg et al. 2006).

Additional References

- Bakermans, M.H., Rodewald A.D., 2009. Think globally, manage locally: the importance of steady-state forest features for a declining songbird. *Forest Ecology and Management* 258: 224–232.
- Barg, J.J., Aiama, D.M., Jones, J., Robertson, R.J., 2006. Within-territory habitat use and microhabitat-selection by male Cerulean Warblers (*Dendroica cerulea*). *Auk* 123(3): 795–806.
- Buehler, D.A., Hamel, P.B., Boves, T., 2013. Cerulean Warbler (*Setophaga cerulea*), *The Birds of North America* (P. G. Rodewald, Ed.). Ithaca: Cornell Lab of Ornithology; Retrieved from the Birds of North America: <https://birdsna.org/Species-Account/bna/species/cerwar>

Table B1. Means (and standard errors) for the forest structural characteristics, and chestnut oak and sugar maple composition, for Cerulean Warbler (CERW) and Ovenbird (OVEN) territory centers, and for Cerulean Warbler non-use locations (CERW_N) for in bold were significantly different ($p < 0.05$). See Appendix A. for field variable descriptions.

Field variable	CERW ($n = 83$)	CERW_N ($n = 56$)	OVEN ($n = 85$)
Basal area	28.30 (1.17)	27.53 (1.53)	29.08 (1.18)
Tree density	17.10 (1.43)	17.66 (1.70)	17.53 (1.63)
Tree height	26.36 (2.14)	<u>24.01 (1.71)</u>	25.81 (1.62)
DBH mean	24.29 (2.19)	24.17 (2.55)	25.31 (2.24)
DBH s.d.	16.40 (2.33)	15.04 (1.95)	15.13 (1.95)
Snag density	0.03 (0.03)	0.05 (0.05)	0.03 (0.03)
Grapevine density	7.17 (33.60)	7.32 (26.08)	2.88 (18.19)
Herbaceous cover	28.30 (8.94)	21.54 (8.22)	20.58 (10.85)
Shrub cover	11.98 (2.90)	<u>17.63 (3.59)</u>	14.71 (3.17)
Sapling cover	17.02 (4.62)	16.98 (4.00)	19.38 (5.27)
Canopy cover	91.84 (1.29)	91.97 (1.22)	92.47 (0.61)
Tree species richness	5.90 (0.81)	6.04 (0.82)	5.35 (1.22)
% Chestnut oak	0.15 (0.56)	0.18 (0.56)	0.20 (0.51)
% Sugar maple	0.22 (0.13)	0.23 (0.16)	0.32 (0.18)

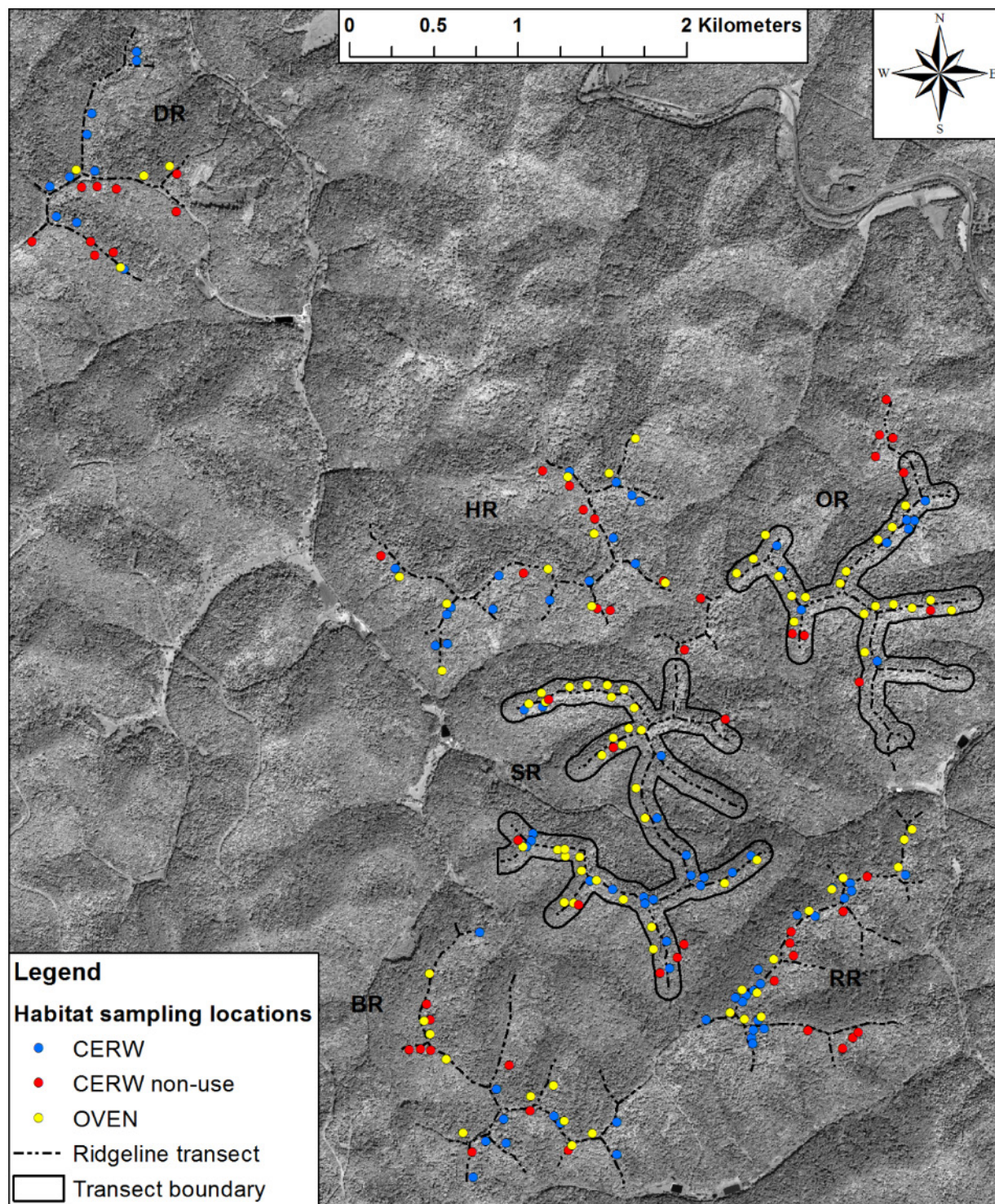


Figure B1. The Cerulean Warbler (CERW) and Ovenbird (OVEN) territory centers, and Cerulean Warbler non-use locations, at which the habitat sampling occurred (data collected as described for a subplot in section 2.2.). The transect boundaries used as sampling windows for the point pattern analysis of the species' complete territory center data on the SR and OR transects are shown.

Appendix C. List of remote sensing variables with subplot statistics and data transformations.

Source ^a	Summary ^b	Processing	Label	Mean	s.d.	min, max	Units ^c	Transformation
PAN	mean	n/a (original image)	PAN _{AVG}	52.66	4.43	41.26, 66.25	DN	none
PAN	s.d.	n/a (original image)	PAN _{SD}	10.47	2.01	6.15, 16.35	DN	none
PAN	s.d.	2 nd order correlation (9x9 pixel moving window)	PAN _{SD_COR09}	1.03x10 ⁻¹	1.02x10 ⁻²	8.02x10 ⁻² , 1.37x10 ⁻¹	DN	none
PAN	s.d.	1 st order s.d. (41x41 pixel moving window)	PAN _{SD_SD41}	3.54x10 ⁻³	1.34x10 ⁻³	1.11x10 ⁻³ , 9.07x10 ⁻³	DN	log(x)
PAN	mean	1 st order s.d. (3x3 pixel moving window)	PAN _{AVG_SD03}	1.16x10 ⁻²	4.32x10 ⁻³	3.39x10 ⁻³ , 2.64x10 ⁻²	DN	none
PAN	mean	2 nd order contrast (3x3 pixel moving window)	PAN _{AVG_CON03}	6.03	0.34	5.15, 7.01	DN	none
PAN	s.d.	2 nd order contrast (3x3 pixel moving window)	PAN _{SD_CON03}	2.53	0.10	2.31, 2.86	DN	none
PAN	s.d.	2 nd order contrast (9x9 pixel moving window)	PAN _{SD_CON09}	10.14	2.32	5.92, 17.25	DN	log(x)
PAN	s.d.	2 nd order correlation (3x3 pixel moving window)	PAN _{SD_COR03}	1.92x10 ⁻¹	3.67x10 ⁻³	1.81x10 ⁻¹ , 2.03x10 ⁻¹	DN	none
PAN	s.d.	2 nd order correlation (17x17 pixel moving window)	PAN _{SD_COR17}	6.15x10 ⁻²	1.28x10 ⁻²	3.80x10 ⁻² , 1.11x10 ⁻¹	DN	log(x)
PAN	s.d.	2 nd order correlation (41x41 pixel moving window)	PAN _{SD_COR41}	2.44x10 ⁻²	9.38x10 ⁻³	8.38x10 ⁻³ , 6.75x10 ⁻²	DN	log(x)
DEM	mean	n/a (original elevation)	ELEV	418.07	21.13	347.87, 463.92	m	none
DEM	mean	Slope	SLOPE	21.05	4.61	9.03, 34.13	degrees	none
DEM	mean	Cosine(Aspect)	COS	0.03	0.60	-1.00, 1.00	northness	arcsine(x)
DEM	mean	Sine(Aspect)	SIN	-0.03	0.59	-1.00, 1.00	eastness	arcsine(x)

a. Data source (PAN = QuickBird satellite panchromatic image; DEM = digital elevation model)

b. Subplot pixel summary statistic (15 m radius extraction)

c. DN = digital number

Appendix D. Spearman's correlations for the set of remote sensing variables used in the constrained ordinations (top), and over the combined OR and SR transect extent for the species distribution model (SDM) spatial covariates (bottom).

Name	PANAVG	PANSD	PANSD _SD41	PANAVG _SD03	PANAVG _CON03	PANSD _CON03	PANSD _CON09	PANSD _COR03	PANSD _COR09	PANSD _COR17	PANSD _COR41	ELEV	SLOPE	COS	SIN
PANAVG		0.25	0.24	0.16	0.47	0.11	0.46	-0.09	-0.12	-0.13	-0.08	0.16	-0.25	-0.67	0.29
PANSD	0.25		0.33	0.69	0.44	0.44	0.72	-0.18	-0.27	-0.28	-0.42	-0.04	0.11	0.07	0.18
PANSD_SD41	0.24	0.33		0.36	0.03	0.14	0.34	0.02	0.09	0.17	0.39	0.00	-0.02	-0.13	0.19
PANAVG_SD03	0.16	0.69	0.36		0.16	0.27	0.47	-0.09	-0.11	-0.09	-0.15	-0.07	0.01	0.06	0.11
PANAVG_CON03	0.47	0.44	0.03	0.16		0.50	0.48	0.04	-0.19	-0.19	-0.16	0.05	-0.05	-0.01	0.37
PANSD_CON03	0.11	0.44	0.14	0.27	0.50		0.46	0.15	-0.04	-0.03	-0.01	0.07	0.19	0.15	0.13
PANSD_CON09	0.46	0.72	0.34	0.47	0.48	0.46		-0.18	-0.28	-0.28	-0.31	0.03	0.04	-0.14	0.32
PANSD_COR03	-0.09	-0.18	0.02	-0.09	0.04	0.15	-0.18		0.28	0.17	0.23	0.03	0.07	0.13	-0.09
PANSD_COR09	-0.12	-0.27	0.09	-0.11	-0.19	-0.04	-0.28	0.28		0.73	0.40	0.03	0.00	-0.01	0.02
PANSD_COR17	-0.13	-0.28	0.17	-0.09	-0.19	-0.03	-0.28	0.17	0.73		0.54	0.05	0.00	0.00	-0.02
PANSD_COR41	-0.08	-0.42	0.39	-0.15	-0.16	-0.01	-0.31	0.23	0.40	0.54		0.06	-0.02	-0.01	-0.08
ELEV	0.16	-0.04	0.00	-0.07	0.05	0.07	0.03	0.03	0.03	0.05	0.06		-0.10	-0.09	-0.02
SLOPE	-0.25	0.11	-0.02	0.01	-0.05	0.19	0.04	0.07	0.00	0.00	-0.02	-0.10		0.26	0.04
COS	-0.67	0.07	-0.13	0.06	-0.01	0.15	-0.14	0.13	-0.01	0.00	-0.01	-0.09	0.26		-0.11
SIN	0.29	0.18	0.19	0.11	0.37	0.13	0.32	-0.09	0.02	-0.02	-0.08	-0.02	0.04	-0.11	

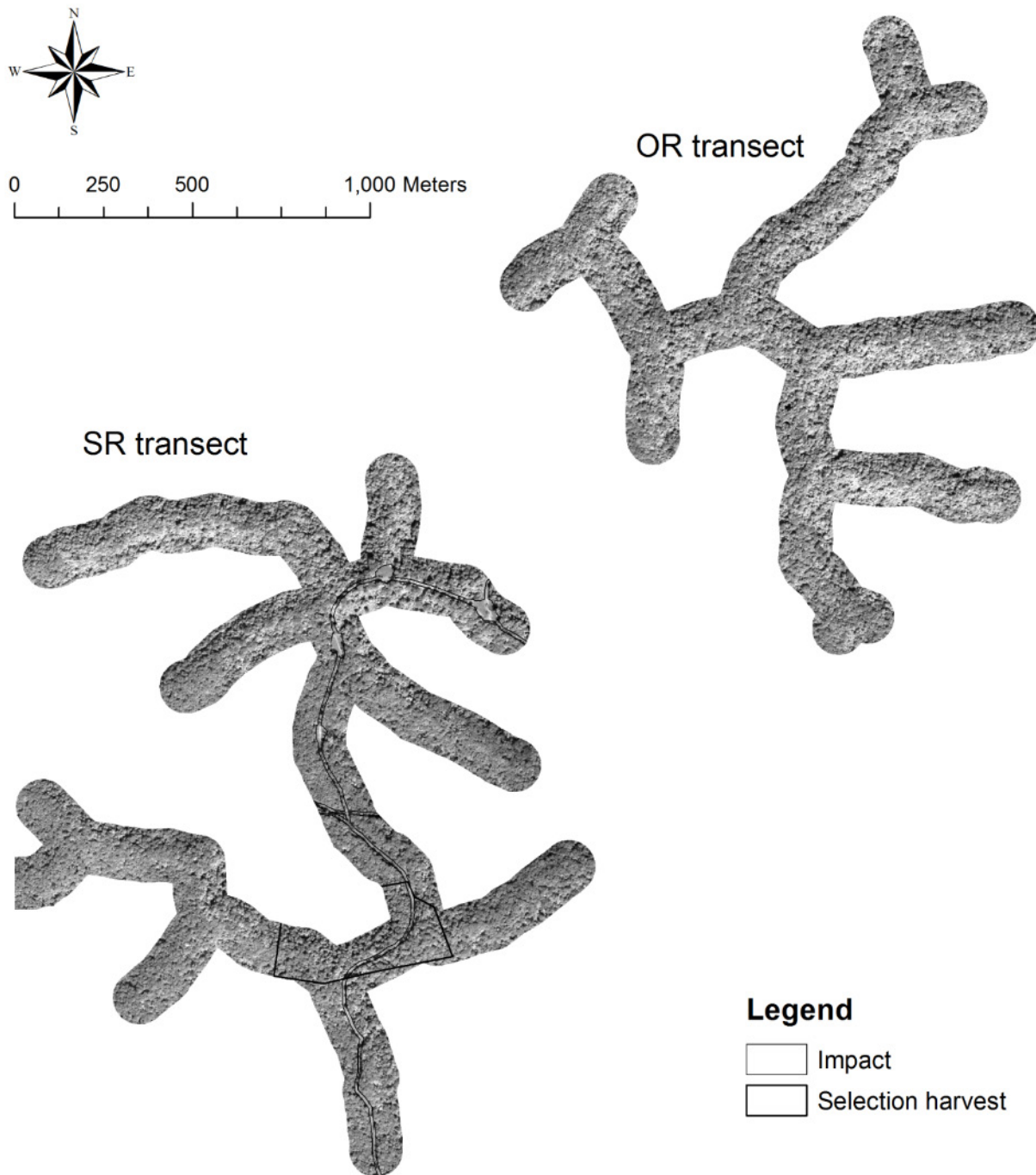
OR and SR transect SDM spatial covariates:

Name	RDA ¹ _S ^a	CCA ¹ _C ^a	RDA ¹ _{S+C} ^a	ELEV	SLOPE	SIN	COS	Knolls	Impact ^b
RDA ¹ _S ^a		0.86	0.96	0.14	-0.17	0.33	-0.14	-0.10	0.02
CCA ¹ _C ^a	0.86		0.92	0.21	-0.06	0.36	0.14	-0.11	0.16
RDA ¹ _{S+C} ^a	0.96	0.92		0.13	-0.10	0.38	0.07	-0.10	0.12
ELEV	0.14	0.21	0.13		-0.28	-0.04	0.04	-0.37	0.23
SLOPE	-0.17	-0.06	-0.10	-0.28		0.05	0.27	0.14	-0.31
SIN	0.33	0.36	0.38	-0.04	0.05		0.03	-0.02	0.00
COS	-0.14	0.14	0.07	0.04	0.27	0.03		-0.04	0.02
Knolls	-0.10	-0.11	-0.10	-0.37	0.14	-0.02	-0.04		-0.12
Impact ^b	0.02	0.16	0.12	0.23	-0.31	0.00	0.02	-0.12	

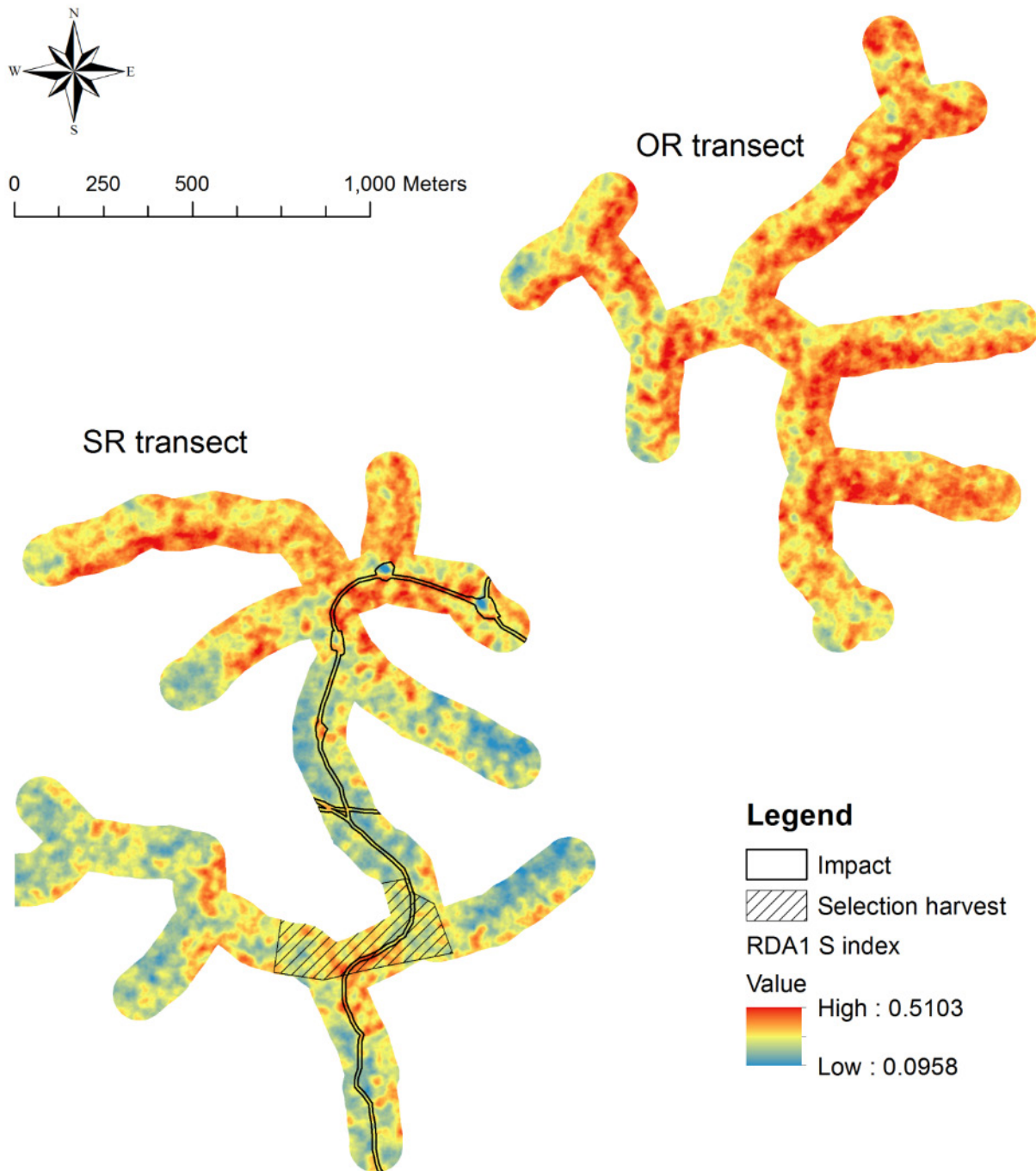
a. A 15 m s.d. Gaussian filter applied to the RDA¹_S, CCA¹_C, and RDA¹_{S+C} indices

b. The correlation based on reclassifying the impact distance at ≤15 m as 1, and > 15 m as 0, at the SR transect only.

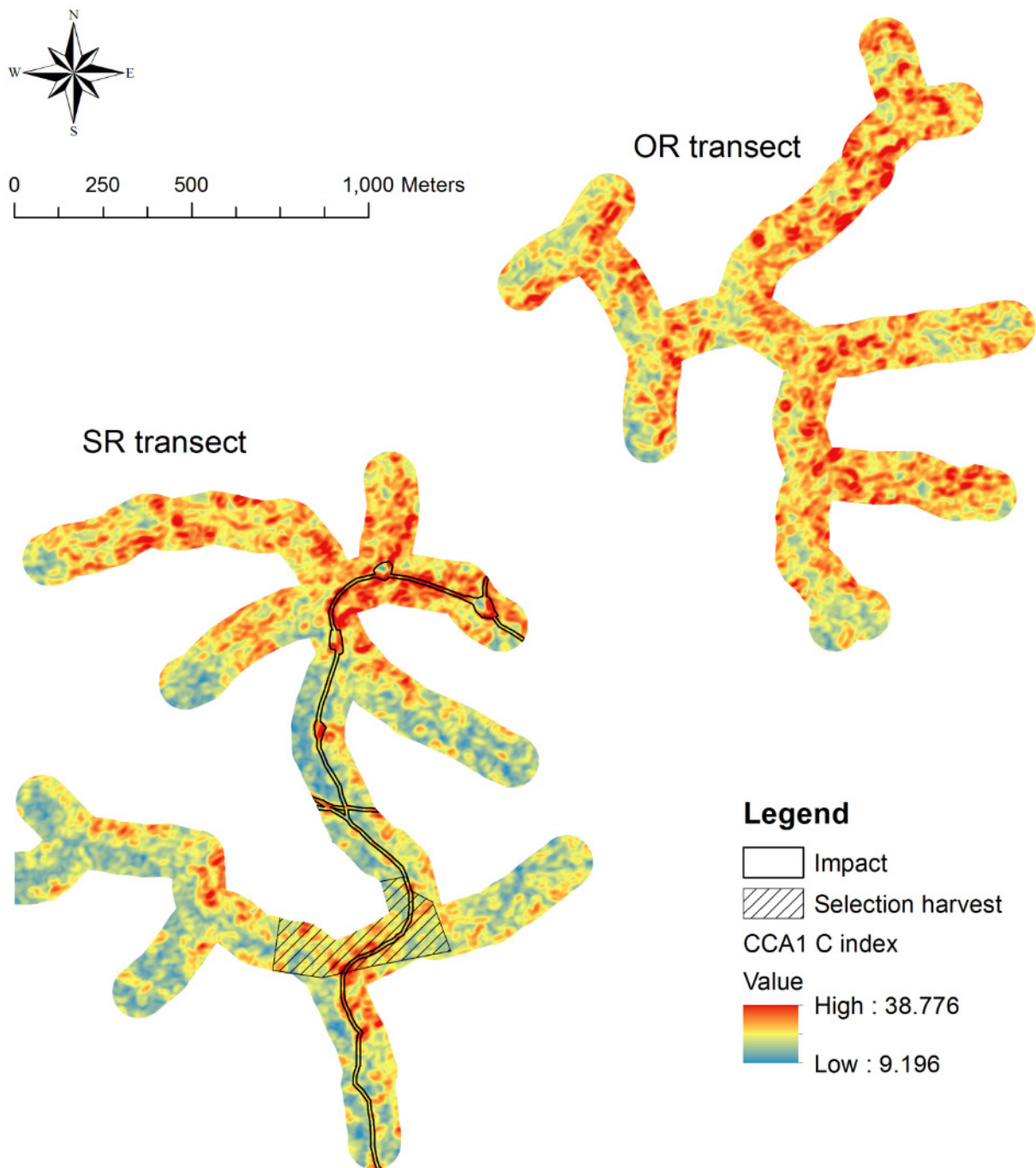
Appendix E. SR and OR transect QuickBird satellite image and remote sensing index maps, and combined-year territory center maps by species.



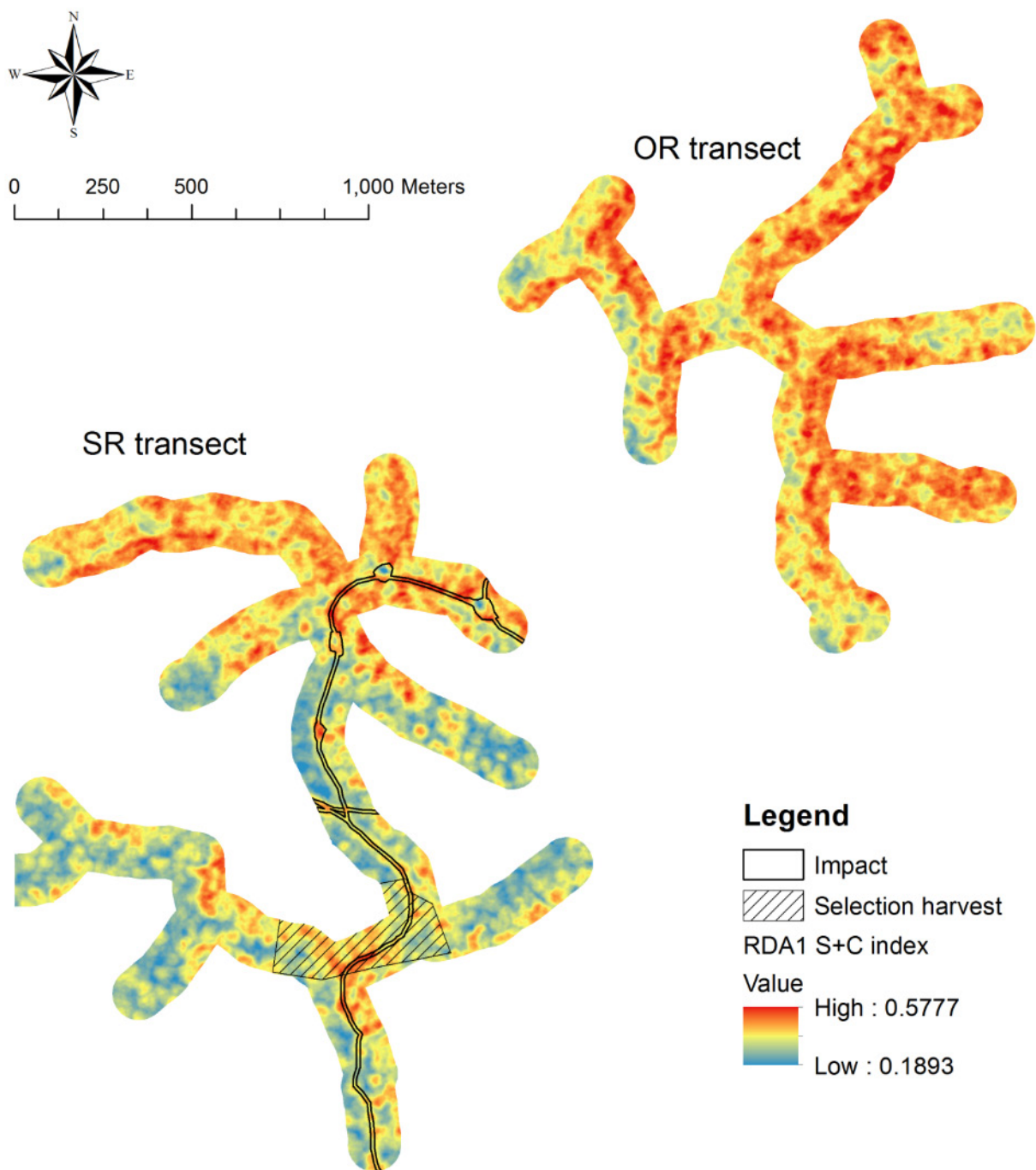
a. QuickBird satellite panchromatic band image (0.6 m spatial resolution; acquired 25 August 2009 at 16:18 GMT, 6° off-nadir) of the two ridgetop transects that were the focus of this study. The edges of the road/pipeline (with four small clearings for conventional gas and oil wells) are indicated, as well as the approximate boundary of the light selection harvest that occurred over the 2006–07 winter.



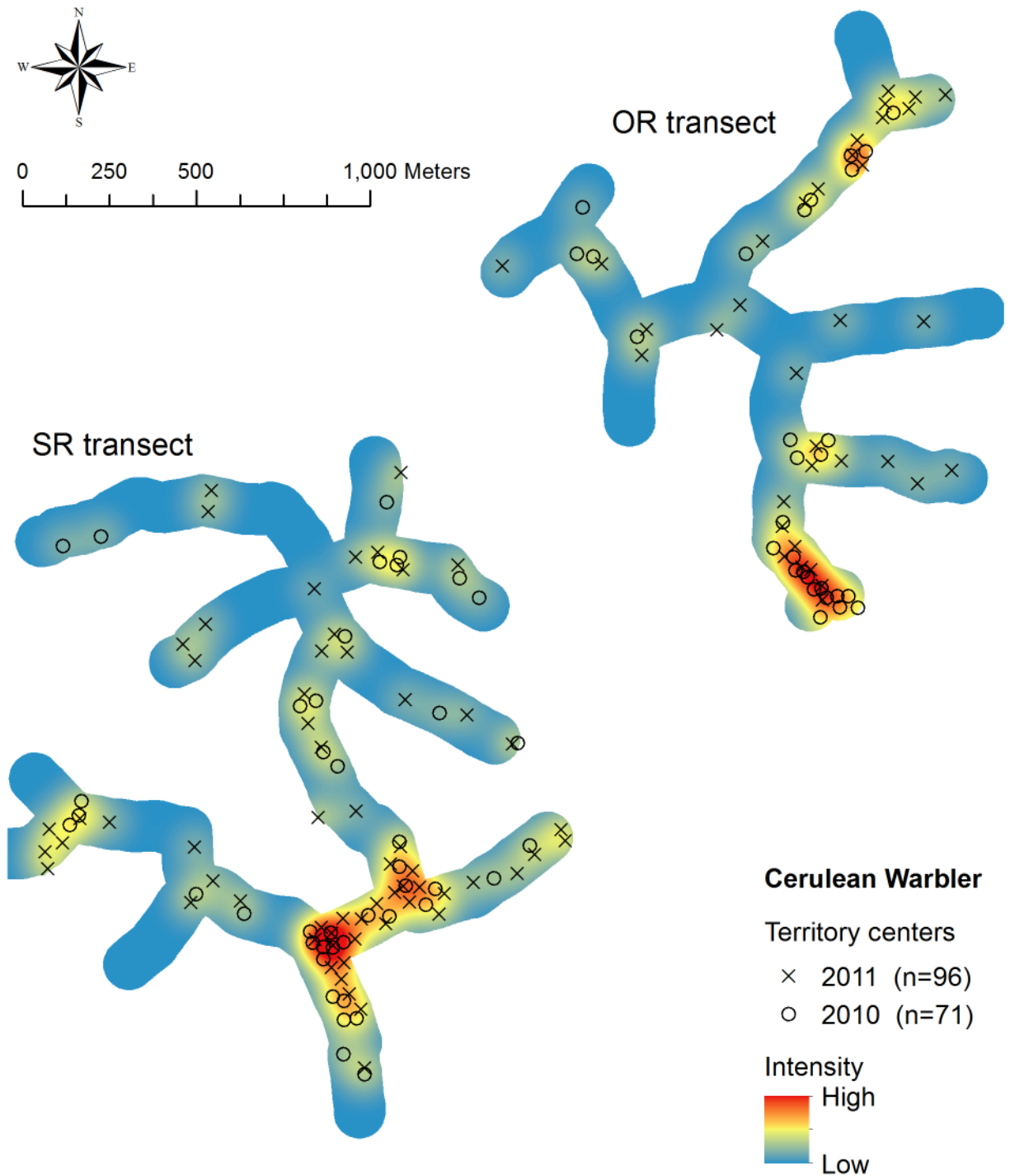
b. RDA¹_s index map, computed as a continuous predictive surface from the RDA_s model coefficients for the linear combinations of remote sensing variables for the first ordination axis (see Figure 2a).



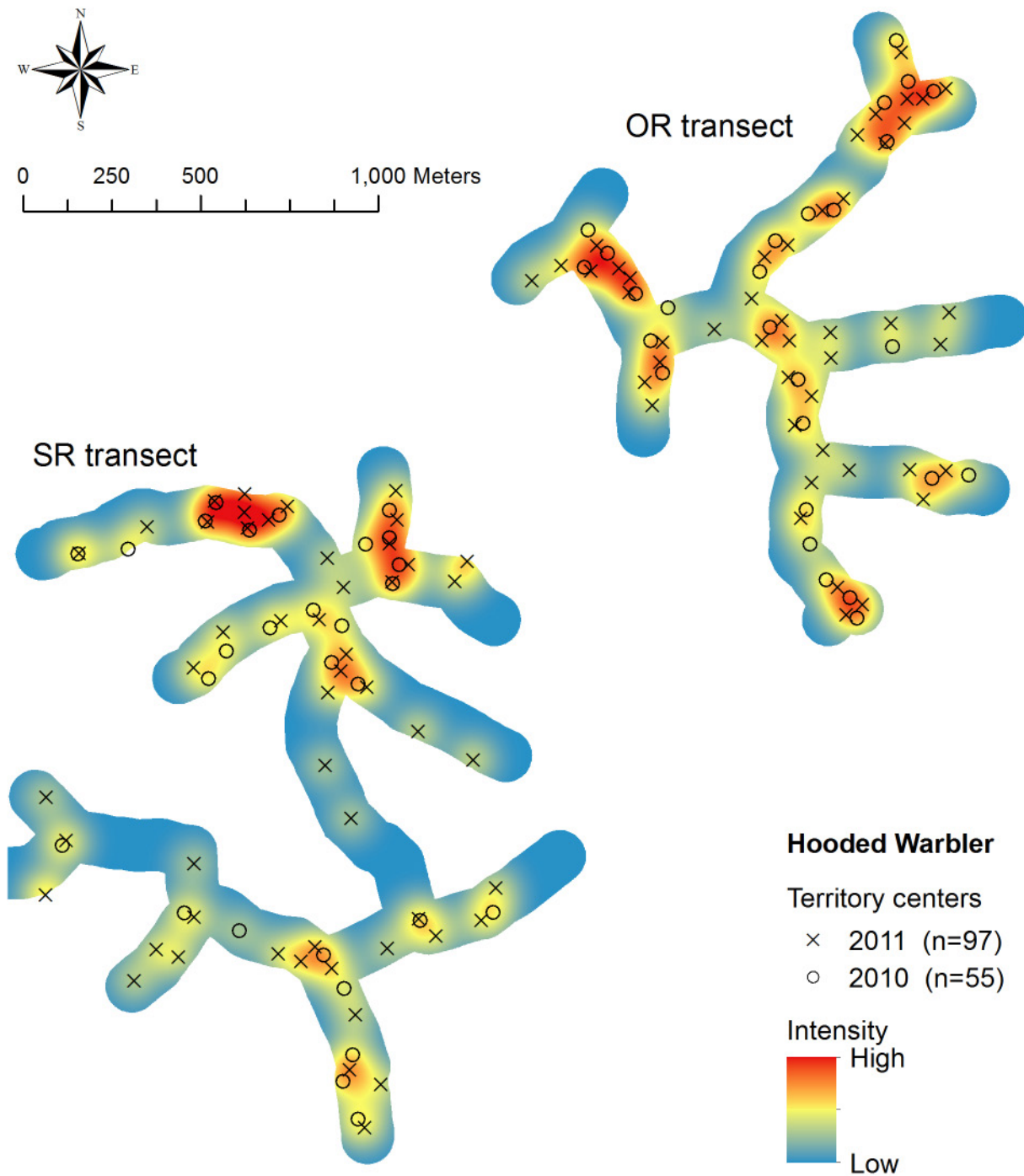
c. CCA¹_C index map, computed as a continuous predictive surface from the CCAs model coefficients for the linear combinations of remote sensing variables for the first ordination axis (see Figure 2b).



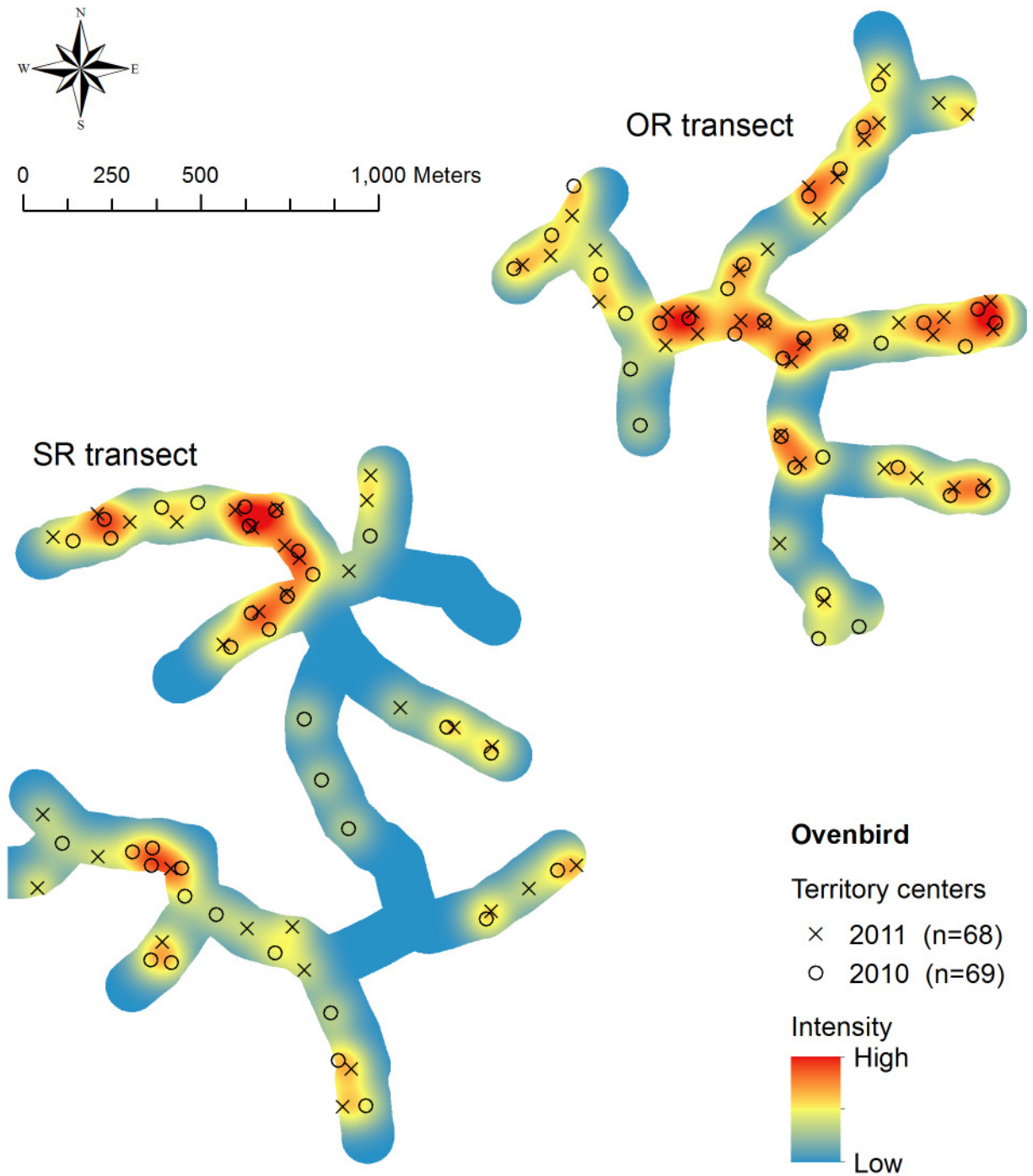
d. RDA^1_{S+C} index map, computed as a continuous predictive surface from the RDA_{S+C} model coefficients for the linear combinations of remote sensing variables for the first ordination axis (see Figure 2c).



e. Cerulean Warbler combined-year territory center map, overlaid on a kernel-smoothed intensity function from the combined year point pattern to help illustrate areas of high between-year selection for territory locations. The intensity function was made using the spatstat R package (Baddeley et al. 2015) *density.ppp* function, with a 50 m standard deviation of isotropic Gaussian smoothing kernel and Diggle's edge correction.



f. Hooded Warbler combined-year territory map, overlaid on a kernel-smoothed intensity function from the combined year point pattern to help illustrate areas of high between-year selection for territory locations. The intensity function was made using the spatstat R package (Baddeley et al. 2015) *density.ppp* function, with a 50 m standard deviation of isotropic Gaussian smoothing kernel and Diggle's edge correction.



g. Ovenbird combined-year territory map, overlaid on a kernel-smoothed intensity function from the combined year point pattern to help illustrate areas of high between-year selection for territory locations. The intensity function was made using the spatstat R package (Baddeley et al. 2015) *density.ppp* function, with a 50 m standard deviation of isotropic Gaussian smoothing kernel and Diggle's edge correction.

Appendix F. Complete annual point process model (PPM) results by species. All single spatial covariate and covariate by transect interaction model results are presented. For models including multiple spatial covariates, those presented vary by species (see section 3.4.). Modeling comments, diagnostic plots, and predicted intensity plots are also provided for select models.

Example PPM (point process model) output:

Parameter estimate, standard error, and lower and upper 95% confidence limits (here do not include 0, and parameter value is negative, so evidence for a negative relation between eastness and point pattern intensity)

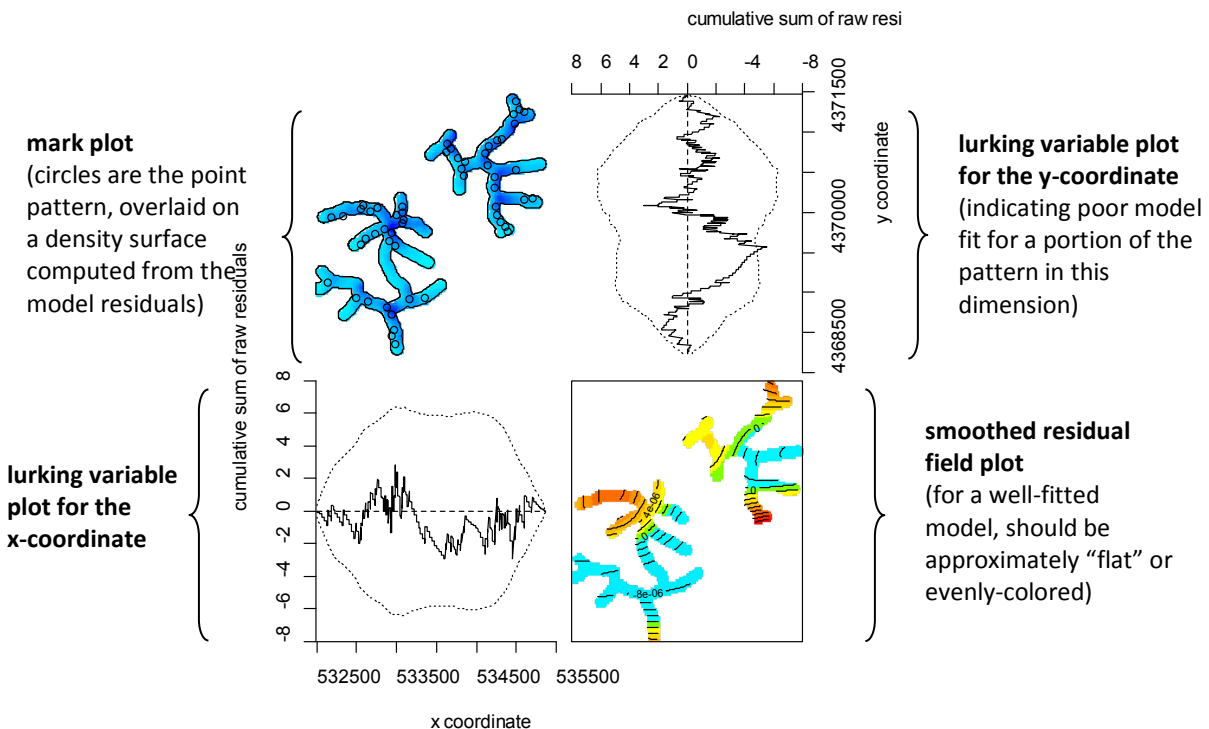
Covariate by transect interaction model result (P -value from likelihood ratio test). Here no evidence for a difference in the slope of the parameter estimates between the transects)

Spatial covariate name and model AIC fit

Eastness (AIC 1510.9)				
	Estimate	S.E.	CI95.lo	CI95.hi
(Intercept)	-10.285	0.142	-10.563	-10.007
Eastness	-0.619	0.127	-0.868	-0.370

Eastness by transect interaction ($P = 0.976$)				
	Estimate	S.E.	CI95.lo	CI95.hi
(Intercept)	-10.995	0.202	-11.392	-10.598
SR	0.034	0.284	-0.522	0.590
OR:Eastness	-0.623	0.181	-0.978	-0.268
SR:Eastness	-0.615	0.178	-0.965	-0.266

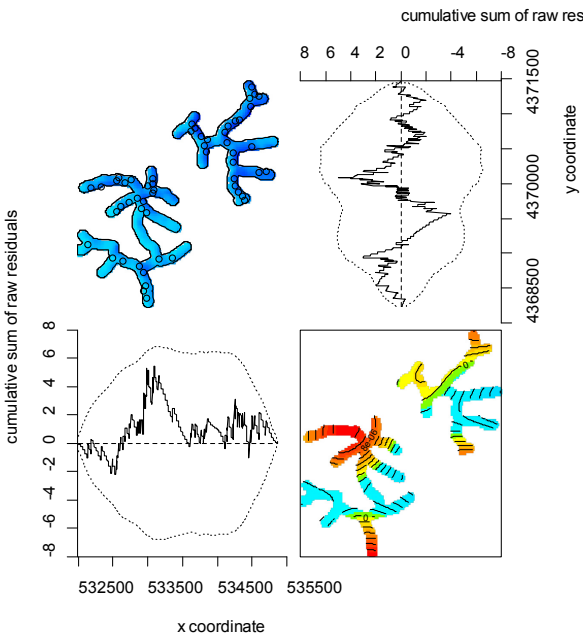
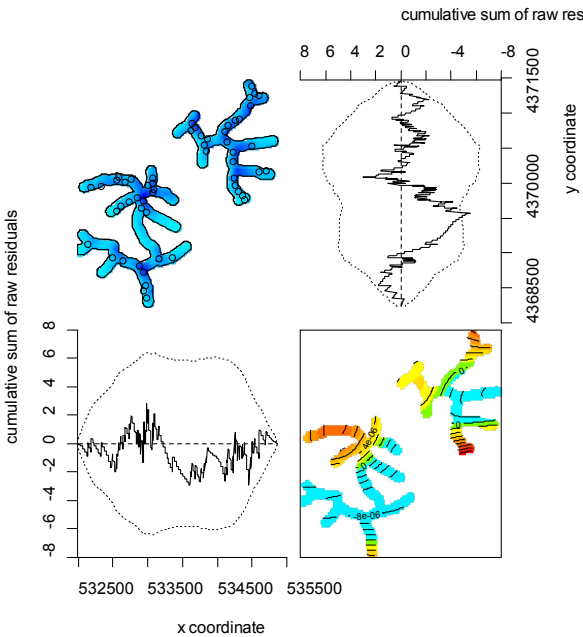
Example 4-panel diagnostic plot for a PPM (also see Baddeley et al. 2015):



2010 Hooded Warbler PPMs: Single covariate and by-transect interaction effects (covariates in bold were also considered in multiple covariate SDMs).

RDA_s (AIC 1239.0)					Elevation (AIC 1242.4)				
	Estimate	S.E.	CI95.lo	CI95.hi		Estimate	S.E.	CI95.lo	CI95.hi
(Intercept)	-10.443	0.150	-10.737	-10.149	(Intercept)	-10.406	0.145	-10.691	-10.121
RDA _{1s}	0.475	0.145	0.191	0.760	Elevation	0.404	0.147	0.115	0.693
RDA_s by transect interaction (<i>P</i> < 0.001)					Elevation by transect interaction (<i>P</i> < 0.001)				
	Estimate	S.E.	CI95.lo	CI95.hi		Estimate	S.E.	CI95.lo	CI95.hi
(Intercept)	-11.635	0.304	-12.232	-11.039	(Intercept)	-11.047	0.193	-11.426	-10.668
SR	0.630	0.358	-0.073	1.332	SR	-0.397	0.330	-1.044	0.251
OR:RDA _{1s}	1.148	0.250	0.658	1.637	OR:Elevation	-0.092	0.187	-0.460	0.275
SR:RDA _{1s}	-0.026	0.189	-0.397	0.345	SR:Elevation	1.008	0.233	0.552	1.464
RDA_{1s+c} (AIC 1239.6)					Slope (AIC 1248.3)				
	Estimate	S.E.	CI95.lo	CI95.hi		Estimate	S.E.	CI95.lo	CI95.hi
(Intercept)	-10.441	0.150	-10.735	-10.146	(Intercept)	-10.348	0.137	-10.617	-10.079
RDA _{1s+c}	0.474	0.151	0.178	0.769	Slope	-0.190	0.132	-0.448	0.069
RDA_{1s+c} by transect interaction (<i>P</i> < 0.001)					Slope by transect interaction (<i>P</i> = 0.920)				
	Estimate	S.E.	CI95.lo	CI95.hi		Estimate	S.E.	CI95.lo	CI95.hi
(Intercept)	-11.834	0.348	-12.515	-11.153	(Intercept)	-11.062	0.196	-11.447	-10.678
SR	0.824	0.396	0.048	1.600	SR	0.041	0.274	-0.496	0.579
OR:RDA _{1s+c}	1.393	0.293	0.819	1.967	OR:Slope	-0.203	0.188	-0.572	0.165
SR:RDA _{1s+c}	-0.100	0.187	-0.468	0.267	SR:Slope	-0.177	0.185	-0.540	0.186
CCA_{1c} (AIC 1243.2)					Knolls (AIC 1241.6)				
	Estimate	S.E.	CI95.lo	CI95.hi		Estimate	S.E.	CI95.lo	CI95.hi
(Intercept)	-10.402	0.144	-10.685	-10.119	(Intercept)	-10.426	0.149	-10.719	-10.134
CCA _{1c}	0.373	0.141	0.096	0.650	Knolls	-0.476	0.175	-0.819	-0.133
CCA_{1c} by transect interaction (<i>P</i> < 0.001)					Knolls by transect interaction (<i>P</i> = 0.384)				
	Estimate	S.E.	CI95.lo	CI95.hi		Estimate	S.E.	CI95.lo	CI95.hi
(Intercept)	-11.441	0.266	-11.963	-10.920	(Intercept)	-11.091	0.203	-11.489	-10.694
SR	0.434	0.327	-0.207	1.074	SR	-0.077	0.302	-0.669	0.516
OR:CCA _{1c}	0.919	0.226	0.477	1.361	OR:Knolls	-0.331	0.233	-0.788	0.125
SR:CCA _{1c}	-0.075	0.189	-0.444	0.295	SR:Knolls	-0.637	0.263	-1.152	-0.121
Eastness (AIC 1241.8)					SR transect Impact (AIC N/A)				
	Estimate	S.E.	CI95.lo	CI95.hi	note: distance to impact tested at SR transect only (AIC comparison with other covariates in this table is not valid)				
(Intercept)	-10.421	0.147	-10.709	-10.132					
Eastness	0.411	0.144	0.129	0.694					
Eastness by transect interaction (<i>P</i> = 0.013)						Estimate	S.E.	CI95.lo	CI95.hi
	Estimate	S.E.	CI95.lo	CI95.hi	(Intercept)	-10.516	0.196	-10.901	-10.132
(Intercept)	-11.364	0.256	-11.865	-10.863	Impact	-0.271	0.213	-0.688	0.147
SR	0.353	0.319	-0.272	0.977					
OR:Eastness	0.815	0.232	0.360	1.270					
SR:Eastness	0.086	0.191	-0.288	0.459					
Northness (AIC 1249.6)									
	Estimate	S.E.	CI95.lo	CI95.hi					
(Intercept)	-10.338	0.136	-10.605	-10.072					
Northness	-0.121	0.136	-0.387	0.145					
Northness by transect interaction (<i>P</i> = 0.160)									
	Estimate	S.E.	CI95.lo	CI95.hi					
(Intercept)	-11.045	0.193	-11.423	-10.666					
SR	-0.010	0.277	-0.553	0.532					
OR:Northness	0.070	0.192	-0.306	0.446					
SR:Northness	-0.314	0.196	-0.698	0.071					

2010 Hooded Warbler multiple covariate PPMs.

Eastness+RDA ¹ s (AIC 1237.5)					Eastness+RDA ¹ s diagnostics				
	Estimate	S.E.	CI95.lo	CI95.hi					
(Intercept)	-10.484	0.155	-10.789	-10.179					
Eastness	0.363	0.195	-0.020	0.746					
RDA1s	0.373	0.153	0.074	0.672					
Notes: Above effects partly not separable (indicated by parameter estimate changes when combined, compared to single covariate estimates).									
Elevation+RDA ¹ s (AIC 1234.9)					Eastness+Elevation+RDA ¹ s diagnostics				
	Estimate	S.E.	CI95.lo	CI95.hi					
(Intercept)	-10.511	0.160	-10.824	-10.197					
Elevation	0.375	0.155	0.071	0.679					
RDA1s	0.443	0.147	0.155	0.732					
Eastness+Elevation+RDA ¹ s (AIC 1232.5)									
	Estimate	S.E.	CI95.lo	CI95.hi					
(Intercept)	-10.555	0.165	-10.878	-10.232					
Eastness	0.408	0.197	0.022	0.794					
Elevation	0.395	0.153	0.095	0.696					
RDA1s	0.318	0.157	0.010	0.625					
Notes: Above effects partly not separable (indicated by parameter estimate changes when combined, compared to single covariate estimates). Inclusion of elevation also resulted in a model fit issue, as indicated by y-coordinate lurking variable plot (although the x-coordinate lurking variable plot looks somewhat improved versus the Eastness+RDA ¹ s model).									

2011 Hooded Warbler PPMs: Single covariate and by-transect interaction effects (covariates in bold were also considered in multiple covariate SDMs).

RDA¹_s (AIC 2083.8)					Elevation (AIC 2081.8)				
	Estimate	S.E.	CI95.lo	CI95.hi		Estimate	S.E.	CI95.lo	CI95.hi
(Intercept)	-9.810	0.106	-10.018	-9.601	(Intercept)	-9.818	0.107	-10.028	-9.608
RDA1s	0.299	0.105	0.093	0.505	Elevation	0.343	0.110	0.128	0.559
RDA¹_s by transect interaction (P < 0.001)					Elevation by transect interaction (P = 0.003)				
	Estimate	S.E.	CI95.lo	CI95.hi		Estimate	S.E.	CI95.lo	CI95.hi
(Intercept)	-11.027	0.223	-11.463	-10.590	(Intercept)	-10.510	0.147	-10.799	-10.221
SR	0.592	0.265	0.072	1.112	SR	-0.101	0.224	-0.541	0.338
OR:RDA1s	1.063	0.186	0.697	1.428	OR:Elevation	0.023	0.148	-0.267	0.313
SR:RDA1s	-0.245	0.139	-0.518	0.027	SR:Elevation	0.677	0.162	0.359	0.995
RDA¹_{s+c} (AIC 2085.1)					Slope (AIC 2090.4)				
	Estimate	S.E.	CI95.lo	CI95.hi		Estimate	S.E.	CI95.lo	CI95.hi
(Intercept)	-9.803	0.106	-10.011	-9.596	(Intercept)	-9.771	0.102	-9.972	-9.571
RDA1s+c	0.278	0.107	0.068	0.488	Slope	-0.131	0.100	-0.327	0.065
RDA¹_{s+c} by transect interaction (P < 0.001)					Slope by transect interaction (P = 0.293)				
	Estimate	S.E.	CI95.lo	CI95.hi		Estimate	S.E.	CI95.lo	CI95.hi
(Intercept)	-11.085	0.235	-11.546	-10.624	(Intercept)	-10.509	0.147	-10.799	-10.220
SR	0.642	0.276	0.101	1.184	SR	0.078	0.206	-0.326	0.481
OR:RDA1s+c	1.159	0.208	0.752	1.567	OR:Slope	-0.018	0.147	-0.307	0.270
SR:RDA1s+c	-0.276	0.137	-0.546	-0.007	SR:Slope	-0.229	0.136	-0.496	0.038
CCA¹_c (AIC 2085.7)					Knolls (AIC 2088.6)				
	Estimate	S.E.	CI95.lo	CI95.hi		Estimate	S.E.	CI95.lo	CI95.hi
(Intercept)	-9.800	0.105	-10.006	-9.593	(Intercept)	-9.783	0.104	-9.986	-9.580
CCA1c	0.262	0.104	0.057	0.466	Knolls	-0.207	0.115	-0.432	0.019
CCA¹_c by transect interaction (P < 0.001)					Knolls by transect interaction (P = 0.998)				
	Estimate	S.E.	CI95.lo	CI95.hi		Estimate	S.E.	CI95.lo	CI95.hi
(Intercept)	-10.803	0.190	-11.175	-10.431	(Intercept)	-10.529	0.151	-10.824	-10.234
SR	0.388	0.237	-0.076	0.851	SR	0.103	0.208	-0.304	0.510
OR:CCA1c	0.781	0.168	0.452	1.110	OR:Knolls	-0.207	0.167	-0.535	0.120
SR:CCA1c	-0.148	0.139	-0.422	0.125	SR:Knolls	-0.206	0.159	-0.517	0.104
Eastness (AIC 2081.9)					SR transect Impact (AIC N/A)				
	Estimate	S.E.	CI95.lo	CI95.hi	note: distance to impact tested at SR transect only (AIC comparison with other covariates in this table is not valid)				
(Intercept)	-9.825	0.108	-10.036	-9.613					
Eastness	0.334	0.107	0.125	0.544		Estimate	S.E.	CI95.lo	CI95.hi
Eastness by transect interaction (P = 0.050)					(Intercept)	-9.896	0.142	-10.174	-9.617
	Estimate	S.E.	CI95.lo	CI95.hi	Impact	-0.169	0.150	-0.463	0.125
(Intercept)	-10.673	0.172	-11.011	-10.336					
SR	0.254	0.223	-0.183	0.691					
OR:Eastness	0.566	0.165	0.244	0.889					
SR:Eastness	0.144	0.142	-0.135	0.423					
Northness (AIC 2091.5)									
	Estimate	S.E.	CI95.lo	CI95.hi					
(Intercept)	-9.766	0.102	-9.966	-9.567					
Northness	-0.075	0.102	-0.274	0.125					
Northness by transect interaction (P = 0.373)									
	Estimate	S.E.	CI95.lo	CI95.hi					
(Intercept)	-10.510	0.147	-10.799	-10.221					
SR	0.091	0.205	-0.311	0.492					
OR:Northness	0.020	0.147	-0.268	0.308					
SR:Northness	-0.161	0.142	-0.439	0.116					

2011 Hooded Warbler multiple covariate PPMs.

Eastness+RDA ¹ _s (AIC 2080.3)					Eastness+RDA ¹ _s diagnostics	
	Estimate	S.E.	CI95.lo	CI95.hi		
(Intercept)	-9.844	0.110	-10.059	-9.629		
Eastness	0.264	0.114	0.040	0.488		
RDA1s	0.206	0.111	-0.011	0.423		
Notes: Above effects partly not separable (indicated by parameter estimate changes when combined, compared to single covariate estimates).						

Elevation+RDA ¹ _s (AIC 2077.6)					Eastness+Elevation+RDA ¹ _s diagnostics	
	Estimate	S.E.	CI95.lo	CI95.hi		
(Intercept)	-9.857	0.112	-10.076	-9.639		
Elevation	0.319	0.114	0.097	0.542		
RDA1s	0.264	0.107	0.054	0.474		
Notes: Above effects partly not separable (indicated by parameter estimate changes when combined, compared to single covariate estimates). Inclusion of elevation also resulted in a model fit issue, as indicated by y-coordinate lurking variable plot (the x-coordinate lurking variable plot also looks somewhat worse versus the Eastness+RDA ¹ _s model).						

Eastness+Elevation+RDA ¹ _s (AIC 2072.7)				
	Estimate	S.E.	CI95.lo	CI95.hi
(Intercept)	-9.897	0.115	-10.122	-9.671
Eastness	0.300	0.115	0.074	0.526
Elevation	0.342	0.112	0.122	0.562
RDA1s	0.148	0.114	-0.076	0.373

2010 Ovenbird PPMs: Single covariate and by-transect interaction effects (covariates in bold were also considered in multiple covariate SDMs).

RDA¹_s (AIC 1531.6)	Elevation (AIC 1535.5)
Estimate S.E. CI95.lo CI95.hi (Intercept) -9.855 0.154 -10.158 -9.552 RDA1s -0.182 0.148 -0.471 0.107 RDA1s^2 -0.309 0.139 -0.583 -0.036	Estimate S.E. CI95.lo CI95.hi (Intercept) -10.110 0.121 -10.347 -9.872 Elevation 0.113 0.124 -0.130 0.355
RDA¹_s by transect interaction (P = 0.001)	Elevation by transect interaction (P = 0.048)
Estimate S.E. CI95.lo CI95.hi (Intercept) -10.862 0.180 -11.215 -10.509 SR -0.047 0.262 -0.560 0.465 OR:RDA1s 0.315 0.179 -0.035 0.666 SR:RDA1s -0.508 0.172 -0.845 -0.171	Estimate S.E. CI95.lo CI95.hi (Intercept) -10.820 0.173 -11.159 -10.481 SR -0.025 0.249 -0.513 0.464 OR:Elevation -0.121 0.166 -0.446 0.205 SR:Elevation 0.367 0.184 0.007 0.728
RDA¹_{s+c} (AIC 1534.6)	Slope (AIC 1532.3)
Estimate S.E. CI95.lo CI95.hi (Intercept) -10.115 0.122 -10.354 -9.877 RDA1s+c -0.156 0.119 -0.389 0.077	Estimate S.E. CI95.lo CI95.hi (Intercept) -10.132 0.124 -10.375 -9.890 Slope -0.239 0.117 -0.469 -0.010
RDA¹_{s+c} by transect interaction (P < 0.001)	Slope by transect interaction (P = 0.675)
Estimate S.E. CI95.lo CI95.hi (Intercept) -10.862 0.180 -11.215 -10.508 SR -0.094 0.267 -0.617 0.430 OR:RDA1s+c 0.316 0.184 -0.043 0.676 SR:RDA1s+c -0.588 0.170 -0.922 -0.254	Estimate S.E. CI95.lo CI95.hi (Intercept) -10.853 0.178 -11.203 -10.504 SR 0.053 0.248 -0.433 0.538 OR:Slope -0.289 0.166 -0.614 0.036 SR:Slope -0.190 0.165 -0.515 0.134
CCA¹_c (AIC 1532.7)	Knolls (AIC 1535.4)
Estimate S.E. CI95.lo CI95.hi (Intercept) -10.129 0.123 -10.370 -9.887 CCA1c -0.229 0.120 -0.465 0.007	Estimate S.E. CI95.lo CI95.hi (Intercept) -10.111 0.121 -10.349 -9.874 Knolls -0.125 0.130 -0.380 0.130
CCA¹_c by transect interaction (P = 0.002)	Knolls by transect interaction (P = 0.455)
Estimate S.E. CI95.lo CI95.hi (Intercept) -10.824 0.174 -11.164 -10.483 SR -0.136 0.263 -0.652 0.380 OR:CCA1c 0.149 0.174 -0.193 0.491 SR:CCA1c -0.604 0.175 -0.947 -0.260	Estimate S.E. CI95.lo CI95.hi (Intercept) -10.836 0.176 -11.180 -10.491 SR 0.052 0.244 -0.426 0.531 OR:Knolls -0.229 0.197 -0.614 0.156 SR:Knolls -0.034 0.173 -0.373 0.304
Eastness (AIC 1510.9)	SR transect Impact (AIC N/A)
Estimate S.E. CI95.lo CI95.hi (Intercept) -10.285 0.142 -10.563 -10.007 Eastness -0.619 0.127 -0.868 -0.370	note: distance to impact tested at SR transect only (AIC comparison with other covariates in this table is not valid)
Eastness by transect interaction (P = 0.976)	Estimate S.E. CI95.lo CI95.hi
Estimate S.E. CI95.lo CI95.hi (Intercept) -10.995 0.202 -11.392 -10.598 SR 0.034 0.284 -0.522 0.590 OR:Eastness -0.623 0.181 -0.978 -0.268 SR:Eastness -0.615 0.178 -0.965 -0.266	(Intercept) -9.974 0.217 -10.399 -9.550 Impact 0.507 0.236 0.044 0.970 Impact^2 -0.362 0.188 -0.731 0.006
Northness (AIC 1536.3)	
Estimate S.E. CI95.lo CI95.hi (Intercept) -10.104 0.120 -10.340 -9.868 Northness -0.019 0.120 -0.254 0.216	
Northness by transect interaction (P = 0.108)	
Estimate S.E. CI95.lo CI95.hi (Intercept) -10.827 0.174 -11.168 -10.486 SR 0.022 0.245 -0.459 0.503 OR:Northness 0.176 0.171 -0.160 0.512 SR:Northness -0.212 0.172 -0.549 0.125	

2010 Ovenbird multiple covariate PPMs.

Eastness+RDA ¹ _s (AIC 1510.1)				
	Estimate	S.E.	CI95.lo	CI95.hi
(Intercept)	-10.074	0.177	-10.420	-9.728
Eastness	-0.637	0.136	-0.904	-0.370
RDA1s	0.055	0.158	-0.254	0.364
RDA1s^2	-0.255	0.141	-0.532	0.021

Notes: Small AIC improvement versus Eastness only model (AIC = 1510.9); effects partly not separable (indicated by parameter estimate changes when combined, compared to single covariate estimates).

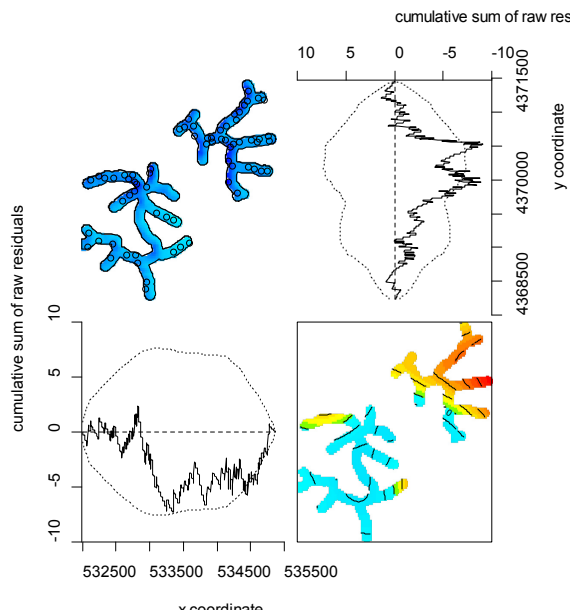
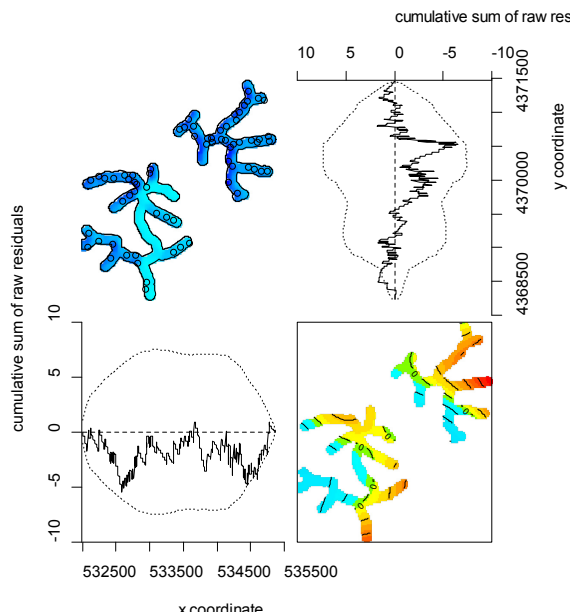
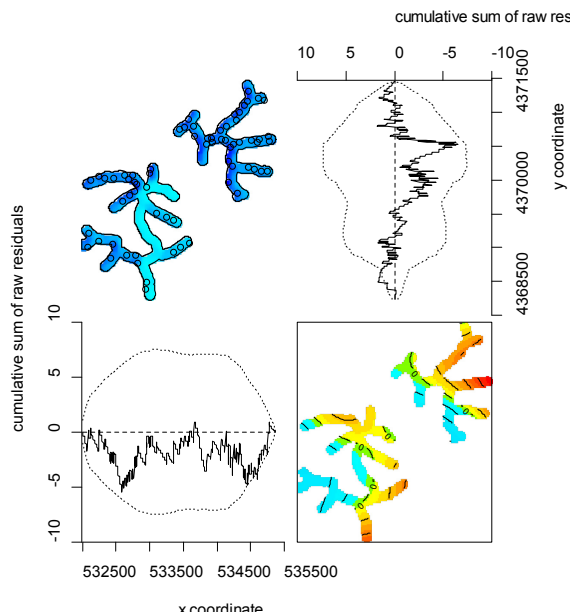
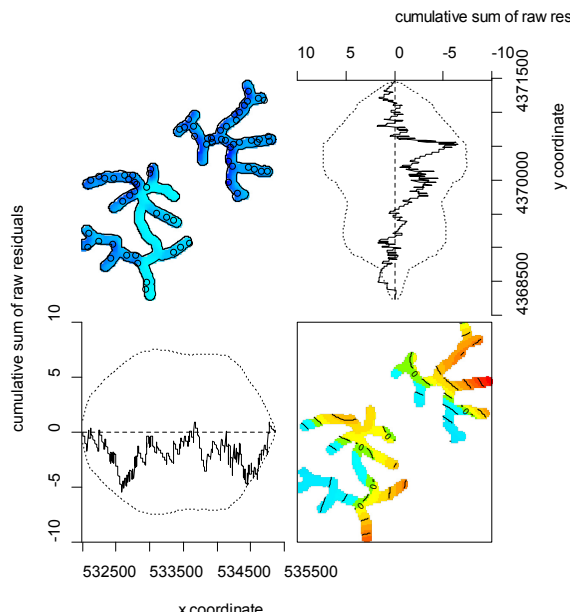
Below: Including a 75 m truncated distance to impact covariate with eastness and the index improved model AIC and residual diagnostics somewhat. While model fit was about the same when the index was removed, residual diagnostics indicated more fit issues (not shown). Topographic slope was an additional effect that further reduced model AIC, but with residual diagnostics unchanged versus the Eastness+RDA¹_s+Impact model.

Eastness+RDA¹_s diagnostics				
x coordinate				
Eastness+RDA¹_s+Impact (AIC 1508.9)				
	Estimate	S.E.	CI95.lo	CI95.hi
(Intercept)	-10.923	0.566	-12.031	-9.814
Eastness	-0.623	0.137	-0.891	-0.355
RDA1s	-0.007	0.160	-0.321	0.307
RDA1s^2	-0.251	0.140	-0.526	0.023
Impact (75 m)	0.013	0.008	-0.003	0.028
Eastness+RDA¹_s+Impact diagnostics				
x coordinate				
Eastness+Impact (AIC 1509.0)				
	Estimate	S.E.	CI95.lo	CI95.hi
(Intercept)	-11.209	0.554	-12.296	-10.123
Eastness	-0.634	0.128	-0.886	-0.383
Impact (75 m)	0.014	0.008	-0.001	0.029
Eastness+RDA¹_s+Impact+Slope (AIC 1506.6)				
	Estimate	S.E.	CI95.lo	CI95.hi
(Intercept)	-11.141	0.572	-12.262	-10.020
Eastness	-0.591	0.139	-0.863	-0.319
RDA1s	-0.080	0.163	-0.399	0.239
RDA1s^2	-0.260	0.142	-0.539	0.019
Impact (75 m)	0.015	0.008	0.000	0.031
Slope	-0.263	0.126	-0.510	-0.017

2011 Ovenbird PPMs: Single covariate and by-transect interaction effects (covariates in bold were also considered in multiple covariate SDMs).

RDA¹_s (AIC 1515.1)					Elevation (AIC 1514.0)				
	Estimate	S.E.	CI95.lo	CI95.hi		Estimate	S.E.	CI95.lo	CI95.hi
(Intercept)	-10.127	0.122	-10.366	-9.887	(Intercept)	-10.134	0.123	-10.376	-9.893
RDA1s	0.122	0.123	-0.119	0.363	Elevation	0.183	0.126	-0.065	0.430
RDA¹_s by transect interaction (P < 0.001)					Elevation by transect interaction (P = 0.633)				
	Estimate	S.E.	CI95.lo	CI95.hi		Estimate	S.E.	CI95.lo	CI95.hi
(Intercept)	-10.905	0.194	-11.284	-10.525	(Intercept)	-10.735	0.166	-11.060	-10.410
SR	-0.078	0.274	-0.614	0.459	SR	-0.199	0.248	-0.685	0.288
OR:RDA1s	0.607	0.182	0.249	0.964	OR:Elevation	0.128	0.169	-0.203	0.460
SR:RDA1s	-0.401	0.181	-0.755	-0.046	SR:Elevation	0.250	0.190	-0.123	0.622
RDA¹_{s+c} (AIC 1515.4)					Slope (AIC 1509.2)				
	Estimate	S.E.	CI95.lo	CI95.hi		Estimate	S.E.	CI95.lo	CI95.hi
(Intercept)	-10.125	0.122	-10.364	-9.885	(Intercept)	-10.169	0.127	-10.419	-9.920
RDA1s+c	0.103	0.124	-0.139	0.346	Slope	-0.312	0.117	-0.541	-0.083
RDA¹_{s+c} by transect interaction (P < 0.001)					Slope by transect interaction (P = 0.048)				
	Estimate	S.E.	CI95.lo	CI95.hi		Estimate	S.E.	CI95.lo	CI95.hi
(Intercept)	-10.926	0.198	-11.315	-10.537	(Intercept)	-10.869	0.185	-11.232	-10.505
SR	-0.074	0.279	-0.621	0.473	SR	-0.037	0.258	-0.543	0.469
OR:RDA1s+c	0.653	0.194	0.272	1.034	OR:Slope	-0.518	0.155	-0.822	-0.214
SR:RDA1s+c	-0.442	0.178	-0.790	-0.093	SR:Slope	-0.052	0.179	-0.402	0.298
CCA¹_c (AIC 1516.1)					Knolls (AIC 1513.3)				
	Estimate	S.E.	CI95.lo	CI95.hi		Estimate	S.E.	CI95.lo	CI95.hi
(Intercept)	-10.119	0.121	-10.357	-9.881	(Intercept)	-10.141	0.124	-10.385	-9.898
CCA1c	0.022	0.122	-0.217	0.260	Knolls	-0.222	0.138	-0.493	0.048
CCA¹_c by transect interaction (P = 0.002)					Knolls by transect interaction (P = 0.067)				
	Estimate	S.E.	CI95.lo	CI95.hi		Estimate	S.E.	CI95.lo	CI95.hi
(Intercept)	-10.824	0.174	-11.164	-10.483	(Intercept)	-10.827	0.183	-11.186	-10.468
SR	-0.136	0.263	-0.652	0.380	SR	-0.077	0.256	-0.580	0.425
OR:CCA1c	0.149	0.174	-0.193	0.491	OR:Knolls	-0.488	0.214	-0.908	-0.068
SR:CCA1c	-0.604	0.175	-0.947	-0.260	SR:Knolls	0.018	0.177	-0.330	0.365
Eastness (AIC 1504.4)					SR transect Impact (AIC N/A)				
	Estimate	S.E.	CI95.lo	CI95.hi	note: distance to impact tested at SR transect only (AIC comparison with other covariates in this table is not valid)				
(Intercept)	-10.199	0.131	-10.456	-9.942					
Eastness	-0.416	0.123	-0.657	-0.174		Estimate	S.E.	CI95.lo	CI95.hi
Eastness by transect interaction (P = 0.761)					(Intercept)	-10.157	0.230	-10.608	-9.707
	Estimate	S.E.	CI95.lo	CI95.hi	Impact	0.590	0.257	0.087	1.094
(Intercept)	-10.795	0.175	-11.138	-10.451	Impact^2	-0.318	0.189	-0.689	0.053
SR	-0.207	0.264	-0.724	0.310					
OR:Eastness	-0.382	0.166	-0.707	-0.056					
SR:Eastness	-0.457	0.183	-0.816	-0.097					
Northness (AIC 1515.6)									
	Estimate	S.E.	CI95.lo	CI95.hi					
(Intercept)	-10.123	0.122	-10.361	-9.884					
Northness	0.087	0.121	-0.150	0.325					
Northness by transect interaction (P = 0.508)									
	Estimate	S.E.	CI95.lo	CI95.hi					
(Intercept)	-10.741	0.167	-11.067	-10.414					
SR	-0.163	0.245	-0.644	0.317					
OR:Northness	0.161	0.165	-0.162	0.484					
SR:Northness	0.000	0.180	-0.352	0.352					

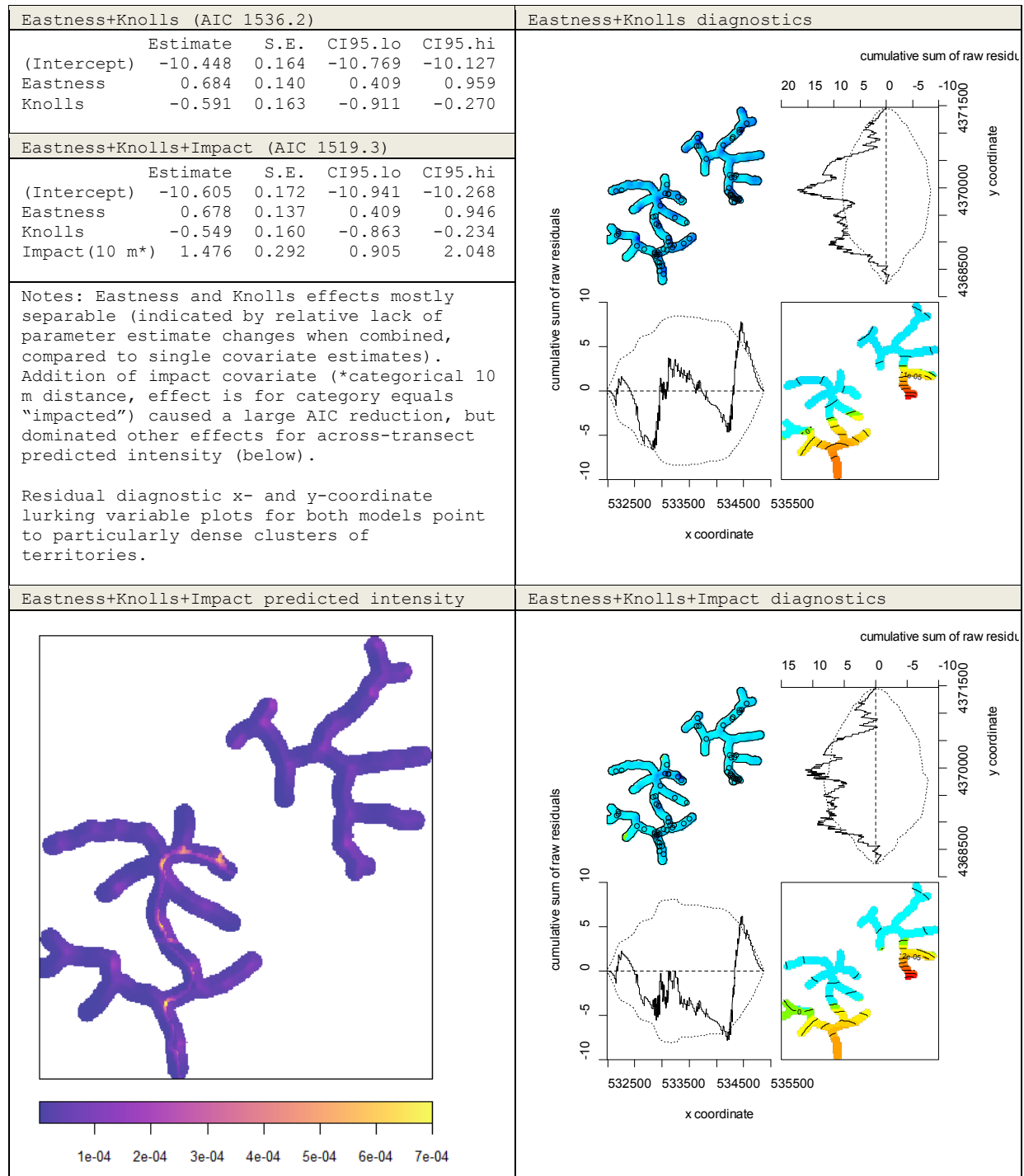
2011 Ovenbird multiple covariate PPMs.

Eastness+RDA ¹ _s (AIC 1501.7)				
	Estimate	S.E.	CI95.lo	CI95.hi
(Intercept)	-10.144	0.175	-10.488	-9.800
Eastness	-0.524	0.135	-0.788	-0.260
RDA1s	0.331	0.146	0.045	0.616
RDA1s^2	-0.110	0.126	-0.357	0.137
Notes: AIC improvement versus Eastness only model (AIC = 1510.9) when index added as a quadratic polynomial).				
Below: Including a 75 m truncated distance to impact covariate with eastness and the index improved model AIC and residual diagnostics somewhat (although the first-order index effect was reduced somewhat). While model fit was about the same when the index was removed, residual diagnostics indicated more fit issues (not shown). Topographic slope was an additional effect that further reduced model AIC, but with residual diagnostics unchanged versus the Eastness+RDA ¹ _s +Impact model (also note the additional reduction in the index effect).				
				
Eastness+RDA ¹ _s +Impact (AIC 1494.2)				
	Estimate	S.E.	CI95.lo	CI95.hi
(Intercept)	-12.173	0.907	-13.950	-10.396
Eastness	-0.494	0.136	-0.760	-0.228
RDA1s	0.229	0.146	-0.057	0.515
RDA1s^2	-0.104	0.124	-0.348	0.139
Impact (75 m)	0.029	0.012	0.005	0.053
				
Eastness+Impact (AIC 1493.9)				
	Estimate	S.E.	CI95.lo	CI95.hi
(Intercept)	-12.467	0.908	-14.246	-10.687
Eastness	-0.433	0.125	-0.679	-0.187
Impact (75 m)	0.032	0.012	0.008	0.057
				
Eastness+RDA ¹ _s +Impact+Slope (AIC 1489.2)				
	Estimate	S.E.	CI95.lo	CI95.hi
(Intercept)	-12.409	0.897	-14.166	-10.651
Eastness	-0.443	0.138	-0.714	-0.173
RDA1s	0.132	0.149	-0.161	0.424
RDA1s^2	-0.119	0.127	-0.369	0.130
Impact (75 m)	0.032	0.012	0.008	0.056
Slope	-0.339	0.127	-0.587	-0.091
				

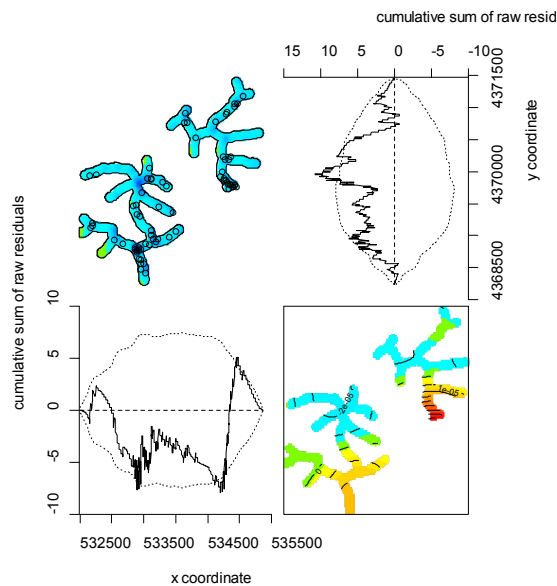
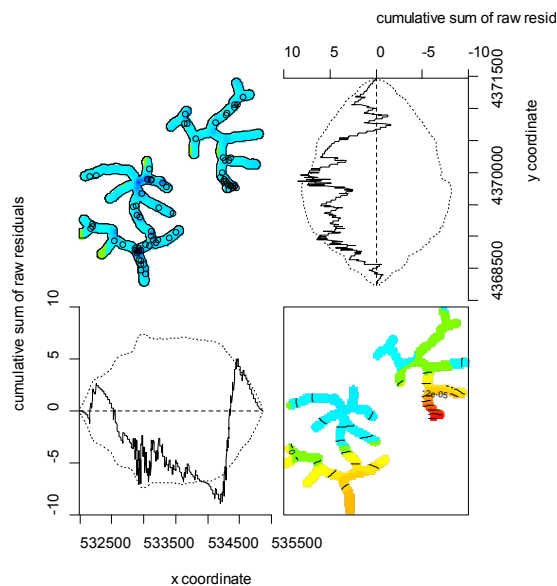
2010 Cerulean Warbler PPMs: Single covariate and by-transect interaction effects (covariates in bold were also considered in multiple covariate SDMs).

RDA ¹ _s (AIC 1576.4)					Elevation (AIC 1552.8)				
	Estimate	S.E.	CI95.lo	CI95.hi		Estimate	S.E.	CI95.lo	CI95.hi
(Intercept)	-10.078	0.119	-10.311	-9.845	(Intercept)	-10.466	0.159	-10.778	-10.155
RDA1s	0.063	0.120	-0.172	0.298	Elevation	0.416	0.098	0.224	0.609
					Elevation^2	0.246	0.055	0.139	0.354
RDA ¹ _s by transect interaction (P < 0.001)					Elevation by transect interaction (P < 0.001)				
	Estimate	S.E.	CI95.lo	CI95.hi		Estimate	S.E.	CI95.lo	CI95.hi
(Intercept)	-11.235	0.235	-11.695	-10.775	(Intercept)	-11.001	0.191	-11.375	-10.627
SR	0.575	0.286	0.014	1.135	SR	-0.063	0.293	-0.637	0.511
OR:RDA1s	0.745	0.214	0.326	1.165	OR:Elevation	-0.236	0.174	-0.578	0.105
SR:RDA1s	-0.352	0.155	-0.655	-0.049	SR:Elevation	1.036	0.190	0.664	1.409
RDA ¹ _{s+c} (AIC 1575.9)					Slope (AIC 1560.1)				
	Estimate	S.E.	CI95.lo	CI95.hi		Estimate	S.E.	CI95.lo	CI95.hi
(Intercept)	-10.082	0.120	-10.316	-9.848	(Intercept)	-10.189	0.131	-10.446	-9.932
RDA1s+c	0.110	0.121	-0.128	0.348	Slope	-0.468	0.113	-0.690	-0.247
RDA ¹ _{s+c} by transect interaction (P < 0.001)					Slope by transect interaction (P = 0.027)				
	Estimate	S.E.	CI95.lo	CI95.hi		Estimate	S.E.	CI95.lo	CI95.hi
(Intercept)	-11.194	0.229	-11.642	-10.745	(Intercept)	-11.278	0.234	-11.737	-10.819
SR	0.570	0.278	0.025	1.115	SR	0.644	0.283	0.089	1.200
OR:RDA1s+c	0.693	0.224	0.255	1.132	OR:Slope	-0.763	0.173	-1.103	-0.423
SR:RDA1s+c	-0.223	0.152	-0.521	0.075	SR:Slope	-0.256	0.150	-0.550	0.039
CCA ¹ _c (AIC 1575.9)					Knolls (AIC 1561.1)				
	Estimate	S.E.	CI95.lo	CI95.hi		Estimate	S.E.	CI95.lo	CI95.hi
(Intercept)	-10.082	0.120	-10.316	-9.848	(Intercept)	-10.211	0.137	-10.480	-9.943
CCA1c	0.107	0.120	-0.129	0.343	Knolls	-0.578	0.161	-0.894	-0.262
CCA ¹ _c by transect interaction (P = 0.309)					Knolls by transect interaction (P = 0.403)				
	Estimate	S.E.	CI95.lo	CI95.hi		Estimate	S.E.	CI95.lo	CI95.hi
(Intercept)	-11.006	0.192	-11.383	-10.629	(Intercept)	-11.188	0.232	-11.642	-10.734
SR	0.405	0.247	-0.078	0.888	SR	0.493	0.288	-0.071	1.057
OR:CCA1c	0.257	0.192	-0.119	0.633	OR:Knolls	-0.751	0.271	-1.282	-0.220
SR:CCA1c	0.007	0.155	-0.297	0.311	SR:Knolls	-0.472	0.200	-0.864	-0.080
Eastness (AIC 1550.3)					SR transect Impact (AIC N/A)				
	Estimate	S.E.	CI95.lo	CI95.hi	note: distance to impact tested at SR transect only (AIC comparison with other covariates in this table is not valid)				
(Intercept)	-10.294	0.145	-10.579	-10.010					
Eastness	0.658	0.136	0.392	0.925					
Eastness by transect interaction (P = 0.907)						Estimate	S.E.	CI95.lo	CI95.hi
	Estimate	S.E.	CI95.lo	CI95.hi	(Intercept)	-11.503	0.434	-12.354	-10.652
(Intercept)	-11.202	0.230	-11.652	-10.752	Impact	0.229	0.423	-0.601	1.058
SR	0.390	0.296	-0.191	0.971	Impact^2	1.638	0.430	0.795	2.481
OR:Eastness	0.678	0.214	0.258	1.098	Impact^3	-0.753	0.268	-1.279	-0.227
SR:Eastness	0.645	0.176	0.300	0.991					
Northness (AIC 1571.4)									
	Estimate	S.E.	CI95.lo	CI95.hi					
(Intercept)	-9.779	0.165	-10.102	-9.457					
Northness	-0.159	0.139	-0.433	0.114					
Northness^2	-0.354	0.152	-0.653	-0.055					
Northness by transect interaction (P = 0.103)									
	Estimate	S.E.	CI95.lo	CI95.hi					
(Intercept)	-11.040	0.199	-11.430	-10.651					
SR	0.440	0.252	-0.054	0.933					
OR:Northness	-0.378	0.196	-0.762	0.005					
SR:Northness	0.024	0.154	-0.278	0.326					

2010 Cerulean Warbler multiple covariate PPMs.



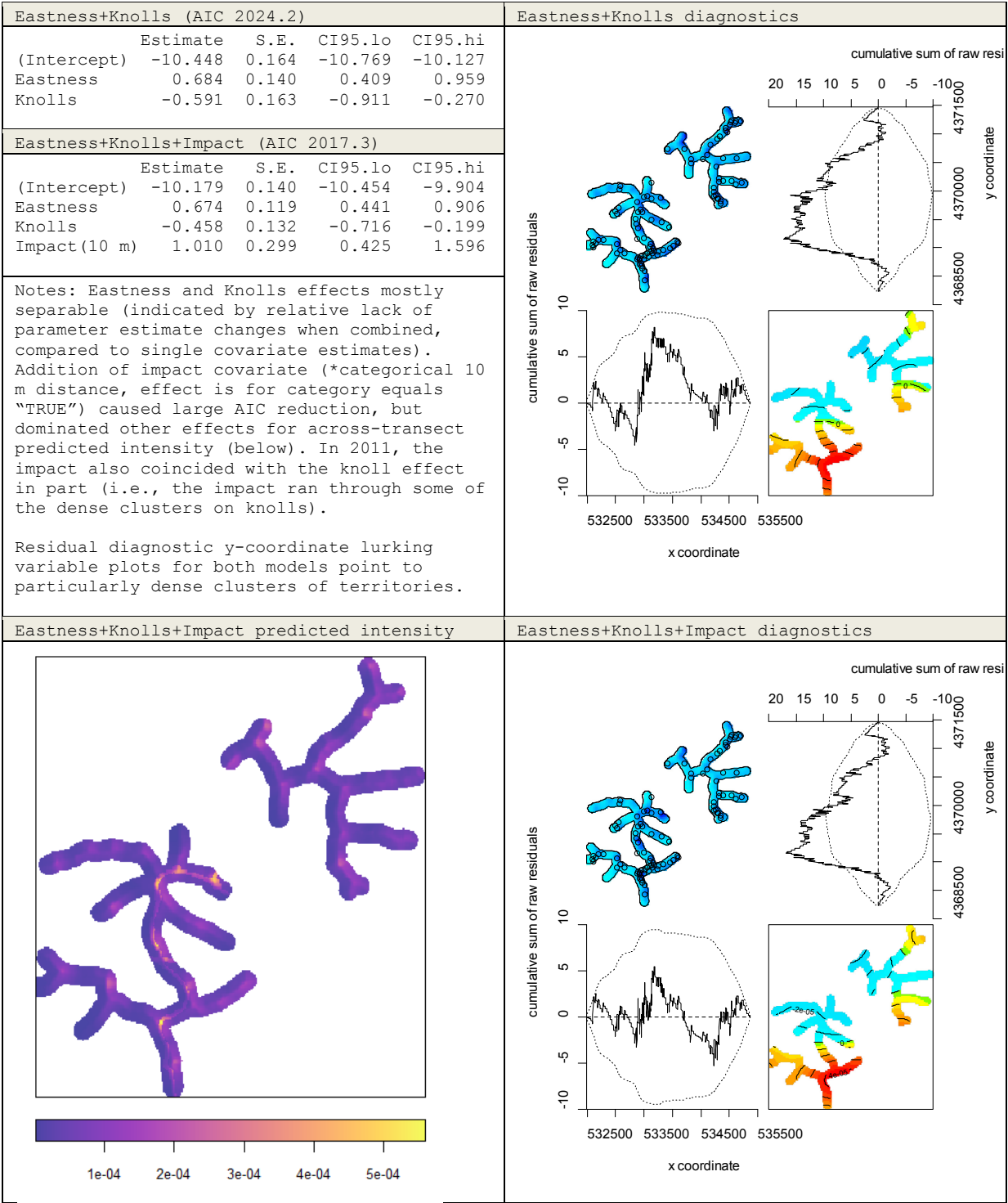
2010 Cerulean Warbler multiple covariate PPMs (additional).

Eastness+Knolls+Elevation (AIC 1518.8)					Eastness+Knolls+Elevation diagnostics				
	Estimate	S.E.	CI95.lo	CI95.hi					
(Intercept)	-10.772	0.193	-11.149	-10.394					
Eastness	0.689	0.141	0.412	0.965					
Knolls	-0.433	0.171	-0.770	-0.097					
Elevation	0.278	0.116	0.050	0.506					
Elevation^2	0.242	0.058	0.129	0.355					
Notes: Elevation and Knoll distance effects related (indicated by parameter estimate changes when combined, compared to single covariate estimates). Model fit issues likely caused by the dense clusters remained.									
Eastness+Knolls+Elevation+Impact (AIC 1513.8)					Eastness+Knolls+Elevation+Impact diagnostics				
	Estimate	S.E.	CI95.lo	CI95.hi					
(Intercept)	-10.820	0.192	-11.197	-10.443					
Eastness	0.673	0.139	0.401	0.946					
Knolls	-0.456	0.171	-0.791	-0.120					
Elevation	0.150	0.124	-0.092	0.393					
Elevation^2	0.199	0.061	0.079	0.319					
Impact(10 m)	1.160	0.326	0.520	1.800					
Notes: Elevation effect further reduced but knoll effect somewhat strengthened by addition of impact covariate. Model fit issues likely caused by the dense clusters remained.									

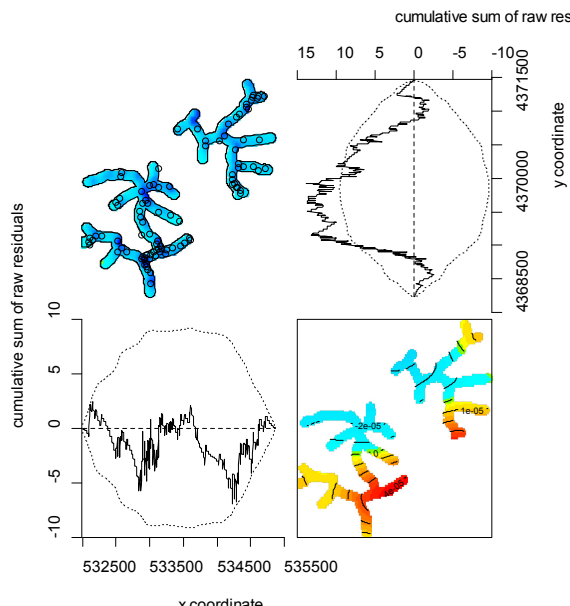
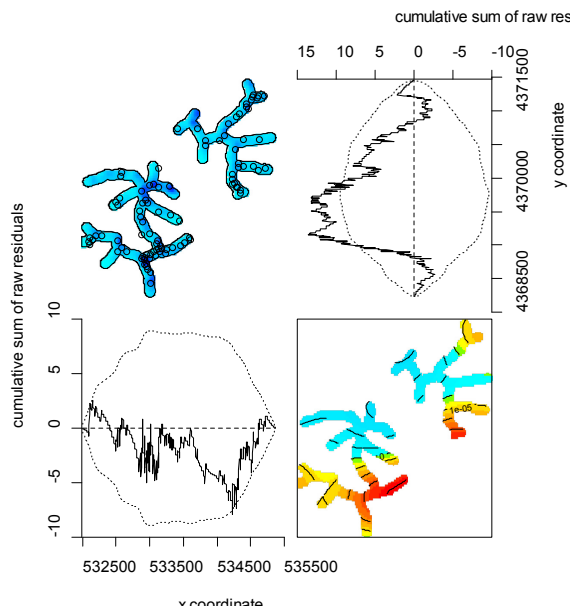
2011 Cerulean Warbler PPMs: Single covariate and by-transect interaction effects (covariates in bold were also considered in multiple covariate SDMs).

RDA ¹ _s (AIC 2072.1)					Elevation (AIC 2055.2)				
	Estimate	S.E.	CI95.lo	CI95.hi		Estimate	S.E.	CI95.lo	CI95.hi
(Intercept)	-9.777	0.102	-9.977	-9.576	(Intercept)	-9.869	0.112	-10.088	-9.649
RDA1s	0.071	0.103	-0.130	0.272	Elevation	0.455	0.113	0.233	0.676
RDA ¹ _s by transect interaction (P < 0.001)					Elevation by transect interaction (P = 0.010)				
	Estimate	S.E.	CI95.lo	CI95.hi		Estimate	S.E.	CI95.lo	CI95.hi
(Intercept)	-11.402	0.271	-11.934	-10.870	(Intercept)	-10.787	0.170	-11.120	-10.454
SR	1.083	0.305	0.485	1.682	SR	0.349	0.230	-0.102	0.799
OR:RDA1s	1.171	0.221	0.739	1.603	OR:Elevation	0.098	0.173	-0.240	0.436
SR:RDA1s	-0.434	0.129	-0.686	-0.181	SR:Elevation	0.686	0.148	0.396	0.977
RDA ¹ _{s+c} (AIC 2071.0)					Slope (AIC 2065.4)				
	Estimate	S.E.	CI95.lo	CI95.hi		Estimate	S.E.	CI95.lo	CI95.hi
(Intercept)	-9.783	0.103	-9.985	-9.581	(Intercept)	-9.811	0.106	-10.018	-9.603
RDA1s+c	0.128	0.104	-0.077	0.332	Slope	-0.267	0.099	-0.461	-0.074
RDA ¹ _{s+c} by transect interaction (P < 0.001)					Slope by transect interaction (P = 0.007)				
	Estimate	S.E.	CI95.lo	CI95.hi		Estimate	S.E.	CI95.lo	CI95.hi
(Intercept)	-11.454	0.285	-12.013	-10.895	(Intercept)	-10.980	0.198	-11.369	-10.591
SR	1.176	0.315	0.558	1.794	SR	0.751	0.236	0.287	1.214
OR:RDA1s+c	1.263	0.245	0.782	1.743	OR:Slope	-0.611	0.158	-0.920	-0.301
SR:RDA1s+c	-0.325	0.126	-0.572	-0.079	SR:Slope	-0.058	0.127	-0.307	0.192
CCA ¹ _c (AIC 2070.4)					Knolls (AIC 2057.7)				
	Estimate	S.E.	CI95.lo	CI95.hi		Estimate	S.E.	CI95.lo	CI95.hi
(Intercept)	-9.787	0.103	-9.989	-9.584	(Intercept)	-9.866	0.113	-10.087	-9.645
CCA1c	0.152	0.104	-0.051	0.355	Knolls	-0.469	0.132	-0.728	-0.210
CCA ¹ _c by transect interaction (P < 0.001)					Knolls by transect interaction (P = 0.295)				
	Estimate	S.E.	CI95.lo	CI95.hi		Estimate	S.E.	CI95.lo	CI95.hi
(Intercept)	-11.039	0.211	-11.453	-10.625	(Intercept)	-10.958	0.203	-11.355	-10.560
SR	0.803	0.248	0.318	1.289	SR	0.671	0.245	0.191	1.150
OR:CCA1c	0.726	0.189	0.355	1.098	OR:Knolls	-0.666	0.238	-1.133	-0.198
SR:CCA1c	-0.143	0.128	-0.393	0.108	SR:Knolls	-0.370	0.158	-0.680	-0.061
Eastness (AIC 2037.5)					SR transect Impact (AIC N/A)				
	Estimate	S.E.	CI95.lo	CI95.hi	note: distance to impact tested at SR transect only (AIC comparison with other covariates in this table is not valid)				
(Intercept)	-9.990	0.125	-10.234	-9.746					
Eastness	0.653	0.117	0.424	0.883					
Eastness by transect interaction (P = 0.169)						Estimate	S.E.	CI95.lo	CI95.hi
	Estimate	S.E.	CI95.lo	CI95.hi	(Intercept)	-10.287	0.274	-10.824	-9.749
(Intercept)	-11.156	0.234	-11.613	-10.698	Impact	0.120	0.306	-0.479	0.719
SR	0.778	0.276	0.237	1.320	Impact^2	0.786	0.306	0.186	1.387
OR:Eastness	0.880	0.209	0.470	1.290	Impact^3	-0.397	0.191	-0.771	-0.022
SR:Eastness	0.537	0.142	0.259	0.815					
Northness (AIC 2072.3)									
	Estimate	S.E.	CI95.lo	CI95.hi					
(Intercept)	-9.775	0.102	-9.975	-9.575					
Northness	0.052	0.102	-0.147	0.252					
Northness by transect interaction (P = 0.422)									
	Estimate	S.E.	CI95.lo	CI95.hi					
(Intercept)	-10.784	0.169	-11.116	-10.452					
SR	0.550	0.213	0.133	0.967					
OR:Northness	-0.056	0.169	-0.387	0.276					
SR:Northness	0.114	0.128	-0.136	0.365					

2011 Cerulean Warbler multiple covariate PPMs.



2011 Cerulean Warbler multiple covariate PPMs (additional).

Eastness+Knolls+Elevation (AIC 2016.4)					Eastness+Knolls+Elevation diagnostics				
	Estimate	S.E.	CI95.lo	CI95.hi					
(Intercept)	-10.137	0.138	-10.407	-9.867					
Eastness	0.683	0.118	0.451	0.915					
Knolls	-0.301	0.143	-0.582	-0.021					
Elevation	0.368	0.122	0.130	0.607					
Notes: Elevation and Knoll distance effects related (indicated by parameter estimate changes when combined, compared to single covariate estimates). Model fit issues likely caused by the dense clusters remained.									
Eastness+Knolls+Elevation+Impact (AIC 2012.9)					Eastness+Knolls+Elevation+Impact diagnostics				
	Estimate	S.E.	CI95.lo	CI95.hi					
(Intercept)	-10.192	0.141	-10.468	-9.916					
Eastness	0.682	0.118	0.451	0.912					
Knolls	-0.315	0.143	-0.595	-0.035					
Elevation	0.300	0.123	0.059	0.542					
Impact(10 m)	0.789	0.311	0.178	1.399					
Notes: Elevation effect further reduced but knoll effect somewhat strengthened by addition of impact covariate. Model fit issues likely caused by the dense clusters remained.									

CHAPTER 4: Modeling the distributions of three Appalachian deciduous forest songbirds as point patterns using fine-scale remote sensing data.

ABSTRACT

Fine-scale spatial patterns in the distributions of breeding territorial songbird species should provide valuable information on the processes involved in their habitat selection. In dense forests, however, collecting location data on these visually cryptic species is challenging. Fortunately, the singing males of these species can provide abundant, albeit often estimated, acoustic location data. Advances in species distribution modeling techniques suggest that these data can be analyzed as spatial point processes. We mapped Cerulean Warbler (*Setophaga cerulea*), Hooded Warbler (*Setophaga citrina*), and Ovenbird (*Seiurus aurocapilla*) singing males as point patterns over three periods of the breeding season on ridgetops in a mature Appalachian deciduous forest in WV, USA. We used point process models (PPMs) that incorporated fine-scale remote sensing data to examine environmental factors underlying these point patterns, as well as intraspecific spacing behavior over a distance of 0–300 m. All three species' patterns exhibited short-distance regularity (likely indicative of competition for territorial space), which we accounted for in hard core interaction PPMs. We detected significant ($p < 0.05$) clustering in the patterns beyond the hard core distances for all three species based on evaluating the L -function (a linearized form of Ripley's K -function) in Monte Carlo simulation envelope tests. Based on evaluating an inhomogeneous version of the L -function in these tests, remotely-sensed environmental covariates included in the PPMs fully explained the clustering in the Hooded Warbler and Ovenbird, but only partially in the Cerulean Warbler. Including inter-point attraction effects in hybrid interaction (hard core-Geyer saturation) PPMs accounted for the

remaining Cerulean Warbler clustering, supporting conspecific attraction as an effect on its distribution. Overall, the PPMs likely produced more realistic environmental parameter estimates when inter-point interaction effects were included, and suggested considerable divergence among the species in their fine-scale habitat use and spacing behavior.

Keywords: Forest birds, remote sensing, spatial point process models, spacing behavior, species distribution models

INTRODUCTION

How species are spatially distributed in relation to the environment is a long-standing and fundamental question in ecology (Sutherland 2013). Species distribution models use a wide variety of statistical techniques to combine species location data with environmental data for purposes including ecological insight and predicting species distributions in space and time (Elith and Leathwick 2009). Increasingly refined distribution models may now be possible because of new, spatially-continuous environmental predictor variables derived from remote sensing data (He et al. 2015). For example, these new sources of environmental information allow models to be of increasingly higher spatial resolution over larger areas (Velázquez et al. 2016). Among the statistical developments, the use of point process models (PPMs) as species distribution models has received much attention (reviewed in Renner et al. 2015). These models treat the locations of a species as a point pattern that is the realization of a spatial point process, and can test how environmental factors as well as interactions between the points (attraction and repulsion) or other spatial processes (e.g., dispersal limitation: Lin et al. 2011) are involved in their distribution.

Many different kinds of distribution data have been used in species distribution models, which in turn have been applied to diverse taxa. Distribution data as point patterns are often comprised of the locations of fixed objects in space such as the trees in a forest (Lin et al. 2011) or the nests of birds (Gießelmann et al. 2008) or ants (Li et al. 2016); but also can be snapshots of the locations of moving organisms such as whales (Waagepetersen and Schweder 2006) and wild ungulates (Hibert et al. 2010). While the objects themselves may be idealized as infinitesimal points in PPMs (for an exception, see Wiegand et al. 2006), in reality this is often false (e.g., a tree has a crown). However, by making the spatial scale of the investigation

sufficiently large relative to the size of the objects, they can be considered approximately point-like (Baddeley et al. 2015) and valid inference can be achieved. As extreme examples, abiotic events occurring over relatively large areas such as fires and earthquakes have been analyzed using PPMs (Liu et al. 2012, Van Lieshout and Stein 2012).

Environmental data are usually incorporated in PPMs as continuous spatial grids, which provide the data values for both the observed (i.e., presence) points and some (usually large) number of background points within the observation window where the object of interest was not observed. These background points may represent true absences, perhaps obtained from a completely mapped pattern assuming sufficient positional accuracy and detection probability, but often this is not possible. Much of the motivation for using PPMs as species distribution models (e.g., see Warton and Shepard 2010) was to overcome the perceived limitations of other techniques for modeling presence-only data, which may be the only location data available (e.g., museum voucher specimens; Fithian et al. 2015). For presence-only data, the background points in a PPM make the analysis essentially similar to a habitat use-availability analysis (Aarts et al. 2012), and with a large enough number of background points PPMs can closely approximate other commonly used species distribution modeling techniques such as spatial logistic regression and Maxent (Baddeley et al. 2010, Fithian and Hastie 2013). Spatial autocorrelation (i.e., non-independence) in species distribution data is frequent and can strongly bias model coefficients (Dormann et al. 2007), and PPMs by incorporating inter-point interactions can account for spatial autocorrelation and thus allow valid model inferences to be made (Renner et al. 2015).

For this study, we analyzed the estimated locations of singing males of three species of territorial songbirds as point patterns on ridgetops in a mature Appalachian deciduous forest. The patterns encompassed a high degree of topographic complexity over short distances, and forest

that varied in structure, composition, and the presence of recent anthropogenic disturbances. The species, Cerulean Warbler (*Setophaga cerulea*), Hooded Warbler (*Setophaga citrina*), and Ovenbird (*Seiurus aurocapilla*), were among the most abundant breeding passerines in this forest, and have contrasting habitat preferences (e.g., for amount of canopy closure; Sheehan et al. 2014) that would likely promote differences in their spatial distributions. We used PPMs to test, within three periods of the breeding season, how the point patterns of these species were influenced by the environmental heterogeneity in terrain and forest characteristics and examined the patterns for evidence of territorial spacing behavior. We incorporated fine scale environmental heterogeneity in the PPMs through the use of remote sensing data with a high spatial resolution: terrain variables obtained from a 3-m resolution digital elevation model (DEM) and a mapped index of forest structural complexity based on a 0.6-m resolution QuickBird satellite image (Chapter 3).

In a seminal study, Sherry and Holmes (1985) performed a quadrat-based spatial analysis of the distributions of seven abundant breeding songbird species in what appeared to be a mostly homogenous northern hardwood forest. They found that the species exhibited a range of dispersion patterns, from the Least Flycatcher (*Empidonax minimus*) with a highly clumped distribution to several species (the Ovenbird among them) that were more evenly distributed. Sherry and Holmes (1985) used the territory mapping method (Bibby et al. 2000) to draw territories around clusters of singing males of these species recorded over a number of survey dates (thus likely representing relatively stable territories), and then obtained the territory centers for their analysis (as we did in Chapter 3). While territory mapping is of value for this and other purposes (e.g., the analysis of species densities rather than relative abundances; Newell et al. 2013), the drawing of territories does require additional subjectivity on the part of the analyst. It

may be useful, therefore, if spatial analyses could rely on the individual bird locations obtained by the method (perhaps even from single visits without the greater effort involved in territory mapping). In our present study, one of our goals was to contrast the spacing of individual Cerulean Warblers, Hooded Warblers and Ovenbirds, as Cerulean Warbler territories appeared to be more strongly clustered (Chapter 3) and there is evidence for its clustered territoriality elsewhere (Roth and Islam 2007, Barnes et al. 2016). Finding a similar range in the dispersion patterns of the species we studied as that found by Sherry and Holmes (1985) thus may help confirm the singing male locations themselves as a viable level for spatial analysis.

While our singing male point patterns were subject to sampling error (e.g., in the positional accuracy of the estimated locations) and factors influencing detection probability (e.g., males present but not singing; Farnsworth et al. 2002), we believed them to still be valuable for understanding spatial point processes influencing where these species place their breeding territories in this forest. For our first objective, despite the data issues we expected that PPMs containing inter-point interaction effects would help control for spatial autocorrelation and provide more realistic parameter estimates for environmental effects. For our second objective, we assumed that over the relatively short distance we focused on (0–300 m), the point patterns were complete and accurate enough for an investigation of territorial spacing behavior that otherwise would be difficult to achieve over the spatial extent we wished to cover. Controlling for environmental heterogeneity in the PPMs allowed us to assess the likelihood that interactions between individuals were involved in the spatial patterns we observed. Acoustic signaling is a potentially rich data source on fine-scale space use by forest songbirds that is relatively easy and inexpensive to collect. We wish to promote its use in spatially-explicit analyses, given careful consideration of likely data limitations.

METHODS

Study Site

This study was conducted in 2011 on ridgetops in the Lewis Wetzel Wildlife Management Area, in northwestern West Virginia, USA (39.5012°N, 80.6490°W; Figure 1). The site is in the Permian Hills region of the Western Allegheny Plateau, and represents the highly dissected topography and dense deciduous forest cover characteristic of the region (Woods et al. 1999). In 2011, the site was ~93% mature second-growth forest (Farwell et al. 2016), with the remaining area comprised of a variety of anthropogenic forest impacts, including timber harvests, forest roads and pipelines, natural gas and oil well pads, and small clearings managed for wildlife. Elevation of the studied ridgetops was 221–480 m (mean 356 m) above sea level. Major tree species on the ridgetops included chestnut oak (*Quercus montana*), sugar maple (*Acer saccharum*), northern red oak (*Q. rubra*), red maple (*A. rubrum*), hickories (*Carya* spp.), black oak (*Q. velutina*), white oak (*Q. alba*), and black locust (*Robinia pseudoacacia*) (see Chapter 2 for additional site details).

Field Data Collection

Six ridgetop transects, totaling 28 km in length, were established for mapping the singing males of the three bird species (Figure 1). Each transect was a network of primary and secondary ridge centerlines obtained by hydrological modeling of the DEM. The transects were placed to cover the range of ridgetop forest habitat conditions and topographic diversity existing at the site, given logistical constraints (ease of access and efficient travel routes). Each transect contained locally high and low elevations (knolls and saddles) and a variety of ridge orientations. One transect (OR) was located completely within mature forest, with no obvious signs of human disturbance.

The other five transects included some recent anthropogenic disturbances (see details in the Appendix Figure 6), but overall were located primarily within mature forest.

The transects were surveyed by J.S. over three replicate sampling bouts in May and June, 2011, to approximately coincide with the early (mean day = 5/8; range: 5/5–5/12), mid (mean day = 5/25; range: 5/19–5/31), and late (mean day = 6/10; range: 6/1–6/20) periods of the peak breeding season for these species based on overall seasonal trends in their singing activity, and prior bird survey work conducted at this site (included in Sheehan et al. 2014, Farwell et al. 2016). Within a bout, each transect's survey was completed over 1–3 days, depending on the transect length that could be covered during the peak daily period of singing activity (0–4 hrs after local sunrise). Surveys were conducted only during optimal conditions for bird activity (calm winds, no precipitation or heavy fog). During a survey, the transect was walked at a slow, regular pace (~1–2 km per hr), with short (<5 min) pauses as necessary to aurally estimate the locations of the singing males and record them on detailed field maps (1:5,000 scale). The maps included the transect ridgelines with points placed at 50 m intervals. A Garmin 60CSX Geographic Positioning System unit (WAAS-enabled ± 5 –10 m positional accuracy) containing these points was used to ensure accurate positioning for estimating the singing locations.

Because of transect side branches and multiple-day surveys, topographic features (e.g., ridgeline intersections and prominent knolls) were used to perform the surveys in segments to which even survey effort was applied. When starting a new segment, the previous map was examined to avoid double-recording the same individual. Determining new individuals was also assisted by the frequent, simultaneous location of conspecifics (males of all three species regularly countersinging). In the absence of countersinging, new individuals were not used if they were within 50 m (for Cerulean and Hooded Warblers) or 100 m (for Ovenbirds; generally

spaced further apart) of a previously mapped individual. A singing male was recorded as soon as possible after it was first heard and its location could be estimated, with adjustments for better accuracy when possible for individuals that continued to vocalize and did not appear to move. Lines were drawn on the maps to denote countersinging and individual movements. All individuals estimated to be within 100 m to either side of the transect were recorded. The completed maps were scanned and then georeferenced (UTM NAD 83, Zone 17 N) and manually digitized in ArcGIS 10.1 (Environmental Systems Research Institute, Redlands, CA, USA) to obtain the coordinates of the singing males.

Analyses

The PPMs were conducted using the spatstat 1.46-1 package (Baddeley et al. 2015) in R 3.3.1 (R Core Team 2016). The polygon observation window containing the singing male locations (the point patterns) was the combined area of the six transects buffered at 85 m (Figure 1), which encompassed >95% of the singing males (by species per bout). We used 85 m instead of the 100 m maximum recording distance to help ensure that the most distant males, which were more difficult to place accurately, were in fact present within the observation window boundary. We combined the transects rather than analyze them separately or use spatially replicated models (see chapter 16 in Baddeley et al. 2015) to increase sample sizes and to more easily include both broad- and fine-scale spatial trends in the models. We considered the sampling bouts as providing three separate snapshots of singing activity over the course of the breeding season, which we examined for potential changes. For example, the early bout likely encompassed initial settlement patterns caused by variation in arrival dates, while the late bout likely encompassed post-breeding singing activity (which also could vary temporally; e.g., by species). Aside from our interest in the potential changes, three separate analyses also allowed us to assess the results

for stability. Finding consistent spacing within the species across the sampling bouts, for instance, would help support the general applicability of analyzing these data as point patterns.

Point pattern analysis background. A point pattern exists within a defined region and may exhibit first-order effects, which manifest as spatial variation in point density (often termed ‘intensity’) and second-order effects, which are interactions (e.g., attraction or repulsion) between the points (Diggle 2003). The simplest spatial point process is the homogenous Poisson process, in which the points exhibit ‘complete spatial randomness’ (CSR). CSR is defined as a constant point intensity across the region and no interactions between the points (Diggle 2003). In contrast, a spatial point process often considered for species distribution models is the inhomogeneous Poisson process (Renner et al. 2015). In this process, the points do not interact, but their intensity varies spatially in relation to environmental heterogeneity (e.g., in soils, elevation). This intensity can be estimated from the point pattern itself, through the use of parametric (e.g., functions of Cartesian coordinates; Diggle 2003) and non-parametric (e.g., kernel density estimation; Baddeley et al. 2000) techniques. These techniques are often used to control heterogeneity as a nuisance effect, with the primary purpose being to assess the pattern for second-order effects. Alternatively, as in our study, environmental data can be obtained to model heterogeneity directly, which can be useful for also gaining insight into environmental effects on the patterns (e.g., see Li et al. 2016).

Testing whether an observed point pattern is explained by a particular spatial point process can be done by considering the process as the null model, and comparing spatial properties obtained from the observed point pattern to the same properties obtained from point patterns that are Monte Carlo-based simulated realizations of the null model (Law et al. 2009). For example, a distance-based summary function such as the Ripley’s K -function (Ripley 1976) can be

calculated from the simulated patterns to obtain the upper and lower bounds of a graphical envelope representing the null model, to compare to the same function graphed for the observed point pattern. Ripley's- K function calculates the average number of neighboring points within circles of increasing radii around the points of the pattern, to provide an assessment of their spatial randomness, clustering, or regularity. With a homogeneous Poisson process as the null model, a departure from CSR is indicated if, along the x-axis of the distance range the K -function is calculated for, the observed function wanders outside the simulation envelope. Where the function is above or below the envelope suggests spatial clustering or regularity; respectively, in the points, at a statistical significance level that is based on the number of simulations.

In the case of an inhomogeneous Poisson process as the null model, there are inhomogeneous versions of summary functions (e.g., the inhomogeneous K -function; Baddeley et al. 2000) that employ the techniques described above to control for heterogeneity in assessing the spatial properties of the point pattern. In addition to incorporating heterogeneity, null models can be made considerably more complex by specifying the type of interaction between the points. We used Gibbs processes (Møller and Waagepetersen 2007) for flexibility in specifying the types of interactions for our models. Gibbs processes are commonly used to model repulsion but can also model moderately strong clustering (Baddeley et al. 2015). We were specifically interested in considering hybrid models that combine Gibbs processes, as these models are useful when interactions occur at different spatial scales (Baddeley et al. 2013).

Assessing and controlling for first-order intensity trends in spatstat PPMs involves the use of quadrature points. These points provide background values for an environmental covariate over the sampling window to compare with the covariate values obtained for the observed point pattern. To accurately estimate the background, it is important that the number of quadrature

points be sufficiently large (Renner et al. 2015), and it is also important that the spatial resolution of the covariate be sufficiently fine so that individual points of the observed pattern do not share the same pixel (Aarts et al. 2012). For modeling second-order interaction effects, it is also often important to use some kind of edge correction, particularly when the pattern is contained within a complex observation window. Summary functions such as Ripley's- K are influenced by points having fewer neighbors for estimating the function because they are nearer to the edge, but the pattern actually occurs within some larger unbounded region (Perry et al. 2006). Which particular edge correction method to use is often less important than the use of one (Baddeley et al. 2015), and edge correction is particularly important when the purpose, as in our study, is to parameterize a specific point process model (Yamada and Rogerson 2003).

Environmental covariates. The remote sensing data layers used as covariates for environmental heterogeneity in the PPMs were based on preliminary modeling of the species' mapped territories (as opposed to individual singing male locations) on two of the transects over two breeding seasons (SR and OR in 2010 and 2011; Chapter 3). We used the ArcGIS zonal statistics function to spatially smooth the layers processed from the 3-m DEM (± 3 m vertical accuracy; source: <http://viewer.nationalmap.gov/>) to reduce the potential for the high resolution of the DEM to result in too much detail in the topographic covariates and a subsequent loss of explanatory power (Cavazzi et al. 2013). To represent topographic variation, we applied a 15-m focal mean to the sine (east–west) and cosine (north–south) linear derivations of 0–360° topographic aspect. This amount of smoothing preserved the diversity of topographic aspects possible on the ridges, which in the preliminary models was a dominant factor influencing the local (i.e., within-ridge) spatial distributions of these species (notably, east-facing aspects for the Cerulean and Hooded Warbler and west-facing aspects for the Ovenbird). To more generally

represent elevation gradients across the transects, we applied a 100 m focal mean to the DEM elevation values. Specifically for the Cerulean Warbler, we calculated a continuous distance grid from the tops of obvious knolls, obtained as point features through 3-dimensional modeling of the DEM and verified in the field.

The mapped index of forest structural complexity (RDAs) was obtained from a redundancy analysis of field-collected forest structure data using the panchromatic band from a QuickBird 2 (DigitalGlobe, Westminster, CO, USA) satellite image and the DEM, as fully described in Chapter 3. In brief here, RDAs was mainly comprised of a linear combination of several image variables, the strongest being a fine scale measure of image texture (the 0.6 m pixel standard deviation). RDAs indicated structural complexity that was primarily related to forest canopy openness, with a more closed forest canopy associated with greater tree basal area and a more open forest canopy associated with greater herbaceous understory cover and grapevine (*Vitis* spp.) density. RDAs was also correlated (Spearman's $\rho = 0.71$) with another multivariate analysis-derived index based on tree composition data, suggesting that this structural complexity was also related to a chestnut oak (a more closed forest canopy) to sugar maple (a more open forest canopy) dominance gradient. We selected RDAs over the composition index because forest structure was more predictable based on external cross-validation, and RDAs more strongly modeled the Hooded Warbler, the species most directly linked to the presence of canopy gaps with well-developed understories in this forest. We applied a 15-m standard deviation Gaussian filter to RDAs (using the spatstat *blur* function) based on preliminary testing that indicated this amount of smoothing preserved the spatial patterns in the index and maximized how strongly it could model the species (Chapter 3).

Recent anthropogenic disturbances (all types combined) were represented by an impacted forest categorical covariate, with impacted forest defined as that existing ≤ 100 m from forest disturbance edges (hand-digitized in ArcGIS) which also incorporated the timber harvest areas. We selected this edge effect distance because it is often used in studies of the effects of anthropogenic forest disturbances on birds, including at this site (Farwell et al. 2016). While distance to edge itself was potentially interesting as a fine scale effect, directly modeling this across the combined transect extent was complicated because the disturbances were localized to five of the six transects. The majority of disturbances were narrow (roads and pipelines) or small in size (well pads and wildlife clearings), so we assumed that these disturbances caused similar, primarily habitat edge-related effects on these forest bird species. The potential effects of timber harvests likely differed because they could also contain the species in the habitat within their boundaries. However, we relied on the impacted forest covariate to also account for any effects from these somewhat larger but still isolated areas, rather than additionally represent them.

Modeling procedure. Because the point patterns of each species clearly exhibited spatial regularity over the shortest inter-point distances that was consistent with territorial male spacing behavior, we first fit PPMs to each species in each sampling bout that included a simple hard core interaction (we subsequently refer to these as hard core models). With a hard core model as the null model, the points in the pattern cannot be closer than the hard core interaction distance, but at larger distances they do not interact (Baddeley et al. 2015). The hard core interaction distances were the species-specific minimum inter-point distances observed within the survey bouts. We fit both homogeneous hard core models (assuming no environmental heterogeneity) and inhomogeneous hard core models that contained environmental covariates to the patterns. Although a homogeneous hard core process was a priori likely false as a null model given the

species' different habitat preferences, these models provided a valuable initial assessment of the spatial properties of the patterns for guiding subsequent modeling (Baddeley et al. 2015).

Particularly, we assessed whether apparent deviations from the homogenous hard core models were controlled through the use of environmental covariates in the inhomogeneous hard core models. Finding evidence against such control subsequently led us to test PPMs containing hybrid interactions (described below) to further determine the species' spacing patterns.

For the simulation envelope-based testing to evaluate the goodness of fit of the PPMs, we used the rank envelope test available in the `spptest` 0.04 R package (Myllymäki et al. 2016). This is a global envelope test, in that it avoids an inflated statistical Type I error rate caused by the problem of multiple testing of distances over which the function may deviate from the envelope. The test further provides a p -value interval for the observed function, with clear evidence for rejecting the null model if the upper p -value is below the specified significance level (we used $\alpha = 0.05$) and some evidence for rejecting the null model if the specified significance level is between the upper and lower p -value (Myllymäki et al. 2016). Low point sample sizes appeared to be the cause of simulation issues for the Ovenbird, which we solved by excluding the transect (DR) with the fewest points from its analysis.

We assessed the properties of the L -function (Besag 1977) and an inhomogeneous version of the L -function (Baddeley et al. 2000), both available in `spatstat`, with the rank envelope tests. The L -function is a linear transformation of Ripley's K -function, with the advantages that it helps to stabilize variance (Mencuccini et al. 2010) and as a linear transformation it is easier to examine the behavior of the function at short distances. Because of our complex observation window comprised of separate, relatively convoluted and narrow transects, we restricted testing for deviations from the fitted model envelopes by the observed L -functions over a distance range of

the hard core distances up to 300 m. The functions were also fairly stable over this range according to the different edge correction methods available in spatstat (Baddeley et al. 2015).

Based on the results of the rank envelope testing of the inhomogeneous hard core models, we tested the use of a hybrid hard core-Geyer saturation interaction model (we subsequently refer to these as hard core-Geyer models) to attempt to obtain a better fit. As used here, the hard core-Geyer models could fit the existence of additional clustering or regularity in the point patterns up to moderate distances beyond the hard core distance. We examined profile plots of the model pseudolikelihood (spatstat *profilepl* function), which is a strength of fit measure, to estimate the best interaction radius (r) and saturation value (σ ; the number of neighboring points typically involved in the interaction) to set as parameters for the Geyer saturation (Geyer 1999) part of the hybrid, evaluating r at 5 m intervals above the hard core distance up to 150 m, and 2–5 neighboring points for σ .

To reduce computation time and still satisfy the resolution requirement (Aarts et al. 2012), we resampled the environmental covariates to a 5 m pixel resolution. Based on an evaluation tool (the *parres* function) and the Akaike Information Criterion (AIC) measure available in spatstat, linear terms were best for modeling all of the covariates but the RDAs index, for which we considered second-order polynomials. We tested each covariate individually with the different interaction models, and also with a Poisson model to obtain baseline parameter estimates for comparison. We then used a stepwise forward-backward procedure based on AIC (the R *step* function) to obtain the most parsimonious set of covariates to account for environmental heterogeneity in the different types of models. While the covariates were relatively uncorrelated (pairwise Spearman's $\rho < |0.38|$), some correlation in their effects when combined was apparent from preliminary modeling. We were generally unconcerned over correlated effects as long as we

achieved a stronger parsimonious model, and attempted to interpret them. However, because of our focus on the fine scale knoll distance effect for the Cerulean Warbler, we excluded elevation from its stepwise procedure (higher elevations were often knolls). For all PPMs, we used a 25x25 m grid quadrature scheme for the background points ($n = \sim 8,000$) as a compromise between maximizing the model fit and processing speed, and the translation edge correction.

RESULTS

Evaluated simply as the raw numbers of singing males, the Ovenbird was relatively stable across the survey bouts (early $n = 103$, mid $n = 97$, and late $n = 113$). The Cerulean Warbler was more variable, with greater numbers in the mid ($n = 198$) and late bout ($n = 180$) than in the early bout ($n = 156$). The Hooded Warbler increased across the bouts (early $n = 116$, mid $n = 152$, and late $n = 173$). Considered within bouts, the minimum inter-point distances were shortest for the Cerulean Warbler (early = 21.8 m, mid = 26.9 m, and late = 22.0 m), followed closely by the Hooded Warbler (early = 23.8 m, mid = 34.5 m, and late = 28.7 m), and more substantially by the Ovenbird (early = 57.1 m, mid = 46.8 m, and late = 46.5 m). Overall, the environmental covariate parameter estimates from the univariate hard core models utilizing these inter-point distances indicated some strengthening of effects compared to the Poisson models (Table 1). The final hard core models obtained from the AIC step procedure also indicated this strengthening (with several additional covariates also selected for the Ovenbird), and they were improved over the final Poisson models based on AIC (Table 2). The specific covariates are described in the context of the individual species results below, but these initial results supported the use of a hard core interaction to account for short-distance repulsion in all three species' point patterns.

Based on the rank envelope tests, the Cerulean Warbler homogeneous hard core null models

were clearly rejected for all survey bouts (upper $p < 0.05$), with the L -function suggesting that individuals were clustered up to the largest distance we evaluated (300 m) beyond the hard core distance (Figure 2; left). The departure of the function above the envelope was greatest for the late bout, indicating stronger clustering. This was qualitatively supported by changes in local Cerulean Warbler densities evident in the point patterns (contained in the Appendix for all species) that suggested it became more spatially concentrated in the late bout, with increases particularly in two locations within impacted forest (on the SR and RR transects, see the Appendix Figure 7) which had relatively higher densities in the early and mid bouts. Along with these increases there also appeared to be general decreases elsewhere.

The univariate Cerulean Warbler inhomogeneous hard core models indicated positive effects for east-facing aspects and proximity to knolls across the survey bouts, for higher RDA_s index values for the early and mid bouts, and for impacted forest for the mid and late bouts (Table 1). The final inhomogeneous hard core models for each bout contained the east-facing aspect and knoll effects, with the impacted forest effect also included for the mid and late bouts (Table 2). We attributed the lack of inclusion of the RDA_s index effect in the early and mid bout final models to the inclusion of the stronger east-facing aspect effect, based on a positive correlation between these effects. While the rank envelope tests indicated that the final inhomogeneous hard core models (Figure 2; right) fit the Cerulean Warbler patterns better than the homogeneous hard core models, not all of the observed clustering appeared to be accounted for by the environmental covariates. For the early and mid bouts, clustering was indicated by the L -function departing above the envelope at distances < 100 m. For the late bout, the departure was more substantial, peaking at ~ 150 m before falling within the envelope by ~ 250 m.

We applied the hard core-Geyer models to the Cerulean Warbler patterns to attempt to

account for this remaining clustering. Profile plots indicated rather clear peaks in the pseudolikelihood for selecting the interaction radius r and saturation parameter σ for each survey bout, ranging from 80–90 m for r and increasing from 3–5 for σ across the bouts. The AIC step procedure for the hard core-Geyer model selected the same environmental covariates as the hard core model in each bout, although in contrast to the hard core models, the spatial covariate parameter estimates were somewhat weakened with the addition of a positive interaction effect (Tables 1 and 2). Based on the rank envelope test (Figure 3), these hard core-Geyer models substantially improved the fit over the hard core models (also supported by AIC; Table 2), with no evidence of clustering remaining. Across the survey bouts, the 95% CIs for the interaction parameter estimates were >0 (listed in Figure 3). As these CIs were from hybrid interaction models, they provided relatively strong evidence for inter-point attraction occurring beyond the initial repulsion indicated by the hard core interaction distance. The increase in σ across the bouts also suggested an increase in the typical number of interacting males.

For both the Hooded Warbler and Ovenbird, some clustering beyond the hard core distance was suggested by the rank envelope tests of the homogeneous hard core null models (Figures 4 and 5; left), although unlike the Cerulean Warbler this did not occur for all survey bouts for either species. Clustering for the Hooded Warbler was suggested for the mid and late bouts up to 150 m where the L -function was at or slightly above the envelope. While larger sample sizes relative to the early bout were perhaps involved in detecting this clustering, a general increase in local Hooded Warbler densities across the survey bouts was apparent in the point patterns, particularly within some transects (e.g., HR, OR, and the northern part of SR; Appendix Figure 8). Clustering for the Ovenbird was suggested only for the late bout, with the L -function at or slightly above the envelope across nearly the full range of distances beyond the hard core

distance. As Ovenbird numbers were fairly stable across the survey bouts, this increase in clustering suggested that individuals became more concentrated spatially by the late bout, and this was also apparent as density increases in the point pattern in some locations (e.g., overall within the OR transect; Appendix Figure 9).

The univariate Hooded Warbler inhomogeneous hard core models indicated positive effects for east-facing aspects, higher elevations, and higher RDAs index values across the survey bouts (Table 1). Based on AIC, second-order polynomials more strongly modeled the RDAs index for the mid and late bouts. There were also positive effects found for impacted forest for the early bout, and for south-facing aspects for the mid bout. The final Hooded Warbler inhomogeneous hard core models contained the individual effects found for the respective survey bouts, with two exceptions likely related to the influence of the RDAs index (Table 2). A positive effect for north-facing aspects was included for the early bout, with the index apparently helping to clarify that there were higher densities on some north-facing aspects with greater structural complexity according to the index. Also, based on a positive correlation between effects, the south-facing aspect effect was not included for the mid bout because of the inclusion of the stronger RDAs index effect. Rank envelope tests of the final Hooded Warbler inhomogeneous hard core models no longer detected clustering (Figure 4; right). In the late bout, short distance regularity was nearly suggested (lower $p = 0.06$), perhaps indicating that for this bout the simple hard core interaction was not the best choice to model repulsion. Regardless, this model was a substantial improvement over a Poisson inhomogeneous model based on AIC (Table 2).

The univariate Ovenbird inhomogeneous hard core models indicated positive effects for west-facing aspects and negative effects for impacted forest across the survey bouts, and a positive effect of elevation for the late bout (Table 1). The final Ovenbird inhomogeneous hard

core models included these respective effects, and several additional effects depending on the bout (Table 2). A positive north-facing aspect effect was included for the early and late bouts, whereas a positive elevation effect was included for the early and mid bouts. The RDA_S index was included in the late bout as a positive linear effect, but in the early bout as a second-order polynomial effect that modeled higher density for intermediate index values. The reasons for the variation in covariate inclusion were difficult to discern, although for the RDA_S index in the late bout the apparent spatial distribution changes were implicated (e.g., more individuals utilizing the OR transect, which had generally higher RDA_S index values). In any case for the Ovenbird, based on AIC the final inhomogeneous hard core models were improved even if rather complex, and the rank envelope test of the late bout model no longer detected clustering (Figure 5; right).

DISCUSSION

In this study, we found support for treating the locations of the singing males of these three forest songbirds as point patterns that are likely realizations of spatial point processes. Clear and consistent differences among the species emerged, despite rather atypical point pattern data in terms of the locations being estimated by ear, and the dynamic nature of singing activity both within a survey and over the breeding season. All three species were abundant with broadly overlapping spatial distributions, yet the models indicated there were substantial differences in their fine-scale distributions in relation to the environment. The models also suggested that the Cerulean Warbler diverged considerably from the Hooded Warbler and Ovenbird in its territorial spacing. In the following discussion, we contrast the species patterns and also address how the types of conspecific interactions they exhibited affected the interpretation of environmental

effects. Finally, we identify some limitations of considering our survey data as point patterns and suggest ways to move forward in using such data to study ecological complexity.

A well-recognized difficulty in analyzing the spatial properties of point patterns is that it may not be possible to distinguish the effects of inter-point interactions (first-order effects) from the effects of heterogeneity due to the environment (second-order effects), without making use of additional biological information (Diggle 2003). It is likely that both first- and second-order effects, perhaps operating at different spatial scales, are involved in the spatial distribution of the points. Particularly for plants, environmental influences are thought to dominate at broader spatial scales, whereas mechanisms such as attraction and repulsion operate at finer spatial scales (Wiegand et al. 2007). We suspect this general characteristic is also true for the point patterns of the singing males of the three forest bird species we studied, at least over the distance range we evaluated. For all three species, the most obvious spatial property of the patterns was for initial regularity as indicated by the hard core distances. These minimum inter-point distances did not appear to be an observer bias, for example, in not recording signaling individuals that were in very close proximity, because this was simply not observed. We believe it is much more likely that the initial regularity indicated competition for territorial space used to attract a mate, which itself is a primary driver of the evolutionary development of vocal signaling behavior in birds (Searcy and Andersson 1986). In dense tropical forests, song provides a means of non-visual communication between individual territorial males (Aubin et al. 2004), and this advantage was presumably important in the forest we studied as well.

At distances beyond the hard core, the rank envelope tests indicated that environmental heterogeneity as measured by the remote sensing data explained clustering in the point patterns for all species, but to a much lesser extent for the Cerulean Warbler. The hard core models

indicated that the unexplained (or ‘leftover’) Cerulean Warbler clustering primarily occurred over moderate distances (<150 m), which increases the possibility it involved direct interactions between individual males. This observation led to the use of the hard core-Geyer models, which adequately controlled the leftover clustering while still including the environmental explanation. We cannot conclude that this leftover clustering was caused by some conspecific attraction mechanism and not by environmental heterogeneity we were unable to measure, however. Other studies have found that the Cerulean Warbler exhibits clustered territoriality (Roth and Islam 2007, Barnes et al. 2016), but unlike some songbird species (e.g., Black-throated Blue Warbler, *Setophaga caerulescens*; Hahn and Silverman 2007) there is only weak experimental evidence through the use of artificial stimuli that conspecific attraction is involved and more study is needed (Barnes et al. 2016). Still, the very high densities of several of the clusters is at least suggestive of more than just an environmental explanation. Regardless, our results supported a very different spatial pattern for the Cerulean Warbler in terms of its potential for dense clustering, and indicated a spatial scale over which to investigate this potential further.

We did not need hard core-Geyer models for the Hooded Warbler and Ovenbird point patterns because incorporating environmental heterogeneity sufficiently accounted for their observed clustering. To the best of our knowledge, there have been no Ovenbird studies and only one Hooded Warbler study (Melles et al. 2009) suggesting they exhibit clustering. Methodological differences with our study complicate direct comparisons, but Melles et al. (2009) found that nests were significantly clustered, mostly at scales between 240 and 420 m, within available nesting habitat as indicated by a habitat map obtained by classifying fine-scale satellite (Ikonos) imagery. For our study, even with the Hooded Warbler numeric increase over the survey bouts there was no marked increase as with the Cerulean Warbler in its clustering

according to the homogeneous L -functions. The initial regularity of the pattern, along with the relatively strong control over its heterogeneity by the environmental covariates, suggested a general expansion by Hooded Warblers to more fully occupy available habitat over the breeding season. Studies of clustering probably should consider abundance, as the Hooded Warbler was much more abundant in our study area compared to the Melles et al. (2009) Southern Ontario, Canada, study area near the northern extreme of its range. Conspecific attraction may be easier to support if there are few individuals relative to available habitat and they exhibit clustering.

Although the simple inclusion of a hard core interaction had a relatively small effect on the parameter estimates for the environmental covariates compared to those obtained from the Poisson models, the estimates tended to consistently increase. Intuitively, this result is suggestive of competition by these species for limited resources as the covariates indicated them, with territorial individuals keeping other individuals from accessing these resources and thus driving up their importance. For example, an increase in the negative effect of impacted forest on Ovenbird intensity was indicated for the hard core models (Table 1; although note the overlapping 95% CIs with the Poisson models). An Ovenbird preference for undisturbed mature forest was thus supported by both models, but the hard core models suggested an increase in the importance of this habitat as a potential limiting factor on Ovenbird density. For all species, the minimum inter-point distances appeared to provide a rough, albeit likely conservative estimate of spacing behavior (e.g., if obtained from a pair of individuals singing near the boundaries of their respective territories), and assuming the existence of competition for space, led to more realistic parameter estimates (and for the Ovenbird selected additional covariates; Table 2).

In contrast to the general strengthening of the environmental covariate effects obtained from the hard core models, the Cerulean Warbler hard core-Geyer models showed some weakening of

these effects. From a modeling perspective, this occurred because part of the environmental heterogeneity effect was instead accounted for by the attraction effect of the inter-point interaction. This has biological implications because conspecific attraction may exaggerate the importance of local environmental features involved in habitat selection (Roth and Islam 2007). Notably, the positive impacted forest effect on Cerulean Warbler intensity was substantially weakened in the late sampling bout by the addition of an attraction effect, which suggested some uncertainty over the underlying cause for the very large clusters observed in the impacted forest later in the breeding season. It is also possible that by then a substantial number of individuals were engaged in post-breeding activities such as caring for fledglings or prospecting for territories for next season (e.g., as may occur in the Black-throated Blue Warbler; Betts et al. 2008). If so, these individuals apparently still exhibited similar spacing behavior and habitat selection, however. Among the species we studied, the Cerulean Warbler distribution appeared to be particularly dynamic, perhaps as a consequence of clustering behavior coupled with changes in the individuals involved in clustering over the breeding season.

In addition to supporting spacing differences among the species, the PPMs indicated much contrast in their habitat use. The strongest such contrast involved topographic aspect. While selection of certain aspects for breeding has been found for the Cerulean Warbler (e.g., Hartman et al. 2009: east-facing aspects; Weakland and Wood 2005, Barnes et al. 2016: northeast-facing aspects), we were unable to find any Hooded Warbler or Ovenbird studies of this phenomenon. At least for the Hooded Warbler, the RDA_s index effects on its intensity suggested that higher forest structural complexity on east-facing aspects was an important factor in its distribution. For the Cerulean Warbler, the east-facing aspect preference could involve higher grapevine density, as grapevines may be a preferred source of nest material for the species (Bakermans and

Rodewald 2009). East-facing aspects on knolls also may have provided the internal forest edges the Cerulean Warbler appears to prefer (Barnes et al. 2016). An alternative or complementary factor may be that topographic aspect influences microclimate, and microclimatic preferences may differ among these species. For example, perhaps the Ovenbird's strong west-facing aspect preference was because these aspects often had greater canopy cover and were thus more shaded. However, another consequence of this greater canopy cover was more open areas with deep leaf-litter (see Chapter 2), which the Ovenbird may prefer to nest in (Mattsson and Niemi 2006).

There are several limitations regarding our use of singing male locations as point patterns. One issue was detection probability, as this is well known to decline as a function of distance from the observer (Emlen 1971), can be influenced by a variety of temporal, environmental, and observer-related factors (see Ralph and Scott 1981), and it is likely that territorial males were present during a survey but not recorded because they did not sing (Farnsworth et al. 2002). It is also not possible to know if all of the recorded individuals had well-established territories. Further, because it was not generally possible to see the individuals, not all of them were necessarily male (female song in warbler species: Najar and Benedict 2015) or even their purported species (Cerulean Warbler singing a Hooded Warbler song: Boves et al. 2010). Despite these issues, we believe these snapshots of singing activity by these species over the course of the breeding season were at least minimally adequate for examining their territorial spacing, and how the environment influenced their spatial distributions. With separate analyses by sampling bout, we not only assessed the patterns for potential changes over the breeding season, but also gained confidence in the results by finding consistency among the species in their spacing as well as habitat use.

Our study site likely provided an ideal situation for the fine scale study of these small territorial songbirds. All three species were abundant, which increased the potential for the statistical detection of effects. Another advantage was the high degree of topographic complexity over relatively short distances, as topography alone provided much contrast among the species' habitat use, and it was possible to effectively survey this topographic complexity from the ridgetops. Our study further benefited from the availability of a high spatial resolution DEM which allowed fine scale terrain modeling, and it was valuable to have at least for modeling the Hooded Warbler a measure of forest structural complexity through the QuickBird satellite-derived RDA_s index. Future comparative studies using the locations of birds as point patterns could benefit from satellite and/or aerial remote sensing data on fine-scale environmental heterogeneity applicable to multiple species (e.g., lidar, a type of active remote sensing data, would likely have been a useful addition to our study for the Cerulean Warbler; see Barnes et al. 2016). More rigorous study designs for testing the relative influence of environmental heterogeneity and interactions on point patterns are also possible (e.g., see Getzin et al. 2008). The use of observation windows with a larger area to perimeter ratio (e.g., square or rectangular) may make edge correction less of a potential bias. Finally, studies in flatter terrain may allow more thorough coverage for collecting more accurate and complete location data on individuals.

Conclusions

Using the locations of singing males in PPMs, we found a number of apparent habitat associations among the three forest songbirds we studied. Several of these do not appear to have been quantified to date, such as the Cerulean Warbler association with knolls, and the Hooded Warbler and Ovenbird association with particular topographic aspects (opposite ones at our study site). These alone are interesting, as are the implications of including inter-point

interactions on the parameter estimates for environmental effects in general. Perhaps most intriguing, however, was that the inter-point interaction PPMs suggested a range in the dispersion patterns of the small, territorial forest songbirds we studied that was similar to the range found by Sherry and Holmes (1985) using a different spatial analysis technique applied to territory centers. For our study it was the Cerulean Warbler exhibiting the highly clumped distribution similar to that of the Least Flycatcher, and the Ovenbird in both of our studies exhibiting a more evenly dispersed distribution. We emphasize that we are comparing our analysis of singing male locations to their analysis of territory centers obtained from a more intensive method, but the similarities we found between our studies located in different forests and using different analysis methods appear to help confirm the usefulness of our approach.

We see an important parallel between our study and Sueur and Farina (2015), who suggested greater use of environmental sound to study ecological complexity. While our estimated singing location data was rather primitive compared to the acoustic data Sueur and Farina (2015) primarily consider (e.g., that obtained from automatic field recording devices), we found it very informative with respect to complex processes underlying how these species were distributed in this forest. We also cannot envision how else to feasibly collect this amount of singing location data over the spatial extent we covered, at the resolution needed for our analysis. As far as the data limitations, there may be ways to overcome them in point pattern analyses (e.g., use of covariates to account for detectability; Waagepetersen and Schweder 2006). Sherry and Holmes (1985) emphasized the relative rarity (which also appears to exist presently) and high value of comparative analyses of bird distribution patterns for understanding how habitat and interactions between individuals determine species distributions at multiple spatial scales. Much would appear to now be possible to achieve in this regard, given improved remote sensing data on the

environment and avian singing behavior as a reliable source of information on species' habitat use and spacing behavior.

ACKNOWLEDGMENTS

We thank D. Blood, B. Miller, M. Napoli, and numerous other field technicians for their assistance with data collection and Wheeling Jesuit University for providing field housing. West Virginia Department of Natural Resources and U.S. Geological Survey West Virginia Cooperative Fish and Wildlife Research Unit provided logistical support.

Funding statement: This research was funded by NETL Department of Energy, U.S. Fish and Wildlife Service, National Fish and Wildlife Foundation, and West Virginia University Division of Forestry and Natural Resources.

Author contributions: J.S. with P.B.W. conceived the idea and design of the study, J.S. processed the remote sensing data, performed the analyses, and with input from P.B.W. wrote the manuscript.

LITERATURE CITED

- Aarts, G., J. Fieberg, and J. Matthiopoulos (2012). Comparative interpretation of count, presence–absence and point methods for species distribution models. *Methods in Ecology and Evolution* 3:177–187.
- Aubin, T., N. Mathevon, M. L. D. Silva, J. M. Vielliard, and F. Sebe (2004). How a simple and stereotyped acoustic signal transmits individual information: the song of the White-browed Warbler *Basileuterus leucoblepharus*. *Anais da Academia brasileira de Ciencias* 76:335–344.

- Bakermans, M. H. and A. D. Rodewald (2009). Think globally, manage locally: the importance of steady-state forest features for a declining songbird. *Forest Ecology and Management* 258:224–232.
- Baddeley, A., J. Møller, and R. Waagepetersen (2000). Non- and semiparametric estimation of interaction in inhomogeneous point patterns. *Statistica Neerlandica* 54:329–350.
- Baddeley, A., M. Berman, N. I. Fisher, A. Hardegen, R. K. Milne, D. Schuhmacher, R. Shah, and R. Turner (2010). Spatial logistic regression and change-of-support in Poisson point processes. *Electronic Journal of Statistics* 4:1151–1201.
- Baddeley, A., R. Turner, J. Mateu, and A. Bevan (2013). Hybrids of Gibbs point process models and their implementation. *Journal of Statistical Software* 55:1–43.
- Baddeley, A., E. Rubak, and F. Turner (2015). *Spatial Point Patterns: Methodology and Applications with R*. London: Chapman and Hall/CRC Press. 810 pp.
- Barnes, K. W., K. Islam, and S. A. Auer (2016). Integrating LIDAR-derived canopy structure into cerulean warbler habitat models. *The Journal of Wildlife Management* 80:101–116.
- Besag J. (1977). Contribution to the discussion of Dr. Ripley's paper. *Royal Statistical Society B* 39:193–195.
- Betts, M. G., A. S. Hadley, N. Rodenhouse, and J. J. Nocera (2008). Social information trumps vegetation structure in breeding-site selection by a migrant songbird. *Proceedings of the Royal Society Biological Sciences Series B* 275:2257–2263.
- Boves, T. J., D. A. Buehler, and P. C. Massey (2010). Interspecific song imitation by a Cerulean Warbler. *Wilson Journal of Ornithology* 122:583–587.
- Cavazzi, S., R. Corstanje, T. Mayr, J. Hannam, and R. Fealy (2013). Are fine resolution digital elevation models always the best choice in digital soil mapping?. *Geoderma* 195:111–121.

- Diggle, P. J. (2003). *Statistical Analysis of Point Processes*. Academic Press, London.
- Dormann, C. F., J. M. McPherson, M. B. Araújo, R. Bivand, J. Bolliger, G. Carl, R. G. Davies, A. Hirzel, W. Jetz, W. D. Kissling, I. Kühn, R. Ohlemüller, P. R. Peres-Neto, B. Reineking, B. Schröder, F. M. Schurr, R. Wilson (2007). Methods to account for spatial autocorrelation in the analysis of species distributional data: a review. *Ecography* 30:609–628.
- Elith, J., and J. R. Leathwick (2009). Species distribution models: ecological explanation and prediction across space and time. *Annual Review of Ecology, Evolution, and Systematics* 40:677–697.
- Emlen, J. T. (1971). Population densities of birds derived from transect counts. *The Auk* 88:323–342.
- Farwell, L. S., P. B. Wood, J. Sheehan, and G. A. George (2016). Shale gas development effects on the songbird community in a central Appalachian forest. *Biological Conservation* 201:78–91.
- Fithian, W., and T. Hastie (2013). Finite-sample equivalence in statistical models for presence-only data. *The annals of applied statistics* 7:1917–1939.
- Farnsworth, G. L., K. H. Pollock, J. D. Nichols, T. R. Simons, J. E. Hines, and J. R. Sauer (2002). A removal model for estimating detection probabilities from point-count surveys. *The Auk* 119:414–425.
- Fithian, W., J. Elith, T. Hastie, and D. A. Keith (2015). Bias correction in species distribution models: pooling survey and collection data for multiple species. *Methods in Ecology and Evolution* 6:424–438.
- Getzin, S., T. Wiegand, K. Wiegand, and F. He (2008). Heterogeneity influences spatial patterns and demographics in forest stands. *Journal of Ecology* 96:807–820.

- Geyer, C. J. (1999) Likelihood Inference for Spatial Point Processes. Chapter 3 in Stochastic Geometry: Likelihood and Computation (O. E. Barndorff-Nielsen, W. S. Kendall and M. N. M. Van Lieshout, Editors). Chapman and Hall / CRC, Monographs on Statistics and Applied Probability, number 80.
- Gießelmann, U. R. S., T. Wiegand, J. Meyer, M. Vogel, and R. Brandl (2008). Spatial distribution of communal nests in a colonial breeding bird: benefits without costs? *Austral Ecology*, 33: 607–613.
- Hahn, B. A., and E. D. Silverman (2007). Managing breeding forest songbirds with conspecific song playbacks. *Animal Conservation* 10:436–441.
- Hartman, P. J., D. S. Maehr, and J. L. Larkin (2009). Habitat selection by Cerulean Warblers in eastern Kentucky. *The Wilson Journal of Ornithology* 121:469–475.
- He, K. S., B. A. Bradley, A. F. Cord, D. Rocchini, M. N. Tuanmu, S. Schmidtlein, W. Turner, M. Wegmann, and N. Pettorelli (2015). Will remote sensing shape the next generation of species distribution models? *Remote Sensing in Ecology and Conservation* 1:4–18.
- Hibert, F., C. Calenge, H. Fritz, D. Maillard, P. Bouché, A. Ipavec, A. Convers, D. Ombredane, and M. N. de Visscher (2010). Spatial avoidance of invading pastoral cattle by wild ungulates: insights from using point process statistics. *Biodiversity and Conservation* 19:2003–2024.
- Law, R., J. Illian, D. F. Burslem, G. Gratzer, C. V. S. Gunatilleke, and I. A. U. N. Gunatilleke (2009). Ecological information from spatial patterns of plants: insights from point process theory. *Journal of Ecology* 97:616–628.

- Li, K., J. H. Vandermeer, and I. Perfecto (2016). Disentangling endogenous versus exogenous pattern formation in spatial ecology: a case study of the ant *Azteca sericeasur* in southern Mexico. *Royal Society Open Science* 3:160073.
- Liu, Z., J. Yang, Y. Chang, P. J. Weisberg, and H. S. He (2012). Spatial patterns and drivers of fire occurrence and its future trend under climate change in a boreal forest of Northeast China. *Global Change Biology* 18:2041–2056.
- Lin, Y. C., L. W. Chang, K. C. Yang, H. H. Wang, and I. F. Sun (2011). Point patterns of tree distribution determined by habitat heterogeneity and dispersal limitation. *Oecologia* 165:175–184.
- Mattsson, B. J., and G. J. Niemi (2006). Factors influencing predation on Ovenbird (*Seiurus aurocapilla*) nests in northern hardwoods: Interactions across spatial scales. *The Auk* 123:82–96.
- Mencuccini, M., J. Martinez-Vilalta, J. Piñol, L. Loepfe, M. Burnat, X. Alvarez, J. Camacho, and D. Gil (2010). A quantitative and statistically robust method for the determination of xylem conduit spatial distribution. *American journal of botany* 97:1247–1259.
- Melles, S. J., D. Badzinski, M. J. Fortin, F. Csillag, and K. Lindsay (2009). Disentangling habitat and social drivers of nesting patterns in songbirds. *Landscape Ecology* 24:519–531.
- Møller, J., and R. P. Waagepetersen (2007). Modern statistics for spatial point processes. *Scandinavian Journal of Statistics* 34:643–684.
- Myllymäki, M., T. Mrkvicka, P. Grabarnik, H. Seijo, and U. Hahn (2016). Global envelope tests for spatial processes. *Journal of the Royal Statistical Society: Series B (Statistical Methodology)*. doi:10.1111/rssb.12172

- Najar, N., and L. Benedict (2015). Female song in new world wood-warblers (Parulidae). *Frontiers in Ecology and Evolution* 3:1–13.
- Newell, F. L., J. Sheehan, P. B. Wood, A. D. Rodewald, D. A. Buehler, P. D. Keyser, J. L. Larkin, T. A. Beachy, M. H. Bakermans, T. J. Boves, and A. Evans (2013). Comparison of point counts and territory mapping for detecting effects of forest management on songbirds. *Journal of Field Ornithology* 84:270–286.
- Perry, G. L., B. P. Miller, and N. J. Enright (2006). A comparison of methods for the statistical analysis of spatial point patterns in plant ecology. *Plant ecology* 187:59–82.
- R Core Team (2016). R: A language and environment for statistical computing. R Foundation for Statistical Computing, Vienna, Austria. URL <https://www.R-project.org/>.
- Ralph, C. J., and J. M. Scott (1981). Estimating numbers of terrestrial birds. *Studies in Avian Biology* No. 6. Allen Press, Lawrence, Kansas.
- Renner, I. W., J. Elith, A. Baddeley, W. Fithian, T. Hastie, S. J. Phillips, G. Popovic, D. I. Warton, (2015). Point process models for presence-only analysis. *Methods in Ecology and Evolution* 6: 366–379.
- Ripley, B.D. (1976). The second-order analysis of stationary point processes. *Journal of applied probability* 13:255–266.
- Roth, K. L., and K. Islam (2007). Do cerulean warblers (*Dendroica cerulea*) exhibit clustered territoriality? *American Midland Naturalist* 157:345–355.
- Searcy, W. A., and M. Andersson (1986). Sexual selection and the evolution of song. *Annual Review of Ecology and Systematics* 17:507–533.
- Sheehan, J., P. B. Wood, D. A. Buehler, P. D. Keyser, J. L. Larkin, A. D. Rodewald, T. B. Wigley, T. J. Boves, G. A. George, M. H. Bakermans, T. A. Beachy, A. Evans, M. E. McDermott, F.

- L. Newell, K. A. Perkins, and M. White (2014). Avian response to timber harvesting applied experimentally to manage Cerulean Warbler breeding populations. *Forest Ecology and Management* 321:5–18.
- Sherry, T. W., and R. T. Holmes (1985). Dispersion patterns and habitat responses of birds in northern hardwoods forests. In *Habitat Selection in Birds*. (M. L. Cody, Editor). Academic Press, NY, USA.
- Sueur, J., and A. Farina (2015). Ecoacoustics: the ecological investigation and interpretation of environmental sound. *Biosemiotics* 8:493–502.
- Sutherland, W. J., R. P. Freckleton, H. C. J. Godfray, S. R. Beissinger, T. Benton, D. D. Cameron, Y. Carmel, D. A. Coomes, T. Coulson, M. C. Emmerson, and R. S. Hails (2013). Identification of 100 fundamental ecological questions. *Journal of Ecology* 101:58–67.
- Van Lieshout, M. N. M. and A. Stein (2012). Earthquake modelling at the country level using aggregated spatio-temporal point processes. *Mathematical geosciences* 44:309–326.
- Velázquez, E., I. Martínez, S. Getzin, K. A. Moloney, and T. Wiegand (2016). An evaluation of the state of spatial point pattern analysis in ecology. *Ecography* 39:1–14.
- Waagepetersen, R., and T. Schweder (2006). Likelihood-based inference for clustered line transect data. *Journal of Agricultural, Biological, and Environmental Statistics* 11: 264–279.
- Warton, D. I., and L. C. Shepherd (2010). Poisson point process models solve the “pseudo-absence problem” for presence-only data in ecology. *The Annals of Applied Statistics* 4:1383–1402.
- Weakland, C. A., and P. B. Wood (2005). Cerulean Warbler (*Dendroica cerulea*) microhabitat and landscape-level habitat characteristics in southern West Virginia. *Auk* 122:497–508.

- Wiegand, T., C. V. S. Gunatilleke, and I. A. U. N. Gunatilleke (2007). Species associations in a heterogeneous Sri Lankan dipterocarp forest. *American Naturalist* 170:77–95.
- Wiegand, T., W. D. Kissling, P. A. Cipriotti, and M. R. Aguiar (2006). Extending point pattern analysis for objects of finite size and irregular shape. *Journal of Ecology* 94:825–837.
- Woods, A. J., J. M. Omernik, and D. D. Brown (1999). Level III and IV Ecoregions of Delaware, Maryland, Pennsylvania, Virginia, and West Virginia. U.S. Environmental Protection Agency, National Health and Environmental Effects Research Laboratory. Corvallis, OR. accessed 2016 April from: ftp://ftp.epa.gov/wed/ecoregions/reg3/reg3_eco_desc.doc.
- Yamada, I., and P. A. Rogerson (2003). An empirical comparison of edge effect correction methods applied to *K*-function analysis. *Geographical Analysis* 37:95–109.

Table 1. Parameter estimates for the environmental covariates from univariate inhomogeneous Poisson (PS), hard core (HC), and hard core-Geyer (HC-G) point process models by species across the three sampling bouts. Environmental covariate estimate 95% confidence intervals (CI) in bold do not overlap zero.

Parameter ^a	Model	Early bout		Mid bout		Late bout	
		Coef.	(95% CI)	Coef.	(95% CI)	Coef.	(95% CI)
<i>Cerulean Warbler</i>							
Intercept ^b	PS	-10.365	(-10.522, -10.208)	-10.132	(-10.272, -9.992)	-10.222	(-10.368, -10.076)
	HC	-10.298	(-10.455, -10.141)	-10.025	(-10.164, -9.885)	-10.149	(-10.296, -10.003)
	HC-G	-10.855	(-11.143, -10.566)	-10.629	(-10.865, -10.392)	-10.853	(-11.093, -10.612)
Impacted forest	PS	0.166	(-0.158, 0.489)	0.552	(0.272, 0.831)	0.574	(0.281, 0.866)
	HC	0.174	(-0.149, 0.498)	0.597	(0.317, 0.877)	0.601	(0.308, 0.893)
	HC-G	0.154	(-0.116, 0.424)	0.402	(0.177, 0.627)	0.375	(0.130, 0.620)
Eastness	PS	0.545	(0.363, 0.726)	0.597	(0.432, 0.762)	0.731	(0.548, 0.914)
	HC	0.560	(0.374, 0.746)	0.636	(0.468, 0.804)	0.754	(0.559, 0.949)
	HC-G	0.490	(0.304, 0.677)	0.533	(0.371, 0.694)	0.613	(0.425, 0.802)
Northness	PS	0.000	(-0.158, 0.157)	-0.005	(-0.145, 0.135)	0.017	(-0.129, 0.164)
	HC	0.000	(-0.168, 0.168)	-0.007	(-0.160, 0.146)	0.015	(-0.141, 0.170)
	HC-G	0.021	(-0.144, 0.187)	0.023	(-0.122, 0.168)	0.019	(-0.129, 0.168)
Knoll distance	PS	-0.427	(-0.612, -0.242)	-0.498	(-0.667, -0.329)	-0.217	(-0.376, -0.059)
	HC	-0.449	(-0.613, -0.285)	-0.548	(-0.697, -0.400)	-0.225	(-0.372, -0.079)
	HC-G	-0.364	(-0.508, -0.219)	-0.401	(-0.523, -0.280)	-0.172	(-0.276, -0.068)
RDAs index	PS	0.289	(0.102, 0.476)	0.163	(-0.002, 0.327)	0.107	(-0.065, 0.278)
	HC	0.297	(0.117, 0.477)	0.177	(0.006, 0.349)	0.112	(-0.075, 0.299)
	HC-G	0.228	(0.076, 0.380)	0.123	(-0.013, 0.260)	0.105	(-0.044, 0.254)
<i>Hooded Warbler</i>							
Intercept ^a	PS	-10.662	(-10.844, -10.480)	-10.391	(-10.550, -10.232)	-10.262	(-10.411, -10.113)
	HC	-10.597	(-10.779, -10.415)	-10.253	(-10.412, -10.094)	-10.150	(-10.299, -10.001)
Impacted forest	PS	0.456	(0.090, 0.822)	0.124	(-0.206, 0.454)	0.155	(-0.153, 0.462)
	HC	0.475	(0.109, 0.841)	0.137	(-0.192, 0.467)	0.170	(-0.138, 0.478)
Eastness	PS	0.349	(0.152, 0.546)	0.292	(0.122, 0.461)	0.469	(0.301, 0.636)
	HC	0.360	(0.165, 0.555)	0.319	(0.153, 0.484)	0.497	(0.326, 0.667)
Northness	PS	-0.009	(-0.191, 0.173)	-0.183	(-0.343, -0.022)	-0.054	(-0.203, 0.095)
	HC	-0.009	(-0.189, 0.171)	-0.201	(-0.362, -0.040)	-0.057	(-0.202, 0.088)

Elevation	PS	0.200	(0.006, 0.395)	0.275	(0.102, 0.449)	0.191	(0.032, 0.350)
	HC	0.207	(0.008, 0.406)	0.305	(0.130, 0.480)	0.206	(0.051, 0.362)
RDAs index	PS	0.439	(0.219, 0.658)	0.507	(0.274, 0.740)	0.717	(0.462, 0.973)
				-0.209 ²	(-0.428, 0.010)²	-0.368 ²	(-0.603, -0.133)²
	HC	0.453	(0.226, 0.681)	0.553	(0.306, 0.799)	0.765	(0.510, 1.020)
				-0.214 ²	(-0.455, 0.027)²	-0.389 ²	(-0.619, -0.159)²
<i>Ovenbird</i>							
Intercept ^a	PS	-10.709	(-10.908, -10.510)	-10.751	(-10.954, -10.548)	-10.601	(-10.790, -10.413)
	HC	-10.446	(-10.645, -10.247)	-10.576	(-10.780, -10.373)	-10.411	(-10.600, -10.223)
Impacted forest	PS	-0.772	(-1.322, -0.222)	-0.644	(-1.183, -0.106)	-1.062	(-1.642, -0.482)
	HC	-0.928	(-1.478, -0.377)	-0.718	(-1.257, -0.180)	-1.182	(-1.762, -0.603)
Eastness	PS	-0.332	(-0.540, -0.123)	-0.239	(-0.449, -0.029)	-0.320	(-0.517, -0.123)
	HC	-0.369	(-0.591, -0.146)	-0.277	(-0.491, -0.062)	-0.369	(-0.566, -0.171)
Northness	PS	0.131	(-0.071, 0.332)	0.101	(-0.104, 0.307)	0.076	(-0.114, 0.266)
	HC	0.156	(-0.040, 0.352)	0.110	(-0.093, 0.314)	0.083	(-0.116, 0.283)
Elevation	PS	0.120	(-0.088, 0.329)	0.192	(-0.027, 0.410)	0.221	(0.016, 0.426)
	HC	0.141	(-0.102, 0.383)	0.221	(0.000, 0.442)	0.264	(0.075, 0.453)
RDAs index	PS	-0.070	(-0.327, 0.186)	-0.006	(-0.239, 0.228)	0.127	(-0.092, 0.345)
				-0.221 ²	(-0.479, 0.038)²		
	HC	-0.080	(-0.336, 0.176)	-0.008	(-0.237, 0.222)	0.159	(-0.063, 0.380)
				-0.243 ²	(-0.527, 0.041)²		

a. Impacted forest was a categorical covariate, defined as forest existing ≤ 100 m from forest edges due to recent anthropogenic disturbances. Eastness and northness were the sine (east–west) and cosine (north–south); respectively, linear derivations of 0–360° topographic aspect (positive values = east-facing or north-facing aspects; negative values = west-facing or south-facing aspects). Elevation was mean elevation. The RDA_s index was a mapped index of forest structural complexity (Chapter 3). Knoll distance was the distance to the tops of prominent knolls (used only in the Cerulean Warbler models instead of elevation).

b. Intercept-only model; for clarity only the environmental covariate estimate is reported for the other models.

Table 2. Final inhomogeneous Poisson (PS), hard core (HC), and hard core-Geyer (HC-G) point process models by species across the three sampling bouts obtained from the AIC step procedure. The AIC values for the final models are presented for comparison within a species within a sampling bout. The model formula begins with the intercept followed by the covariate coefficients (key: IF = impacted forest, E = eastness, N = northness, EI = elevation, RDA_S = forest structural complexity index, Kd = knoll distance)^a.

Species	Model	Early bout		Mid bout		Late bout	
		AIC	Model formula	AIC	Model formula	AIC	Model formula
Cerulean Warbler	PS	3479.1	$-10.578 + 0.569 E + -0.444 Kd$	4272.6	$-10.590 + 0.474 IF + 0.628 E + -0.494 Kd$	3940.5	$-10.716 + 0.548 IF + 0.749 E + -0.211 Kd$
	HC	3462.2	$-10.542 + 0.589 E + -0.470 Kd$	4223.0	$-10.537 + 0.519 IF + 0.680 E + -0.554 Kd$	3917.0	$-10.686 + 0.580 IF + 0.777 E + -0.223 Kd$
	HC-G	3436.5	$-10.952 + 0.521 E + -0.400 Kd$	4187.4	$-10.876 + 0.417 IF + 0.587 E + -0.447 Kd$	3840.3	$-11.135 + 0.389 IF + 0.630 E + -0.184 Kd$
Hooded Warbler	PS	2675.7	$-11.002 + 0.626 IF + 0.195 E + 0.157 N + 0.519 RDA_S$	3428.6	$-10.378 + 0.205 E + 0.397 RDA_S + (-0.187 RDA_S)^2 + 0.264 EI$	3833.2	$-10.250 + 0.351 E + 0.559 RDA_S + (-0.336 RDA_S)^2 + 0.182 EI$
	HC	2664.6	$-10.981 + 0.661 IF + 0.203 E + 0.168 N + 0.546 RDA_S$	3387.9	$-10.266 + 0.225 E + 0.435 RDA_S + (-0.193 RDA_S)^2 + 0.296 EI$	3795.2	$-10.156 + 0.375 E + 0.600 RDA_S + (-0.358 RDA_S)^2 + 0.201 EI$
Ovenbird	PS	2249.4	$-10.328 + -1.067 IF + -0.301 E + -0.057 RDA_S + (-0.255 RDA_S)^2 + 0.254 EI$	2168.8	$-10.563 + -0.934 IF + -0.223 E + 0.342 EI$	2465.7	$-10.377 + -1.421 IF + -0.298 E + 0.433 EI$
	HC	2190.4	$-10.009 + -1.295 IF + -0.375 E + 0.176 N + -0.002 RDA_S + (-0.285 RDA_S)^2 + 0.324 EI$	2134.2	$-10.372 + -1.097 IF + -0.269 E + 0.417 EI$	2412.3	$-10.200 + -1.585 IF + -0.464 E + 0.163 N + 0.257 RDA_S + 0.540 EI$

a. Impacted forest was a categorical covariate, defined as forest existing ≤ 100 m from forest edges due to recent anthropogenic disturbances. Eastness and northness were the sine (east–west) and cosine (north–south); respectively, linear derivations of 0–360° topographic aspect (positive values = east-facing or north-facing aspects; negative values = west-facing or south-facing aspects). Elevation was mean elevation. The RDA_S index was a mapped index of forest structural complexity (Chapter 3). Knoll distance was the distance to the tops of prominent knolls (used only in the Cerulean Warbler models instead of elevation).

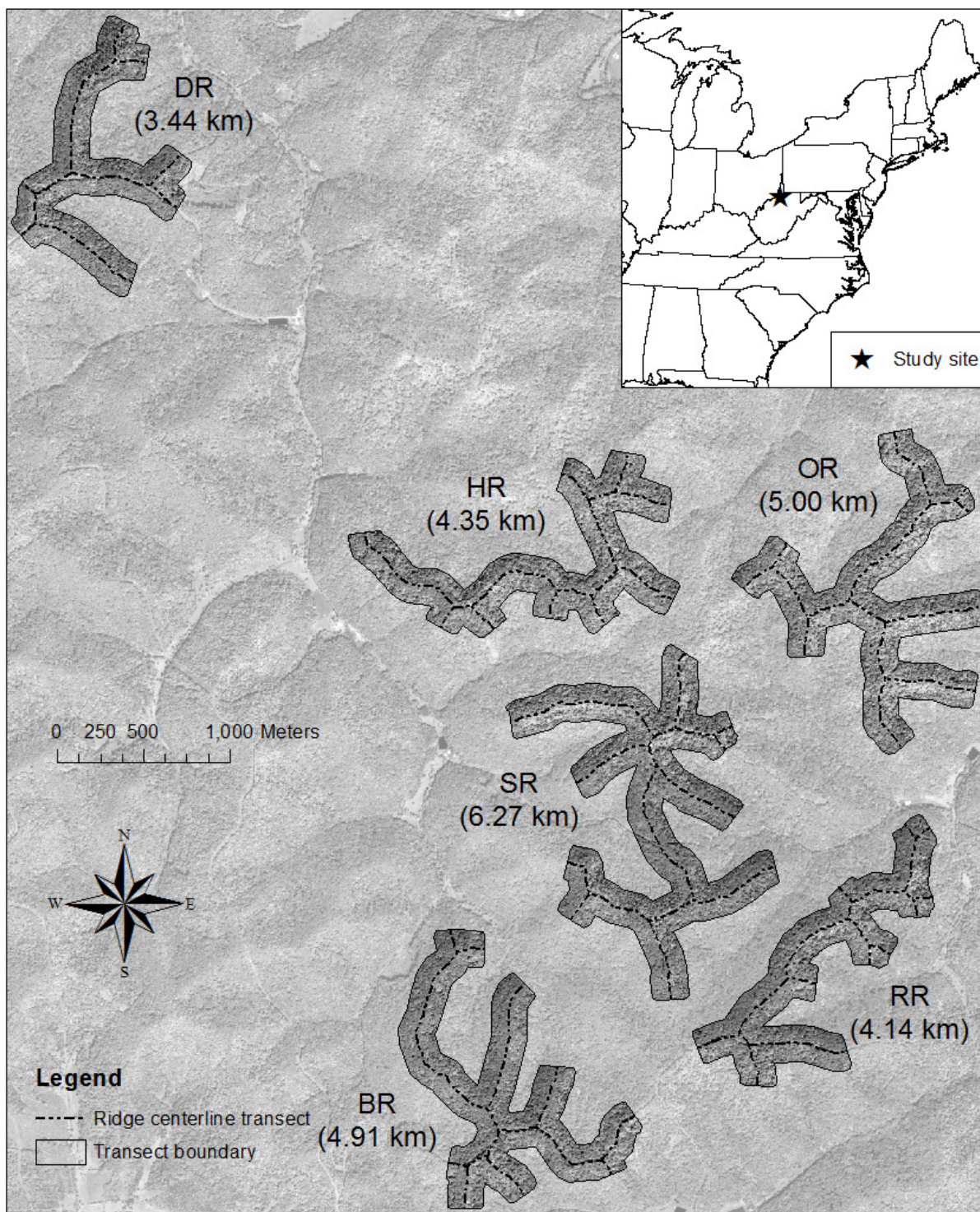
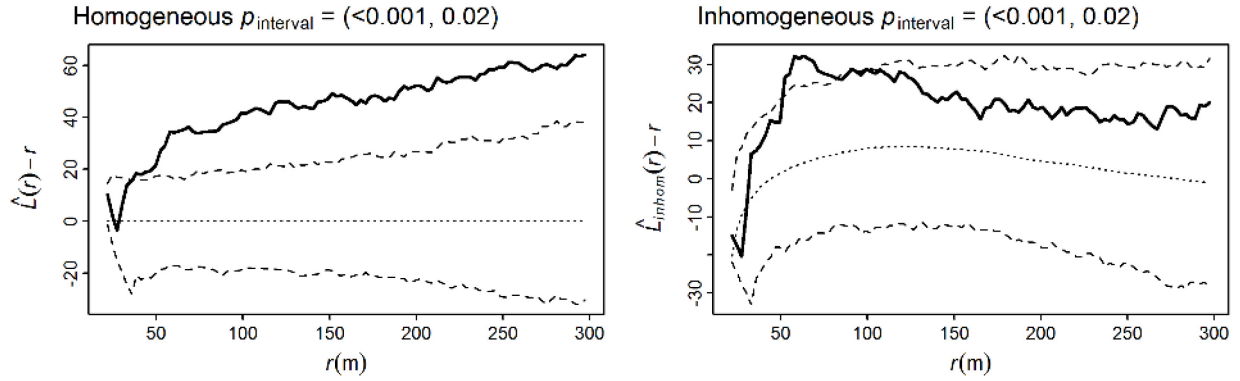
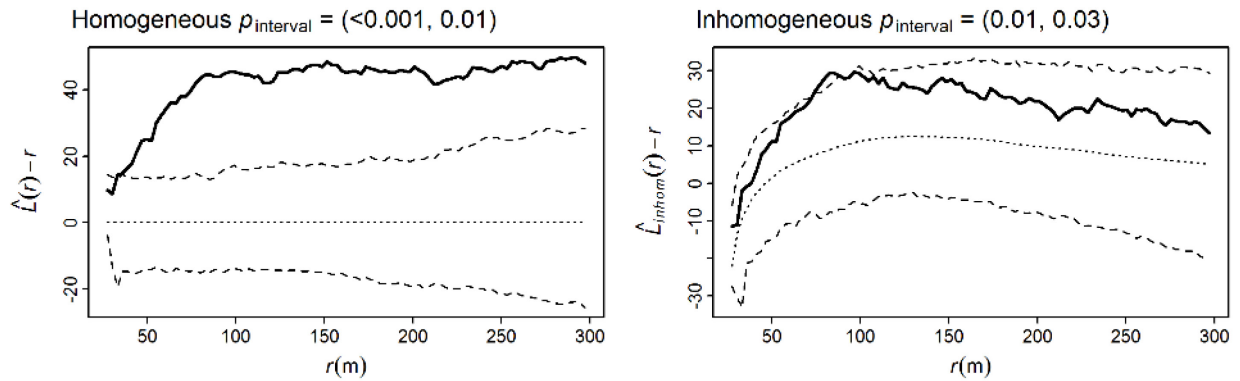


Figure 1. The six ridgetop transects in the Lewis Wetzel Wildlife Management Area, WV, for mapping the locations of Cerulean Warbler, Hooded Warbler, and Ovenbird singing males. See the Appendix for additional transect details.

Early bout ($n = 156$)



Mid bout ($n = 197$)



Late bout ($n = 180$)

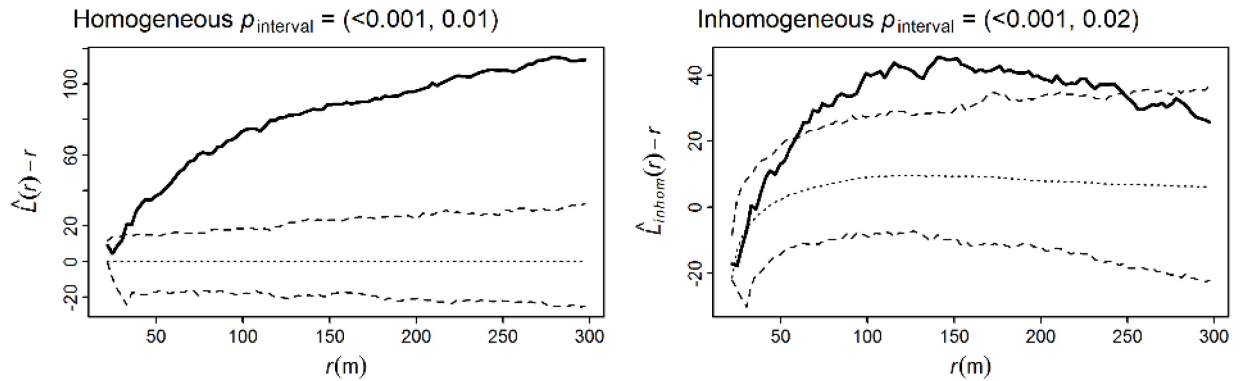


Figure 2. Rank envelope tests of the homogeneous and final inhomogeneous hard core models for the Cerulean Warbler point patterns by survey bout using the centered L - and L_{inhom} -functions ($\hat{L}(r) - r$ and $\hat{L}_{\text{inhom}}(r) - r$; r = distance in m), which are linearized versions of the Ripley's K -function for detecting clustering or regularity in a point pattern. The thick line is the function obtained from the observed point pattern, the dashed lines are the upper and lower bounds of the 95% global envelope for the distance interval (hard core distance to 300 m) based on 2499 simulations of the fitted model, and the dotted line is the simulation mean (i.e., the estimated theoretical expectation of the null hypothesis). The p -value interval for the test is in parentheses (lower p -value, upper p -value) and where the function is above the envelope suggests distances up to which individuals exhibited clustering.

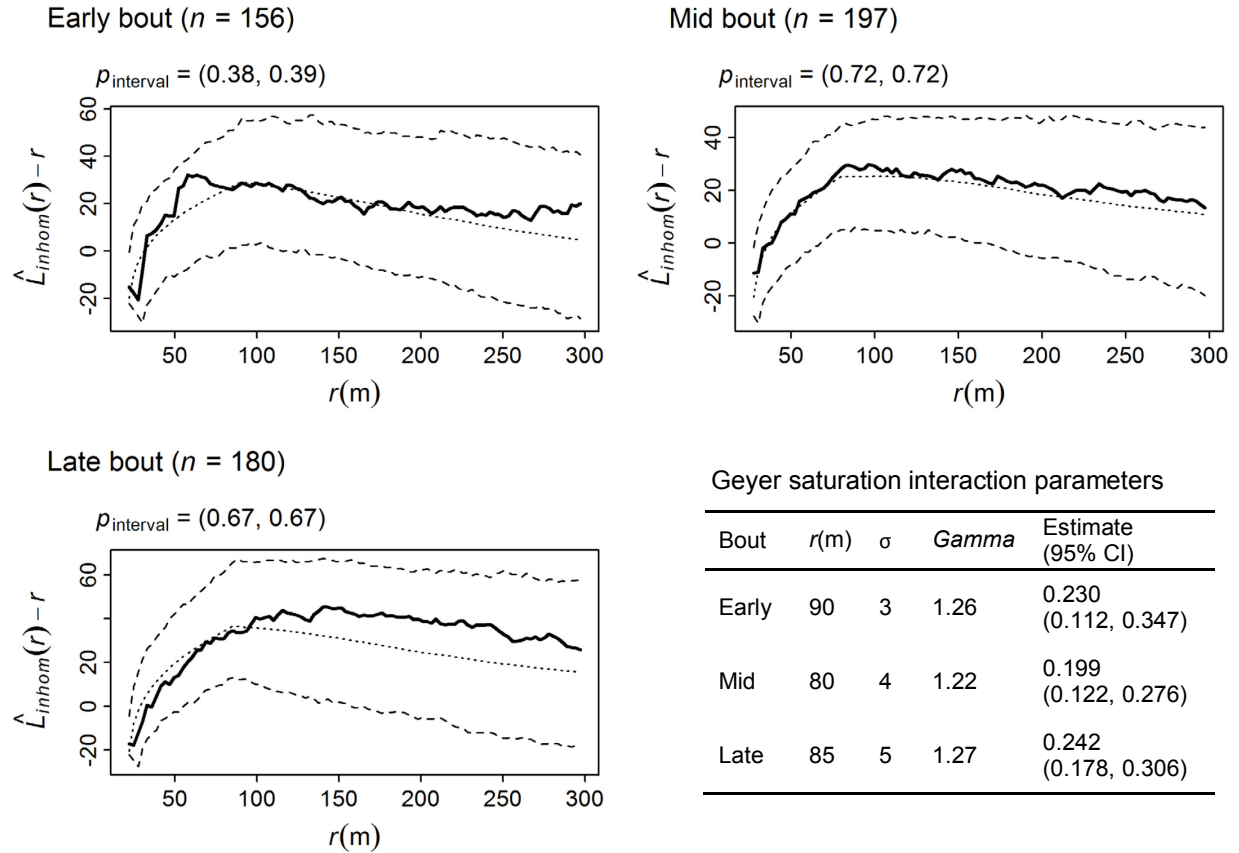
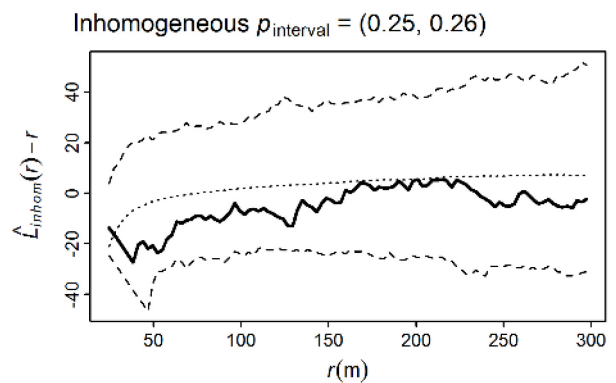
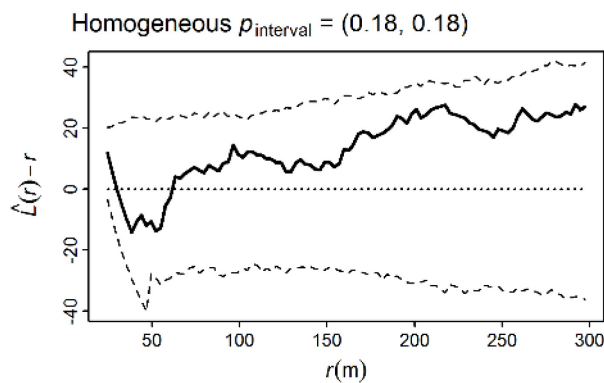
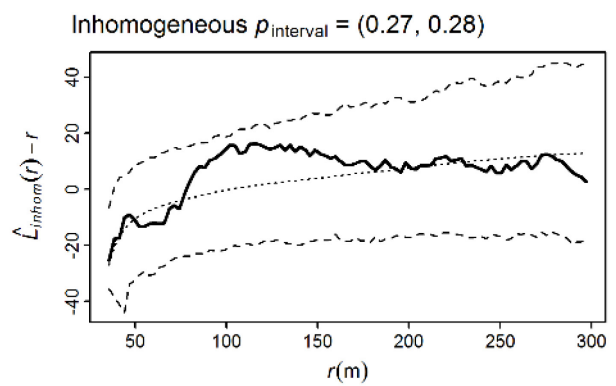
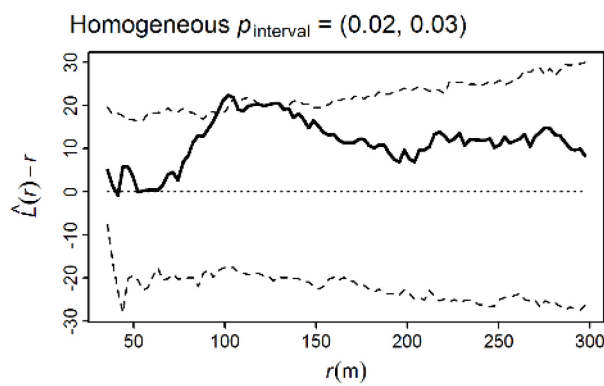


Figure 3. Rank envelope tests of the final inhomogeneous hard core-Geyer interaction hybrid models for the Cerulean Warbler point patterns by survey bout (figure and test descriptions as in Figure 2). The table shows the key parameters for interpreting the Geyer saturation interaction: $r(m)$ is the interaction radius distance, σ is the number of neighboring points typically involved in the interaction, Γ is the interaction parameter (>1 indicates clustering), and the estimate is the positive attraction effect estimate and its 95% confidence interval (CI).

Early bout ($n = 116$)



Mid bout ($n = 152$)



Late bout ($n = 173$)

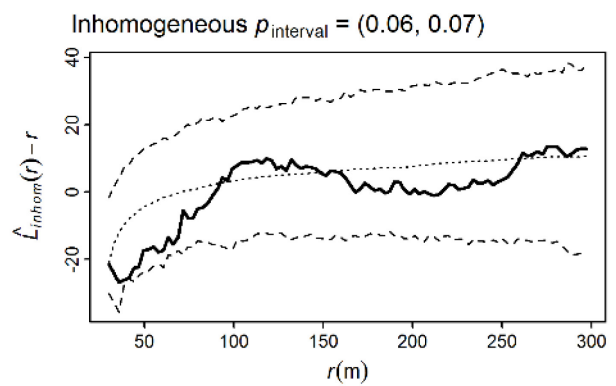
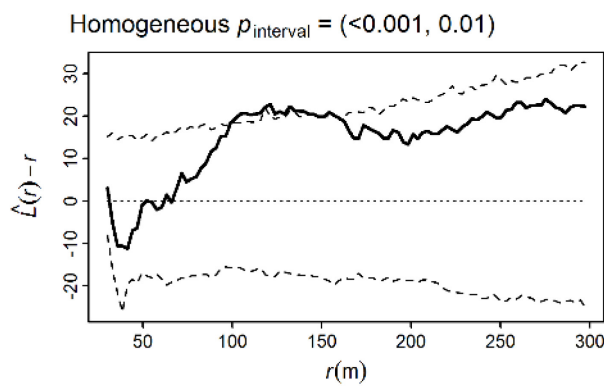
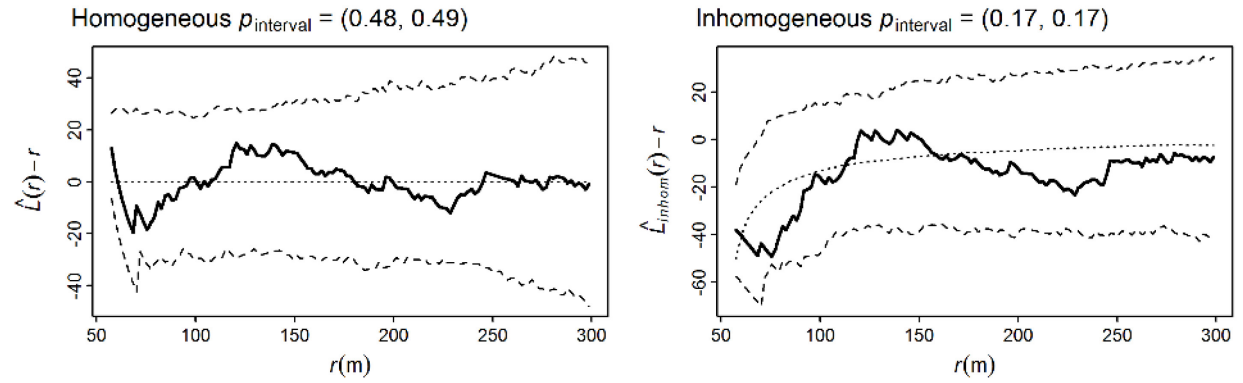
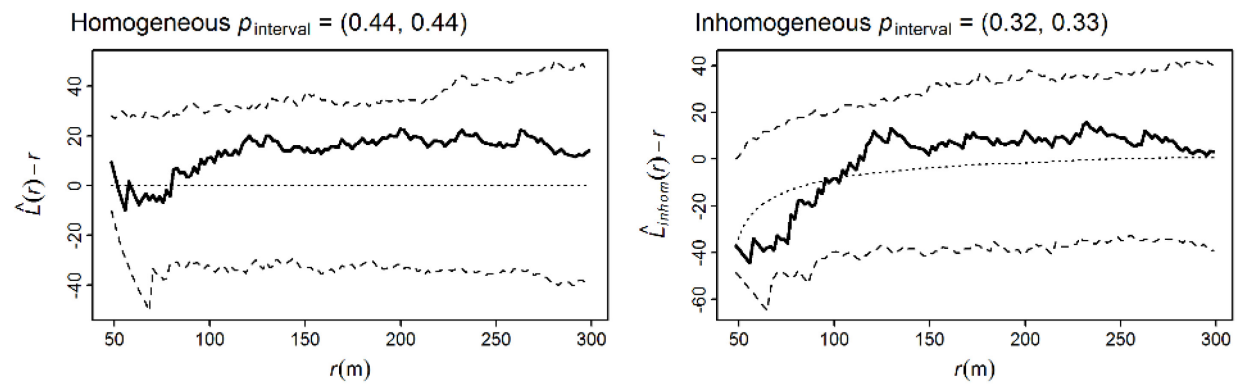


Figure 4. Rank envelope tests of the homogeneous and final inhomogeneous hard core models for the Hooded Warbler point patterns by survey bout (figure and test descriptions as in Figure 2).

Early bout ($n = 97$)



Mid bout ($n = 93$)



Late bout ($n = 108$)

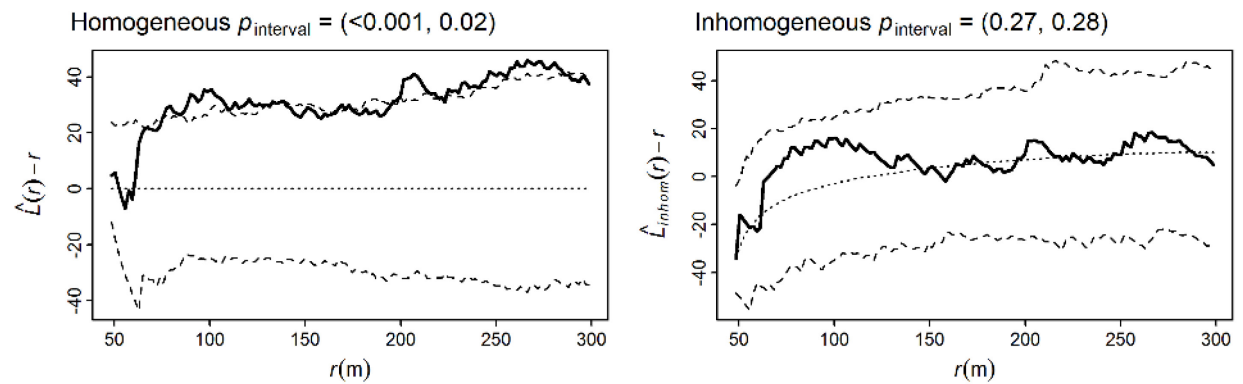


Figure 5. Rank envelope tests of the homogeneous and final inhomogeneous hard core models for the Ovenbird point patterns by survey bout (figure and test descriptions as in Figure 2).

APPENDIX

Forest impacts mapped within the areas of the transects (Figure 6), and the point patterns of the singing male Cerulean Warblers, Hooded Warblers, and Ovenbirds by survey bout (Figures 7-9).

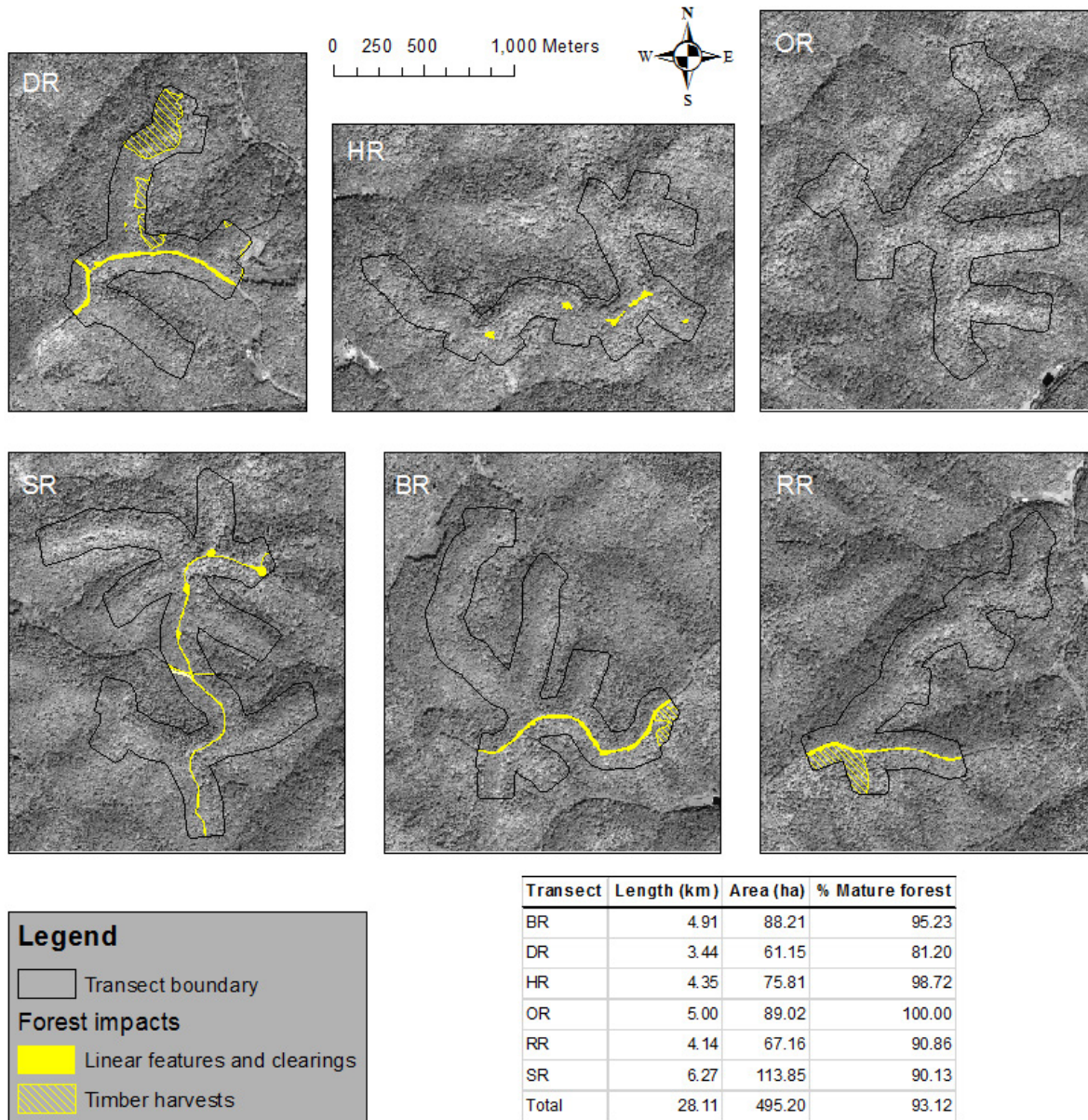


Figure 6. Forest impacts within the areas of the transects delineated using a 2009 QuickBird 2 (DigitalGlobe, Westminster, CO, USA) satellite 0.6 m panchromatic image (acquired 25 August 2009 at 16:18 GMT, 6° off-nadir, solar azimuth = 127°).

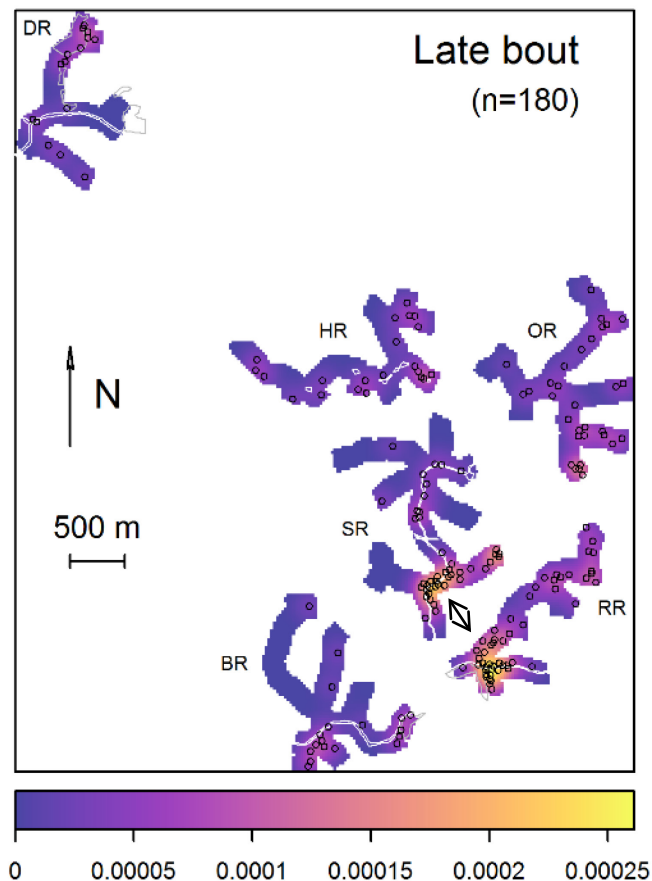
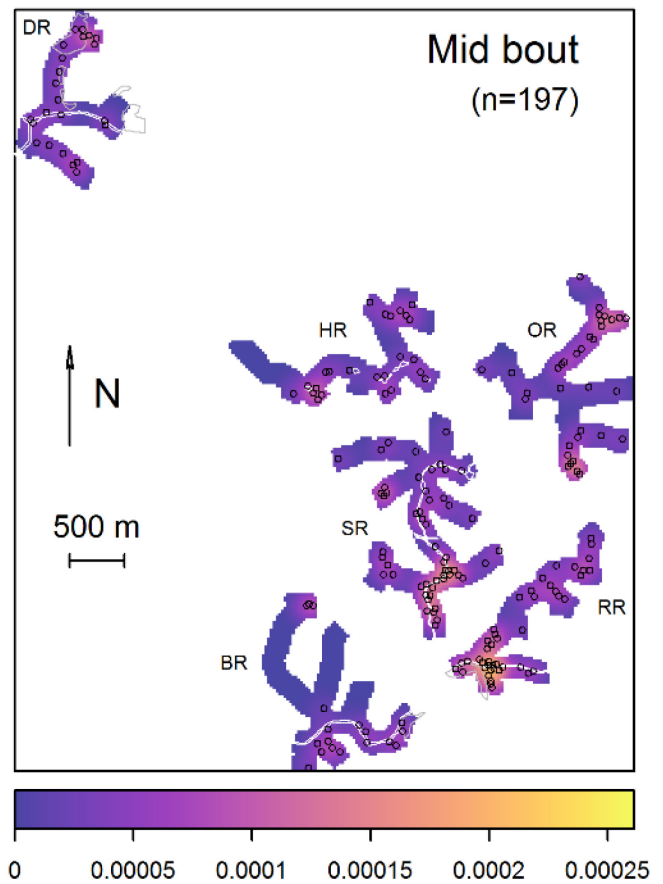
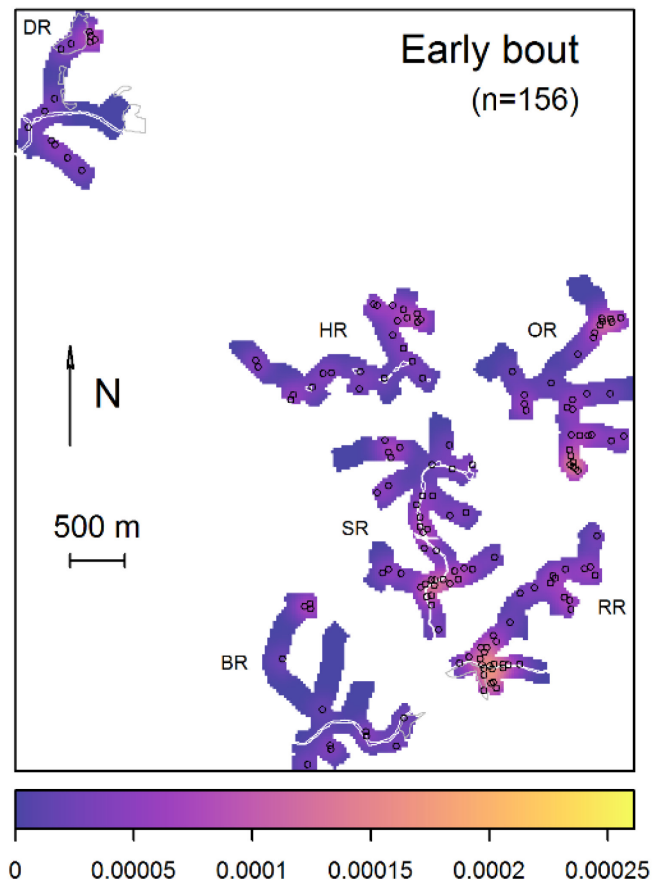


Figure 7. Point patterns of singing male Cerulean Warblers by survey bout, overlaid on point intensity (i.e., density) functions. The intensity functions were made using the spatstat R package (Baddeley et al. 2015) *density.ppp* function, with a 100 m standard deviation of isotropic Gaussian smoothing kernel and Diggle's edge correction. The functions were standardized across the survey bouts to depict changes in local densities. The transect impacts are outlined in white. The arrow points to the two highest local densities in the late bout.

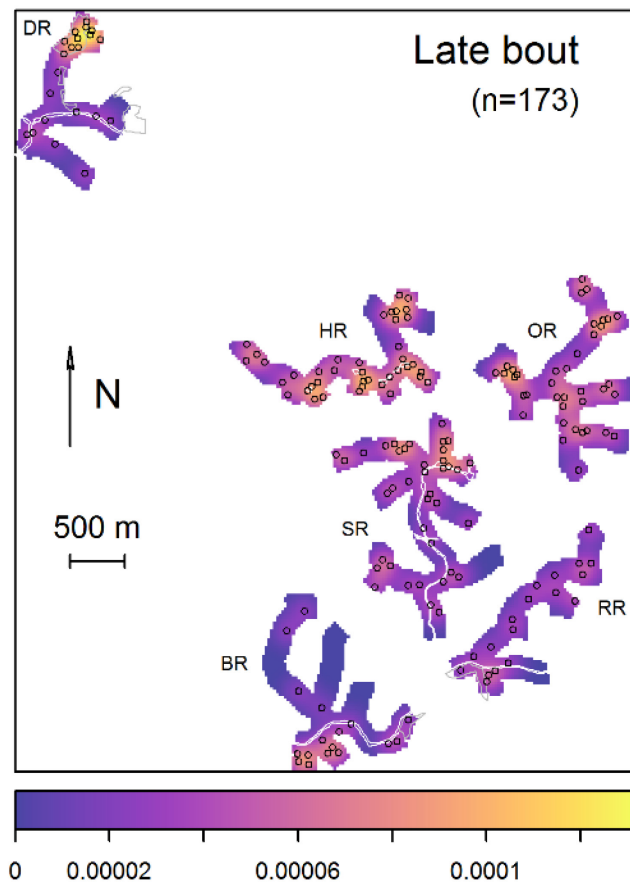
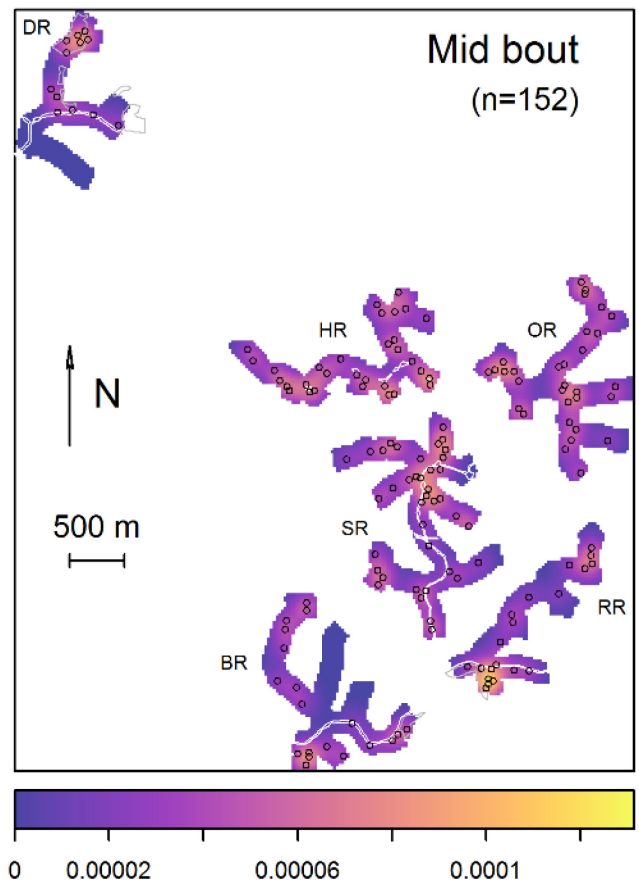
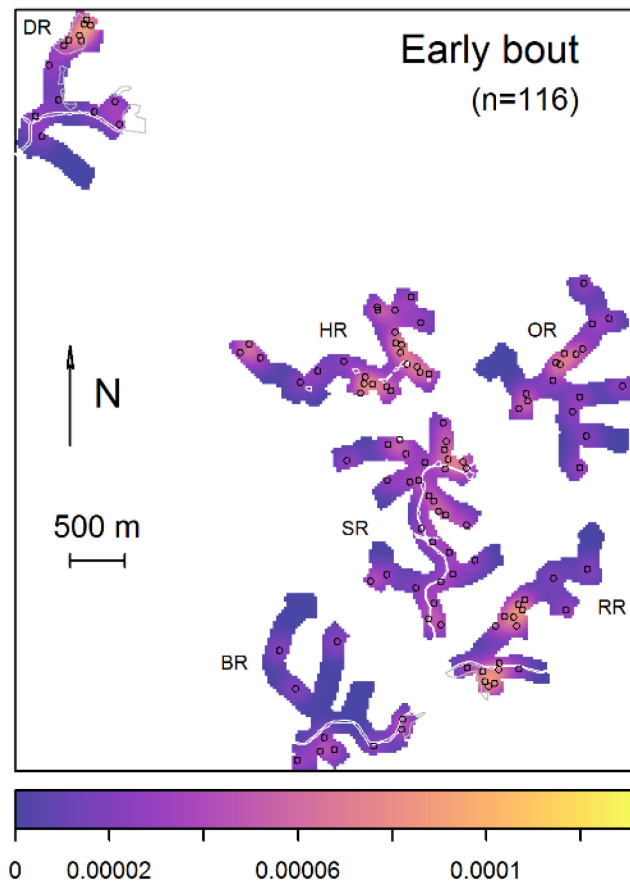


Figure 8. Point patterns of singing male Hooded Warblers by survey bout, overlaid on point intensity (i.e., density) functions. The intensity functions were made using the spatstat R package (Baddeley et al. 2015) *density.ppp* function, with a 100 m standard deviation of isotropic Gaussian smoothing kernel and Diggle's edge correction. The functions were standardized across the survey bouts to depict changes in local densities. The transect impacts are outlined in white.

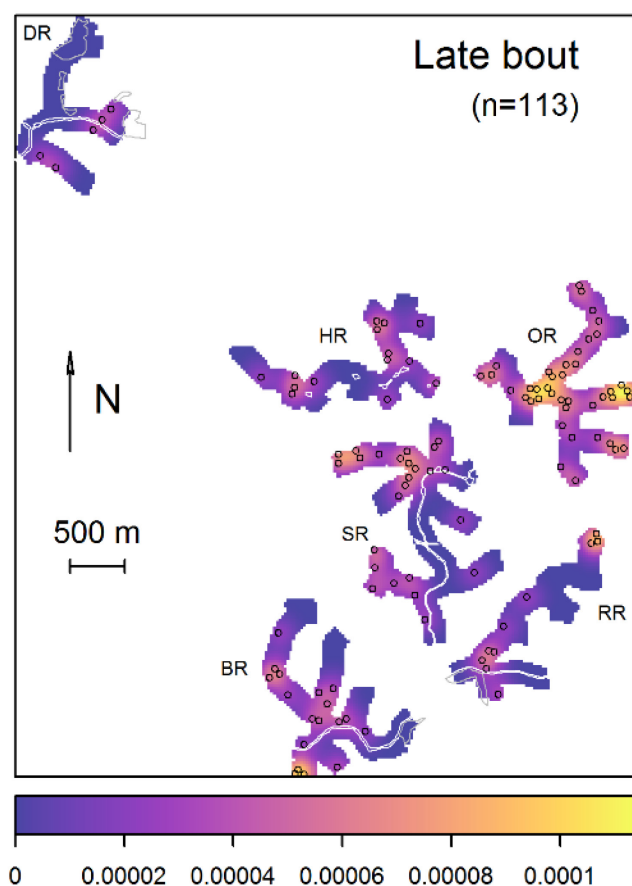
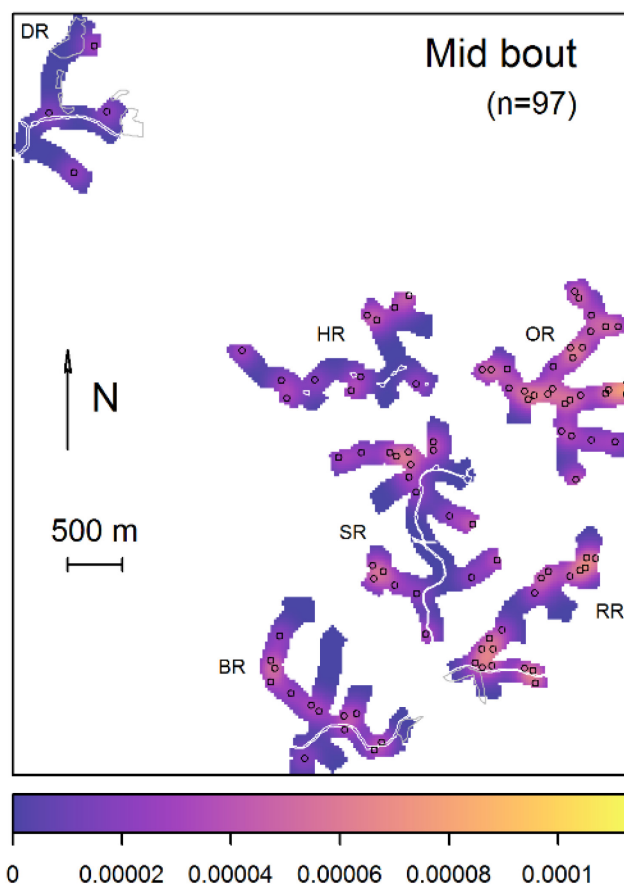
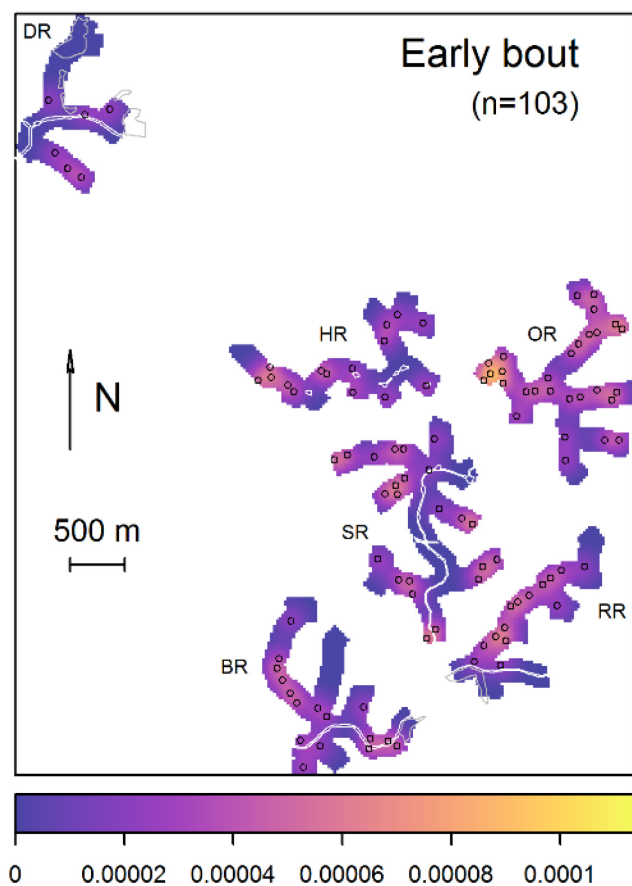


Figure 9. Point patterns of singing male Ovenbirds by survey bout, overlaid on point intensity (i.e., density) functions. The intensity functions were made using the spatstat R package (Baddeley et al. 2015) *density.ppp* function, with a 100 m standard deviation of isotropic Gaussian smoothing kernel and Diggle's edge correction. The functions were standardized across the survey bouts to depict changes in local densities. The transect impacts are outlined in white.